THESIS FOR THE DEGREE OF DOCTOR OF PHILOSOPHY

Charge Breeding and Production of Multiply Charged Ions in EBIS and ECRIS

FREDRIK J.C. WENANDER

Department of Experimental Physics
CHALMERS UNIVERSITY OF TECHNOLOGY
Göteborg, Sweden 2001

Charge Breeding and Production of Multiply Charged Ions in EBIS and ECRIS
FREDRIK J.C. WENANDER
ISBN 91-7291-009-7

Doktorsavhandlingar vid Chalmers tekniska högskola
Ny serie nr 1693
ISSN 0346-718x

Department of Experimental Physics
Chalmers University of Technology
SE-412 96 Göteborg
Sweden
Telephone +46 (0)31-772 1000

Printed at Chalmers Reproservice
Göteborg, 2001

Abstract

The REXEBIS is an Electron Beam Ion Source (EBIS) developed for charge breeding of the exotic and sometimes short-lived isotopes that are produced at ISOLDE for the REX-ISOLDE post accelerator. Bunches of singly charged radioactive ions are injected into the EBIS and charge bred to a charge-to-mass ratio of approximately ¼, and thereafter extracted and injected into a short 3-stage LINAC for acceleration to a few MeV/u. This novel concept, employing a Penning trap to bunch and cool the ions from an on-line mass separator in combination with a charge breeding EBIS, should result in an efficient and compact system. The REXEBIS is based on a 0.5 A electron beam produced in the fringe field of a magnetic solenoid, and compressed to a current density of >200 A/cm^2. The 2 T magnetic field is provided by a warm-bore superconducting solenoid, thus giving easy accessibility but no cryogenic pumping. The EBIS is switched between 60 kV (ion injection) and ~20 kV (ion extraction). This thesis presents the design and construction of the REXEBIS, together with initial commissioning results.

A complete ion injection, breeding and extraction cycle for an EBIS has been simulated to certify high injection and extraction efficiencies. The entire EBIS was modelled using an ion-tracing program, SIMION 3D. Acceptance and emittance phase-spaces were determined for different source settings and ions types. Beam optics parameters such as: lens positions and voltages; accepted beam tilt and displacement tolerances at the focal points were settled. These simulations verified an analytically derived acceptance formula. General conclusions on acceptance, emittance and energy spread of an EBIS were drawn. The correlation between the two transverse emittance phase-spaces was shown to be small.

Various experiments have been performed at an Electron Cyclotron Resonance Ion Source (ECRIS) in order to improve the ion yield. The source is operated in pulsed afterglow mode, and provides Pb^{27+} ions to the CERN Heavy Ion Facility on an operational basis. With the aim to reach higher beam intensities, the effect of a pulsed biased disk was investigated with different pulse structure and voltage settings. Various plasma electrode geometries were tested, including operating the source without a plasma electrode. The use of CF_4 as mixing gas was explored, and high secondary electron emission materials were inserted inside the plasma chamber in an attempt to increase the cold electron density. No proof of absolute higher intensities was seen for any of these modifications. Nevertheless, the yield from a poorly tuned/low-performing source could readily be improved with bias voltage applied and the extracted pulse became less noisy. The fast response to the bias implies that increases/decreases are not due to ionisation processes.

Finally, a design proposal utilising an EBIS for the ion pre-injector for the Large Hadron Collider (LHC) is presented. The LHCEBIS would produce lead ions, as well as lighter ions, that are directly injected into and further accelerated in an RFQ/LINAC arrangement. The source would operate with a repetition rate of 0.8 Hz, and the extracted yield is estimated to $1.6 \cdot 10^9$ Pb^{54+} per pulse. Using fast extraction, the extraction time can be less than 10 μs, possibly allowing single-turn injection into the PS Booster.

Keywords: acceptance, afterglow, beam simulation, charge breeding, EBIS, ECRIS, emittance, highly charged ions, ion injection, LHC, phase-space correlation, post accelerator, radioactive beam, REX-ISOLDE

List of publications

P1. **REXEBIS – a charge state breeder for the REX-ISOLDE post accelerator**
J. Axelsson, M. Björkhage, P. Carlé, L. Liljeby, K-G. Rensfelt, B. Jonson, G. Nyman, F. Wenander, Proc. of the 6th European Particle Accelerator Conference, Stockholm, Sweden, IOP Bristol (1999) p.1412-1414.

P2. **REXEBIS design and initial commissioning results**
F. Wenander, J. Cederkäll, B. Jonson, L. Liljeby, G. Nyman, K-G. Rensfelt, B. Wolf, Ö. Skeppstedt and the REX-ISOLDE collaboration, Proc. of the 8th International Symposium on Electron Beam Ion Sources and Traps and their Applications, Brookhaven National Laboratory, Nov 6-8, 2000. Accepted for publication in AIP Conference Proceedings Series.

P3. **EBIS as charge breeder for radioactive ion beam accelerators**
F. Wenander, Proc. of the 5th Radioactive Nuclear Beam conference, Divonne, France (2000). Accepted for publication in Nucl. Phys. A.

P4. **Experiments on the pulsed afterglow operation of an ECR ion source**
C. E. Hill, F. Wenander, Proc. of the 14th International ECRIS Workshop, ECRIS99, Geneva, Switzerland (1999) p.187-190.

P5. **Effect of a biased probe on the afterglow operation of an ECR4 ion source**
C. E. Hill, D. Küchler, F. Wenander, B. H. Wolf, Proc. of the 8th International Conference on Ion Sources, ICIS99, Kyoto, Japan, Rev. Sci. Inst. **71** no.2 (2000) p.863-865.

P6. **An EBIS as heavy ion source for the LHC pre-injector**
F. Wenander, Proc. of the 8th International Symposium on Electron Beam Ion Sources and Traps and their Applications, Brookhaven National Laboratory, Nov 6-8, 2000. Accepted for publication in AIP Conference Proceedings Series.

P7. **REXEBIS – the electron beam ion source for the REX-ISOLDE project**
F. Wenander, B. Jonson, L. Liljeby, G. Nyman and the REX-ISOLDE collaboration, CERN-OPEN-2000-320.

P8. **CRYSIS emittance simulations**
F. Wenander, Internal report, Manne Siegbahn Laboratory, Stockholm, Sweden (1999) MSL 99-1.

P9. **Simulation of ion injection, charge breeding and extraction for the REXEBIS**
F. Wenander, B. Jonson, G. Nyman. In preparation for Nucl. Instr. Meth. A.

I have furthermore contributed to the following papers

P10. **A preliminary design of the electron beam optics of the electron beam ion source for REX-ISOLDE**
R. Rao, F. Wenander, Nucl. Instr. Meth. **A416** no.2-3 (1998) p.210-220.

P11. **Problems improving the ECR at CERN**
D. Küchler, C. E. Hill, F. Wenander. Accepted for publication in Conference Proceedings of SIF (Italian Society of Physics).

P12. **High yields from the Stockholm electron beam ion source CRYSIS**
R. Rao, M. Björkhage, P. Carlé, Å. Engström, L. Liljeby, G. Rouleau, F. Wenander, 2nd Euroconference on Atomic Physics with Stored Highly Charged Ions, Stockholm, Sweden, (1996) Hyperfine Interactions **108** no.1-3, (1996) p.307-317.

P13. **The REX-ISOLDE bunching and charge breeding system**
F. Ames, G. Bollen, B. Jonson, L. Liljeby, I. Martel-Bravo, G. Nyman, K-G. Rensfelt, P. Schmidt, J. Szerypo, F. Wenander, International Workshop on JHF Science: JHF '98 Tsukuba, Japan, KEK-Proceedings-98-5 v2 JHF-98-2 v2 p.400-403.

P14. **REX-ISOLDE, an accelerator for radioactive ions**
F. Ames, G. Bollen, T. Davinson, D. Habs, A. Huck, M. Huyse, B. Jonson, O. Kester, L. Liljeby, G. Nyman, A. N. Ostrowski, H. Podlech, P. van Duppen, R. von Hahn, R. Rao, U. Ratzinger, R. Repnow, K-G. Rensfelt, K. Rudolph, A. Schempp, P. Schmidt, D. Schwalm, A. C. Shotter, T. Sieber, P. Thirolf, G. Walter, F. Wenander, P. J. Woods, International Workshop on JHF Science: JHF '98 Tsukuba, Japan, KEK-Proceedings-98-5 v2 JHF-98-2 v2 p.237-240.

P15. **The REX-ISOLDE project**
D. Habs, O. Kester, T. Sieber, A. Kolbe, J. Ott, G. Bollen, F. Ames, D. Schwalm, R. von Hahn, R. Repnow, H. Podlech, A. Schempp, U. Ratzinger, L. Liljeby, K-G. Rensfelt, F. Wenander, B. Jonsson, G. Nyman, P. van-Duppen, M. Huyse, A. Richter, G. Shrieder, G. Walter, ISOLDE collaboration, 5th European Conference on Accelerators in Applied Research and Technology (ECAART-5), Eindhoven, Netherlands, 1997, Nucl. Instr. Meth. **B139** no.1-4 (1998) p.128-135.

P16. **The REX-ISOLDE project**
O. Kester, D. Habs, T. Sieber, H. Bongers, S. Emhofer, P. Reiter, P. G. Thirolf, G. Bollen, O. Forstner, H. Ravn, F. Ames, P. Schmidt, G. Huber, L. Liljeby, Ö. Skeppstedt, K-G. Rensfelt, F. Wenander, B. Jonson, G. Nyman, R. von Hahn, H. Podlech, R. Repnow, C. Gund, D. Schwalm, A. Schempp, K-U. Kühnel, C. Welsch, U. Ratzinger, G. Walter, A. Huck, K. Kruglov, M. Huyse, P. van den Bergh, P, van Duppen, L. Weissman, A. C. Schotter, A. N. Ostrowski, T. Davinson, P. J. Woods, J. Cub, G. Schrieder and the REX-ISOLDE collaboration, Hyperfine Interactions **129** no.1-4 (2000) p.43-66.

Charge Breeding and Production of Multiply Charged Ions in EBIS and ECRIS

PART I – THE REXEBIS

PART IV – CONCLUSIONS AND OUTLOOK

Commonly used symbols

A	mass number
α	acceptance (mm·mrad)
B	magnetic field (T)
C	charge (C)
e	elementary charge ($1.6 \cdot 10^{-19}$ C)
E	energy or electrical field (depending on context)
E_e	electron-beam energy (eV)
ε_0	permittivity constant ($8.854 \cdot 10^{-12}$ Fm^{-1})
ε	emittance (mm·mrad)
f	neutralisation / compensation factor
$\Delta\phi$	plasma dip (V)
ϕ	plasma potential (V)
I_e	electron-beam current (A)
j_e	electron-beam current-density (A/m^2)
k	Boltzmann's constant ($1.38 \cdot 10^{-23}$ J/K)
m_e	electron mass ($9.1 \cdot 10^{-31}$ kg)
n_e, n_q	electron and ion (charge state q) density (cm^{-3} or m^{-3} depending on context)
q	ion charge (C) or ion charge-state depending on the context
Q	ion charge-state
R_B	magnetic mirror ratio
r_{ebeam}	electron-beam envelope (m)
ρ_l	electron-beam charge per unit length (C/m)
$\sigma_{q \to q+1}$	ionisation cross-section from q to q+1 (m^2)
T_e, T_i	electron and ion temperature (K)
τ	breeding time (s)
u	nucleon
U_{ext}	extraction voltage (V)
U_t	drift tube potential relative cathode potential (V)
ΔU	electron-beam potential depth (V)
$v_{\parallel}$	velocity component parallel to magnetic field line (m/s)
$v_{\perp}$	velocity component perpendicular to magnetic field line (m/s)
ω_{ecr}	cyclotron resonance frequency (rad/s)

Abbreviations and acronyms

CCD	Charge Coupled Device
CRYSIS	CRYogenic Stockholm Ion Source (EBIS at Manne Siegbahn Laboratory)
CW	Continuous Wave
EBIS	Electron Beam Ion Source
ECRIS	Electron Cyclotron Resonance Ion Source
HV	High Voltage
IH-structure	Interdigital H-structure
ISOL	Isotope Separator On-Line
LEIR	Low Energy Ion Ring
LHC	Large Hadron Collider
LINAC	LINear ACcelerator
MCP	Multi Channel Plate
MCI	Multi Charged Ion
NEG	Non-Evaporable Getter
PROFIBUS	PROcess FIeld BUS
PS	Proton Synchrotron
REX-ISOLDE	Radioactive EXperiment at ISOLDE
RF	Radio Frequency
RFQ	Radio Frequency Quadrupole
TOF	Time Of Flight
UHV	Ultra High Vacuum

Preface

Ever since the invention of the EBIS and ECRIS – probably the two most powerful systems for production of multi-charged ions – both sources have had a given position as ion providers for various kinds of atomic physics experiments. Much of the interest was spurred by the need for data within astrophysics and fusion plasma physics. Clearly, the sources have contributed substantially to the exploration of the physics of highly charged ions [1], and more applications for highly charged ions are to come. For example, the accuracy in mass determination of short-lived nuclei using the Penning trap mass spectrometer technique [2] can be increased; the solid state physics community will profit from the higher ion energy in order to achieve deeper ion implantation; surface bombardment by highly charged radioactive ions is possible; and as a result of the continuous struggle for higher charge states, more precise tests of QED using heavy hydrogen-like ions [3] are made conceivable.

At the present time the goal is not solely to produce ions with highest possible charge states. With the appearance of ion pre-injectors, the need for very high ion yields released within a short time has been raised. Charge breeding of radioactive ions is another new application for sources for highly charged ions, which not only demands a fast breeding time, but also requires a high efficiency and clean extraction spectra among other things. Stretching the present performances and uncovering new techniques are therefore compulsory to reach the recent demands on the sources for highly charged ions.

Naturally, a single universal source able to fulfil the entire range of requirements is not available. Such a superior source would have the daunting mission to produce ion beams with varying charge state, and with an extraction time variable between DC and a few microseconds. While having a high yield capacity, it should also be able to handle very few ions. A minimum of complexity is desirable, in addition to a long lifetime. The beam quality, more specifically the transverse and longitudinal emittance, is of great importance, as it is reflected through the whole accelerator chain (in terms of transmission losses) and at the actual experiment (in terms of luminosity and time structure). The EBIS [4,5] and ECRIS [6,7] are two sources for multiply charged ions based on relatively different concepts that not alone, but in a complementary way, meet the listed specifications. The main goal throughout my doctoral studies has been to explore methods to conform these two source types to the challenging requirements of their new applications.

Principally, the doctoral work of mine can be divided into two major parts. The first concerned the design and development of an EBIS to be used for charge breeding of radioactive ions. Charge breeding is a new concept with the aim to permit short post accelerators, and the methods to use either an EBIS or an ECRIS as breeder are under eager investigation. The project, called REXEBIS [P1,8,P7], is a collaboration between the Manne Siegbahn Laboratory in Stockholm, where most of the design and construction were carried out, and Chalmers University of Technology, Gothenburg. The building-up phase and completion has taken place at ISOLDE [9,10], CERN. The REXEBIS related work is covered in the first section of this thesis. Since the EBIS theory, design simulations and construction aspects, and the REX-ISOLDE post accelerator all were extensively treated in my Licentiate thesis [8,P7], only a brief recapitulation will be given here. Instead, the focus will be on the initial commissioning results of the REXEBIS and how they relate to simulated predictions.

At the PS division, CERN, the second part of the studies was carried out. There, a number of experiments were performed on an existing and operational ECRIS, the lead producing ECR4 [11,12] for LINAC3 [13,14], when the source was liberated from ion delivery to the SPS. The objectives were to theoretically study the beam extraction out of the ECRIS, and to experimentally investigate various methods to boost the afterglow intensity. The latter will be accounted for in the second part of this thesis.

In spite the fact that the EBIS and ECRIS are two rather dissimilar devices and governed to a large extent by different physical processes, the production of highly charged ions unavoidably link them together. This was illustrated in the theoretical evaluation of using an EBIS as an ion source for the pre-injector to the LHC project [15]. Here the two sub-projects became related, and furthermore the perspective on a complete accelerator chain was added to the picture. This work is presented as the last section of this thesis.

Part I – The REXEBIS

1.1 Introduction

1.1.1 Motivation for REXEBIS

The development of REXEBIS [P1,P7], is part of a larger project, the so-called REX-ISOLDE [16,17,18,19], which is a post accelerator connected to the ISOLDE (Isotope Separator On-Line) facility [9,10] at CERN. The nuclear physics community is now turning its attention to the regions far away from nuclear stability, to the neutron and proton drip-lines and the physics with radioactive ions. There, exciting new phenomena may be found, such as changed magic numbers, halo shells etc [16,18]. To reach these extreme regions in the nuclear chart innovative accelerator concepts have to be used. The ISOLDE community has chosen to add a post accelerator to the separator. By doing so, the physicists will have access to the large number of isotopes produced at ISOLDE, and make use of the long experience in radioactive ion production, but now at higher energies. So far, approved experiments at REX-ISOLDE involve studies of the nuclear structure of medium-light neutron-rich nuclei by Coulomb excitation and neutron transfer reactions.

1.1.2 The REX-ISOLDE project

The REX-ISOLDE is designed to boost the energy of radioactive nuclei produced by ISOLDE from 60 keV to energies between 0.8 and 2.2 MeV/u. The idea is schematically depicted in Figure 1. To achieve the energy goal, a novel post accelerator concept will be used utilising a Penning trap as an efficient buncher and cooler (REXTRAP) [20,21,22], and an electron beam ion source (REXEBIS) as a charge breeder. The REXEBIS increases the ion charge from 1^+ to a charge-to-mass ratio of ~1/4, prior to the mass analysis in an achromatic mass separator [23]. Subsequent acceleration is achieved in a three stage LINAC consisting of an RFQ [24,25], an IH-structure [25,26] and three 7-gap resonators [27,28] before the ions impinge at the target. As a result of the increased ion charge state inside the EBIS, a lower acceleration voltage is viable, and the size and cost of the LINAC can be kept within reasonable limits. A more comprehensive description of the REX-ISOLDE project is found, for instance, in ref. [18]. The actual accelerator layout in the ISOLDE hall is illustrated in Figure 2.

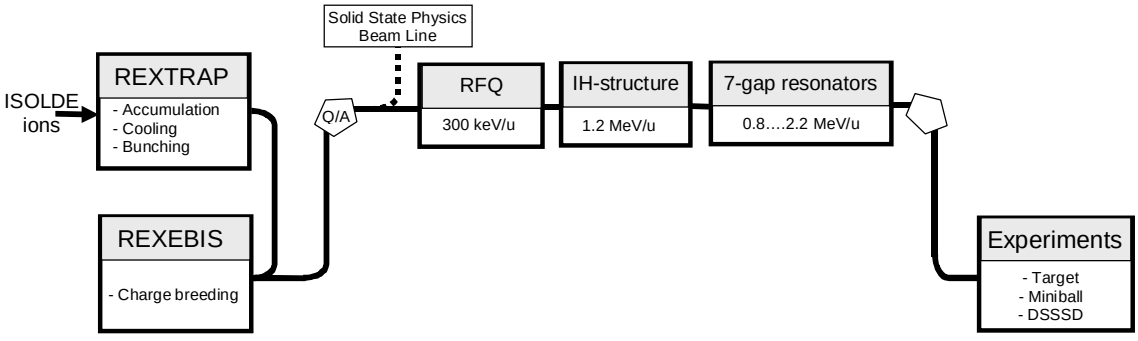

Figure 1. *Flowchart for the REX-ISOLDE concept.*

1.1.3 Fundamental EBIS theory

Inside the REXEBIS the ions are charge bred to a higher charge state. The EBIS [4,5], Figure 3, uses a dense mono-energetic electron beam from an electron gun to further ionise the ions. The electron beam is focused and compressed by a strong magnetic field created by a surrounding solenoid. Ions injected into the EBIS are confined radially by the electrostatic forces from the negatively charged electron beam and the magnetic field, and longitudinally by potential barriers, established by cylindrical electrodes surrounding the beam. Inside the trapping region the high-energy electrons collide with ions, which are stepwise ionised, until they finally are extracted by raising the trapping potential and lowering the extraction barrier simultaneously. The ion motion inside the trap is a combination of radial oscillation in

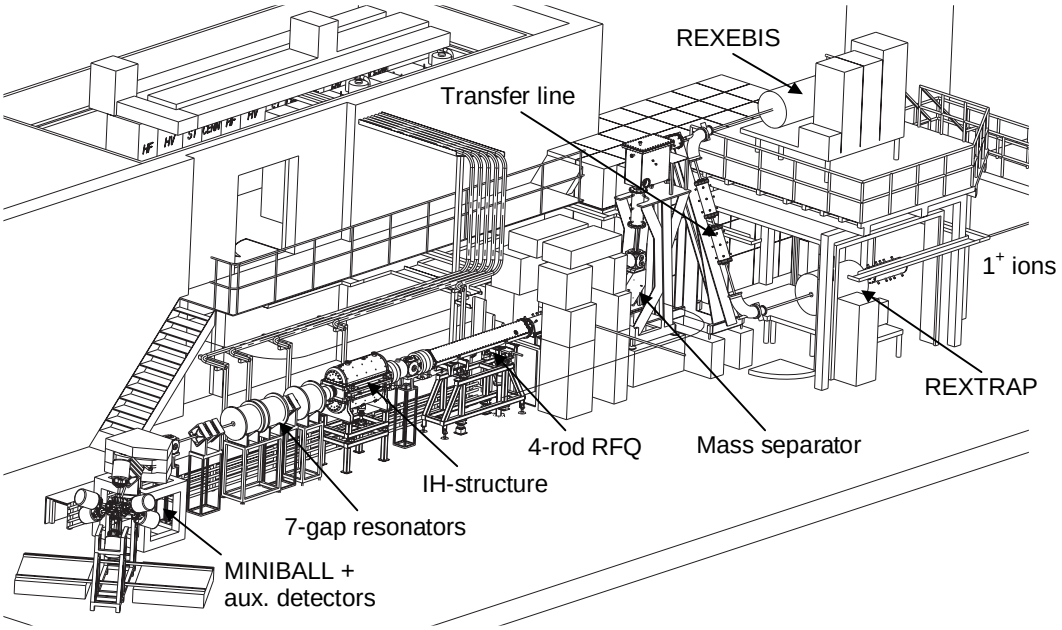

***Figure 2**. Overview of the REX-ISOLDE post accelerator layout in the ISOLDE hall.*

the electrostatic field of the beam with a superimposed azimuthal cyclotron motion around the magnetic field lines, and a relatively non-correlated bouncing between the end barriers [29].

The main characteristic entity describing an EBIS is the product $j_e\tau$, the ionisation factor, of the electron-beam current-density j_e and the breeding time τ. The probability for transition of an ion from charge state q to q+1 is $P_{q\to q+1}=\sigma_{q\to q+1}\cdot j_e\cdot\tau/e$, where e is the elementary charge. Thus, on the average, all ions of charge state q transform to q+1 when $j_e\tau=e/\sigma_{q\to q+1}$. This means that to produce ions of mean charge k from singly charged ions with stepwise ionisation, the ionisation factor $j_e\tau$ has to be:

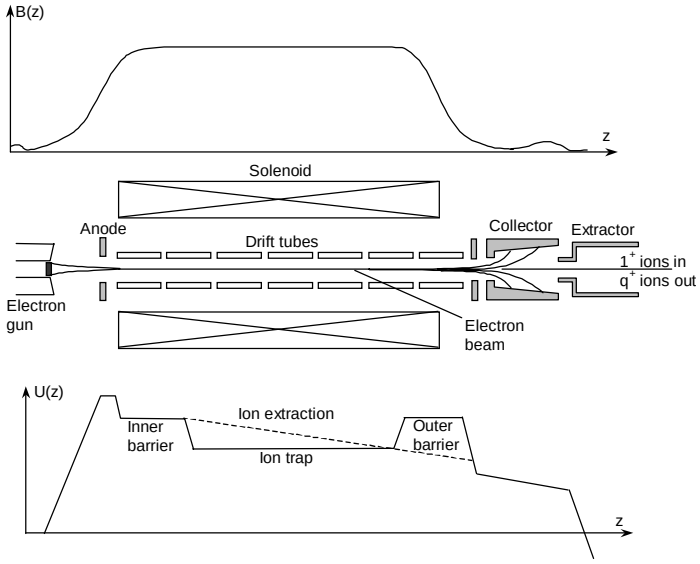

***Figure 3**. Scheme of EBIS with corresponding axial magnetic field and axial potential function.*

$$j_e\tau = \sum_{q=1}^{k-1}\frac{e}{\sigma_{q\to q+1}} \quad \text{(e.g. ~3.3 As/cm}^2\text{ to ionise an Ar atom to 11}^+\text{)} \qquad \textbf{(1)}$$

1.1.4 The REX-ISOLDE bunching/cooling/breeding

One of the novelties with the REX-ISOLDE post accelerator is the unique combination of a Penning trap, in which the semi-continuous radioactive beam from ISOLDE is accumulated, cooled and bunched, and an EBIS, where the charge state of the ions is increased. Major reasons for introducing a trap in the system is the higher injection efficiency into the EBIS for a pulsed beam, and the more narrow charge state distribution. In addition, the large transverse beam emittance of ISOLDE (~35 π·mm·mrad at 60 kV) has to be cooled to be adequately accepted by the EBIS if its emittance is expected to be less than 10 π·mm·mrad at 20 kV as required by the mass analyser. Besides, a pulsed beam out of the EBIS allows the LINAC to operate with a duty factor <10%, and it improves the signal to background ratio for the

physics experiments with low count rates. The Penning trap/EBIS system described below should have a high overall efficiency (up to 30% for Na isotopes), manage short-lived ions (cycle time <40 ms) and handle intensities from a few hundred to 10^8 ions per second.

1.1.4.1 Buncher and cooler

The REXTRAP potential is close to 60 kV permitting the semi-continuous 60 keV ISOLDE beam to enter the trap just over the outer potential barrier. The incoming ions are decelerated by frictional collisions with buffer gas atoms (Ar, Ne or He depending on ion species). The energy loss, ΔE, in the buffer gas during a single oscillation in the trap has to be larger than the energy spread of the ISOLDE beam (effectively 100 eV) for the ions to be trapped. The trapped ions are confined in radial direction by the action of a strong magnetic field (3 T field created by a superconducting solenoid) and in longitudinal direction by the potential of an electrostatic quadrupole (see Figure 4). The electrode structure inside the trap is divided into two regions. The injection side has a high buffer gas pressure of ~10^{-3} mbar and a length of 40 cm, which ensures ion capture with an efficiency close to 100%, while the trapping/extraction zone including the potential minimum of the trap has about one magnitude lower pressure. Using this separation one minimises the energy-spread degeneration caused by the numerous collisions with gas molecules while ejecting the ions, and improves the mass selectivity of the cooling technique.

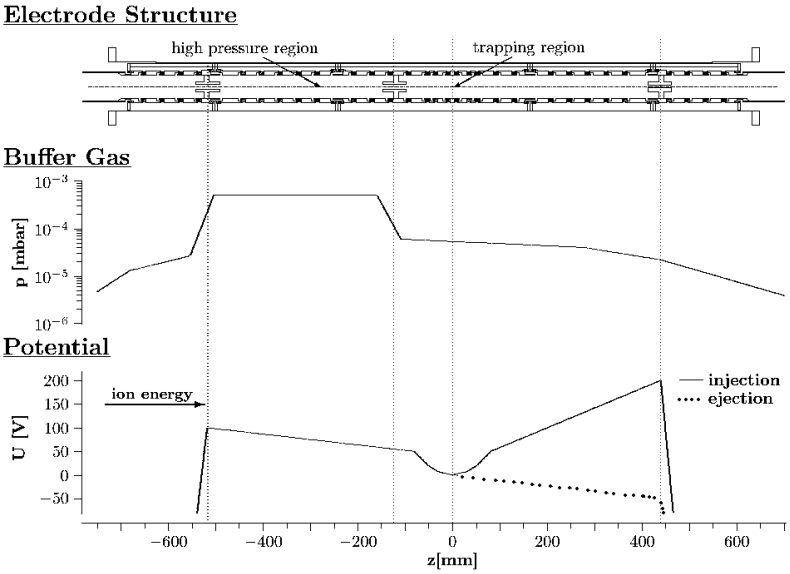

***Figure 4**. Electrode structure, voltage and buffer gas pressure distribution inside the Penning trap [30].*

Inside the trap the ions perform mainly three different eigenmotions (numerically exemplified for A=30): axial (f_z~60 kHz), cyclotron (f_+~1.5 MHz) and magnetron (f_-~1.2 kHz) as illustrated in Figure 5. The amplitudes of the eigenmotions are reduced so the ions end up in the trap centre, and thereby the emittances are improved, as a result of long range Coulomb collisions with the buffer gas combined with a special RF-sideband cooling technique [31]. The cooling time is in the range 10-20 ms, and the transverse emittance of the expelled ion bunches is reduced by at least one order of magnitude with respect to the ISOLDE beam (typically to 3 π·mm·mrad at 60 kV).

In principle the mass selectivity of the cooling technique could be employed for further purification of the ISOLDE beam. So far a mass resolving power R of 300 to 500 has been achieved, but a higher value of R can be reached if even lower gas pressure in the trap region and longer cooling times are used. The Brillouin constraint [32,33] limits the space-charge density in a Penning trap to roughly 10^9 cm^{-3}, hence at maximum ~10^8 ions can be accumulated and cooled per bunch.

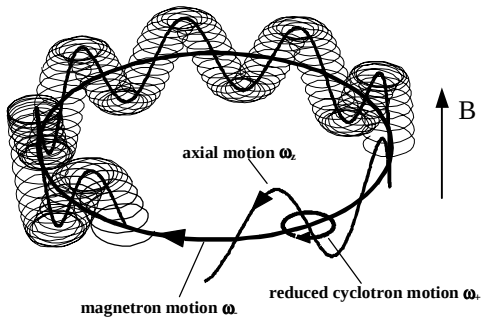

***Figure 5**. Ion eigenmotions in a Penning trap: magnetron, cyclotron and axial motion.*

At the end of the cycle the ions are extracted in a bunch and transported to the EBIS with 60 keV kinetic energy. The extracted pulse length from the trap is in the order of 10 µs and has an energy spread of some eV, thus the ions can be easily injected into an EBIS.

Experiments show that the trap can realistically handle beam intensities from a few hundred up to some 10^6 ions per pulse, at a 50 Hz operation rate. Stable beams from ISOLDE and also from a test ion source were injected with maximum efficiencies of 30% and 45%, respectively, and ion species between ^{7}Li and ^{181}Ta were successfully accumulated, cooled within 20 ms and thereafter extracted [30]. As can be seen in Figure 6, the extracted beam is slightly contaminated by H_2O and Ar (buffer gas). The first radioactive ions to be trapped were ^{25}Na ($t_{1/2}$=59.6 s), ^{26}Na ($t_{1/2}$=1.07 s) and ^{88}Rb ($t_{1/2}$=17.8 min), and no additional background due to the radioactivity was seen. The emittances and the energy spread have yet not been measured due to the very weak signals.

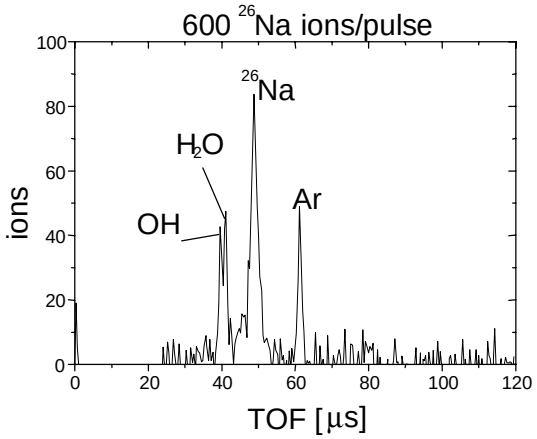

***Figure 6**. Time-of-flight spectrum for bunched $^{26}Na^{1+}$ ions ejected from REXTRAP after accumulation from ISOLDE and cooling [22]. Argon used as buffer gas.*

1.1.4.2 Transfer beam line

After bunching and cooling in the Penning trap, the ions are extracted to ground potential (i.e. 60 keV) and transferred to the REXEBIS via the transport line (see Figure 2). It has an achromatic and symmetric design, and consists of two 7.5º kickers, two 82.5º spherical benders and two electrostatic quadrupole triplets on each side of the symmetry point. The kicker at the REXEBIS side is only active during injection; at extraction from the EBIS the beam goes straight through to the mass analyser. The REXEBIS requires an extremely good residual gas pressure, thus apertures are positioned at the three beam foci to improve the differential pumping between the trap and the EBIS. Beam diagnostic units (FC and MCPs with phosphor screens read out by CCD cameras) are placed at the beam transport entrance, in the middle of the system, and at its exit.

1.1.4.3 Charge breeder

The specifications for the REX-ISOLDE post accelerator, together with the limits set by the Penning trap and the mass separator/LINAC, impose strict requirements on the REXEBIS design. The EBIS should be able to charge-breed elements with mass A<50 to a charge-to-mass ratio of >1/4.5 within a confinement time of <20 ms (i.e. breeding frequency 50 Hz). This short confinement time is dictated by the short lifetime of the radioactive nuclei. For light elements one has the possibility to use an even shorter cycle time (10 ms). The number of ions injected per pulse may vary from a few ions to 10^7. Because of the low production yields of the most exotic radioactive ions the EBIS has to be efficient, i.e. the injection and extraction efficiency should be higher than 50%. Because of the statistical nature of the ionisation process an inherent breeding efficiency, $q_i/\Sigma q_i$ of about 30% is expected (correlated to the ion mass).

To fulfil the above requirements, we have chosen a design utilising a 5 keV electron beam with a current of 0.5 A. The current density is >200 A/cm^2 throughout a 0.8 m long trap region. With these parameters the REXEBIS trap can hold up to ~$6\cdot10^9$ charges for an electron-beam charge-compensation of 10%. This is more than two orders of magnitude larger than the number of ions that can conceivably be delivered by the Penning trap due to its intrinsic space-charge limitations. The most dominant charge states for some typical ions, charge bred for 20 ms in the REXEBIS, are listed in Table 1. Breeding time versus charge state for a selection of elements is plotted in Figure 7.

Element	Charge-state
$_{8}$O	7^+
$_{11}$Na	9^+
$_{12}$Mg	9^+
$_{18}$Ar	11^+
$_{19}$K	11^+
$_{20}$Ca	12^+
$_{36}$Kr	16^+
$_{37}$Rb	18^+
$_{51}$Sb	19^+
$_{54}$Xe	21^+

***Table 1**. Peak charge-state after 20 ms breeding time.*

A small extraction emittance of 3 π·mm·mrad (60 kV) from the Penning trap is required for a high injection efficiency, and the following mass analyser accepts at most an emittance of 40 π·mm·mrad (4σ, 20 kV extraction voltage) for an energy spread of 50 eV/Q.

The EBIS platform voltage is switched between 60 kV (ion injection) and ~20 kV (ion extraction). The low extraction voltage results in a low RFQ injection energy and thus an efficient adiabatic bunching providing better output emittance of the RFQ.

As will be demonstrated below, it is clear that a mass selection system with a good resolution is needed after the REXEBIS to separate the residual gas from the radioactive ions, since the number of rest-gas ions can exceed the radioactive ions with several orders of magnitude. The REX-ISOLDE mass separator [23] has a Q/A-resolution of ~150.

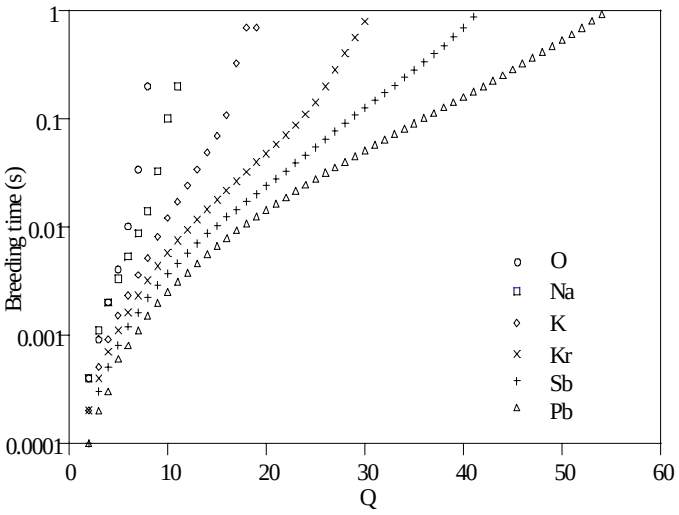

Figure 7*. Breeding time versus charge-state for the REXEBIS design parameters. Not all ions to be used in the REXEBIS at a first stage.*

1.2 The REXEBIS mechanical design

1.2.1 Novelties

For the first time an EBIS is being used to charge breed ions for a post accelerator. The idea of a Penning trap in front of an EBIS has never been tried before, but as already explained, it turns out to be necessary due to the poor beam properties out of the primary on-line source. The possibility of a very small number of injected ions is also a new challenge, as well as the high efficiency requirement. Mechanical EBIS innovations include an open-end collector design to improve the extracted beam quality; warm bore and inner structure that are pumped by Non-Evaporable Getter (NEG) strips; and few drift tubes to minimise the risk for self-excitation.

In the following sections the main components (see Figure 8) of the REXEBIS will be examined, starting with the solenoid. Since an extensive description of the REXEBIS can be found in ref. [P7], only a summary is presented here but previously non-covered material has been added. In Appendix 1 a photo of the REXEBIS can be found.

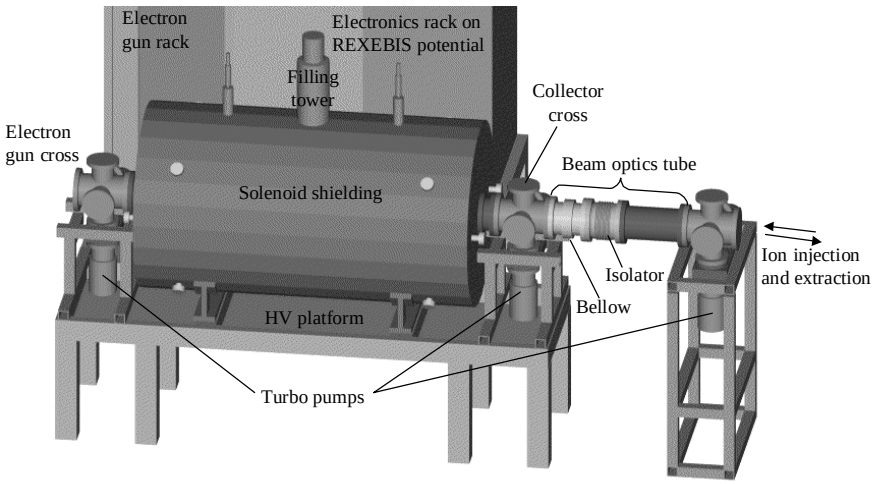

Figure 8*. The REXEBIS positioned on the high voltage platform. The electron gun is found inside the vacuum cross to the left. The transport line from the REXTRAP and the mass separator connecting the EBIS to the LINAC are positioned to the right of the injection/extraction optics.*

1.2.2 Solenoid

The superconducting solenoid [34] (NbTi wire) provides a 2 T magnetic field, both for focusing of the electron beam and to facilitate trapping at ion injection. It is iron shielded with 25 mm thick passive iron bars in a cylindrical configuration. The basic solenoid and iron shielding shapes [P10] were calculated using POISSON [35]. In the present configuration the magnetic field compresses the electron beam from a current density of 25 to >200 A/cm^2.

To optimise the performance of the EBIS, the magnetic field straightness, homogeneity, and stability must be carefully controlled. A simple method was developed to verify the field straightness, and found the traced central field-line to be within a cylinder, with the axis coinciding with the geometrical beam axis, of radius 0.15 mm for the full EBIS length (-800<z<800 mm), see Figure 9. The axial field has a specified homogeneity of 0.3% over ±400 mm, and we measured the homogeneity to be within 0.25%. The relative field decay was specified to be better than $5\cdot10^{-6}$ h^{-1}, but the measured decay amounts $13\cdot10^{-6}$ h^{-1}.

The REXEBIS has a warm bore, i.e. the inner cylinder containing the drift structure is held at room temperature, despite the cryogenic temperatures of the superconducting solenoid. We chose this concept to avoid the memory effect in which gases frozen to a cryogenic surface may re-enter the vacuum by the thermal load from the electron beam going astray. Furthermore, cryogenically unstable operation resulting in solenoid warm-up due to electrons hitting cold surfaces is avoided. The main difficulty is to substitute the inherently efficient cryogenic pumping from a cold bore.

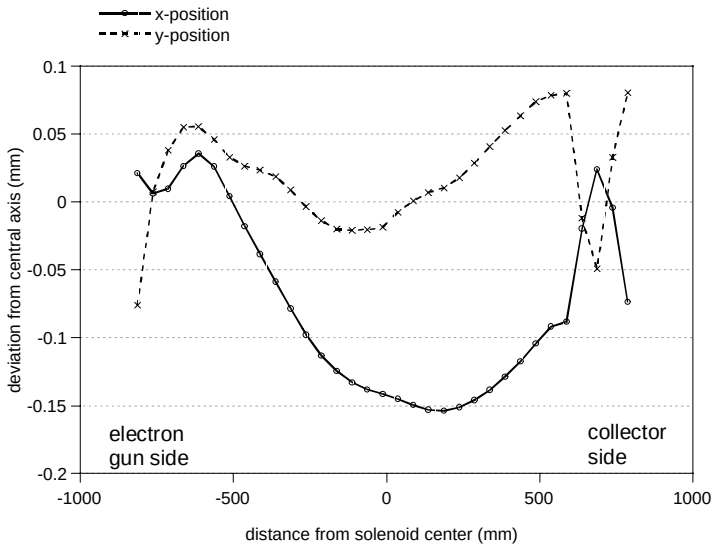

Figure 9*. x-z (solid) and y-z (dashed) plots of the central field line trace. Sag not included.*

Initial problems with too short LqN_2 holding time and coil failure occurring when the magnet was purposely quenched are practically solved. Although, the excessively high field decay-rate remains, as well as the short LqHe effective hold-time of 8-9 days instead of specified >14 days. In any case, the REXEBIS magnet is now believed to be robust to coil failure in connection with a quench.

A compilation of the most important solenoid data can be found in Appendix 2.

1.2.3 Electron gun

The electron gun is of semi-immersed type, positioned at 0.2 T. With U_{anode}=6500 V the electron beam I_e and gun perveance P_{gun} equal 0.46 A and 0.87 μA/V$^{3/2}$, respectively. The electron gun will deliver a current of ~0.5 A at a cathode current-density of 25 A/cm^2. In ref. [P7] the EGUN [36] simulations of the beam propagation in the gun region are presented. The simulated beam profile r_{ebeam} equals ~0.24 mm in full field, corresponding to a full field electron current-density j_e(full field) of 250 A/cm^2, higher than the specified 200 A/cm^2. Photos of the electron gun and the cathode are shown in Figure 10 and Figure 11, while Appendix 2 contains a summary of the electron gun parameters.

As cathode a 1.6 mm diameter lanthanum hexaboride (LaB_6) crystal [37] is used. The lifetime at T_c=1750 K, yielding a cathode current-density j_c of 25 A/cm^2, is approximately 1 year if a surface degeneration of 100 μm is accepted.

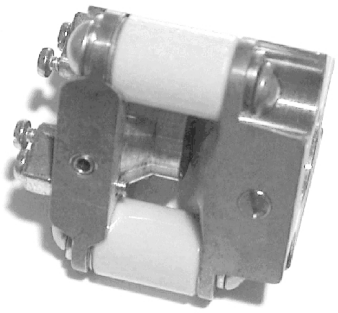

***Figure 10**. Electron gun with Wehnelt and anode electrodes to the left and right, respectively. Cathode surface not visible. Copper (OHFC type) used as electrode material.*

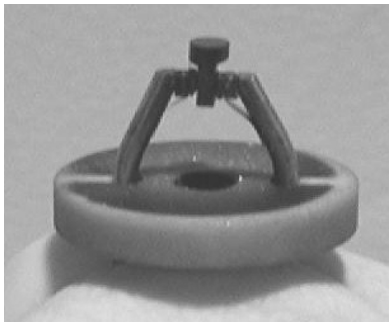

***Figure 11.** The LaB_6 cathode used in the REXEBIS electron gun. Two posts compressively hold pyrolytic graphite blocks, which in turn hold the electron emitting material. The posts are made of a molybdenum-rhenium alloy, which maintains a high modulus of elasticity at high temperatures.*

1.2.4 Inner structure

The inner structure consists of drift tubes, a support structure and NEG strips. All these elements are placed in UHV and near room temperature (warm bore ~15 °C). We have chosen to manufacture most of these details in titanium due to its conceivable gettering property.

The drift tubes have an inner radius of 5 mm. The REXEBIS has three trapping tubes: 100, 230 and 464 mm long, which can be combined to trap lengths of 100, 230, 332, 464, 696 and 798 mm. The trapping tubes are all immersed in full magnetic field. There are no coupling/damping sleeves at the ends of the drift tubes due to pumping reasons, only a 2 mm free space insulation-distance between the flat front faces of the tubes.

With a full length the charge trapping capacity for a 10% electron-beam compensation amounts to $6 \cdot 10^9$ electrical charges. The electron-beam energy is 5 keV. The potential depth of the electron beam at nominal current is 107 V, which is significantly larger than the potential ripple (±5 V) caused by beam scalloping. Ions are injected with a ~10 µs long pulse from the Penning trap, and are ejected by their inherent kinetic energy upon lowering the end-tube trap potential. Utilising this method, virtually no extra energy spread will be introduced. The tube potentials are set by fast switching supplies of type TREK 50/750 (1500 V, 100 mA) [38], with slew rates larger than 125 V/µs. Parts of the inner structure are shown in Figure 12, and relevant parameters are presented in Appendix 2.

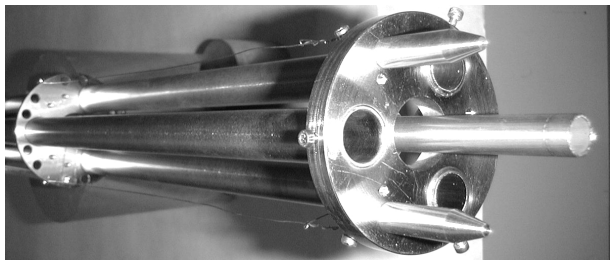

***Figure 12**. Photo of the inner structure taken from the collector side. The outer drift tube is clearly visible to the right.*

1.2.5 Electron collector

A 5 mm thick cylindrical iron shield surrounds the copper (OHFC type) collector. It reduces the magnetic field drastically inside the collector, causing the electron beam to expand rapidly onto the collector surface. The design of the collector is tailored to the electron impact angle so that back-scattering is minimised (see furthermore ref. [P7]). Simulations have shown that the back-scattering breaks

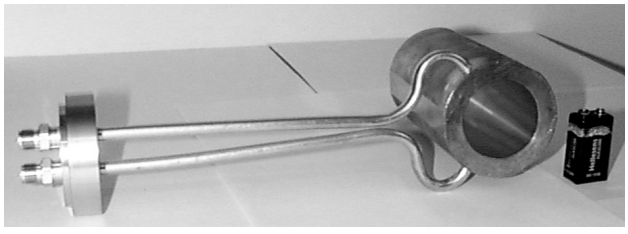

***Figure 13**. Photo of the collector showing the cylindrical copper body and the two cooling water pipes.*

down into <0.1% by direct reflection, <0.1% by inelastic back-scattering, and <0.05% by elastic back-scattering. The collector has a large opening towards the combined injection/extraction beam optics. This minimises ion beam aberrations and increases pumping conductance.

The collector is placed at a +2000 V potential relative to the cathode, yielding 1000 W heat dissipation on the collector surface for a nominal beam current of 0.5 A. The power density on the electron bombarded region is below 8 mA/cm^2. Estimations of out-gassing caused by electron bombardment yields a rest-gas pressure inside the collector in the order of 10^{-11} mbar for a fully baked-out surface. A photo of the collector is presented in Figure 13, while relevant parameters are given in Appendix 2.

1.2.6 Beam optics and diagnostics

From the collector region the ions are accelerated to 20·Q keV by the extraction electrode. The remainder of the beam optics elements is schematically presented in Figure 14, and the steering package is shown on a photo in Figure 15. A few remarks are called for. First, the lenses and beam steerers are used for both injection and extraction, and therefore switched as the beam injection and extraction voltages differ. During injection the inner einzel lens configuration also acts as a retardation system from 60 to 20 keV. The beam steerers are made of cylinders that have been sliced into four 90° sectors, making them axially very compact. The switching voltages for the lenses and the steering plates are generated by TREK 20/20 (±20 kV, 20 mA) and TREK 601B (±500 V, 20 mA) supplies, respectively. The switching is performed in less than 1 ms.

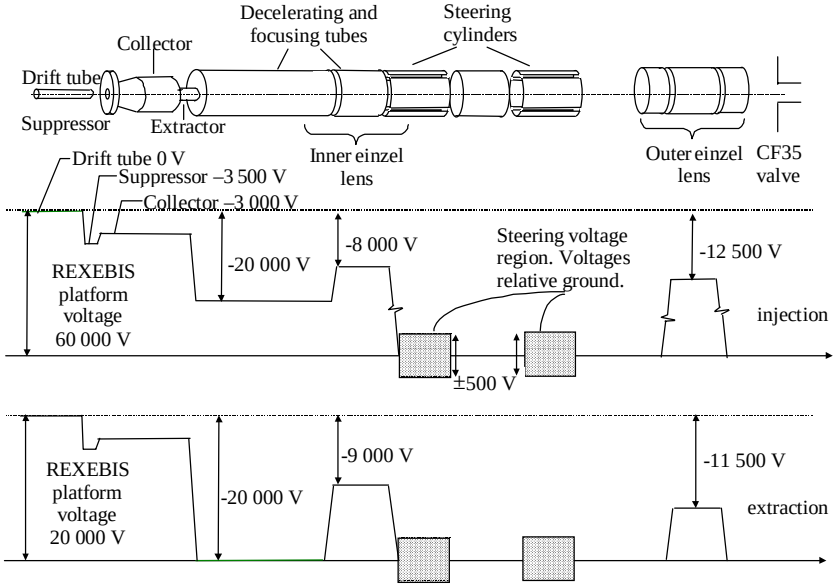

Figure 14*. Schematic picture of the optics elements and the voltage settings during beam injection (top) and extraction (bottom). The einzel lens voltages are switchable between +20 and –20 kV, the steering plates between +500 and -500 V.*

Two beam-diagnostics elements are implemented in order to assure correct conditions for injection and extraction: a FC for registration of higher beam currents and a CCD camera observing the beam profile and position on a phosphorous plate behind a MCP for low yield beams (down to single particles). These detectors are bi-directional, i.e. they either register the injected beam coming from REXTRAP or rest-gas beam going out from REXEBIS. These systems are installed at the EBIS beam focal point outside the outer einzel lens, and at the symmetry point in the transport line. A double-sided MCP diagnostics unit will also be introduced closer to the EBIS.

Figure 15*. Inner and outer beam deflectors with an optional einzel lens in between.*

1.2.7 High voltage switching

The REXEBIS is located on a platform at ~60 kV potential during injection, allowing the cooled 60 keV ions extracted from the REXTRAP to be captured. During the breeding period, the potential is decreased to provide an ion beam with an energy of 5 keV/u for acceleration in the RFQ. This injection energy ensures an efficient, adiabatic bunching and small output emittance from the RFQ. The platform potential during injection and extraction is shown in Figure 16. The platform voltage is generated by a switchable 60 kV/100 mA HV supply from FuG [39] with rise and fall times, between 15 and 60 kV, of 1.1 ms for the 0.8 nF capacitive load generated by the platform itself. It has a voltage accuracy better than 10^{-4}.

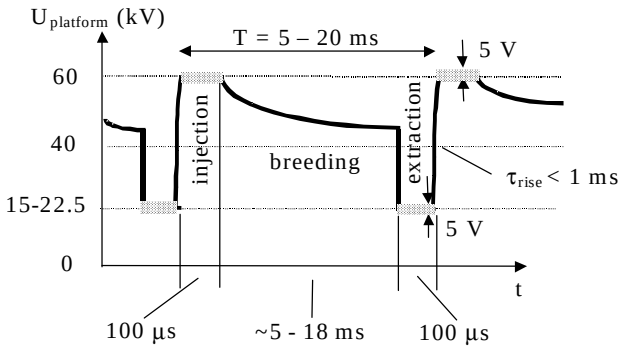

***Figure 16**. REXEBIS platform potential relative to ground during two cycles. (The internal REXEBIS voltages, for instance the barrier tube voltages, are related to this platform potential).*

One of the racks on the HV platform, containing the supplies for the electron gun, the suppressor and the collector, is kept on cathode potential relative to the REXEBIS platform (approximately -5 kV). This has been arranged by insulating the inner shelves from the rack cabinet, so the rack can be placed directly on the platform without electrical insulation. The power to the rack is delivered by a 5 kVA transformer.

1.2.8 Vacuum and pumping system

The REXEBIS vacuum requirements are challenging. This is because of the absence of cryogenic pumping inside the warm-bore REXEBIS and the necessity of being able to charge breed ions without losses. The main vacuum concerns are out-gassing from the inner structure and gas load from the drift tubes and/or electron collector caused by impacting electrons. The backbone in the pumping system is two Pfeiffer TPU180 turbo drag pumps [40], located at the gun and at the collector side (see Figure 8), respectively. The optics system following the EBIS is pumped by a Pfeiffer TPU260. These three pumps are backed by a small turbo on ground potential providing a fore vacuum better than 10^{-5} mbar. A zeolite trap protects the turbo from back-streaming oil from the roughing pump. The system provides a base pressure better than 10^{-11} mbar inside the EBIS. Via a N_2 inlet the system is brought to atmosphere pressure.

Non-evaporative getters (SAES St707 [41]), with a total getter area of 6000 cm^2, are mounted in an octagonal geometry around the inner structure in order to provide additional pumping in the ionisation region (see Figure 17). The getter material has a very high pumping speed of 1 $l/cm^2 \cdot s$ for H_2. The hydrocarbon sorption efficiency is very low, and inert gases are not pumped at all. The complete vacuum system has been, and the second version of the internal parts will be, vacuum fired (the stainless steel parts at 950° C and the titanium at 700° C) to reduce the out-gassing of hydrogen. The whole vacuum system is baked at 350° C, which is needed for activation of the NEG pumps. A 12-channel PLC unit controls the baking cycle.

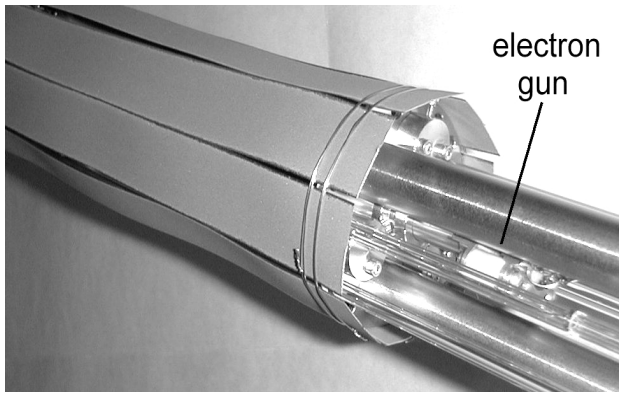

***Figure 17**. NEG strips mounted around the inner structure. Eight 1.5 m long SAES St707 [41] strips provide a total pumping speed of about 6000 l/s for H_2. The electron gun is partially viewed to the right.*

As REXTRAP operates with an Ar (alternatively Ne or He) pressure of about $3 \cdot 10^{-3}$ mbar, five differential pumping stages are introduced along the transport line, with a turbo pump in each section.

This is expected to give a partial Ar pressure at the EBIS beam optics tube (Figure 8) of about 10^{-12} mbar, which is acceptable for EBIS operation.

The absolute number of residual gas ions produced during a breeding period was estimated using a simplified REXEBIS vacuum model [P7] and the resulting Q/A-distribution was deduced. The Q/A-spectrum, with 10 000 injected ^{30}Na ions, is given in Figure 18. The breeding time is set to optimise charge state 8^+. Since the N_2 partial pressure is uncertain, it was conservatively assumed to be same as for O_2. It is evident that the REXEBIS calls for as good residual gas suppression as possible inside the trap region to avoid a complete outnumbering of the few radioactive ions.

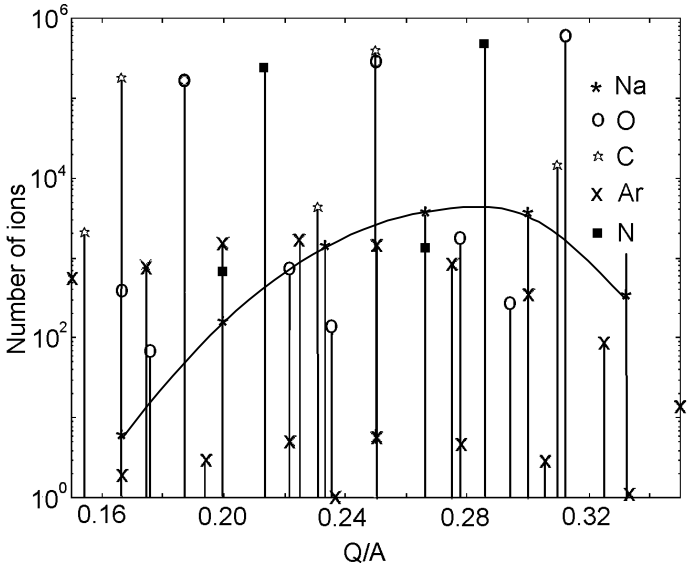

***Figure 18**. Calculated Q/A spectrum showing the absolute number of residual and radioactive ions. Breeding time 13 ms; 10 000 ^{30}Na ions; Ar diffusion from the REXTRAP; ^{16,17,18}O, ^{12,13}C, ^{14,15}N, ^{36,38,40}Ar isotopes are present.*

1.2.9 Control system

The control system of the REXEBIS is presently based on a client-server model where a task-dispatching server process runs on a VME based Motorola 68030 processor under OS/9. The dispatcher receives requests to start different control processes via TCP/IP packets transmitted from the client processes via the local network using socketing. The control hardware for the REXEBIS consists, on the one hand of ADCs and DACs connected to a PROFIBUS line [42] that is controlled by a VME resident PROFIBUS controller and on the other hand by a set of function generators, so-called GFASs [43] that also reside in VME. The PROFIBUS controlled ADCs and DACs are used for the control of static parameters such as e.g. lens voltages and electron-beam control, whereas the function generators drive devices that need to be dynamically controlled. The client processes can be started on a number of control consoles, which in the present concept of the ISOLDE control system means that they may run on any PC that runs Windows95 or NT. At start-up the client process typically connects to a database located on a server to inquire about current settings for the hardware it intends to control. The user subsequently controls the equipment completely via a graphical user interface. The vacuum system is independently controlled via a PLC based (SIMATIC [44]) control system that is connected to a second PROFIBUS line whose controlling process runs under NT.

Due to the potential differences between the three voltage platforms that the REXEBIS system comprises, the control signals for the PROFIBUS ADCs and DACs, as well as for the DACs connected to the function generators, are transmitted via fibre-optic links. The REXEBIS control system is presently undergoing an upgrade in order to make it comply with the general control concept used for REX-ISOLDE as a whole.

1.2.10 Interlock and safety systems

A hardware interlock system probing the cooling water flow (collector, warm bore and turbo pump circuits) and the vacuum has been implemented. It protects for instance the cathode from rest-gas poisoning; the solenoid from overheating during bake-out; the collector from excessive heat load caused by the electron beam; and HV sparking at poor vacuum conditions etc. The solenoid is inherently protected using a field ramping-down procedure when either of the two cooling liquids falls below a lower limit.

The personnel security is mainly provided in terms of a Faraday cage surrounding the whole REXEBIS set-up, with doubled interlocks at each entrance. The 60 kV HV is cut if the interlock chain is broken by

opening one of the two cage doors. No special actions of safety have to be taken because of the magnet, as the solenoid is iron shielded.

1.3 The REXEBIS simulations

The following section covers the ion injection, breeding and extraction simulations carried out at the design stage of the REXEBIS. A few of the most central results are presented, while a full description of the model (mathematical implementation and motivation) and the results are presented in ref. [P7].

1.3.1 Introduction

Extensive ion beam simulations were carried out during the design stage of the REXEBIS to ensure high beam-transport efficiency within the system. That aim was to determine the acceptance and emittance phase-spaces (transverse and longitudinal), vital parameters for interfacing the injected beam from the REXTRAP and the extracted beam to the mass separator. Beam optics parameters such as drift tube potentials, lens positions and voltages, accepted beam tilt and displacement tolerances at the focal points were also settled using the EBIS model described below.

The entire EBIS was modelled using an ion-tracing program, SIMION 3D ver. 6.0 [45], which is a simulation program that models ion optical problems in 2D or 3D electrostatic and magnetic potential arrays. The separate arrays modelling the different elements are positioned in a workbench, thereby allowing simulation of geometrically large problems. The program traces the charged particles and displays them together with the electrostatic/magnetic structure. SIMION 6.0 incorporates user programming – a feature that allows the user to include arbitrary functions, or to superimpose any field on the traced particles. That implies that the user has the possibility to carry out manipulations on the tracked particle at each time-step, an option that was extensively used.

1.3.2 Model

The EBIS model includes the following features:

- Electric field from time-varying potentials on the electrodes.
- Magnetic field from the solenoid (user programming).
- Electric potential from the electron beam (user programming).
- Charge multiplication within the electron beam (user programming).

Not included in the model were:

- Heating/cooling, i.e. momentum transfer in ion-ion or electron-ion interactions.
- Ion-ion or ion-atom interactions leading to electron transfer (charge exchange processes).
- Space charge effects originating from the ions.

In the simulation the injected ions were initialised in the focal plane outside the EBIS. After a completed tracking inside the EBIS the ion beam parameters were recorded in the same plane. To simulate the residual gas emittance the atoms were initially ionised at random radius within the electron beam with no initial kinetic energy, and thereafter conventionally charge bred and extracted.

1.3.3 Simulation results

1.3.3.1 Acceptance

An analytical expression producing an upper limit of the geometrical acceptance[1] was derived (see further ref. [P7]) for ions that are fully confined inside a *non-compensated* electron beam, i.e. an electron beam that is not neutralised by ions:

$$\alpha = \pi \frac{r_{ebeam}}{\sqrt{2U_{ext}}} \cdot \left(Br_{ebeam} \sqrt{\frac{q}{m}} + \sqrt{\frac{qB^2 r_{ebeam}^2}{4m} + \frac{\rho_l}{2\pi\varepsilon_0}} \right) \qquad \textbf{(2)}$$

[1] The term ‘geometrical acceptance’ corresponds to the area of an ellipse that encircles the phase space.

where r_{ebeam}, U_{ext}, q, m and ρ_l represent electron-beam radius (m), ion injection potential (V), ion charge (C), ion mass (kg) and electron-beam charge per meter (C/m). A plot outlining the maximum acceptance phase-space in one dimension for the ions to be fully confined within the electron beam inside the trapping region is shown in Figure 19. The ions were injected into the trapping region with 200 eV excess energy, i.e. enough to almost completely fill the phase space (requires ~215 eV). The acceptance phase-space can be inscribed within an ellipse with an area of ~11 π·mm·mrad, which agrees very well the analytical prediction of 11.4 π·mm·mrad, according to eq. 2. Most importantly, the simulations show that the phase space exceeds the specified acceptance of 3 π·mm·mrad at 60 kV injection voltage.

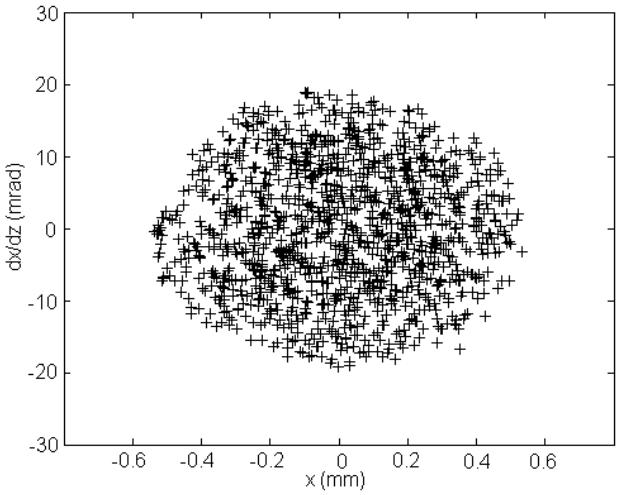

***Figure 19**. Maximum transverse acceptance phase-space for 60 keV $^{30}Na^{1+}$ ions injected into the REXEBIS and confined completely within the electron beam.*

Figure 19 gives in reality an upper estimation of the acceptance phase-space for fully confined ions. It is necessary for the ions, but not sufficient, to start within both a horizontal and vertical phase space as plotted. Due to coupling between the phase spaces still only ~85% of the ions fulfilling this starting condition will be fully confined (assuming uniform distributions in the two phase spaces). The remaining 15% will be confined for at least 90% of the breeding time. To both completely confine, and to achieve 100% injection efficiency, the ions should be injected with a lower injection energy into the trap (~100 eV excess energy) so they automatically become trapped within the electron-beam well ΔU. The acceptance shrinks only marginally compared with the phase space in Figure 19. On the other hand, if a lower fraction of confinement time within the electron beam is acceptable, e.g. 90%, the acceptance increases dramatically, close to 20 π·mm·mrad. Only 45% of the ions are then confined within the electron beam for 100% of the time.

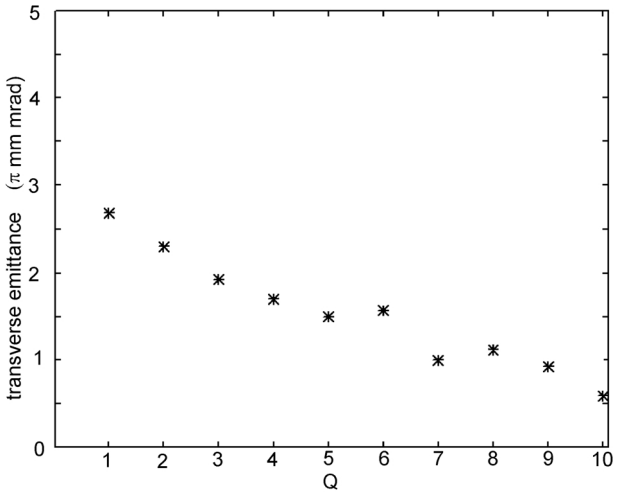

***Figure 20**. RMS emittance vs. charge-state for injected ions fully confined within the electron beam. The emittance decreases with increasing charge-state. (Poor statistics explains the fluctuations.)*

For the REXEBIS the last term in the acceptance expression (eq. 2), originating from the electron-beam space-charge, is completely dominating, implying that the acceptance should be mass, charge and B-field independent. The latter independence was verified by acceptance simulations for B=2 and 5 T. Similarly the acceptance was shown to be mass independent.

1.3.3.2 Emittance

Like the acceptance, also the emittance was shown to be independent of mass and B-field to a first order approximation. This result is of major importance from an EBIS design point of view, since it shows that it is not sufficient to keep the B-field strength low to obtain a small emittance. However, one should keep in mind that this result was obtained for a non-compensated beam. For a compensated beam the emittance (and acceptance) will increase with the B-field. On the contrary to the acceptance, the emittance is charge-dependent. The statistical RMS emittances, defined as:

$$\varepsilon_{RMS} = 4\sqrt{\langle x^2\rangle\langle x'^2\rangle - \langle x\cdot x'\rangle^2}\ \ mm\cdot mrad \qquad \textbf{(3)}$$

where x is position and x' trajectory divergence for the ions. As illustrated in Figure 20 the RMS emittance decreases with increasing charge state. This phenomenon is attributed to a change in mean radius for the ion trajectories within the trap when the ions are successively charge bred. In other words, the radial distribution of the ions becomes more axially centred with higher charge state. One should point out that the amount of radius shrinkage is solely dependent on the average charge state, and not on the ion mass. The geometrical emittance, enclosing all ions in the phase space, should in principle remain constant as there exists a theoretical possibility, if even small, for step-wise ionisation without a decrease in ion trajectory radius. For this reason the statistical RMS definition is used for the emittance.

Sodium ions injected into the maximum acceptance phase-space of 11 π·mm·mrad (ε_{RMS}=2.6 π·mm·mrad) will after charge breeding to $Q=7^+$ or 8^+ have a RMS emittance of approximately 1.3 π·mm·mrad (60 kV), which transforms to $1.3\sqrt{60/20}$ ~2.3 π·mm·mrad for 20 kV extraction voltage. If the ions are injected within the specified 3 π·mm·mrad geometric phase space, the emittance will be even smaller. On the contrary, poorly injected ions ionised to a low charge state will yield REXEBIS emittances larger than 20 π·mm·mrad (60 kV).

The emittance of the residual gas is of major importance for the resolution in the mass separator. The emittance of simulated residual gas breeding represented by oxygen, which was charge bred to 4^+ or 5^+, is shown in Figure 21. The RMS emittance is 1 π·mm·mrad.

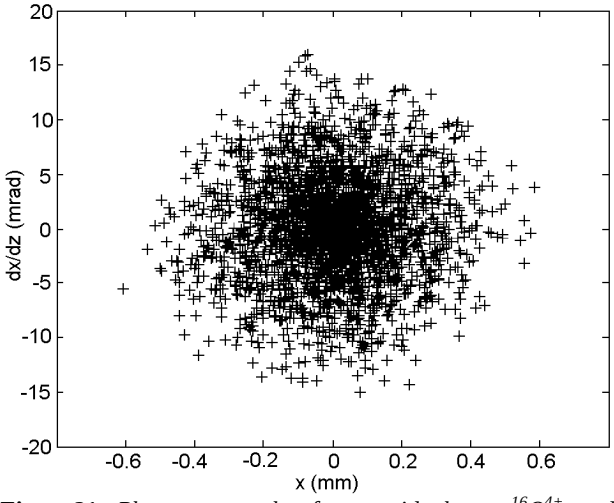

***Figure 21**. Phase space plot from residual gas $^{16}O^{4+}$ and $^{16}O^{5+}$ extracted with 60 kV. The RMS emittance is 1 π·mm·mrad. The true REXEBIS residual gas phase-space would be stretched $\sqrt{3}$ in dx/dz-direction due to the lower extraction voltage of 20 kV.*

1.3.3.3 Energy spread

The ionisation is a random process and can occur at different radii and therefore at different beam potential. That means the ions achieve a potential energy that varies depending on where they are ionised, which is the cause of the breeding energy spread (ionisation heating). The Coulomb heating by the electron beam is negligible, as was shown in ref. [P7]. In Figure 22 the extracted beam energies per Q are plotted for Q varying between 1^+ and 10^+. It can be seen that higher charge states lead to lower extraction energies as expected, since the highly charged ions accumulate around the beam axis. It seems as if the energy spread does not vary with the charge, but the statistics are rather poor. An average energy spread per Q for all charge states would be $\sigma(E_{out})$~15 eV.

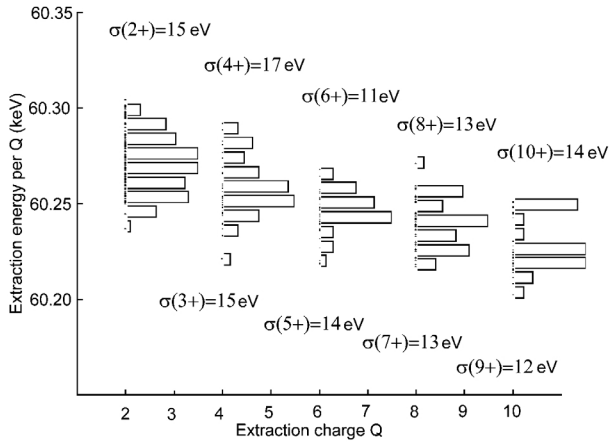

***Figure 22**. Extraction energy per Q vs. charge-state for ions charge bred in the REXEBIS. Histograms for the energy spread (even charges) are plotted vertically in connection to corresponding charge-state. (From the listed energy spread values a numerical error of 3.5 eV (1σ) should be subtracted.)*

The energy spread from an EBIS has been measured several times, for instance at CRYSIS [46], but then with a highly compensated trap. The obtained result was an energy spread of 57 eV/Q for a 300 mA electron beam at 17.4 keV [P12]. This value exceeds the simulation prediction by far and is due to the high electron-beam compensation. The first ions in the extracted pulse leave a compensated trap and have therefore a high energy, while the last extracted ones have a lower energy because of a more attracting electron beam. This phenomenon should be avoided in the REXEBIS.

1.3.3.4 Phase-space correlation

Ions starting inside a cylindrically symmetrical magnetic field have after extraction from the field a rotational kinetic momentum corresponding to the magnetic vector potential they started in (see Figure 23). As a consequence, the transverse emittance is increased. So even if the beam initially has zero emittance inside the EBIS, it would after extraction be non-zero. However, there exists a correlation between the transverse phase spaces [47]. Skew quadrupoles (a quadrupole rotated 45° to the horizontal plane), have the ability to partially de-correlate the phase spaces. The magnetic field from the lens completely counteracts the azimuthal velocity in one direction, while increasing it by a factor two in the other direction, as shown in Figure 24.

For the achromatic mass separator following the REXEBIS in the REX-ISOLDE system, the emittance is of vital importance for the separator resolution. By improving the emittance in one direction (the bending direction), as suggested above, the mass resolution could be improved. This opportunity raised the demands for an investigation of the phase-space correlation out of an EBIS and the need for de-correlating optics.

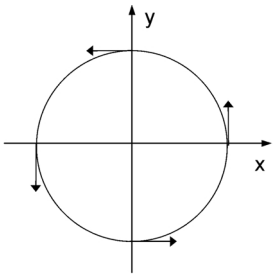

Figure 23. *Azimuthal velocity components due to the coupling between phase spaces.*

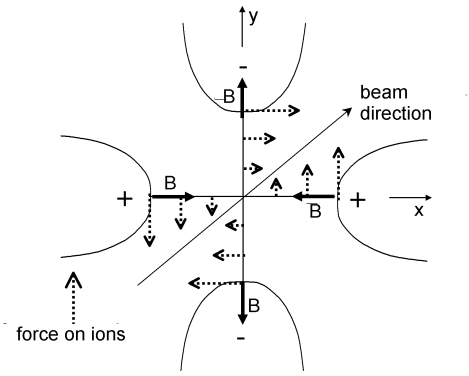

Figure 24. *The effect of a skew quadrupole counter-acting the azimuthal velocity in one plane.*

The result from the investigation is presented in Figure 25 in the form of a velocity vector plot, i.e. a plot containing the velocity vectors for the extracted ions at the focal point outside the EBIS. It is clear that the velocity directions are almost randomly distributed. The correlation was quantified by plotting a histogram of the azimuthal velocity component, see Figure 26, and compare the mean azimuthal velocity $< v_\theta >$ with the standard deviation $\sigma(v_\theta)$. The result is a small correlation, $< v_\theta >$=-1200 m/s, compared with a much wider standard deviation, $\sigma(v_\theta)$ =9750 m/s. The reason is the relatively large transverse energy spread for the injected ions, causing the ions to move with high velocity in random directions. This movement almost swamps the velocity correlation induced by the extraction from the axial magnetic field. Hence, the adding of a skew quadrupole does not improve the emittance notably. On the other hand, if the ions are cooled inside the trap by ion-ion collision, a case similar to rest-gas breeding occurs where the velocity correlation is dominating. For ^{30}Na ions, injected as gas atoms into the EBIS and thereafter charge bred to 7^+ or 8^+, the absolute value of the mean azimuthal velocity, –2750 m/s, is comparable with the standard deviation of 3200 m/s.

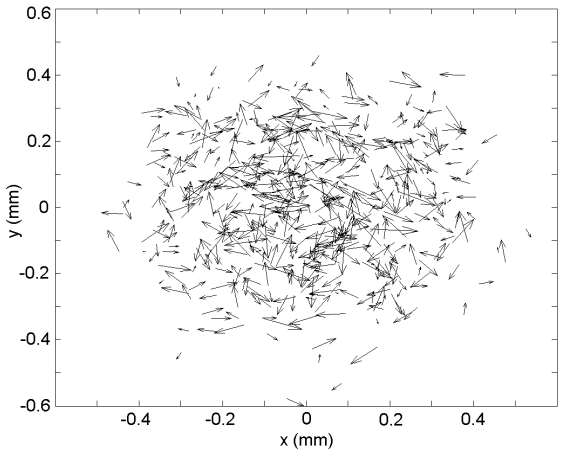

Figure 25. *Velocity vector plot for a beam extracted from REXEBIS.*

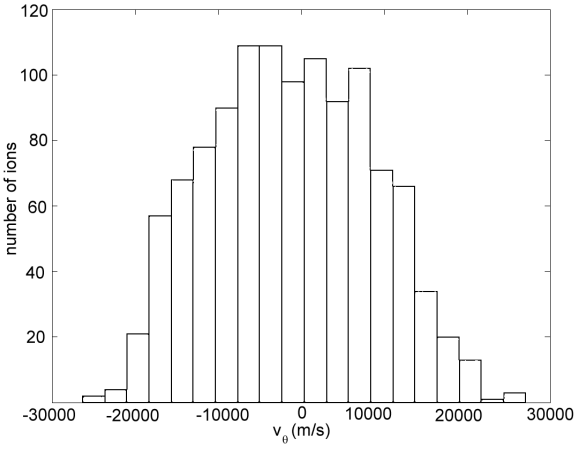

Figure 26. *v_θ histogram with $< v_\theta >$=-1200 m/s and $\sigma(v_\theta)$ =9750 m/s.*

1.4 Experimental results

The most important commissioning results [P2] from the four major experimental runs with the REXEBIS are presented in the following section and related to simulated values. So far, the main emphasis has been on electron-beam investigations and rest-gas extraction, although some early injection tests were also carried out. It should be pointed out that the presented results are preliminary, and that the source has not yet reached its design specifications.

1.4.1 Electron beam

The initial tests showed that the electron beam was well-behaved and not critically sensitive neither to drift tube nor to suppressor or collector voltage settings. A common feature for the tests was the poor vacuum that hampered the performance of the electron beam.

1.4.1.1 Maximum electron current

The electron-beam current, I_e, was maximised during the tests and found to be limited by the loss current (see the following section). Maximum values for different gun perveances are listed in Table 2 below, together with the obtained space-charge capacity. The calculated breeding times for different ionisation energies, ranging from 100 to 1000 eV, are normalised to the design values and plotted in Figure 27. So far, the REXEBIS has reached a calculated breeding time that is ~1.2 times longer than the design value and a space-charge capacity of 84% of the nominal value.

I_e (mA)	P_{gun} (μP) (gun perveance)	E_e (eV) (beam energy)	Percent of nominal space charge capacity
340	1.3	3653	84
375	1.1	5070	78
302	0.66	5450	60

***Table 2**. Top notations for the electron beam current for different gun perveance values.*

1.4.1.2 Electron loss-current

The loss current, I_{loss}, i.e. electrons going to EBIS ground potential instead of to the suppressor and collector, was <0.5% for an electron current of 200 mA. Normal loss current in CRYSIS is between 0.1 to 0.5% of the collector current. At higher electron current the loss increased exponentially as illustrated in Figure 28, and with a power supply limitation of 2.5 mA, a maximum current of 375 mA has been reached. The loss current displayed a variation during the breeding cycle, peaking for a non-neutralised trap (see Figure 29), but over the time the loss current turned-out to be very stable.

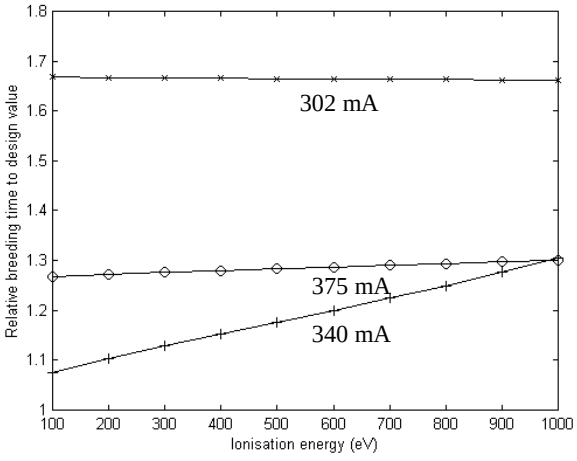

***Figure 27**. Calculated breeding times for different ionisation energies normalised to the design values for the three currents listed in Table 2.*

Less than 3% of the loss current reached the anode and the inner drift tube (electrically connected) and not more than 1% was collected on the trapping tubes. On the other hand, the largest portion (50-70%) went to the drift tube closest to the suppressor. In spite of this, a non-negligible fraction is not accounted for, which is baffling since the system is very closed, both from a geometric as well as electrical potential point of view. Nevertheless, scattered electrons from the collector, and secondary electrons created in the collector region, may have a momentum distribution that allows them to escape.

The excessive loss current could be due to a misalignment of the inner structure with respect to the magnetic field axis. An indication of this is that the loss current is very sensitive to small movements of the EBIS structure. A translation of about 0.2 mm of one end of the structure could occasionally increase the losses by as much as 50%. Another reason could be that the suppressor and collector unit (see Figures 8 and 14) was axially displaced by 5 to 8 mm. The poor vacuum in the collector region most likely contributed to the high loss current.

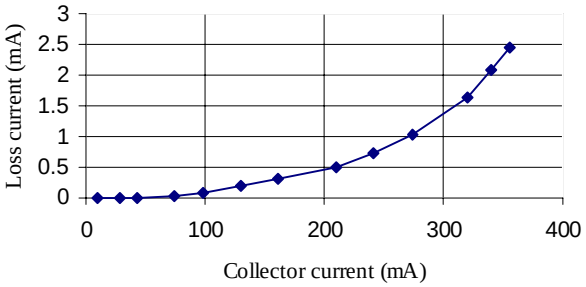

***Figure 28**. Loss current dependence on electron beam current for relatively poor vacuum conditions (10^{-8} mbar). Measured points with fitted curve.*

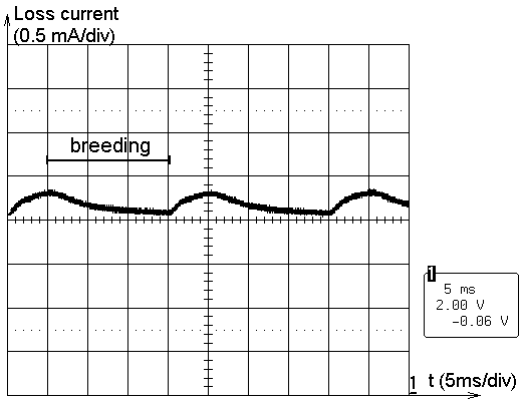

***Figure 29**. Loss current variation during two and a half breeding cycles. The loss current peaks for an uncompensated trap.*

According to the EGUN simulations presented in ref. [P7] the direct reflection, inelastic and elastic back-scattering should add up to less than 0.25% in an aligned and correctly adjusted electron optics geometry. It should, nevertheless, be stated that a high loss current is acceptable as the electrodes of REXEBIS are at room temperature.

1.4.1.3 Electron gun perveance

The gun perveance value, P_{gun}, was found to be 1.55 µP, which exceeds the value of 0.9 µP given by the EGUN simulation. A perveance that exceeds the design value may be favourable since it allows for a lower electron-beam current and energy while maintaining a short breeding time. The beam energy will not restrict the ionisation possibilities at a moderate charge-to-mass ratio of ~1/4 and A<50. Moreover, the change in space charge capacity is small and in any case only 10% of the total capacity is occupied by injected ions.

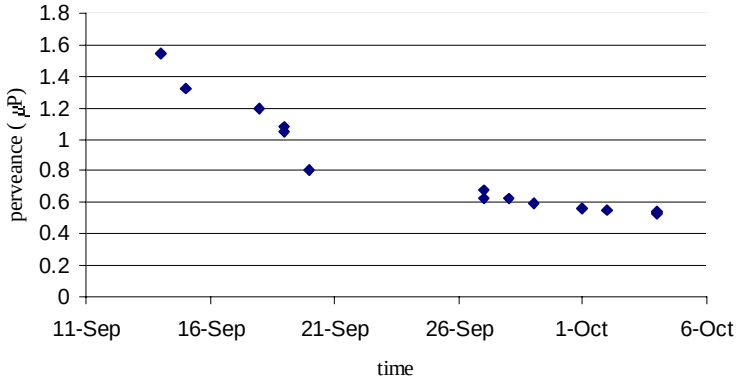

***Figure 30**. Gun perveance as a function of operation time. The perveance was monitored by decreasing the anode voltage so the electron extraction became space charge limited. The abrupt variations in perveance occurred when the filament heating was changed rapidly.*

It has been noted that large and rapid variations in the cathode filament heating caused the perveance to change (Figure 30). The perveance of the electron gun dropped abruptly, typically in steps of 0.1 to 0.2 µP, after each cool-down and warm-up cycle. This can most likely be attributed to an axial movement backwards of the cathode in its support clamps. With a considerably slower warming-up and cooling-down procedure one could possibly avoid this phenomenon. The electron-beam tests have therefore been carried out with a gun perveance going from 1.55 down to 0.6 µP.

1.4.1.4 The LaB_6 cathode

A slow current decrease of a few mA per day was observed (operating at thermionic limit). The lost current could be regained by increasing the filament heating. Besides, an electron emission lower than specified was obtained. This was compensated for by increasing the filament heating to between 15 and 24 W (i.e. far higher than the 7 W specification for the second crystal). The low electron emission could either be due to a (carbon) poisoned cathode, or simply be explained by the fact that the cathode crystal moved backwards in the support clamps whilst tipping its emitting surface. Dismantling supported the latter theory, as it was found that the crystal mounting had failed so the crystal was slanted and partially hidden behind the Wehnelt electrode[2].

[2] The asymmetry could possibly influence the electron beam propagation and thereby also the loss current.

As will be exemplified later on, the mass spectrum was contaminated by ^{11}B and ^{139}La peaks originating from the strongly heated cathode. As the replacement cathode will be run at a lower temperature, the problem should be reduced, although, a small fraction of contamination will most certainly be present. This will inflict an overlap with some radioactive ions, for instance ^{11}Li and ^{11}Be, since they can not be separated from $^{11}B^{3+}$ and $^{11}B^{4+}$ in the mass separator. The boron will therefore unavoidably be accelerated in the LINAC and reach the target. Exploiting other types of cathodes, for example IrCe, would solve this problem. IrCe cathodes have an even higher electron emission, and lifetimes similar to LaB_6. Splitting the present combined anode and inner-barrier drift-tube into two separate tubes with appropriate potentials would also most probably reduce the B and La contamination.

1.4.2 Vacuum

A vacuum superior to 10^{-11} mbar (Penning gauge limit) has been reached inside the gun region, while the collector pressure hovered around 10^{-10} mbar. With the electron beam on and thus an out-gassing from the electron beam load the pressure in the gun and collector regions increases to between 2 and $20 \cdot 10^{-9}$ mbar. The collector bake-out has so far not been optimal, which implies higher base pressure and out-gassing from the electron-beam load. The O_2 and CO/CO_2 partial pressures inside the drift tubes were estimated from rest-gas extraction to be between 2 and $5 \cdot 10^{-9}$ mbar. This is noticeably higher than expected considering that the inner bore contains NEG strips with a total pumping speed of ~6000 *l*/s. However, the pumping effect in the electron-beam region is small due to the severe conductance limitations of the drift tubes.

The electron-beam loss inside the drift tube gives rise to a significant out-gassing, which in the present construction only can be 'pumped away' by ionisation in the electron beam and consequent release from EBIS. In fact, the electron beam empties 20 to 50% of the rest-gas content inside the drift tubes during 20 ms breeding, presuming the vacuum is good enough to avoid compensation.

Improvement of the vacuum inside the drift tubes could be obtained by covering the drift tube and collector surfaces with a NEG coating (ZrTi or ZrTiV) [48], which apart from adding ~200 *l*/s pumping speed (for H_2) directly around the electron beam, also would reduce secondary electron emission [49] and electron stimulated gas emission. Drilling 1500 2 mm diameter radial holes in the drift tubes would contribute with a total conductance in the order of 300 *l*/s. Even more preferable, but on the other hand more complicated, are drift tubes constructed out of a net. At a later stage, when the system is rarely opened, the NEG strips could be removed and all inner parts be covered by a NEG coating to avoid different activation temperatures for strips and coating. The strong out-gassing from the NEG strips before baking is then also circumvented. Vacuum firing of all elements inside the bore, and the use of titanium as construction material for the next generation of drift-tube structure, should facilitate a total pressure $<10^{-11}$ mbar in the trapping region under electron-beam operation.

To facilitate controlled tests of the breeding parameters, as well as repeated mass-separator calibrations even at low base pressure inside the EBIS, a calibrated gas leak will be installed.

1.4.3 Rest-gas ion extraction

The extracted rest-gas ion beam was characterised in a number of ways with respect to pulse shape, extracted charge, DC-background level, rest-gas composition etc. A summary of the results is presented in the following section.

1.4.3.1 Current levels and pulse shape

The peak current of the extracted pulse varied between 20 and 300 µA depending on breeding time and/or extraction time. The latter time was varied by applying either a flat voltage distribution or a 300 V ramp over the two trap tubes at extraction. The extracted DC component was approximately only 1 µA, but with an extraction duty factor of 1‰, it still dominants over the pulsed beam. By switching

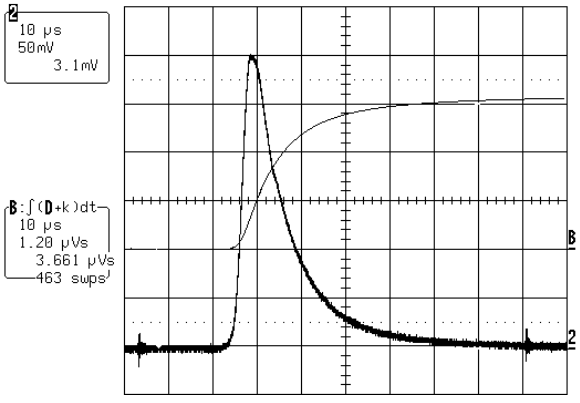

***Figure 31**. Trace 2 represents the extracted EBIS pulse recorded in a FC (1 kΩ load resistor) for ramped extraction from a 279 mA electron beam. FWHM extraction time t_{ext}=9 µs and peak current $\hat{I}$=300 µA. Trace B represents the integrated charge; C_{ext}=3.67 nC.*

the deflection plates in the optics line with an accuracy down to a few μs clean pulses could be obtained. The extracted pulse shape for ramped (FWHM 9 μs) extraction is plotted in Figure 31. On operational basis the extraction will be non-ramped (FWHM 15 μs) to minimise the energy spread. The LINAC has a maximal pulse acceptance of 2 ms. By mechanically and electrically dividing the inner barrier into an anode drift tube and inner barrier, and the outer barrier into an outer barrier and outer drift tube, the DC component ought to be reduced.

1.4.3.2 Extracted rest-gas spectrum

A typical rest-gas spectrum analysed in the REX-ISOLDE mass separator is shown in Figure 32 (DC component gated away). The presence of oxygen and carbon, but also of nitrogen is clear. The neon peaks appear since REXTRAP was operated with neon as buffer gas and the differential pumping system in the transport line was incomplete. The relatively low amount of detected hydrogen is confusing, but could possibly have its explanation in a large emittance because of the low charge state, and therefore a poor transmission out of the EBIS and through the mass separator. Hydrogen may also be heated out of the trap by collisions with heavier elements. From the spectrum the electron current-density j_e could be determined to be between 125 to 150 A/cm^2 (125 A/cm^2 expected from theory).

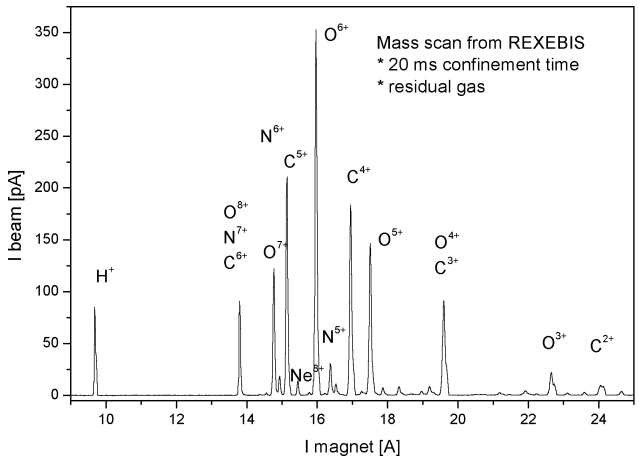

***Figure 32**. Mass analysed rest-gas spectrum from REXEBIS, with an estimated trapping-region pressure of $5 \cdot 10^{-9}$ mbar. REXEBIS parameters: I_e=210 mA and U_t=5440 V.*

Due to the elevated filament heating, significant traces of lanthanum were seen in certain mass spectra, see Figure 33. In fact, the cathode will evaporate away ~$6 \cdot 10^{10}$ La and ~$36 \cdot 10^{10}$ B atoms per second at an operation temperature of 1750 K. At the injection tests the filament heating was reduced, but still, the identification of weak potassium peaks was hampered. Future vacuum improvements aim to improve the rest-gas pressure with at least two orders of magnitude.

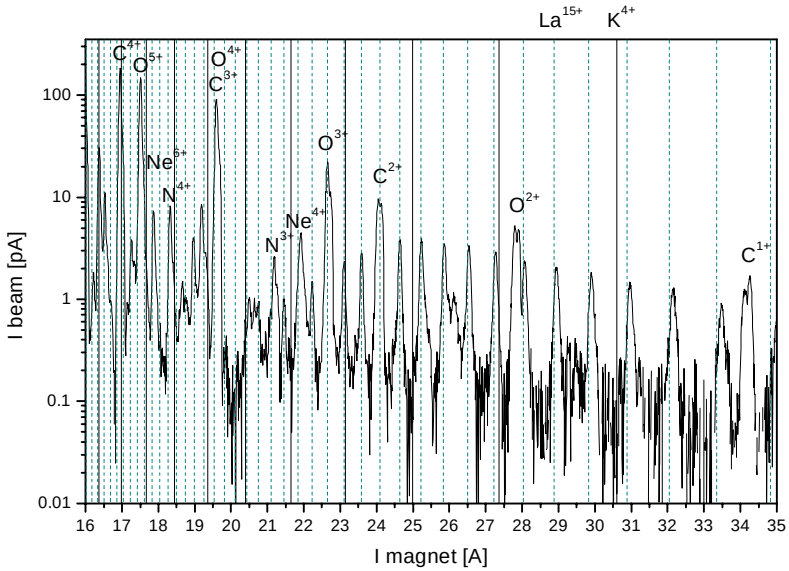

***Figure 33**. Mass analysed rest-gas spectrum from the REXEBIS for 20 ms breeding time. A fence of lanthanum peaks (dashed vertical lines) is present due to the elevated filament heating power. The high rest-gas level hampered the possibility to identify a successful injection of potassium (filled vertical lines).*

1.4.3.3 Beam neutralisation

The electron-beam neutralisation (or compensation) time was investigated and it was found that the extracted charge saturated after 50 ms (Figure 34) at a collector rest-gas pressure of approximately $1 \cdot 10^{-8}$ mbar. It is interesting to note that the extracted charge is not zero even for very short breeding times. This might be explained by a disturbance being induced in the electron beam when the potentials of the trap electrodes are switched. This may force the beam to hit parts of the inner structure and thus cause ion bursts from the surfaces due to out-gassing. The same disturbance also describes the fact that the number of extracted ions is influenced by the cycle time also for a fixed confinement time (for a non-compensated trap). A longer period time resulted in fewer extracted ions per pulse, see Table 3.

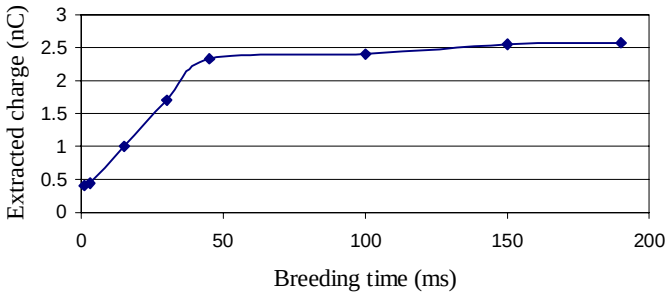

Figure 34. *Extracted charge as a function of breeding time, for I_e=282 mA and U_t=5800 V. The collector rest-gas pressure was $9 \cdot 10^{-9}$ mbar, and the theoretical trapping capacity 5.4 nC.*

Theoretically, the EBIS trap can confine 5.4 nC. After tuning of the extraction optics the extracted charge amounted to about 3.7 nC, i.e. to a compensation level of 68%. An increase of the trap barrier height, with ramped as well as with non-ramped extraction, did not enhance the extracted charge, neither had the extraction time any significance on the amount of extracted charge. A smaller electron current, I_e=150 mA, with a theoretical trap capacity of 3.4 nC, yielded an extracted charge of only 0.89 nC (25% compensation degree).

τ=45 and T_{period}=50 ms	τ=45 and T_{period}=200 ms
C_{ext}=2.33 nC	C_{ext}=1.80 nC

Table 3*. Extracted charge per pulse for high and low duty factor.*

Maximum beam compensation for other EBIS have been measured to be around 60% [50]. The limit can be explained by a decrease in depth of the potential well (i.e. holding voltage) with increased compensation. That will force those rest-gas ions that were 'born' with a large potential energy, i.e. primarily ionised near the electron-beam edges, to leave the trap radially. These ions can either hit the drift tubes and be lost, or be scraped at the apertures during extraction. Ion losses to the drift tube become possible when the tube-to-axis potential depth of the partially compensated (compensation degree f) beam falls below the initially non-compensated electron-beam well-depth ΔU, i.e. when:

$$f \geq 1 = \frac{1}{2} \cdot \frac{1}{\left(ln\left(\frac{r_{ebeam}}{r_{tube}} \right) - \frac{1}{2} \right)} \qquad \textbf{(4)}$$

For the REXEBIS this occurs for f=0.85, i.e. at a somewhat higher compensation degree than measured.

1.4.4 Beam transport properties

The extracted rest-gas beam-profile was recorded using the MCP 0.5 m after the outer einzel lens. Typically, a beam-spot size smaller than 6 mm was obtained for a non-compensated beam. Interesting to note was the size dependence of the breeding time as illustrated in Figure 35. Two possible effects can

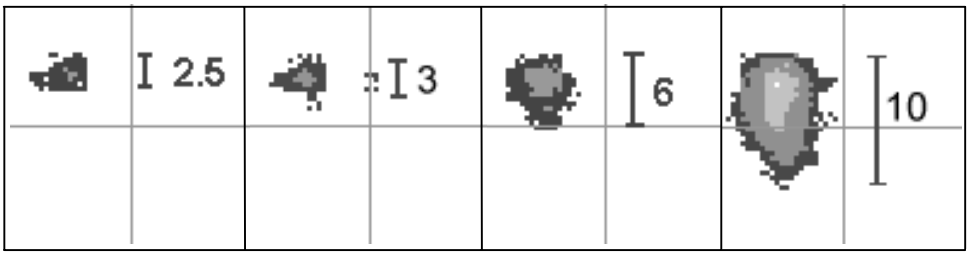

Figure 35*. Beam profile recorded at the MCP after the EBIS exit for varying breeding times. From left to right τ= 5, 15, 45 and 95 ms; T_{period}=100 ms and I_e=239 mA.*

explain this phenomenon. Either a space-charge blow-up of the extracted beam occurs for large extracted currents, or, the longer breeding time forces the ions into trajectories with larger average radius inside the EBIS as described above. The second explanation seems most likely since a ramped extraction did not significantly affect the beam size.

1.4.5 Emittance

The emittance of the extracted non-separated rest-gas beam was investigated during two runs. To my knowledge, systematic emittance measurements on an EBIS have only been carried out at CRYSIS [P8] before. Initial large emittance values for the REXEBIS could be understood and successfully explained. However, attempts to measure on the separated beam failed due to the weak signal for a single Q/A-value.

1.4.5.1 Emittance measurement set-up

The emittance meter used is of so-called slit-grid type [51]. In one experiment it was positioned directly after the REXEBIS, with only a transport tube in between, while a second measurement was carried out with the emittance meter placed in the mass separator line. The ion beam extraction voltage was 20 kV. The relatively week average current, 50-100 nA, out of the EBIS resulted in a modest signal-to-noise ratio in the emittance meter, which in its present version has no gating possibilities. Thus, the determination of the background level and as a consequence the geometrical emittance became problematical. Because of the different set-up for the two occasions, the results are not completely comparable[3].

1.4.5.2 Emittance versus breeding time

Firstly, the effect of the breeding time on the emittance was investigated. With a prolonged breeding time, the geometrical emittance increased from 20 π·mm·mrad (τ=1 ms) to over 60 π·mm·mrad (τ=85 ms). As the electron beam gradually becomes compensated because of the poor vacuum, the ions move with larger and larger radii inside the trapping region, and generate a growing emittance. One can easily show that the maximum beam radius r_{max} for rest-gas ions inside a trap with a compensation f is:

$$r_{max} = r_{ebeam} \cdot exp\left(\frac{f}{2(1-f)}\right) \qquad \textbf{(5)}$$

A compensation level of 70% corresponds to maximum 0.8 mm ion radius inside the REXEBIS. Using the EBIS acceptance formula derived for a non-compensated beam an upper number for the emittance can be assigned. Insertion of I_e=250 mA, A=16 u and Q=4 yields a geometrical emittance prediction of 75 π·mm·mrad, in good agreement with measurements.

1.4.5.3 Emittance versus electron-beam current

A minor emittance improvement was recorded when the electron-beam current was lowered from 240 to 82 mA, that means to a more shallow electron-beam well. A more exact value could not be arrived at due to the low signal-to-noise ratio for the lower current. The result nevertheless agrees with the general expression for the emittance, see eq. 2.

1.4.5.4 Absolute emittance value

No beam was detected at the emittance meter with a statically open trap (i.e. EBIS operated in TOF-mode) using active steerer gating. This verifies that the measured signal originates in the trapping region and that no significant ion production takes place in the collector region. On the other hand, without gating, a detectable current was recorded, and a geometrical emittance of ~15-20 π·mm·mrad was measured. This case simulates an EBIS with a very good vacuum, since the electron beam is almost completely non-compensated, and represents what can be expected for the REXEBIS operating at optimum vacuum conditions. The calculated geometrical emittance for low-charged (1^+) rest-gas ions is 19 π·mm·mrad, which is in good agreement with the measured value. The horizontal phase space for a breeding time of 1 ms is illustrated in Figure 36.

[3] The insertion of several beam apertures and a long drift distance previous to the second investigation may have affected the beam propagation so it became aperture limited, worst case 25 π mm mrad, which is a value very much the same as was measured. This is the most plausible explanation for the small variations in phase space and emittance that were recorded with different settings and the apertures present. Thus, in the following analysis, only the results from the set-up where the apertures were absent are included.

1.4.5.5 Phase-space aberrations

A difference in orientation of the horizontal and vertical phase spaces was recorded. While the horizontal phase space had its beam waist at the emittance meter, the vertical was significantly divergent. This is not an expected effect since the EBIS and its extraction optics, except for the deflectors, have an axial symmetry. The source of this focal difference was most likely caused by wrongly connected deflection plates acting as a quadrupole.

The horizontal phase space showed signs of aberration (see Figure 37), which also could be attributed to a misaligned magnetic field, or to influence of the Penning gauge magnets, or to asymmetric beam scraping. Tests involving displacement of the Penning gauge magnets were not conclusive due to the possible aperture limitation mentioned earlier. As was seen in the REXTRAP, even very small magnetic items inside or directly outside the trapping region can strongly influence the beam quality [52].

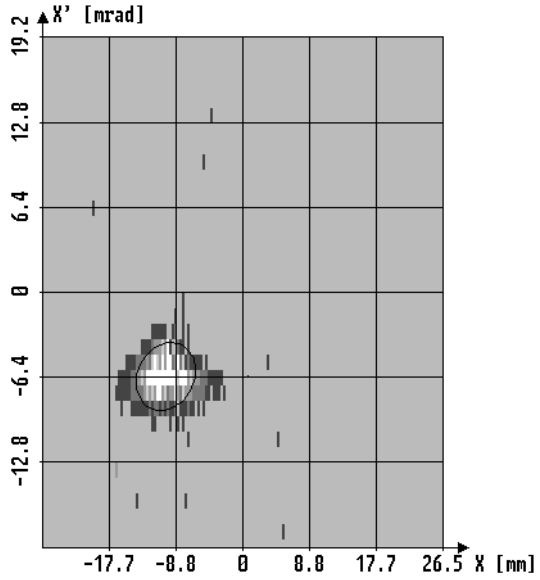

***Figure 36**. Horizontal phase space plot for 1 ms breeding time. The ellipse encloses an emittance of 9.9 π·mm·mrad. REXEBIS parameters: I_e=300 mA and U_t=4960 V.*

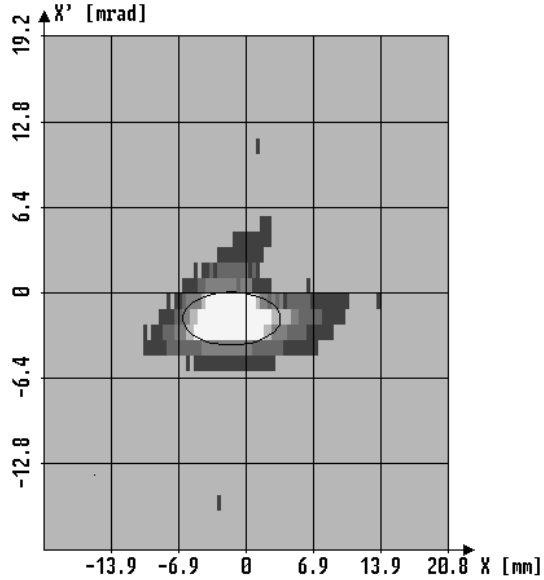

***Figure 37**. Aberrated horizontal phase space for I_e=300 mA and τ=4 ms.*

1.4.5.6 Future emittance investigations

Albeit a large comprehension of the beam emittance has been developed, further systematic studies could imply improved beam properties. By re-measuring the beam emittance directly after the EBIS, thus avoiding aperture limitations, the causes for the beam aberration could be identified. The effects of moving the gun and collector in the magnetic field, the removal of the Penning gauges, and for curiosity the operation with a reversed magnetic field, should be investigated. Emittance measurement on single charge states after the mass separator would reveal the charge-dependency of the emittance.

Even if it has been demonstrated that the emittance most likely will comply with the 10 π·mm·mrad (2σ) specification for short breeding times, one can anticipate an even better emittance. The non-relevant low-charged ions, present both for short and long inclusion times, dominate the border of the phase-space plots and will be sorted out in the mass separator. Similarly, the mass-dependent focusing term caused by the magnetic field results in different orientation of the phase-space ellipses so they together make up a pessimistically large emittance. As already been mentioned, with improved vacuum conditions the beam compensation is avoided and the emittance reduced.

1.4.6 Ion injection tests

One of the most essential tests for the REXEBIS, and for the whole REX-ISOLDE accelerator with its bunching/cooling/breeding concept, is the ion transport from the REXTRAP through the transfer beam line into the trapping region inside the EBIS. A major injection experiment, described here below, was carried out during the fall of 2000.

1.4.6.1 Injected ions and intensities

Two types of ions were used for the injection tests: ^{39,41}K produced in a surface ion source locally supplying ions to the REXTRAP, and radioactive ^{26}Na ($t_{1/2}$~1 s) produced at ISOLDE. The beam out of the REXTRAP had a pulse length of ~10 μs, a period time of 25 ms and an energy spread <10 eV. The injected intensities were very modest; for the stable ^{39,41}K an intensity (averaged current) of <8 pA was recorded at the upper bender Faraday cup (FC) (restricted by the space-charge limitations inside the trap). For the ^{26}Na case, some hundred ions per pulse were delivered to the upper bender. Besides a ~10 pA DC beam of ^{39,41}K passing through the REXTRAP without phase-space cooling was utilised.

1.4.6.2 Beam set-up

The beam was traced by the help of FCs and MCPs from the Penning trap through the transfer line to the upper bender. The transport efficiency through the beam line was limited to ~30% due to the low transport energy of 30 keV. Two different methods for setting up the beam optics parameters for the EBIS were used.

First, the cathode heating was switched off (no electron production) and the injected ion current was measured on the anode/inner barrier tube. The cathode was disconnected from the gun supply (i.e. on the same potential as the inner barrier) to avoid secondary electrons from completely swamping the weak ion signal. All other voltages were applied, including a pulsed outer barrier indicating if the injection timing was correct. Approximately 10% of the signal measured on the upper FC in the transfer line was detected inside the EBIS at a platform voltage of 29 800 V (beam energy 30 000 V). Increasing the platform voltage rapidly decreased the signal. Attempts to measure currents at other elements such as the outer trapping tube, at the extractor tubes etc, failed due to the high number of secondary electrons created by the ion impact on ground potential in front of the EBIS.

The alternative way of setting up the transfer line/EBIS was to extract a rest-gas beam from the EBIS backward through the transfer line towards the Penning trap. For a low degree of compensation, the beam optics should be identical as for injection. Approximately the same steering settings were found for the two methods, although, the focal length of the einzel lenses differed, most probably due to the absence of the strongly focusing electron beam in the first method.

1.4.6.3 Ion detection methods

To detect injected ions after the EBIS the mass separator was used, and for this purpose calibrated on rest-gas and/or lanthanum peaks in the expected Q/A-region. Either the mass spectrum was scanned for subtle differences with the Penning trap alternately open and closed, or the magnet was set on a specific Q/A-peak and the injection parameters were varied. Lower Q/A-values than expected were also scanned because of the possibility of a poor confinement in the electron beam. To detect the ion current a FC (theoretically sensitive down to fA, practically 0.5 pA) and a MCP were used. The MCP signal was either presented visually or 'time-of-flight' analysed. For the radioactive ions a beta detector was used after the ions had been accelerated through the RFQ.

During the experiment the EBIS trapping tube potentials and the HV platform voltage were systematically scanned, as well as the closing time for the outer barrier tube. To a certain extent also the einzel lens and steering plates settings were changed. Finally some adjustments of the REXTRAP and transfer line were carried out.

1.4.6.4 Expected signal levels

The emittance of the beam delivered to the EBIS was unknown. Based on the 30% beam transmission from the Penning trap to the EBIS through the transfer line, which has an acceptance of approximately 40 π·mm·mrad for 30 keV, the assumption of a 15 π·mm·mrad trap emittance is not unreasonable. Independent simulations of the cooling mechanism inside the Penning trap suggest an emittance in this range [22]. Because of the reduced electron current in the EBIS, the nominal acceptance values decreased by a factor of $\sqrt{180\,mA/500\,mA}$ in each dimension. The particle acceptance for focused-matched phase spaces is proportional to $(\alpha_{EBIS}/\varepsilon_{transport\ line})^2$. Furthermore, in the injection estimation below, a 50% particle emittance/acceptance matching has been assumed. The most abundant charge state was assumed to contain 25% of the particles, and the EBIS to mass separator transport efficiency was estimated to 75%. In the cases when the RFQ was used (for the radioactive ^{26}Na), it had a transmission of 70%, and the total efficiency of the β-detector was 15%. Taking this information into account, lower and upper boundaries on the expected current could be stated, as summarised in Table 4. With a noise level of

0.5 pA for the current measurement and a β-detector background level of 5-10 counts per second, one should most likely have been able to detect a signal if the injection, breeding and extraction were fully successful. This was not done.

1.4.6.5 Why were no charge bred ions detected?

Most certainly, several independent circumstances contributed to the failure in detecting charge-bred ions after the mass separator. Note the *extremely small* current of 5 to 10 pA (compare with pulsed injection into CRYSIS with a minimum of 1-2 μA for >20 μs, i.e. a factor ~$2 \cdot 10^5$ larger). The low electron beam in the EBIS reduced the acceptance, and the properties (emittance value and phase-space orientation) of the beam injected into the EBIS might not have been fulfilling the strict EBIS requirements at the interface point of the upper bender [22,52][4]. The relatively high level of rest-gas background inside the EBIS made the identification of injected ions to a difficult task (see Figure 33). Pre-ionisation of the 1^+ ions before they enter the trap region could have reduced the injection efficiency (simulation predicts a pre-ionisation loss smaller than 10%). The barrier timing is critical, but its proper timing was verified at the injection test.

Detected current/particles	Injected current/particles	
	8 pA of ^{39,40}K	50-200 ^{26}Na/pulse
Maximum	1.6 pA	25 β/s
Minimum	0.06 pA	3 β/s

***Table 4**. Upper and lower boundaries for expected current/particles that should have been detected after the EBIS.*

One error during the injection tests has afterward been identified. For the backward beam tracing toward the Penning trap, the EBIS should have been operated with a short enough breeding time in order to avoid compensation. This would have assured identical injection and extraction conditions for the EBIS. The potential difference between injection and extraction (50 to 100 V) was nevertheless taken into account during the test.

1.4.6.6 Suggestions for future ion injection tests

To succeed with ion injection, the properties of the injected beam should be verified. In practice that means to measure the transverse emittance after the transport line, which has not been possible until now due to the non-availability of an emittance meter with enough sensitivity for the weak beams delivered by the Penning trap. Insertion of a double-sided MCP in the EBIS beam line should facilitate the beam guiding. By placing the test ion source directly in front of the transport line, a stronger ion beam (10 to 100 nA) can be obtained. These actions, together with a control system update, a re-alignment of all involved elements, and a number of other improvements, should assure a successful ion transport from the Penning trap into the EBIS.

1.4.7 High voltage switching test

Several acceptance tests of the FuG 60 kV/100 mA power supply for the platform HV switching were carried out before it could be accepted. Most tests indicated that the power supply did not fulfil its specifications concerning the pulse plateaux stability. Finally, a handheld Tektronix P5016A HV probe, rated for 40 kV, was used. The curve-form for switching between 20 and 40 kV was recorded and compared with the curve form of the internal HV divider in the FuG supply. They both showed flat plateaux at the low and high voltages, maximum discrepancy ±5 V. Thus one could safely conclude that the built-in divider indeed shows a correct value. The top switching voltage was then increased to 60 kV and a pulse-form falling within the specifications was measured on the internal divider[5].

1.5 REXEBIS conclusions and outlook

1.5.1 Achievements

The last year has been an exciting year for REX-ISOLDE as the project has fully entered the commissioning stage. All components are completed, tested and most of them are installed at the

[4] In addition, it was later found out that a magnetic wire inside the REXTRAP had been disturbing the beam extraction during the injection tests.

[5] It is interesting to note that four high voltage dividers (one even brand new), which all were rated for the voltage and the switching frequency, showed an incorrect voltage response.

ISOLDE facility. Successful accumulation, cooling and bunching of ions delivered by ISOLDE, has been demonstrated with the Penning trap. Acceleration up to 300 keV/u with the RFQ of ion bunches delivered by the EBIS has been carried out. Separate beam tests on the 7-gap resonators have verified their functionality.

The REXEBIS project was started in autumn 1995 and the bulk of the two first years was spent on beam simulations, interfacing the source to the surrounding elements and design development. The simulation model that was developed gave valuable insight into the performance of a non-compensated EBIS, and important beam parameters such as acceptance and emittance could be predicted. Generally, a great effort was devoted to verify the different design aspects theoretically using simulations and calculations.

After nearly three years of installations the build-up phase of the REXEBIS at ISOLDE is almost completed. A large part of this time has been filled with miscellaneous acceptance tests of equipment and verification of design solutions. Throughout the most recent period the work has focused on actual commissioning tests of the complete REXEBIS system. This stage has been fruitful as a deeper understanding for the actual behaviour of the source was created. The performance and anomalies could be related to the simulations, which in turn could be extrapolated to make certain predictions about a compensated EBIS.

Although the design values have not been fully reached so far, the results are promising, and several important commissioning results have been achieved. We have demonstrated that the REXEBIS works reliably as a rest-gas source, providing stable beams of different charge state, intensity and extraction time to the following LINAC for its installation tests. At electron currents lower than the design value the losses are minimal and the electron beam easy to operate. The emittance measurements have verified the small emittance of an EBIS for short breeding times. In addition, the measurements have revealed the strong dependence on the degree of beam compensation and further stressed the need for an extremely good vacuum inside the trapping region.

1.5.2 The future

The commissioning tests have pointed out the direction for further improvements concerning the design and construction. To reach the nominal design values for electron current, electron current-density, emittance etc, the REXEBIS has to be mechanically upgraded in line with the suggestions in '*The REXEBIS mechanical design*' section. The most important issues to deal with are:

- The electron-beam losses preventing operation at full electron-beam current. Reducing the losses would enable operation with full electron-beam current and thereby an enlarged ion beam acceptance, larger space-charge capacity and shorter breeding time. The vacuum would most certainly improve as well.
- Inadequate vacuum conditions in the trapping region. An improved vacuum situation would automatically yield smaller emittance, less rest-gas in the mass spectra, longer compensation time and most probably a lower electron-beam load.
- Possible misalignment of the inner structure, optics elements and of the magnetic axis to the geometric axis. Diminished emittance aberrations, less beam steering and simplified ion injection are expected by aligning the geometric and magnetic axes.

In the immediate future, when the REXEBIS has been modified, a new series of studies will commence. On the agenda is:

- Precise determination of the electron current-density and residual gas composition.
- Emittance measurement for different charge states using a deflector-type emittance meter and a photo-detector.
- Most importantly, further ion injection tests of ions from the Penning trap. The properties of the injected beam have to be pinpointed, and separate high-intensity injection tests carried out to identify the correct injection settings. Thereafter the injection/breeding/extraction efficiencies can be established.

So far it has been shown that the Penning trap and the EBIS work well as separate units. Now it remains to interlace the buncher/cooler with the breeder to a high performance unit producing multiply charged ions with high efficiency.

Part II – Yield improving experiments on an ECR4 ion source

2.1 Introduction

2.1.1 Motivation

In autumn 1994 the new CERN Heavy Ion Accelerating Facility [13,14] was brought into operation and a lead beam of $2.9 \cdot 10^7$ ions per pulse was accelerated in the SPS to an energy of 158 GeV/u. The ion source, an ECRIS, quickly met the specifications of 80 eμA of Pb^{27+}, and annually provides the heavy ion experiment programme at CERN [53] with currents between 80 and 100 eμA. Needless to say, the search for higher beam intensities has continued. Present physics experiments have a constant call for more particles, and when the LHC project goes into operation with heavy ions, the lead ion production has to be increased by almost an order of magnitude compared with present values to fulfil the specifications set by the experiments (see further Part III).

Several techniques to improve the yield of a continuous wave (CW) ECRIS exist, but not all have been systematically evaluated for the afterglow mode. Theoretical calculations were carried out on alternative carrier gas combinations [54], which when experimentally tried on the CERN ECR4 [11,12] ion source did not match the expectations [55]. In the search for higher intensities the CERN team performed a number of experiments on the source, for instance the extraction gap distance was varied, the carrier gas composition changed, and the effect of a biased electrode was tried out [56,57]. These experiments have now been followed up and refined. Two different approaches to boost the yield were tried: either to increase the total number of ions in the plasma, or to extract the available ions in a shorter pulse (presently the extracted pulse length from the ECRIS exceeds the typical 400 to 500 μs accepted by the synchrotron).

As the source is subject to operational restrictions, no major design changes could be carried out as that would have jeopardised the beam delivery to the physics experiments.

2.1.2 The LINAC3

The Heavy Ion Accelerating Facility has now completed seven periods of operation. Each year, the ion intensity and the integrated number of ions delivered to the physics targets have increased (except in 1999 when higher intensity was not requested). The increase is partly due to a performance enhancement of the ECRIS and the linear accelerator (LINAC3), illustrated in Figure 38.

The ion source produces a charge-state distribution of lead ranging from about 18^+ to 31^+, on which oxygen peaks are superimposed, for instance O^{2+} overlapping Pb^{26+}. The ions are electrostatically extracted with a pulse length of 1 to 2 ms, utilising the afterglow phenomenon (see sec. 2.1.3.7). Even though the LINAC runs at 0.8 Hz (optionally 10 Hz), the source is pulsed with 10 Hz to obtain a higher pulse to pulse stability. The RFQ requires an injection energy of 2.5 keV/u, that translates to a pre-acceleration voltage of about 20 kV, depending on the charge state of the lead ion.

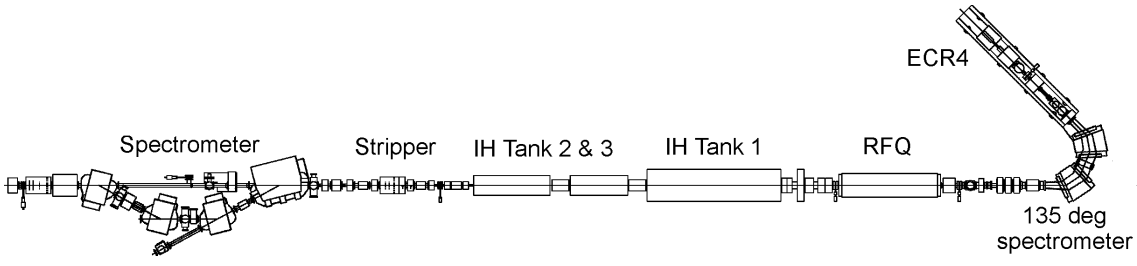

Figure 38. *Over-view drawing of LINAC3.*

After a drift of approximately 1 m the beam is focused by a solenoid onto the entrance slit of the 135º spectrometer (resolution $\Delta p/p=0.003$). At the end of the spectrometer, the beam passes through an exit slit, and the analysed current is measured in a FC at this point. The subsequent four-rod RFQ, which accelerates the beam from 2.5 to 250 keV/u, has four modulated vanes that act as the accelerating and focusing structure. Three IH-linac tanks, running at 101.28 and 202.56 MHz, boost the energy to a final 4.2 MeV/u. At this stage the Pb^{27+} is stripped in a carbon foil to charge states ranging from 49^+ to 57^+. A second spectrometer is then used to select Pb^{53+} for further acceleration in the synchrotrons.

2.1.3 ECRIS theory

As the complete theory of an ECRIS is very extensive and complex (moreover not fully understood) – involving plasma physics, atomic physics, charged particle motion, magnet theory, wave-plasma interaction etc – a full coverage will not be given (see for details ref. [6]). Below follows a short introduction to the theory, with qualitative arguments since most quantitative formulae produce uncertain predictions, and a few more detailed sections on topics linking to the experiments that were carried out.

2.1.3.1 Fundamental concept

An ECRIS can be considered to be a composition of three entities: a magnetic field, a microwave field (RF) and a low-pressure ionised gas. Mechanically it is based around a vacuum chamber, which serves as a microwave cavity. The chamber is situated inside a magnetic field created by a set of solenoids and a multi-pole magnet. RF is coupled into the source and a plasma is ignited by microwave ionisation, thereafter maintained and developed by electron impact ionisation. Electrons heated by the RF contribute to the successive ionisation of the ions that escape mainly longitudinally from the plasma.

2.1.3.2 Electron heating

At a surface inside the plasma chamber, there is a magnetic field strength forcing the electrons to spiral around the field lines with a gyrofrequency $\omega_{ecr}=e\cdot|B|/m_e$ that coincides with the frequency of the externally fed RF. Electrons in this electron cyclotron resonance (ECR) zone will stochastically gain[6] energy from the electric field E of the microwave radiation, more specifically, the electric field component of the microwave perpendicular to the magnetic field. In multi-mode chambers the ECR condition is assured as there is always a component of the electric field of the waves that is perpendicular to the magnetic field lines.

The ECR heating transfers energy to the electron momentum in a direction perpendicular to the magnetic field lines, so an electron velocity anisotropy $v_\perp/v_\parallel>1$ arises which improves the electron confinement in the magnetic mirror field compared to that for a classical thermalised electronic population. Furthermore, the high energy electrons suffer practically no collisions and are hence easily confined. The electrons can however move back and forth along the magnetic field lines, and thus undergo a large number of oscillations, while the ions get progressively ionised by electron impact.

Likewise the electrons pass repeatedly through the resonance and gain in total energy, up to several 100 keV in low-pressure devices. The hot electrons in the ECR plasma are far from thermodynamical equilibrium, even if the concept of electron temperature T_e is frequently used. In fact several electron populations exist (low temperature electrons with some 10 to a few 100 eV, and higher energy populations with several keV or tens of keV).

2.1.3.3 Magnetic confinement

Magnetic field is required for confinement of the plasma. Most ECRIS producing multi-charged ions are of minimum B-field configuration type, i.e. they have a centre region with a minimum B-field strength. The min-B ECRIS has superior trapping properties for ions and electrons; the ion confinement time is long, and the conditions for multi-charged ion production are radically improved compared with a simple mirror ECRIS. A set of solenoid coils provides a magnetic mirror field for axial confinement, while the radial confinement is achieved by a strong radial field created by a magnetic multi-pole. A closed, ellipsoidal resonance surface within the vacuum chamber is formed. The plasma is confined only within closed magnetic isobars [58].

The axial confinement is not perfect, which is not entirely a drawback, since it otherwise would be impossible to extract the ions. The mirror ratio R_B, defined as the ratio between the maximal and minimal

[6] Depending on the phase of the microwave field relative to the cyclotron motion, the electron may gain or lose transverse velocity $v_\perp$ at a single ECR crossing, but averaged over a random phase angle, the energy gain is positive.

axial magnetic field in the plasma chamber, i.e. $R_B=B_{max}/B_{min}$ (of the order of 3), is an important factor for the determination of the leak rate of electrons and ions. Starting from two conserved quantities, the invariance of the magnetic moment μ and the kinetic energy W_0 (assuming the absence of electric field), one can derive the escape condition for a charged particle. If the particle has parallel and perpendicular velocities, $v_{\parallel 0}$ and $v_{\perp 0}$, with respect to the magnetic field direction at the B-field minimum, the condition for reflection in the magnetic mirror can be written as:

$$v_{\perp 0}^2 \cdot \left(1-\frac{1}{R_B}\right) \geq v_{// 0}^2 \qquad \textbf{(6)}$$

In velocity space this corresponds to a loss cone (see Figure 39). Nevertheless, for electrons a non-negligible population, even within the loss cone, is hindered from leaving due to the perpendicular heating that occurs when the electrons pass the ECR zone (RF assumed to be on). The loss cone for electrons is modified into a hyperboloid [59]. The phenomenon closing the open-ended trap in an ideal situation is generally known as the ECR mirror plug. Furthermore the electrostatic potential dip $\Delta\phi$ (see sec. 2.1.3.5) distorts the shape of the loss cone for ions and plugs the ion leaks [59].

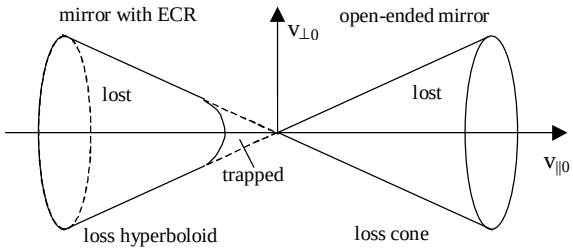

Figure 39. *Losses in velocity space for a simple mirror (right) and an ECR mirror (left).*

2.1.3.4 Microwave feeding

The microwave power is coupled into the source through a waveguide, either axially, off-axis or radially, but optimally the RF should be launched along the axis. Multi-mode conditions occur if the cavity dimensions are large with respect to the wavelength. The plasma is transparent to RF for frequencies higher than the plasma frequency, given as:

$$\omega_p = \left(\frac{n_e e^2}{m_e \varepsilon_0}\right)^{1/2} \qquad \textbf{(7)}$$

while waves at lower frequencies do not propagate into the plasma body. For a fixed frequency this condition translates to a maximum attainable plasma density $n_{cut\text{-}off}$, which can be expressed as:

$$n_{cut-off} = 1.2 \cdot 10^{10} f_{RF}^2 \ \ cm^{-3} \qquad (f_{RF} \text{ in GHz}) \qquad \textbf{(8)}$$

For a microwave frequency of 14.5 GHz $n_{cut\text{-}off}$ equals $2.6 \cdot 10^{12}$ cm^{-3}. By increasing the microwave frequency a higher plasma density is achievable, but more RF power is needed in addition.

2.1.3.5 Plasma potential and plasma dip

Inside an ECRIS the plasma usually has a positive potential of some tens of volt with respect to the walls [60]. This plasma potential ϕ is related to the sheath and the ambipolar diffusion between the wall and the plasma. Since the cold electrons in an ECRIS have a higher mobility and leave the plasma faster than the ions, ϕ assumes a positive value in order to accelerate the ions and to retard the electrons, so that the plasma neutrality can be retained. The plasma potential is strongly dependent on the ion charge-state distribution as a high charge state partially compensates for a low mobility, thereby lowering ϕ.

In the core of the plasma inside an ECRIS where $T_e >> T_i$, the ions are generally scattered faster than the electrons into the loss cone by 90° Spitzer collisions. It is therefore claimed that a small negative potential dip $\Delta\phi$ appears in the core [61] in order to retain the ions together with the trapped hot electrons. This potential is superimposed on the

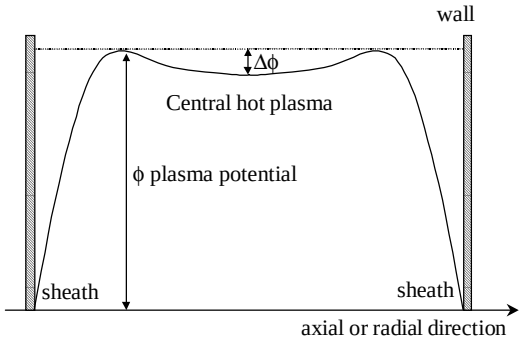

Figure 40. *Electrostatic potential distribution along the axis or radius inside an ECRIS.*

plasma potential. In Figure 40 the total potential along the axis or radius of a min-B trap is represented, showing the electrostatic dip $\Delta\phi$ that traps the ions and the ambipolar plasma potential ϕ necessary to confine the thermal electrons. $\Delta\phi$ is usually much smaller than 1 V.

2.1.3.6 Ion production

The elements of interest are introduced into the plasma either by gas injection or as vapour gas, where they are step-by-step ionised by the energetic electrons. The attainable charge state is mainly dependent on the electron density n_e, the confinement time τ and the electron energy distribution. The ion confinement time can be increased by decreasing the energy of the ions (typically some eV) for example by gas mixing or, as demonstrated above, by increasing the mirror ratio R_B of the magnetic bottle. Furthermore a good vacuum (~10^{-6} mbar) is required to minimise charge exchange reactions between the ions and neutral atoms. A steady-state ECRIS has an inherent contradiction between a good confinement (high charge state) and an intense leakage current. The highly charged ions diffuse to the extraction end of the ion source because of the magnetic configuration, where they are axially extracted by a high voltage. For hexapolar radial confinement the loss region has a triangular shape.

2.1.3.7 Afterglow

If the microwave feeding is abruptly turned off, the steady-state regime is replaced by the so-called afterglow [62]. In a source optimised for pulsed discharge, this is characterised by a current spike (see Figure 41), which has a fast rise time of 100-300 µs. The decay constant depends on the confinement conditions and the recombination rate of the ions, and can for a quiescent afterglow be very long. The ECR4 current either decreases exponentially over more than 10 ms or ends in a sharp break down after 1-2 ms (Figure 53), depending on the tuning of the source [55]. Most importantly, a current boost of 2-3 times larger intensities than the steady state is common in the afterglow, and for single high ionisation states the relative increase can be considerably higher (>100 [57]). This phenomenon can be understood as a plasma potential disruption inducing a rapid diffusion of the highly charged ions contained in the plasma. The high peak intensity and short pulse make the afterglow operation suitable for synchrotron injection. Different theoretical explanations for the afterglow exist, and the most widely accepted one, based on the expulsion of ions from the potential dip $\Delta\phi$, is described in the following section (following the outline in ref. [63]).

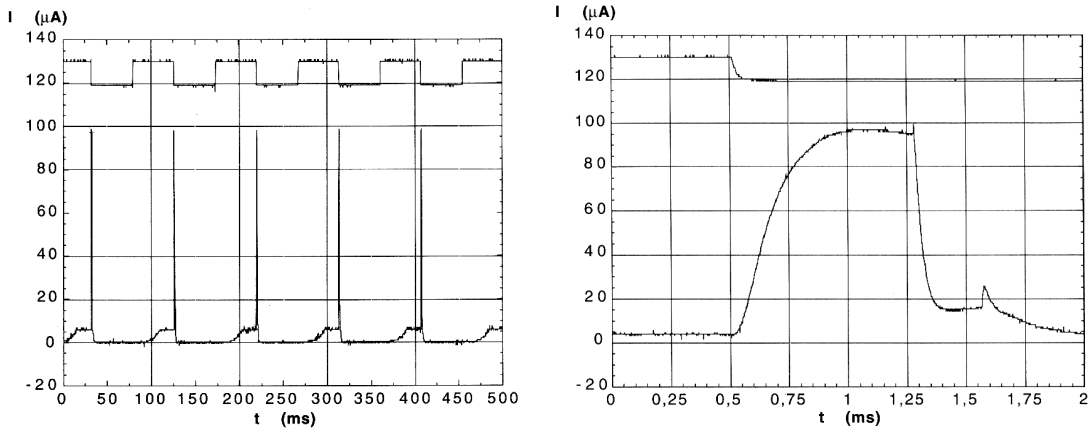

Figure 41. *A typical afterglow pulse shape for Pb^{27+} extracted from the CERN ECR4 ion source (shown in different time-scales) [14]. RF timing (upper curves) and extracted current (lower curves).*

The electrons leaving the loss hyperboloid during steady-state mode drag a number of ions along with them towards the extraction gap. The extractable ion current originating from ions with charge state q can be expressed as:

$$I_q \sim \frac{1}{2} n_q q e V_x / \tau_q \qquad \textbf{(9)}$$

where n_q and τ_q represent the density and the confinement time of ions of charge state q, and V_x the plasma volume that maps along the field lines into the extraction hole (factor ½ because of the two mirror ends of the magnetic configuration). Using West's model [64] the confinement time dependence on the potential dip $|\Delta\phi|$ is approximately:

$$\tau_q \sim R_B L_z \sqrt{\frac{m_i}{kT_i}} \cdot exp\left(\frac{qe|\Delta\phi|}{kT_i}\right) \qquad \textbf{(10)}$$

where T_i is the ion temperature and L_z the axial length of the plasma. The ions leaking out of the source are ions that have escaped the potential dip, which is maintained as long as the hot electrons are mirroring inside the magnetic field.

When the microwave transmission is stopped, the ECR plug is eliminated and a first bunch of electrons immediately leave the trap since they are no longer perpendicularly energised. Thus, the electron flux can temporarily increase over the steady-state flux. With the escape of the electrons the potential dip $|\Delta\phi|$ is decreased and the ion confinement time τ_q shortened, therefore an increased ion flow reaches the extraction gap. The relative current increase for a certain charge state q to the steady-state current I_q can approximately (assuming for instance homogeneous density and thermalised ion-population temperatures) be expressed as [61]:

$$\frac{I_q(afterglow)}{I_q(steady)} \propto exp\left(qe\frac{|\Delta\phi|}{kT_i}\right) \qquad \textbf{(11)}$$

The relation indicates that highly charged ions are favoured in the ion spike as has been verified for example with the ECR4 source. For a relative increase of a factor 100 for $q=27^+$, $e|\Delta\phi|/kT_i$ assumes a value of ~0.17.

Not all ions are expelled during the first afterglow pulse. The hot collisionless electron population with $v_\perp/v_\parallel > 1$ decays only slowly, and therefore ions are kept in the remaining potential dip. A further collapse of the electron population occurs however as the electron heating no longer exists and the electron temperature T_e therefore decreases. Moreover, there is a reduction of some cold electron sources, such as primary ionisation of carrier-gas and secondary emission from hot electrons impinging on the walls. The confined highly charged ions are compelled to leave the plasma at the same speed because of charge neutrality.

2.1.3.8 Electron starvation

Electron starvation is an important issue in the min-B ECRIS. Without a permanent supply of rather cold electrons to the plasma, the electron density is not large enough to maintain efficient ionisation. There are different methods for supplying these electrons, for example, the first-stage ECR discharge in a high pressure region is the most classical donor of electrons to the second-stage low pressure region. An ECR plasma cathode was developed at RIKEN [65], which in principle was an electrode for electron extraction at low energy and injection into the main stage. Wall coatings having high secondary electron emission yields, e.g. ThO_2, SiO_2, Al_2O_3, have proven to be very efficient. A negatively biased disc on axis may reduce the electron losses and/or provide new electrons from secondary emission of impinging plasma particles [66]. Finally, it is believed that gas mixing also acts against electron starvation [67]. Nevertheless, the electron starvation can be minimised by improving the mirror ratios (axial and radial) in the min-B structure. This is the case for the ECR4, which has no dedicated cold electron supplier except for the mixing gas.

2.1.3.9 Gas mixing

A common way to reach higher charge states is to add a mixing gas, lighter than the main element and dominant in density. The yield increasing effect by a mixing gas has various interpretations. For instance, it could be explained by a dilution effect lowering the mean ion charge $q_{eff} = \sum n_q q^2 / n_e$ and reducing the electron loss rate (i.e. increasing the average energy confinement time τ_e of the electrons). This becomes obvious from:

$$\tau_{coll} \sim \frac{5 \cdot 10^3}{q_{eff}} \frac{T_e^{3/2}}{n_e} \quad (T_e \text{ in eV and } n_e \text{ in } cm^{-3}) \qquad \textbf{(12)}$$

where τ_{coll} (s) is the Spitzer collision time, which is close to τ_e. The positive effect could also be explained by an increased electron density as a result of better ionisation efficiency of the carrier gas. The most widely accepted model for the gas-mixing effect is that ion-ion collisions between higher-charged ions and gas-mixing ions lead to a cooling effect of the former because of the mass effect [68]. A lower ion temperature T_i leads to a longer ion confinement in the $\Delta\phi$ potential well according to eq. 10.

2.1.4 The ECR4 lead ion source

The ECR4 at LINAC3 was developed at GANIL from their standard CAPRICE type machine [69], see Figure 42 for a schematic layout. The source, of min-B type, was originally designed as a CW source, but it has capabilities to operate in pulsed afterglow mode (repetition rate 10 Hz, 50% duty cycle). One of the main characteristics of the source is its coaxial wave launcher whose inner conductor reaches into the source almost up to the back resonance surface. The source is operated at 14.5 GHz and with a typical RF power of 1.3 kW, optimal for Pb^{27+} production. The transition from the wave launcher to the multi-mode chamber is tuned by a motorised plunger tuner to maintain optimum plasma conditions. The optimal performance is not necessarily found at the point of minimum reflected power.

The source has a high magnetic gradient and consequently a small resonance area (B_{ECR}=0.52 T at 14.5 GHz). The axial confinement, which optimises the charge-state distribution, is provided by two independent, water-cooled coils operating at 900-1100 A and producing a maximal axial field of 1.1 T (mirror ratio 2.8). The radial confinement is achieved by a strong radial field created by a Fe-Nd-B permanent magnet hexapole. Along the radius of the plasma chamber, the field varies between 0.4 and 1.2 T. The solenoids are fully enclosed in an iron yoke terminated near the hexapole by two pole pieces acting as flux concentrators. The plasma electrode and the tip of the oven electrode are each ~8 mm inside the axial magnetic field peaks.

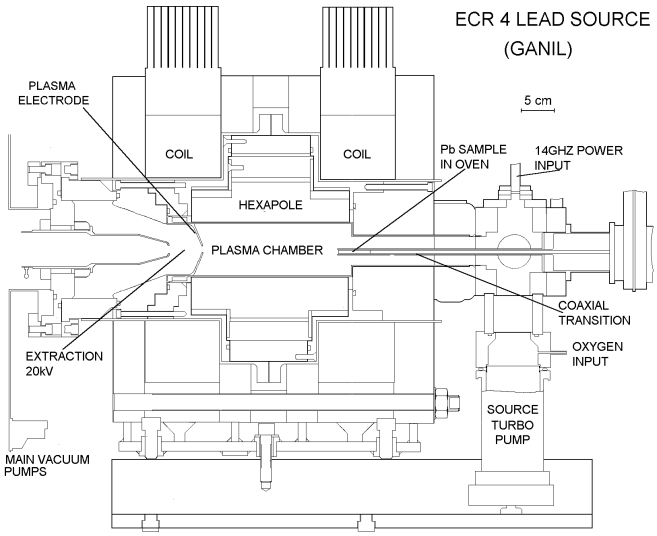

Figure 42. *Schematic layout of the central parts of the CERN ECR4 ion source.*

Oxygen is introduced into the source at the injection side near the RF inlet and used as carrier gas. The possibility for injection of an additional sample gas exists. Isotopically pure ^{208}Pb is evaporated into the plasma using a 6 mm diameter micro oven which is situated inside the coaxial RF feed line, and heated up to 600-800 °C. The plasma chamber, a water-cooled double-wall chamber made of stainless steel, is together with the RF cavity on positive high voltage (~20 kV) and insulated from the rest of the source (coils, iron yoke etc) that are kept on ground potential.

Two pumping systems are used at the source. On the extraction side two larger turbomolecular pumps attain a pressure of $2 \cdot 10^{-7}$ mbar or better, whilst a smaller turbo pump is used to pump the RF transition near the gas injection to a base pressure of about $3 \cdot 10^{-7}$ mbar. With servo controlled oxygen injection, this pressure rises to around $1 \cdot 10^{-5}$ mbar.

The ion beam is electrostatically extracted via a 16 mm diameter aperture in the plasma electrode (at plasma chamber potential) by a single 15 mm diameter extraction electrode (puller) at ground potential. The fixed extraction gap is varied between 42 and 47 mm. The ion source HV is dynamically stabilised using a 'bouncer' during the afterglow beam loading.

The most important properties and design parameters for the CERN ECR4 are listed in Appendix 3.

2.2 Experiments and discussion

2.2.1 General test procedure

Various experiments were performed on the CERN ECR4 source in order to increase the afterglow yield. The requirements of a high pulse-to-pulse stability and a flat pulse top were not relinquished. Similarly the transverse emittance constraint remained, even if the emittance was not monitored. The injection beam line for LINAC3 is presented in Figure 43. The ion intensity was measured in Faraday cups either before (FC1) or after (FC2) the spectrometer or after acceleration in the RFQ (FC3).

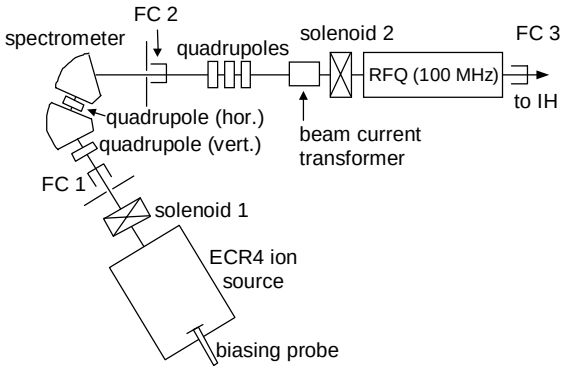

Figure 43. *Layout of the injection part for the LINAC3 beam line.*

The general procedure throughout the tests was to first optimise the source before introducing the change, and thereby obtain a yield reference value. Thereafter the modification was carried out, and the source was once again re-tuned to an optimal performance, which was compared with the reference value and the highest hitherto achieved current of 100 eμA in FC3.

2.2.2 Biased axial electrode

2.2.2.1 The idea

It is often claimed that a negatively biased electrode (zero to a few hundred volt), positioned on axis near the plasma at the injection side, may reduce the electron losses out of the magnetic bottle and/or influence the electron density positively due to the injection of cold electrons, created by bombardment of the electrode with loss electrons and ions [66]. This method has been regularly used at ECR ion sources operated mainly in CW mode. Similarly, the presence of a biased electrode in the vicinity of the plasma improved the performance and stabilised the afterglow in an ECRIS for sulphur ions (a MiniMafios with off axis microwave coupling) [70]. The real reason for the improvement remains unclear, however, recent investigations suggest that the ion yield increase is mainly due to improved extraction conditions [71,72] or plasma potential optimisation [73,74].

Biased electrode tests have previously been carried out at the ECR4 ion source, but no gain in current could be observed [56] at the time. We nonetheless pursued this idea and expanded the experiment from static to pulsed biased voltage, and allowed for a positive biasing voltage as well. Thus, there was the opportunity to vary both the voltage, the pulse length and the timing of the pulse relative to the end

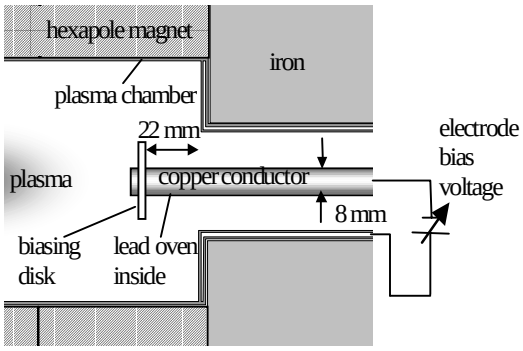

Figure 44*. Schematic drawing of the lead oven arrangement acting as a biased electrode. (The biasing disk was not used in all experiments.)*

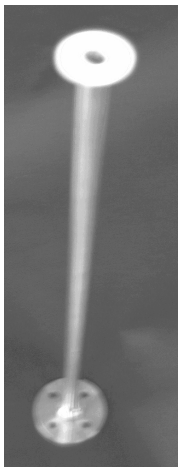

Figure 45*. The biased electrode containing the oven. A disk is here attached to the end of the electrode.*

of the RF pulse. The idea was to prevent the cold electrons from escaping the magnetic bottle and to feed secondary electrons into the plasma by applying a negative bias to the electrode during the breeding phase. In a similar way a positive bias pulse applied after the RF off flank may facilitate the extraction of the electrons from the plasma, and repel the ions owards the extraction side.

2.2.2.2 Experimental method

On the ECR4 ion source a bias could be applied to the inner conductor of the coaxial transition, which contains the sample oven (see Figures 44 and 45). The electrode penetrates the plasma chamber 8 mm inside the maximum axial field peak at the injection side. The switching between two voltages, positive or negative, was managed by a Behlke HTS31 switch [75]. Due to insulation problems the bias voltage was limited to 300 V. During normal non-biased operation the electrode and the plasma chamber are at the same potential.

A load resistor of <1 kΩ was necessary to keep the probe potential below ~1 V during the microwave pulse, i.e. to discharge the (ion) current of about 1.5 mA. Higher resistor values would act like a DC bias voltage, as was the case for the biased probe experiments presented in ref. [P4] where a 22 kΩ resistor was utilised.

Disks of different material (Ta, and Al_2O_3) and shapes were mounted at the end of the electrode to increase the area as shown in Figure 45. Complete test results are found in ref. [P4,P5].

2.2.2.3 Results and discussion

Electron temperature and plasma potential

Before the pulsed bias tests were underway, the floating potential of the source was measured with a high impedance probe while the source was under full RF power (1300 W) and no extraction voltage applied. Figure 46 shows that, after the plasma ignites, the co-axial electrode rapidly rises to around 400 V with respect to the plasma chamber and continues rising during the heating phase to 500 V. This potential collapses almost instantaneously with the removal of the RF heating to practically 0 V during the afterglow pulse.

If an electrode is floating, the potential across the sheath will acquire the value that will cause the ion and electron currents to exactly balance. Making three assumptions the floating potential of the electrode can be approximated with [76]:

$$V_{float} = \frac{kT_e}{2e} ln\left(\frac{2m_i}{3m_e}\right) \qquad \textbf{(13)}$$

The formula assumes: that virtually all of the electrons are maxwellianized, which is not true inside an ECRIS with its hot and cold electron distributions; that the influence of the magnetic field on charged particle trajectories is small; and that there are a substantial number of primaries (singly charge ions). Even if neither of these presumptions are completely valid, the formula can be used to assign an electron 'temperature' that assumes a value between 80 and 100 eV. The Bohm criterion [76] requires the plasma potential to be around $kT_e/2e$, i.e. about 50 V (in agreement with for example ref. [60]). Such a considerable energy should have a positive influence on the inherent emittance of an ECRIS [77].

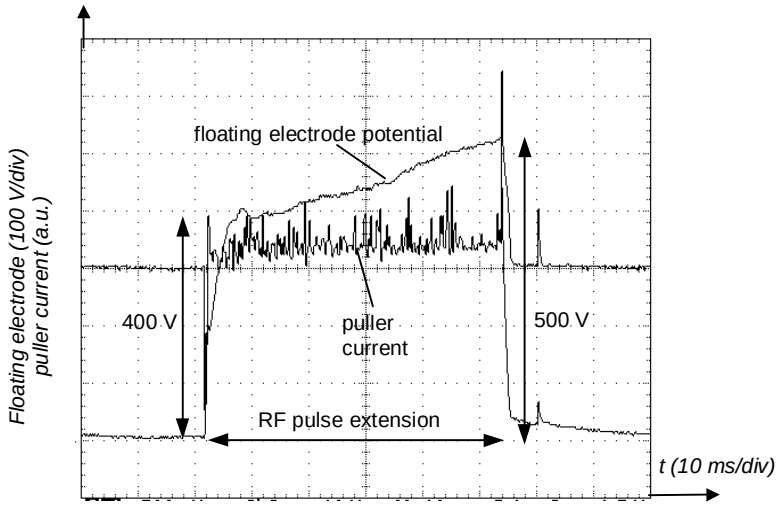

***Figure 46**. Change of floating electrode potential with RF pulse. The load current on the puller is included as well.*

Response times

The first very important conclusion from the pulsing of the electrode was the rapid response (within some μs) to a change in the bias voltage; too short to change the charge-state distribution in the ECR plasma (see Figure 47).

Influences by disk characteristics

The early bias tests on the ECR4 ion source were carried out using only the oven electrode as a biased probe [56,P4]. It was later considered that the electrode was possibly too small to have any effect. Thus the electrode surface was increased by the addition of metallic or dielectric disks to the coaxial line and the tests were repeated (see Figure 45). First a 20 mm diameter Ta disk was mounted at the end of the tube. This made the conditioning and operation of the ion source very difficult and the RF tuning had to be adjusted for high reflected power of about 150 W. Obviously the disk interfered with the propagation of the RF into the cavity. The disk was replaced by one made from pure insulating Al_2O_3. Conditioning was accompanied by gas bursts from the disk and needed much more time than usual, but the final operation of the source was similar to that without disk. To reduce the obstruction of the RF propagation triangularly shaped Ta-disks were produced and oriented either parallel or opposite to the hexapole loss lines (see Figure 48). The tuning became much easier compared to the full disk. A moderately larger current was measured for the parallel compared with the opposite configuration, which could be explained by a larger overlap between the loss triangle and the biased disk in the former case.

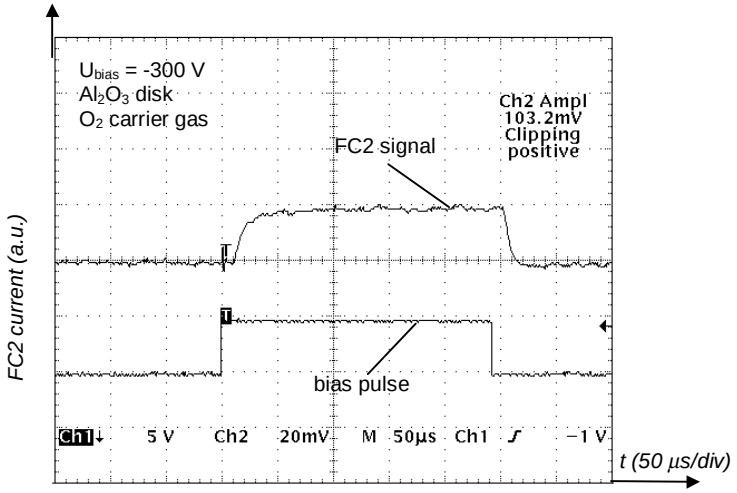

***Figure 47**. Time response to bias pulse in the main pulse region.*

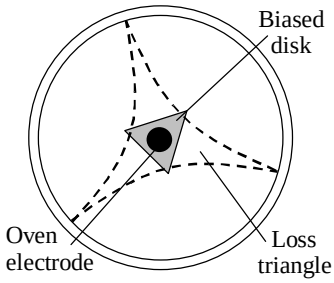

***Figure 48**. Schematic drawing showing a biased disk mounted on the oven electrode opposite to the hexapole loss lines.*

The effect of varying pulse timing

For all geometries we found similar reaction to the timing of the bias voltage pulse. For instance, if the bias pulse is active only during the RF pulse, there is a gain in ion current for the O^{2+}+Pb^{26+} for all cases, in agreement with the positive experience of biased probes used in pulsed and CW sources. The performances for the afterglow optimised Pb^{27+}, however, varied between the different disk types (Figure 49). The gain during the main pulse had no influence on the afterglow if the biasing pulse was switched off before or with the RF.

If the bias pulse is both on the main and the afterglow region, it tends to destabilise the growth of the afterglow, creates a pre-pulse or a faster initial growth of the afterglow, which later slows to the maximum of the Pb^{27+} current.

With a bias pulse active only during the afterglow the current changes only during the on-time and depends on the applied voltage. This, together with the fast response described for in sec. 0, can not be accounted for by the established biased probe theory, i.e. an additional ion production. The phenomenon is instead interpreted as an evidence for a modified extraction condition with the bias pulse active as was suggested in ref. [71,72]. For example, the formation of a beam of energetic electrons oscillating between the puller and the biased probe may affect the extraction and ion transport conditions. A change in the plasma potential as was proposed in ref. [73,74] is also in agreement with our results.

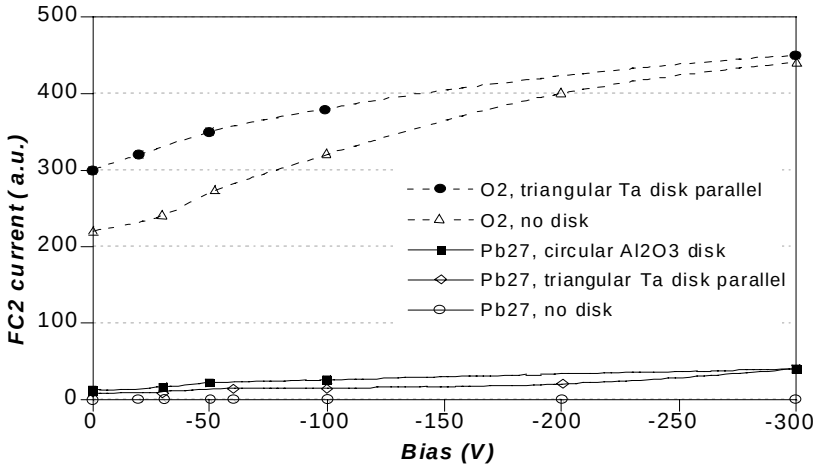

***Figure 49**. Ion yields during the main pulse as function of bias voltage. A clear trend shows higher yields for increased bias voltage as is also observed in most CW sources.*

The effect of varying bias voltage

The afterglow current (in FC2) dependence on the bias voltage for the different geometries is shown in Figure 50. Usually the ion current increases by <10% at around –15 V (depending on the disk) and decreases to a minimum at about -30 V. For lower bias the Pb^{27+} current increases monotonically down to -100 V, usually to values above the level at 0 V bias. For lower bias the current increases only marginally or remains constant. The same behaviour can be seen for the O^{2+}+Pb^{26+} afterglow yield. In fact, without a disk present at the electrode the current increase in FC2 going from 0 to –300 V could be as high as 90%. Maximum recorded peak current was above previous highest achievement of 140 μA in FC2 [78]. However, the acceptance angle (slit size) had most likely been increased in front of FC2, so the results are not completely comparable. The real current increase after the RFQ was <20% for the higher biasing voltages, and always below the record of 100 μA. Nevertheless, with high biasing voltages one could readily produce a large current also for a non-tuned source. Moreover, in general the bias voltage had a noise reducing effect and a long stable afterglow pulse could be achieved (Figure 51).

Other support gases such as Ar and He were also tried. Both gave lower yields of Pb^{27+} ions than with oxygen (57 and 9 μA respectively), but the biased probe could partially compensate for the decrease. In addition to negative bias voltages, a positive pulse of up to +300 V and of different lenghts was applied after the RF-off flank. The idea was to facilitate the ejection of the electrons from the plasma, and to repel the positive ions. No significant enhancement of the ion current was seen neither with nor without (Al_2O_3) disk, only a small noise reduction.

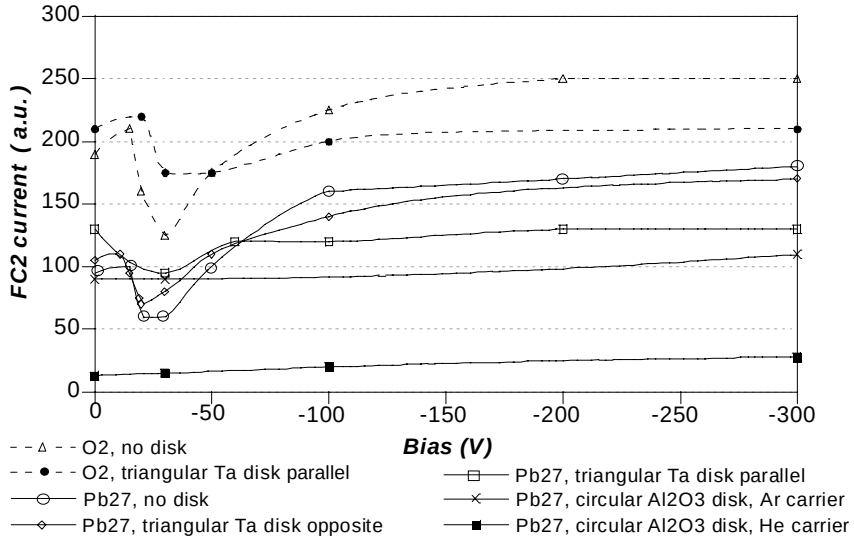

***Figure 50**. Afterglow yields measured in FC2 for Pb^{27+} and O^{2+}+Pb^{26+} as function of bias voltage for various disk and gas combinations.*

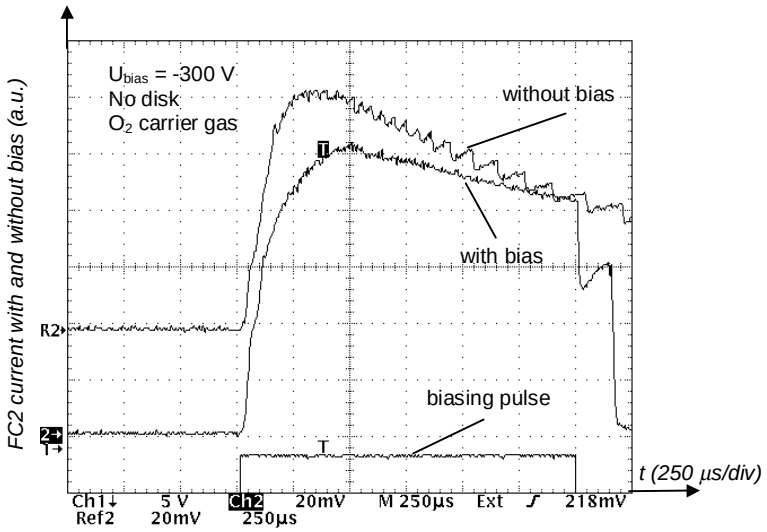

***Figure 51**. Afterglow pulse of Pb^{27+} on FC2. The yield increase is evident and the pulse less noisy. Note the sharp breakdown with bias off.*

2.2.3 Insertion of internal electron donors

2.2.3.1 The idea

As was described in sec. 2.1.3.8 the supply of cold electrons to the ECRIS magnetic trap is necessary to produce large electron density and thereby obtain an efficient ionisation. Plasma chamber coatings with high secondary emission have been tested in several CW ECRIS with a positive effect on the ion current [79]. A chamber liner of aluminium has previously been inserted in the CERN ECR4, but no improvement in the Pb^{27+} current was noticed for afterglow operation.

2.2.3.2 Experiment realisation and results

This time a slab of Al_2O_3 ($40 \cdot 10 \cdot 4\ mm^3$) was inserted in the chamber at the pole tip of the hexapole magnet to be bombarded by plasma particles. Unfortunately, the RF power could not be increased to its nominal value due to heavy discharging. The Al_2O_3, melted by the plasma bombardment, caused this misbehaviour, which started a violent out-gassing and vacuum perturbations.

Next a small sample of LaB_6 (~$50\ mm^2$) was placed just behind the plasma electrode. After adjustments we reached 93% of the nominal intensity for this set-up. Moreover, we had to start up the source fairly slowly in order to avoid discharges and a high load current. Possibly a better result could be obtained with a larger piece of LaB_6 positioned further into the plasma chamber where the plasma particle bombardment rate is higher.

Common weaknesses for both tests was the insufficient cooling of the inserted species, and the far too small emitting surfaces to make a substantial contribution to the electron density in the plasma.

2.2.4 Gas mixing test

2.2.4.1 The idea

Under normal operation oxygen is used as mixing gas for the ECR4 source at CERN. The oxygen abundance completely dominates over the lead. Other gas combinations, such as He, Ar and Ne, have been tried out in the past, without any improvement [56]. As an alternative to oxygen, CF_4 was tried as mixing gas mainly for two reasons:

- F has similar properties as O (mass, electro-negativity).
- The CF_4 molecules (if not immediately dissociated) has several metastable states in the region of 10 to 20 eV that could be excited by lead collisions and act cooling on the lead.

2.2.4.2 Experiment realisation

During the experiment both O_2 and CF_4 were supplied as mixing gases. The source was first optimised using exclusively oxygen, and thereafter CF_4 was introduced to the source in varying quantities. For each

value of CF_4 gas flow, the oxygen in-flow was varied. A clear correlation between the injected amount of CF_4 gas and the extracted Pb^{27+} current was found: the more injected gas, the less extracted current. The Pb^{27+} current decreased to about a tenth of its nominal value for a CF_4 gas pressure in the same region as the optimal oxygen pressure. At a higher CF_4 pressure, the source was almost entirely quenched. First after one day with pure oxygen the source could finally be re-tuned to reach its pre-test current.

2.2.4.3 Discussion

The experiment showed a much poorer yield than expected, and the reasons for this could be manifold. In the case of non-dissociated CF_4 molecules, in spite of the RF, large charge-exchange cross-section between the molecule and the multiply charged lead ions may have impeded the production of highly charged ions. The excitation energies for the metastable states were probably too high to have any influence on the cooling.

It is indeed interesting to note the strong yield quenching effect by the addition of the CF_4. Even after the gas was disconnected, and a good vacuum had been obtained, it was still almost impossible to ignite the plasma. It is suspected that a surface coating on the plasma chamber wall had been created, which produced this "memory effect", or that an inhibiting compound at the oven was formed. Since the yield was quenched only after a combination of CF_4 and an applied RF field[7], it is believed that the memory effect was due to the fluoride and not the CF_4 since the latter should dissociate when the plasma is ignited. We were later informed by other groups about inferior performance using fluorine.

2.2.5 Plasma electrode variations

2.2.5.1 The idea

The objective was to maximise the emptying of the plasma volume from ions. By varying the aperture of the plasma electrode different plasma sizes could be mapped along the magnetic field lines to the extraction hole. Magnetic field calculations performed with POISSON [35] suggest that an aperture larger than the standard plasma electrode is necessary to achieve a complete emptying. However, a maximum aperture size is not evidently optimal as meniscus bulging and ion beam matching to the extraction system become difficult with a large aperture. Moreover, for a large hole the influence of the hexapole field on the ion-beam shape becomes significant and will increase the beam-halo losses. Different plasma electrode apertures were therefore tested, including the complete removal of the plasma electrode. The ECR4 source was originally designed with a 6 mm diameter extraction hole, but is normally operated with a 16 mm hole because of its higher performance.

2.2.5.2 Results and discussion

After more than 40 days of stable operation the 16 mm plasma electrode was exchanged for the smaller with a 6 mm opening. The source showed an extremely poor yield, a factor 1/75 compared to the unmodified set-up, while simulations predicted a current of ~1/8. In spite of tuning, the low current persisted, so the experiment was abandoned and the plasma electrode changed back. Nevertheless, the yield still remained low and spontaneous runaways occurred. Possible explanations for this behaviour could be a malfunctioning oven or too high out-gassing, and therefore no direct conclusions can be drawn from this test.

Following an idea of Geller in ref. [7], the plasma electrode was completely removed. Without a plasma electrode, the plasma should be confined by the magnetic field lines from the hexapole magnet. When tested, Penning discharges occurred in the extraction region, and the nominal extraction voltage could not be reached. A probable explanation is that the differential pumping, usually obtained by the small plasma electrode hole, did not exist anymore and therefore the gas pressure in the extraction region became too high. The only way to prevent discharges was to lower the gas pressure. A shorter gap distance would also have been essential to shape the plasma meniscus.

2.2.6 Moveable puller

An axially moveable puller was designed to allow a continuous variation of the distance between plasma electrode and puller without dismantling the source as in the old design. A current increase is expected for distances larger than tested so far [55]. With a moveable extractor it would be easy to vary

[7] The source performed normally after the CF_4 gas pressure calibration, which was carried out without the RF on.

the distance between the plasma electrode and the extractor in order to optimise the yield and beam profile/emittance for different ion species, charge states and ion currents.

2.2.6.1 Set-up

A replica of the existing puller was made with a few simplifying design modifications. Firstly, no vacuum pumping holes were incorporated at the cylindrical part of the puller, neither a tungsten sheet inside the puller. The rear end of the puller was not threaded but flat to permit sliding inside a Teflon cylinder. Finally, the lip in front of the threaded section was discarded. (See Figure 52 for a comparison between the standard and new puller.) The electrode slides in the Teflon insulator cylinder and is externally adjustable via a gear drive. In addition, a titanium puller was produced with exactly the same geometry as the new puller.

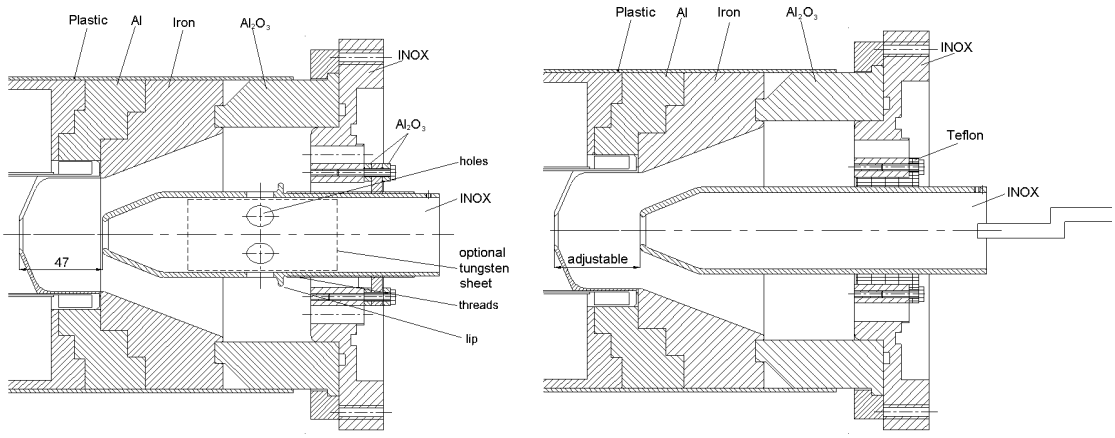

Figure 52. *Standard (left) and new movable (rihgt) puller mounted in the extraction region. The optional tungsten sheet in the old design is not necessary for a functional puller.*

2.2.6.2 Results and discussion

In spite of major efforts we did not manage to condition the movable puller at the first trial, i.e. to apply a nominal extraction voltage of 20 kV, while having the other source parameters as normal. A continuous discharge (several mA) current was drained between the source and ground. Thus, we did not have the opportunity to perform extraction tests with a varying puller-to-plasma electrode distance. A similar general behaviour was seen for the Ti-puller.

With no magnetic field, nor RF applied (and thus no plasma), a normal discharge current between 0.1 and 0.14 mA was noticed for U_{ext}=20 kV, however, with magnetic field on, the discharge current increased abnormally. The vacuum conditions were similar as for normal operation. The explanation for the high discharge current had to be found within the changes introduced with the new puller designs, that meant in either of the following four categories: a ferromagnetic puller material, changed geometry, higher out-gassing rate, or different surface properties.

As was pointed out the discharge current was strongly dependent on the magnetic field in the extraction region and the extraction voltage, not on the RF status. POISSON and PGBUN [80] were used to calculate the magnetic and electric field strengths generated by the solenoids and the extraction system. Penning discharges occur for a field configuration with E perpendicular to B, which can be found in the fairly large volume between the main insulator and the cylindrical side of the puller. The condition for a resonant discharge (correct gas pressure, E- and B-field) could easily be fulfilled because of the varying field gradients. This hypothesis is supported by the noteworthy observation that the holding voltage was independent of the gap distance between the plasma electrode and the puller. Traces of discharges were also seen on the cylindrical part of the puller and at the ceramic insulator.

Remarkable enough, it was sufficient to add a lip to the puller that was similar to the standard configuration to disturb the resonance condition. With the ring on place the full extraction voltage could be applied both on the movable (stainless steel) and the titanium puller with the magnetic field as well as the RF applied. Unfortunately, due to heat expansion of the puller/Teflon cylinder with the RF and extraction active, the moveable puller had a tendency to stick and the tests had to be abandoned until next period of operation. A reconstruction of the mechanism is foreseen, as a moveable puller is highly desirable.

2.3 Final remarks on the afterglow experiments

2.3.1 Conclusions

An extensive investigation of the possibilities to increase the afterglow yield have been carried out. Similar tests to those summarised here have resulted in ion current improvements for ECR ion sources operating in pulsed or CW mode. For the CERN source operating in afterglow mode, no significant current increases have been observed in any of these or previous experiments [55,56]. Nevertheless, with a high negative bias applied, even a non-tuned source was able to deliver a high current, close to the top values. In addition, the bias voltage had a noise reducing effect and a long stable afterglow pulse could be achieved. In spite of these positive features it was decided not to use the probe for routine operation since the source did perform, after long and careful conditioning, with similarly high values. In different situations, where the ion species and the source conditions are more often changed, the biased probe will help to reach optimum performance in a much shorter time.

The biased probe study confirmed that the probe does not influence the total ion content of the ECR plasma to a first approximation. The fast response to the pulsed biased voltage is not consistent with the time constant for production of highly charged ions. Affected extraction conditions is a more likely explanation.

There seems to be an absolute maximum Pb^{27+} ion current extractable under normal stable operation conditions. Either the yield enhancement 'tricks' are not applicable on the afterglow mode, or the ECR4 ion source performance may already be maximised, i.e. an enhanced production of highly charged ions, or a more rapid extraction of the ions only result in instabilities or break down of the afterglow reservoir.

One may discuss if the plasma cut-off is reached or not. For 14.5 GHz the plasma cut-off occurs at $n_e=2.4\cdot10^{12}$ cm^{-3}. Assuming that the effective trapping volume for the ions is restricted to be within the ECR boundaries (approximate 6 cm long, 2 cm radius $\Rightarrow$ 75 cm^3), the stored charge is ~30 μC. The ions leave the source in two directions, thus ~15 μC should be collected at the extraction side (neglecting radial losses to the hexapole). The measured total extracted ion current is about 2.6 mA during the main pulse (RF on) and increases (over about 300 μs) to approximately 5 mA after the RF is switched off. For a 1 ms long afterglow pulse, this corresponds to 5 μC, a factor three below what can be expected for the source near the plasma cut-off. Considering that the radial losses were neglected and that the volume estimation was very approximate, the cut-off hypothesis can not be ruled out. The saturation in ion yield for an RF power >1300 W may support this theory as well.

Two different phenomena could explain why the afterglow could not be compressed in time. Either the reason is a limited effect of the biased electrode on the internal ion release from the source, or transport limitations in the extraction system. The first argument suggests that an abrupt and critical disturbance of the plasma (i.e. plasma instability) causing the ions to leave the plasma could not be created with the moderate bias voltage used in the tests. Considering the short Debye length inside the plasma (~0.1 mm) and the strong confinement of the hot electron population, this is comprehensible. An alternative is the PuMa method with a fast pulsed magnetic field [81], but this would imply a totally new source design. The second argument is based on the fact that the extraction system has a limited perveance. The approximate formula:

$$I_q = \frac{\varepsilon_0}{9}\sqrt{\frac{2q}{m_i}}\cdot\frac{\pi d^2}{L^2}V^{3/2} \qquad \textbf{(14)}$$

gives the maximal extractable current from a convergent plasma meniscus with diameter d (m) in a magnetic field free region and with a gap distance L (m). Inserting ECR4 parameters, one arrives at a current of ~5 mA (compare with a measured afterglow peak in FC1 of about 5 mA). The transportable current estimation is a somewhat pessimistic, and according to beam extraction simulations that were carried out the ECRIS field picture (magnetic and electrostatic) allows the plasma meniscus to be less convergent than for the non-magnetic case and a higher current is therefore transportable. Nevertheless, for an increased plasma density and/or increased afterglow yield, a shorter gap distance than 47 mm could be advantageous to adjust the plasma meniscus shape.

2.3.2 Outlook

The afterglow investigations are still going on, and in the near future three experimental projects are foreseen. First of all a plasma chamber of aluminium has been manufactured, but not yet tested. The aluminium surface is naturally oxidised, and could conceivably act as an electron donor to the plasma.

Given that the cause for the HV sparking with the moveable puller has been eliminated, the optimisation of the extraction-gap distance can be performed in a controlled way without having to open up the source. The optimal setting, with respect to yield, beam focusing and emittance, should be easy to find for different ion species.

Not reported here, since the experiment is only in its starting-up phase, is the installation of a completely new high-performance x-ray measuring system for the ECR source. The detector has been installed and some initial measurements have been carried out. An x-ray diagnostics system based on a Ge-crystal detector with an 8 µm Be-window will give information about the characteristic x-rays of the ions and bremsstrahlung from the electrons emitted from the ECR plasma. The wide energy-range of the detector, 500 eV to ~500 keV, allows determination of the energies for both the cold and hot elect rons. Since the measurement is time-resolved, the plasma build-up and release can be studied, and hopefully contribute to the understanding of the processes in the plasma and the afterglow ion release.

In the drive for higher beam intensities the extraction system must not be neglected. Space-charge effects are evident in the extraction region and the plasma meniscus may be distorted for higher plasma densities. As a consequence of the higher plasma density and higher extracted current, one may end up with a strongly divergent beam, which is difficult to transfer and inject into the RFQ. For this reason, extensive beam extraction simulations, using different particle tracking programmes as KOBRA3 [82], IGUN [83] and PBGUN [80], have been carried out. The properties of the propagated beam have been found to be strongly dependent on the starting conditions of the ions. Varying the unknown user-input parameters, such as particle distribution inside the plasma, electron temperature and initial ion velocity, within plausible limits could bring about completely different results. Still, simulations utilising these programmes could give guidelines for improved extraction systems (multi-electrode systems to allow for higher extraction voltage, grids etc).

In summary one can state that the knowledge of the afterglow has increased with these experiments, especially the understanding of the biased probe effect which has been given an alternative explanation. However, further investigation is essential to find the answers to some of the important questions for future ECRIS development that remain unanswered, for instance:

- What scaling laws apply for the afterglow?
- Is there a gain using a larger source volume?
- Could higher afterglow currents be expected from the next generation of ECR sources with higher RF frequency and/or magnetic field?

Part III – The LHCEBIS proposal

3.1 LHC and its ion pre-injectors

With the advent of the Large Hadron Collider (LHC) [15] in 2006 the request for higher ion beam intensities than presently available from the CERN heavy ion pre-injector, LINAC3 [13,14], arises. The idea of using an EBIS as ion source has therefore been theoretically investigated, and instead of looking in the direction of RHIC [84] with its high performance next-generation EBIS [50,85,86], an innovative concept with the REXEBIS as base was explored. The feasibility study resulted in a proposal [87,P6], which will be discussed in a condensed form here. First, however, the upcoming LHC accelerator will be explained in a few sentences; thereafter follows a summary of the alternative injector chains that are foreseen, together with the possible ion source solutions.

3.1.1 The Large Hadron Collider

The Large Hadron Collider, currently under construction at CERN, will become the accelerator with the world's highest energy when it starts up in 2006. With its 27 km circumference, it will also be the world's largest cryo-installation since the superconducting magnets will be cooled down to 1.4 K by superfluid helium. The LHC will be a versatile accelerator that can collide proton beams with energies around 7 TeV and with beam crossing points of unsurpassed luminosity providing the experiments with high interaction rates. Furthermore, it can collide beams of ions (Pb, In, Ar, He) for the ALICE detector [88] with a total collision energy in excess of 1150 TeV (for lead). The energy available for collisions between the constituents of the protons (the quarks and gluons) will reach the TeV range, that is about 10 times that of LEP and the Fermilab Tevatron. In order to maintain an equally effective physics program at the higher energy E the luminosity of a collider should increase in proportion to E^2, which generates stringent conditions on the beam quality, thus also on the ion source.

3.1.2 The injector chain

3.1.2.1 Beam requirements

In order to have a reasonable collision rate in the ALICE detector (608 bunches per ring, $1 \cdot 10^8$ Pb^{82+} per bunch, 9 min. filling per ring), the particle production rate of the injector chain to the LHC has to be increased dramatically from the level obtainable with the present scheme. The maximum lead beam, produced from the present ECR4 lead source (see sec. 2.1.4), that is accelerated in LINAC3 before stripping has a luminosity which is a factor ~150 too low. That means the number of ions, N, per bunch needs to be increased by a factor of ~10.

A higher ion production rate is not adequate since the intensity increase must fit within an unchanged transverse emittance, ε, because: (i) the collider luminosity is proportional to N^2/ε; (ii) ion losses at injection into the collider are reduced with a smaller emittance reducing the risk of quenching a superconducting magnet. The higher ion production may be achieved in several ways, and four pre-injector ion source scenarios are summarised below. A schematic picture of the full LHC injector complex is presented in Figure 53.

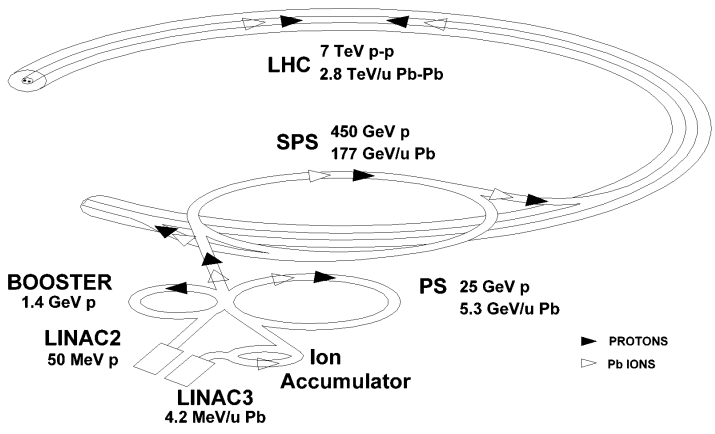

***Figure 53**. The LHC injector complex indicating the acceleration scheme for protons and ions. The LHC has two separate beam tubes for particles rotating in each direction.*

3.1.2.2 Present ECR4 lead source in combination with LEIR

If the present ECR4 ion source is to be used, the former Low-Energy Antiproton Ring (LEAR) will be converted into a Low-Energy Ion Ring (LEIR) [89]. LEIR is to act as a low-energy accumulator where the ion beam is stacked and cooled (with the help of an electron-cooler) to reach the required intensity and emittances. An intensity of 100 μA of Pb^{27+} is expected in the afterglow pulse (sec. 2.1.3.7) for 100 to 300 μs (repetition rate 10 Hz). The beam will be accelerated to 4.2 MeV/u and subsequently stripped to Pb^{54+}. The goal is to multi-turn inject the 150 μs pulse from LINAC3 into LEIR (~50 turns), and accumulate $1.2 \cdot 10^9$ ions/cycle for a 3.6 s duration. After having accumulated and cooled the beam down to the required emittance the ion beam is bunched, accelerated to 14.8 MeV/u and transferred to PS. The beam is accelerated in the PS and fully stripped prior to transfer to the SPS (see Figure 54, top). An upgrading of the LEIR vacuum and cooling time is necessary for this scheme to be successful [89,90].

3.1.2.3 The PHOENIX ECRIS option

A new type of ECRIS is under development, the so-called PHOENIX [91]. This is an improvement of the ECR4 source, operating with a higher mirror ratio and with a 2.5 times larger plasma volume. Typically a factor of 10 increase in extracted current, i.e. 1 emA of Pb^{27+} in the afterglow, is expected based on volume and frequency scaling. This would mean that the luminosity goal could be reached without using LEIR. Consequently, the LINAC3 beam could be directed to the PS Booster instead, for further acceleration in PS at the next stage. Using LEIR anyhow would smooth out the afterglow variations.

3.1.2.4 The Laser Ion Source option

The Laser Ion Source (LIS) [92] concept makes use of CO_2 laser to produce a short (~5 μs) high current (5.5 mA) pulse of $\sim 7.5 \cdot 10^9$ Pb^{25+} ions/s. In the same way as above, the ions are accelerated in LINAC3 and stripped at the carbon foil to Pb^{54+}, and thereafter single-turn injected into the PS Booster instead of LEIR. With a stripping efficiency of η=0.2, the number of ions out of LINAC3 amounts to $1.2 \cdot 10^9$ per pulse. The main advantage is the single-turn injection viability, thus no need for LEIR.

3.1.2.5 The LHCEBIS option

The ion expulsion out of an EBIS can be very fast, in the range of 5 to 10 μs, thus allowing single-turn or a few turn injection into the PS Booster in a similar way as for the LIS concept. The source would operate with a repetition rate of 0.8 Hz, and the extracted yield should be $1.6 \cdot 10^9$ Pb^{54+} per pulse. Ions would be accelerated in LINAC3, but the need for the first stripper foil is avoided, and thereafter directly accelerated in the PS Booster (see Figure 54, bottom part).

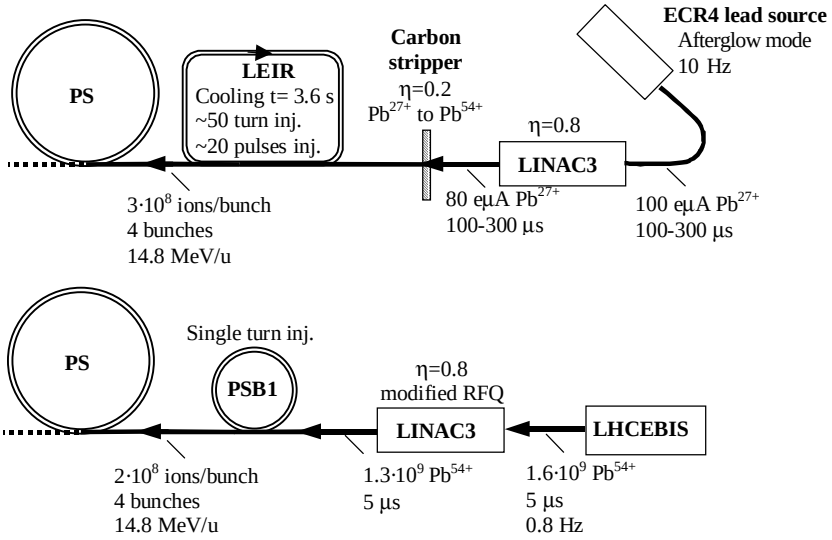

***Figure 54**. The first elements in the LHC injector chain schematically depicted for two different concepts. The present ECR4 lead source in combination with LEIR (top), and single-turn injection into PS Booster with ions produced in an EBIS.*

3.2 The LHCEBIS concept

3.2.1 Introduction

The use of an EBIS as ion source for large heavy-ion collider projects such as LHC or RHIC is by no means new [93]; in fact the RHIC project is investigating the possibility experimentally. The main challenge when using an EBIS as an ion source for a large heavy-ion injector is to create sufficient negative space charge to confine the large positively charged ion-cloud. So far the standard solution to the space-charge problem has been to increase the electron-beam current, which has required the development of a new generation of EBIS. Nevertheless, my approach is different, as the LHCEBIS makes use of the high space-charge capacity, C, of the trap for low electron-beam energies, demonstrated by:

$$C = \frac{1.05 \cdot 10^{13} \cdot I_e L}{\sqrt{E_e}} f \quad elementary\ charges \qquad \textbf{(15)}$$

where L (m) is the trap length, f the degree of compensation (0<f<1), I_e (A) and E_e (eV) the electron current and energy, respectively. As seen from the formula, one way to increase the negative charge is to decrease the electron-beam energy E_e (the lower limit for a specific I_e is set by the perveance). A low electron-beam energy is adequate for the LHCEBIS since the lead ions do not have to be fully stripped. The second idea is to make use of the so-called closed shell-effect. That means boosting the fraction of ions in the desired charge state from about 20% (normal breeding) to at least 50% by choosing the electron-beam energy just below the ionisation energy of the next charge state. Operation with a closed shell-effect breeding leads to a more effective use of the confining negative space charge (i.e. the electron current), which can therefore be decreased by a factor of two. Keeping the electron-beam current low has several advantages [P6] but the design involves some new and unexplored areas and the implications had to be investigated.

3.2.2 General design aspects and theory

3.2.2.1 Basic design

The proposed EBIS has a design very similar to the REXEBIS [P1,P7] even if the former is to be used for a completely different purpose (see sec. 1.1.4.3). The constructional changes that are needed to adapt an REXEBIS to LHCEBIS performances concern mainly the electron gun, which will have to deliver 1.5 A instead of 0.5 A. Furthermore the drift tube structure should allow for fast extraction, and the ion extraction system should be capable of handling high currents. See Figure 55 for a schematic drawing of the LHCEBIS.

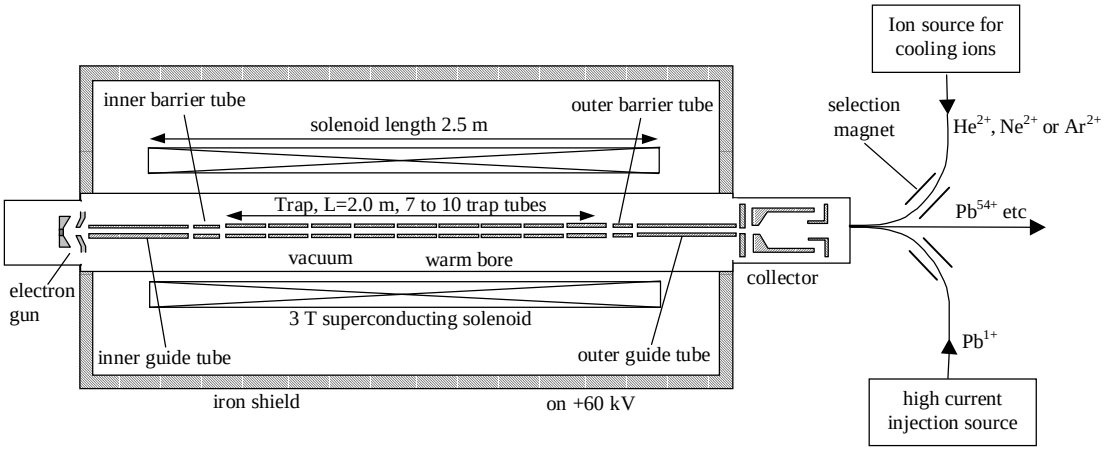

***Figure 55**. Schematic drawing of the LHCEBIS showing the most important elements. (Not to scale.)*

3.2.2.2 Charge-state

The LHCEBIS would deliver lead ions with charge state 54^+, meaning that the first stripper stage at 4.2 MeV/u after LINAC3 becomes obsolete. As a consequence of the transition from electronic n- to m-shell, the ionisation potential for lead 53^+ and 54^+ ions increases significantly from about 3.3 keV to 5.4 keV [94]. That means by operating the EBIS at an electron-beam energy below 5.4 keV, most ions will end up as Pb^{54+} after some time of breeding. The charge-state development for lead ions bombarded with 5 keV electrons is shown below (Figure 56). Note that the calculation shown in the left plot does not include any recombination processes, neither ion loss effects due to ion heating by electron Coulomb scattering. The dielectronic recombination with the electron beam will be negligible (the recombination rate with secondary electrons, however, is not fully known) in the LHCEBIS. The charge exchange probability between a neutral gas (assume a H_2 pressure of 10^{-11} mbar) and a Pb^{54+} ion (150 eV kinetic energy) during 1 s is calculated to be about 2% using Müller and Salzborn's formula [95] for electron transfer from atoms or molecules to highly charged ions. The narrow charge-state distribution, which is a consequence of the pulsed injection, leads to a very small charge exchange rate between lead-ions. As will be demonstrated below, the ion losses due to heating and subsequent radial escape can also be kept small. Nevertheless, the radiative recombination seems to be non-negligible [96] and the cross-section ratio ($\sigma_{ion}/\sigma_{radiative}$) for electron-beam energies close to the next charge state (55^+) is approximately 2, calculated with radiative recombination cross-section formula described in ref. [97]. When taking the radiative recombination into account, the charge-state evolution is modified as shown in the right plot in Figure 56. One has to keep in mind that both the ionisation and recombination cross-sections are based on theoretical calculations, meaning that the real number of Pb^{54+} ions may be larger or smaller.

3.2.2.3 Space charge

The proposed LHCEBIS has a total trap capacity of 70 nC, which means, assuming a maximal trap compensation of 50% (>60% reached at the REXEBIS [P2], see also ref. [86]), a useful space charge of ~35 nC. From the charge evolution graph in Figure 56 (including radiative recombination) it is clear that the relative abundance of Pb^{54+} ions can be 50%, which equals an effective trap capacity of $\sim 2 \cdot 10^9$ Pb^{54+} ions.

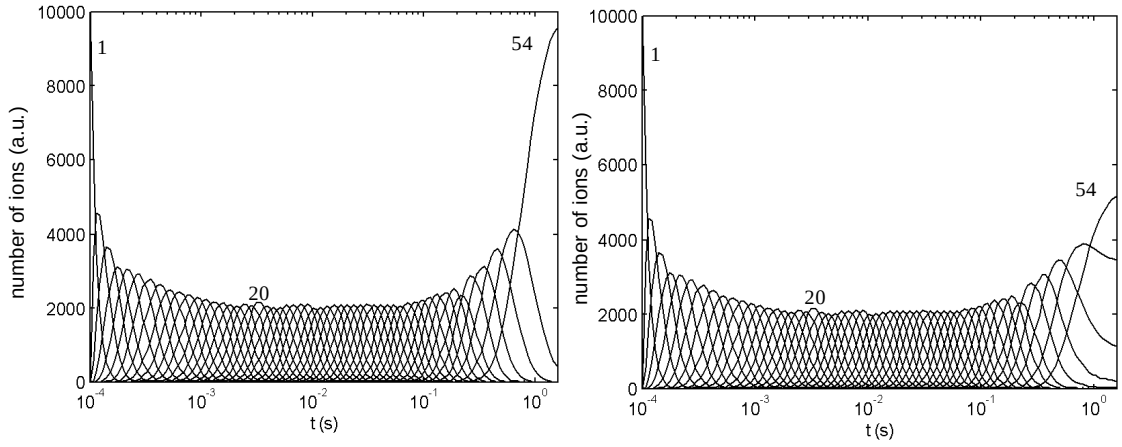

Figure 56*. Relative charge-state abundance for Pb stepwise ionised by a 5 keV electron beam (radiative recombination excluded and included in left and right plot, respectively).*

The number of cooling ions, and therefore the amount of uselessly occupied negative space charge, has never been measured for lead in an EBIS and therefore remains to be investigated experimentally. Residual gases are also ionised and trapped within the electron beam. A total residual gas pressure of 10^{-11} mbar should be achievable inside the trap region yielding a space-charge compensation of less than 5% for a 1 s breeding period. A positive side effect of the residual gas is its evaporative cooling effect on the hot lead ions.

An EBIS is virtually indifferent to the ion species that are injected for breeding. Thus, the EBIS is also capable of breeding for example O, Ca and Nb as shown in Table 4.

Ion	Peak charge	Breeding time	Abundance	Ions per pulse
Lead (Pb)	54^+	1 s	50%	$2{\cdot}10^9$
Lead (Pb)	27^+	0.01 s	20%	$8{\cdot}10^8$
Oxygen (O)	8^+	0.1 s	50%	$1.7{\cdot}10^{10}$
Calcium (Ca)	18^+	0.5 s	50%	$7{\cdot}10^9$
Niobium (Nb)	31^+	0.3 s	50%	$4{\cdot}10^9$

***Table 4**. Ion yield per pulse for the proposed LHCEBIS assuming 50% compensation and j_e=400 A/cm^2. Closed shell effects used in all cases except for Pb^{27+} and Nb^{31+}; the former is presented for comparison.*

3.2.3 The breeding cycle

3.2.3.1 Injection

The lead is introduced into the trap region by external ion injection, i.e. Pb^{1+} ions are produced in a high-current external ion source (for example an RF-source or a MEVVA [98]) and then injected into the EBIS.

In principle, two different injection scenarios are possible. The first implies pulsed injection (~15 μA during 50 μs), corresponding to a total number of ~$4.7{\cdot}10^9$ Pb^{1+} ions. This is only slightly more lead ions than needed for LHC, thus, very little boiling-off during the breeding phase is allowed. To ensure a minimal degree of boiling-off and radial heating, evaporative ion cooling can be used. In addition, the 1^+ ions should be injected into the very bottom of the electron-beam potential[8]. It then follows that the ions are completely trapped inside the electron beam, and they have a low initial temperature.

The alternative method is to completely fill the trap with Pb^{+1} ions, i.e. to compensate it already at injection. Since the external ion sources are limited in current, slow injection has to be used; that means a 2.5 μA[9] beam is injected for some ten milliseconds over a previously raised outer barrier. The temperature of these ions inside the trap is higher than in the previous alternative, and during breeding most of the Pb ions are boiled-off, so only a fraction of the initial number of ions remains when the bunch of Pb^{54+} is extracted.

The need for lowering the trap tube potential as the breeding progresses and the electron-beam space charge becomes neutralised to keep the electron-beam energy at 5 keV is a shortcoming of the first method. For the second method the trap is fully compensated at injection, and the trap tube voltage can be kept fixed during breeding. Experiments have to decide which of the methods (or a mixture of both) provides the highest number of Pb^{54+} after the breeding has finished.

3.2.3.2 Breeding

As was shown in Figure 56, a breeding time of ~1 s is needed to reach Pb^{54+} at a current density of 400 A/cm^2. Thus, the EBIS can work with a repetition rate of almost 1 Hz if one assumes complete trapping within the electron beam, because the extra time required for injection, extraction and cleaning is negligible.

According to ref. [5], the radial holding voltage, i.e. the radial voltage needed to prevent the Pb^{54+} ions from escaping due to the elastic small-angle Coulomb scattering with the electron beam, is in the order of 20 V, which is much less than the radial voltage from the electron-beam well. Thus, there is little danger from an ion loss perspective. However, since the ions may not be perfectly injected into the bottom of the potential well of the electron beam, after compensation a certain fraction will have the energy to leave the electron-beam potential well regardless of heating or not. If the injection energy exceeds 160 eV (see sec. 3.2.5.3), temporal beam escape will occur when the compensation level reaches 50%. This has to be compensated for by an increase in confinement time or electron current-density. In fact, the 1.2 s confinement requirement is based on an electron density of 400 A/cm^2, but in reality one can expect a density of 450 A/cm^2 from the design. However, an even higher current density might be necessary due to the neutralisation.

[8] Due to the small acceptance for ion injection at the bottom of the electron beam potential [P7], the injection current might have to be larger than 15 μA if the emittance of the external ion source is poor.

[9] With an injection time of 15 ms, the injection current has to be 2.5 μA to fill the trap to 50% (~35 nC). However, due to a low efficiency for continuous injection, the injection current may have to be two orders of magnitude larger.

To reduce the temperature of the lead ions evaporative ion cooling is suggested. The cooling ions could either be introduced into the trapping region via ordinary gas injection, or by slow external ion injection. Using the latter method one would gain control over the exact amount of injected coolant, as well as the timing for cooling. Nevertheless, for this method to be successful, the cooling ions have to be injected into the trapping region with a very low energy.

3.2.3.3 Extraction

After breeding, the ions are extracted from the trap region by fast extraction. That means, an axial electric field gradient extending over the whole trapping region is applied during the extraction phase to push the ions out and, by doing so, single turn injection into the Booster is attainable. Experiments with fast extraction have already proven that it is possible to reach very short extraction times, e.g. 10 μs FWHM for Xe ions in a 750 mm long trap [50]. In case the requirement of 5.5 μs (the revolution time of the Booster) is unreachable for practical reasons, and the transverse emittance is sufficiently low, one could consider 2 to 4 turn injection into the Booster.

An additional method, the so called accelerated potential wall has been suggested in ref. [99] and, if successfully applied at the LHCEBIS, all ions may be extracted with the same low radial energy dispersion of the 50% neutralised beam. The effectiveness of this has not yet been proven experimentally.

The injection energy into the present RFQ in LINAC3 is 2.5 keV/u, resulting in a low extraction voltage of 10 kV for Pb^{54+}. A more convenient extraction voltage, from a space charge and energy spread point-of-view, would be 50-60 kV. The extraction efficiency out of the EBIS should exceed 80%.

3.2.4 Beam properties

3.2.4.1 Transverse emittance

The optimal non-normalised transverse emittance for the LHCEBIS at an extraction voltage of 60 kV is estimated to 4 π mm mrad (2σ) using the acceptance formula in ref. [P7]. This very small emittance presumes a full compensation of the electron beam in the active trapping region during the whole extraction cycle, a requirement that is not possible to attain. Furthermore all ions should be fully trapped within the radius of the electron beam. With 50% compensation the emittance may increase to a value of 40 π mm mrad (2σ) (ε_n=0.06 μm). This is within the 0.1 μm LHC specifies as maximum emittance for the ion source. The accelerated wall concept is essential to keep the compensation level high throughout the extraction phase. Even so, in the collector region where the ions are separated from the electrons and still move with a relatively low velocity, space-charge blow-up may occur which could blow-up the emittance unless precaution is taken.

3.2.4.2 Energy spread

Ions extracted from an EBIS in general have a finite energy spread caused by: finite injection energy; ion heating due to elastic electron-ion collisions; ion heating due to ionisation at different radii (i.e. at different electrostatic potentials); trap potential decrease during the extraction phase; and linear axial electrical field gradient inside the trap needed for fast extraction. When using fast extraction the latter is dominant. This means an energy spread of approximately ±500·Q eV to ±2000·Q eV for t_{ext}=10 μs and 5 μs, respectively. Thus, the analysing magnets in the present LEBT at LINAC3 can not be employed. Instead the beam, mainly containing Pb^{54+}, should be injected directly into an RFQ with a high energy-spread acceptance. Simulations have shown that a very high transmission, >95%, through an RFQ can be obtained for an energy spread as high as 20% [100] if all matching conditions are perfectly fulfilled.

3.2.4.3 Space charge blow-up

Due to the short extraction time, the peak ion-current is as high as 4 mA. Therefore the EBIS to RFQ distance should be minimised to avoid space-charge blow-up. Moreover, a short distance reduces the charge-exchange losses with the residual gas, even if the losses should be negligible for a pressure better than 10^{-9} mbar (a pressure necessary to reach the intended good vacuum inside the EBIS). One lens is obligatory to focus the beam into the RFQ.

3.2.5 Mechanical design

3.2.5.1 Solenoid

Similar to the REXEBIS, the solenoid, with a full field length of 2.0 m (total length 2.5 m), is iron shielded and of warm-bore type, i.e. the inner cylinder is at room temperature. Some of the advantages of this was explained in sec. 1.2.2.

3.2.5.2 Electron gun

The electron beam will be generated in a semi-immersed gun (cathode field ~0.2 T). The flat cathode, LaB_6 with 310-crystal orientation, can have high emission density (j_c~30 A/cm^2) with a lifetime of approximately 1 year (somewhat higher emission density is possible with an IrCe cathode). With an anode voltage of 10 000 V the gun perveance becomes a moderate 1.5 microperv for a 1.5 A electron beam. After the emission from the electron gun, the beam is compressed by the increasing magnetic field strength (approximately linearly to B) when entering the solenoid, resulting in an electron current density of >400 A/cm^2 in full magnetic field. At the axial position corresponding to a field strength of about 1 T, the electron-beam energy is decreased from 10 to 5 keV, and thereby the perveance is increased to a relatively high value of 4.2 microperv.

3.2.5.3 Drift tube structure

The system of drift tubes, defining the extension of the trap in longitudinal direction and the electron-beam energy, is shown in Figure 55. The drift tube structure will be mounted in vacuum inside the room temperature bore of the solenoid. To reach UHV (10^{-11} mbar) inside the EBIS, turbopumps on each side of the solenoid, and NEG strips or other getter pumping inside the trapping region are necessary.

With a large drift tube radius, or more correctly, tube-to-electron-beam radius ratio, the radial ion losses are kept low because of the considerable potential well. When the electron beam becomes compensated and the radial holding voltage therefore decreases, the ions may have sufficient energy to leave the electron beam radially and be lost at the drift tubes. To keep this radial ion loss as low as possible, and to minimise beam instabilities, it is desirable to have a large tube radius. On the other hand, the perveance limits the tube radius to maximum 4 mm.

A non-compensated electron beam of 1.5 A creates a potential well ΔU of 320 V, and a total beam-axis to drift-tube voltage of 2100 V for 0.25 mm beam radius and 4 mm tube radius. Even with a 50% trap compensation, the radial holding voltage is ~1000 V which exceeds by far the radial heating (in the order of 20 eV). Thus, the ion losses in radial direction are expected to be low, and can be made very small also in the longitudinal direction if the barrier potentials are high enough.

Because of the axial electric field gradient necessary to obtain a fast extraction, 7 to 10 trapping tubes are required to create the field. Additionally four tubes (barrier as well as inner and outer guide tubes) are needed, in total 11 to 14 tubes. More tubes are undesirable as it increases the risks of self-induced RF generation. Instead of several separated cylindrical tubes, the same field gradient effect can be obtained by a few electrodes, which intermesh without touching each other [101].

3.2.5.4 Electron collector

With a collector potential of +3 kV relative to the cathode, the deposited energy on the collector surface, which has to be cooled, is 4.5 kW. Compared to many other EBIS, the collector has an open design with a large diameter extractor extending into the collector, see Figure 57. A large, open end should ensure that the ion beam aberrations are kept small and the vacuum good. No extra bucking or transverse magnet correcting coils are foreseen. However, the collector will be surrounded by an iron cylinder to decrease the magnetic field inside the collector region, and thereby improve the electron-beam expansion and collection.

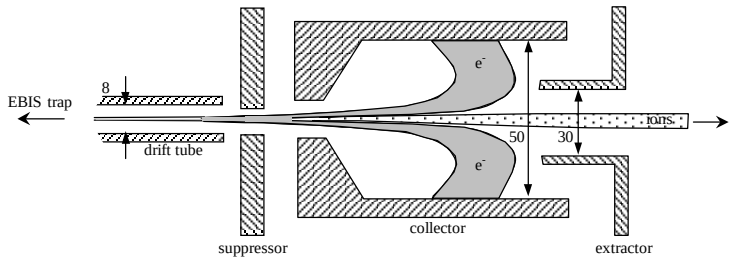

Figure 57*. Schematic drawing of the electron collector. Note the open collector end and the large extractor diameter. (Not to scale. Typical dimensions and beam shapes indicated.)*

3.3 Experimental test at CRYSIS

3.3.1 Motivation and goal

Lead breeding tests were carried out at CRYSIS [46], the EBIS installed at the Manne Siegbahn Laboratory, in Stockholm. The goal of the experiment was to determine the maximum attainable ratio of $\frac{Pb^{54+}}{\sum_i Pb^{i+}}$ in the pulse extracted from CRYSIS. This means essentially to determine the equilibrium-state between radiative recombination, charge exchange (between Pb^{54+} and rest-gas or lower charged lead ions), heating losses and production of Pb^{54+} by ionisation, for a low electron-beam energy of 5 keV. From the result one can conclude whether closed-shell breeding is favourable compared to ordinary EBIS breeding with its higher electron-beam energy and consequently broader charge-state distribution.

3.3.2 Set-up and experimental procedure

Lead ions of low charge were produced in a CHORDIS [102,103]. Singly charged ions were selected in the separator magnet and thereafter transferred via the INIS beam line [103] at 20 kV to CRYSIS (660 nA measured beam intensity at the FC in the INIS line and at the transparent harp close to CRYSIS). At the EBIS platform the beam was retarded to 1 keV, and injected over the outer barrier into the trapping region.

Due to the inherent properties of CRYSIS, only a modest electron beam of about 45-50 mA could be produced at 5 keV electron energy. As a result, the electron-beam density was very low, and therefore a long breeding was necessary. The electron-beam well ΔU was only 10 V, while the beam-axis to trapping-tube potential difference was 60 V. The trapping capacity of the electron beam reached 1.1 nC.

3.3.3 Breeding results

The experiment was a success in view of the fact that injection into an electron beam of less than 50 mA at an energy of 5 keV (unusual running parameters for CRYSIS) was feasible. A maximum neutralisation of 60% was attained. The electron-beam current-density was determined to be between 12 and 14 A/cm^2, in good agreement with the theoretical value of 12 A/cm^2 [P12].

Due to the very low electron-beam current-density, a confinement time of ~50 s was necessary to produce Pb^{54+}. For such long breeding times no ions were found in the TOF spectra. After a confinement time of 10 s the TOF spectrum peaked at Pb^{38+} and the highest detectable charge state corresponded to Pb^{45+}. Neon gas was introduced into the source with the aim of increasing the higher charge states, and indeed an intensity increase of a factor 2.5 was recorded at shorter breeding times, but the charge-state distribution was not shifted to higher charge states.

3.3.4 Discussion and conclusions

The goal, to produce Pb^{54+} ion, was not reached in this experiment. Several possible explanations can be found:

- For example, the ion heating voltage from the electron beam was predicted to be close to 20 V, a value of the same order as ΔU. Thus, radial boil-off was unavoidable.
- Charge exchange between highly charged lead ions and lead ions of lower charge or rest-gas ions could have reduced the Pb^{54+} feeding. The cross-section for charge exchange between Pb^{45+} and hydrogen is approximately 10^{-13} cm^2. With a hydrogen rest-gas pressure of 10^{-11} mbar, a lead ion kinetic energy of 30 eV, and breeding times longer than 10 s, the probability for charge exchange reaches close to 10%.
- The optimal beam transport settings may have changed when going from low to high-charged ions in case of the presence of a magnetic stray field. Finally, problems of technical nature might have seriously hampered the performance for breeding times longer than ~15 s.

All these effects can nonetheless be avoided in a dedicated LHCEBIS.

3.4 LHCEBIS conclusions and outlook

3.4.1 Prospective

The argumentation has shown that an EBIS could meet the requirements imposed on an ion injector for LHC if direct injection into the PS Booster were to be used instead of accumulation in the LEIR. Table 5 shows an estimation of the ion balance for the LHCEBIS concept, with a pulse yield after the LINAC3 exceeding the constraint of $1.25 \cdot 10^9$ Pb^{54+} ions required for single-turn injection into the Booster. Consequently, it might not be necessary to develop and exploit a high current and high energy EBIS, nor to use four separate EBIS (one for each Booster ring). Instead, an alternative route with a design similar to the REXEBIS can be taken, which makes use of an electron beam with relatively low current and energy, and utilises the closed shell effect. Table 6 summaries its design properties.

3.4.2 Reservations

Nevertheless, the LHCEBIS design has a few uncertainties that need further investigation before one can confidently claim that the concept will fulfil its promises. The electron beam has a high perveance that can make the propagation through the drift tubes difficult. Besides, the relatively small drift tube radius can possibly cause alignment problems and excessive ions losses. It is not clear what fraction of the available negative space charge will be occupied by cooling gas ions and, most important, it remains to examine experimentally how the radiative recombination will effect the abundance of Pb^{54+}. Finally, the fast extraction brings about a high space charge in the collector region before the ions are accelerated to 60·Q keV, which could cause emittance enlargement. The high peak current has to be transported to and injected efficiently into a large energy spread accepting RFQ.

Total available space-charge	$4.4 \cdot 10^{11}$ elementary charges
50% attainable space-charge	$2.2 \cdot 10^{11}$ elementary charges
50% Pb^{54+} abundance (due to radiative recombination, rest-gas, cooling gas etc)	$2.0 \cdot 10^9$ Pb^{54+} ions
80% EBIS extraction efficiency	$1.6 \cdot 10^9$ Pb^{54+} ions
80% LINAC transmission (Pb^{54+} after LINAC)	$1.3 \cdot 10^9$ Pb^{54+} ions

Table 5. *Space-charge availability and number of ions for the different steps in the LHCEBIS concept.*

Cross-section measurements as well as cooling gas studies (determining optimal gas type, quantity and its space-charge occupation) could most likely be performed at the REXEBIS at ISOLDE when it becomes fully operational. Additionally, the substantial task of time-resolved extraction simulations (including space charge and charge-state distribution) remains in order to verify the feasibility of the proposal. Further results from the studies of an RFQ for the RHIC EBIS are highly anticipated.

Electron energy (gun) / (trap)	10 keV / 5 keV
Electron current	1.5 A
Electron current density	>400 A/cm^2
Extracted ion energy spread	0.3 to 1 keV/u
Trap length	2.0 m
Full magnetic field	3 T
Total charge capacity	$4.4 \cdot 10^{11}$ elementary charges
Yield Pb^{54+}	$1.6 \cdot 10^9$ ions
Normalised transverse emittance	0.06 μm
Ion extraction energy	~15.6 keV/u

Table 6*. Design parameters for the proposed EBIS for the LHC lead ion pre-injector.*

Part IV – Conclusions and outlook

4.1 The REXEBIS

REX-ISOLDE is a pioneering project for post-acceleration of radioactive beams and will provide abundant opportunities for the new generation of experiments that are planned at the on-line mass separator facility ISOLDE. A key component is the charge breeding REXEBIS, part of the important novel bunching/cooling/breeding concept that will be utilised for the first time at REX-ISOLDE. Since charge breeding of radioactive ions is an unexplored territory with special requirements, the EBIS design had to be adapted with respect to intensity, breeding time, and efficiency constraints, among other things. The simulations and design, the construction and building-up phase, and the initial commissioning tests of the REXEBIS charge breeder have been presented in this thesis. The simulations have furthermore given valuable insight into beam acceptance and emittance for EBIS in general.

Much time of my doctoral work was spent bringing the REXEBIS into an operational state before any tests could be performed. Presently the commissioning is in full progress and the REXEBIS has been shown to work, not according to all specifications, but it is well under way. The major task that remains is to merge the EBIS with the Penning trap and transfer line, and to experimentally prove the anticipated advantages of the TRAP/EBIS concept.

The claimed superiority of using an EBIS as charge breeder for the 1st generation of radioactive beam post accelerators is based on: the fast breeding (some tens of milliseconds); the high breeding efficiency; the indifference to the ion species (hydrogen to superheavy elements); the exceptional beam properties (transverse and longitudinal emittance); and the low contamination of the extracted beam (capable of handling down to a few ions per pulse). The question remains how to improve its performance, and adapt it to the higher yield that is expected from the 2nd generation Radioactive Nuclear Beam facilities. Three prominent matters have to be dealt with – shorter cycle time, continuous injection and higher yields.

- A shortened breeding time results in higher efficiency for short-lived species. Thus both higher cathode current-density (e.g. utilising IrCe cathodes) and higher beam compression are of great interest. Generally, breeding fully stripped Be ions, or Na to 9^{+}, in the order of 5 ms is within reach with existing EBIS technology, implying that short-lived nuclei such as ^{35}Na ($t_{1/2}$=1.5 ms) can be accelerated.
- Using continuous injection into the EBIS would eliminate the need for the bunching Penning trap and consequently the space-charge restrictions set by it. Nonetheless, so far the continuous injection mode has shown very poor efficiency, most probably due to a small acceptance [P7]. A promising solution would be to make use of a gas-filled RFQ guiding structure to shrink the emittance by at least a factor 10 (in each phase plane) [104,105].
- A direct action to increase the yield of ions in a Penning trap/EBIS system is to raise the repetition rate. The possibility to extend the Penning trap radius and length always remains, but the consequences for the transverse and longitudinal emittances have to be investigated [106]. An RFQ cooler as a replacement for the Penning trap plus various evolutions of high performing EBIS open up opportunities for higher beam intensities. A high performance EBIS could be, for instance, a RHICEBIS or a LHCEBIS with a breeding capacity of some 10^{13} charges per second. Yet another project under development is the investigation of the reflex mode EBIS (RefEBIS [107]), where the electron beam is reflected repeatedly (several hundred times) inside the EBIS.

Nevertheless, the EBIS is not the only charge breeding solution. The $1^{+} \rightarrow n^{+}$ ECRIS charge breeder, latest version based on the PHOENIX source, has already produced very impressive results. The global efficiency (stating the fraction of captured 1^{+} ions) has reached the same level for metallic as for gaseous ions, i.e. 70 %. The most abundant charge may reach 10 to 15 % depending on the mass, and the breeding time has been reduced significantly, for example to 25 ms for Ag^{19+} [108]. The high space-charge capacity of an ECRIS is highly attractive from a 2nd radioactive beam-facility point of view. A charge breeding ECRIS will later be installed at ISOLDE for comparative measurements with the Penning trap/EBIS system.

4.2 The ECR4 lead ion source

Considerable knowledge about the afterglow phenomenon was acquired during the experiments, especially increased the understanding of the biased probe effect. Afterglow enhancing tricks similar to the ones that have been successful on ECRIS operating in pulsed or CW mode were tried out on the CERN ECR4 source. In spite of a number of different experiments, no evidence was found for an absolute yield increase over the record notation that was obtained for a carefully optimised, normally operated source. Consequently, the experience gained from CW sources seems not to be directly applicable on an ECR source running in afterglow mode. A relative increase <20% for the Pb^{27+} afterglow yield was noticed for bias voltages more negative than –100 V, but the detected current after the RFQ never exceeded the previously obtained top current. There seems to be an absolute maximum Pb^{27+} ion current under normal stable operation conditions. The ECR4 ion source performance may already be optimised, or the extraction system in its present state can not handle an increased afterglow current. Regardless, the ECR4 is a stable and well-behaving ion source in its original configuration.

A successor to the ECR4 ion source, the PHOENIX source, is presently in the commissioning stage at ISN, Grenoble. Running at higher RF frequency, with a larger mirror ratio and making use of a larger plasma volume, typically a factor of 10 increase in extracted current, i.e. 1 emA of Pb^{27+} in the afterglow is expected.

4.3 The LHCEBIS

In the last section it was demonstrated that an EBIS could possibly meet the LHC specifications for lead production and therefore advantageously be used as an alternative to the ECRIS and LIS concepts. Instead of developing and exploiting a high current and high energy EBIS, an alternative route can be taken which makes use of an electron beam with relatively low current and energy, and utilises the effect of boosted charge-state. An LHCEBIS could furthermore fulfil the constraints of an ion source dedicated for hadron therapy accelerators. Nevertheless, an experimental verification of a number of uncertain parameters has to be performed before one can confidently claim that the concept will fulfil its promises. Some of them could be carried out at an operative REXEBIS.

In complement to this, a successful development of a new generation of EBIS is already under way. A research programme at Brookhaven National Laboratory aims for using an EBIS as an injector for RHIC, which will have a 10 A and 20 keV electron beam, an electron current-density higher than 400 A/cm^2, and an estimated trap capacity of $5 \cdot 10^{11}$ charges. Some very promising results have already been achieved.

4.4 General final remarks

Both the EBIS and ECRIS are ion sources of utmost interest for the future and can be used as charge breeders, or as ion sources for various injectors, or feed physics experiments directly. They have the ability to produce multi-charged ions with so far unparalleled performances. The strength of the EBIS is the high charge states attainable, the straightforward change between elements and charge states, and that its beam properties match synchrotron injection-conditions well. The ECRIS has on the other hand a superior yield, large acceptance for ion injection and not at least the back-up of a large number of serious research teams. However, catching up from behind is the Laser Ion Source concept where a large amount (9 mA) of highly charged ions (Ta^{20+}) can be produced and released within a few microseconds [109]. The prospect of running such a source at 1 Hz, which is attainable within a year (2001) at CERN, is very attractive.

Acknowledgements

During my long time as a doctoral student, I have stood on several platforms – Chalmers, MSL, PS and ISOLDE at CERN. Unavoidably, a large number of people have been confronted with my deeds, and I would like to express my gratitude to at least a few.

My sincere thanks go to supervisor Göran Nyman and group leader Björn Jonson for always being behind the scenes pulling the right strings all the time. They have given me a lot of responsibility and a free hand to form my situation, which has been both tough and rewarding in many aspects. My second gratitude is directed to 'supervisor' Leif Liljeby for explaining one or two things about EBIS, and to my third supervisor, Charles Hill, for sharing his knowledge about ECRIS magic. Bernhard Wolf plays in the same league as a consequence of his great assistance with both the ECRIS and EBIS, and as a consultant for the writing of this thesis.

Moreover, I am indebted to Gerhard Huber for his willingness to share his economical wealth with me. The Knut and Alice Wallenberg Stiftelse, Sweden, are acknowledged for their generous contribution to the REXEBIS project.

As groups I would like to mention the Subatomic group at Chalmers for good companionship (Christian, Halina, Karin, Kate, Lasse, Leif, Martin, Mikael, Mikail and Thomas); the Manne Siegbahn Laboratory colleagues (Håkan, Jan, K-G, Lasse, Micke och Örjan); the friends from "Denmark and Spain" (Andreas, Haik, Hans, Karsten, Katarina, Luis, Maria, Olof and Uffe); the people at PS (Andreas, Christiano, Detlef, Henri, and Mats and all others); all ISOLDE friends and my REX-ISOLDE allies (Friedhelm, Joakim, Oliver F, Oliver K and Pit).

Finally, I owe my sincere thanks to my parents, for supporting me in many ways and for always encouraging me to proceed along any path that I have chosen even if they rarely know where I have been, where I am, or where I am going.

Anna – not forgotten. Always on my mind.

Appendix 1. *Photo of the REXEBIS installation from the gun side.*

Appendix 2. *A compilation of the most important design parameters for the REXEBIS.*

Solenoid	
Central magnetic field	variable between 0.1and 2.0 T
Field homogeneity over ±400 mm on axis	0.25% (measured) 0.3% (specified)
Field straightness	$r_{central}$<0.15 mm over -800<z<800 mm (measured) $r_{central}$<0.5 mm over -825<z<825 mm (specified)
Relative field decay	$13 \cdot 10^{-6}$ h^{-1} (measured) $5 \cdot 10^{-6}$ h^{-1} (specified)

Inner structure	
Trap length	100, 230, 332, 464, 696 or 798 mm
Trap capacity	$6 \cdot 10^{10}$ charges
Number of drift tubes	6
Drift tube inner radius	5 mm
Electron-beam energy	5 keV
Electron-beam radius	0.25 mm
Electron-current density	>200 A/cm^2 (~250 A/cm^2)
Tube-to-beam axis voltage	-750 V
Electron beam potential depth	107 V
Beam ripple	±5 V
Drift tube material	titanium

Collector	
Collector voltage relative to cathode	2000 V
Suppressor voltage relative to cathode	1500 V
Extractor voltage relative to collector	-17 000 V
Power dissipation	1000 W
Material	OHFC
Electron load	<8 mA/cm^2
Direct reflected, back-scattered and secondary electrons	<0.1%, 0.1%, 0.05%

Electron gun	
Gun type	Semi-immersed
Cathode material	LaB_6 310-crystal orientation
Cathode temperature T_c	1750 K
Cathode life-time	1 year
Cathode current density j_c	25 A/cm^2
Cathode diameter	1.6 mm
Magnetic field at cathode B_c	0.2 T
Electron beam current I_e	0.46 A
Anode voltage U_{anode}	6500 V
Perveance P	0.87 A/V$^{3/2}$
Post anode voltage $U_{post\ anode}$	~10 000 V (optional)
Compression	from 25 to >200 A/cm^2 (~250 A/cm^2)
ω_L/ω_p in full field	5.1
Radial gun misalignment Δr_c	<1.3 mm
Gun tilt $\Delta(dr/dz)_c$	<4 mrad
Axial gun misalignment Δz_c	<±5 mm

Turbo pumps	
Two 180 *l*/s	One 260 *l*/s
Compression N_2 >$1 \cdot 10^{12}$, He $2 \cdot 10^8$, H_2 $5 \cdot 10^5$	Compression N_2 >$1 \cdot 10^9$, He $3 \cdot 10^5$, H_2 $1.3 \cdot 10^4$

NEG pumps	
H_2 pumping speed	0.5 *l*/cm^2·s
O_2, N_2 and CO_x pumping speed relative H_2	65%, 15% and 40%
Hydrocarbon sorption efficiency relative H_2	<0.1%

Ion beam properties (simulated)	
Specified geometrical acceptance	3 π·mm·mrad (60 kV)
Maximum geometrical acceptance	11 π·mm·mrad (60 kV)
Geometrical emittance	<19 π·mm·mrad (20 kV)
Extracted energy spread per Q	15 eV (1 σ)

Appendix 3. *Main parameters for the CERN ECR4 ion source.*

Magnetic field	
Mirror ratio	2.8
Hexapole material / radial confinement	Nd-Fe-B permanent magnet (VACODYN 370HR)
Pole tip B-field at hexapole	1.2 T
Minimum B-field	0.4 T
Peak axial B-field	1.1 T
Coil current	Typically 900 to 1100 A
RF heating	
Frequency	14.5 GHz
RF power source	Klystron amplifier
Heating pulse length	50 ms (40 to 50% duty cycle)
Repetition rate	10 Hz
RF power	<2.2 kW
Plasma	
Resonant field	0.518 T
Cut-off plasma density $n_{cut\text{-}off}$	$2.4 \cdot 10^{12}$ cm^{-3}
ECR region extension	~ 6 cm length, ~ 4 cm width
Plasma gas	Oxygen
Metallic sample feed	By micro oven
Geometry	
Plasma chamber dimensions	66 mm diameter, 179 mm long
Extraction gap	42 to 47 mm
Plasma electrode hole	16 mm
Beam extraction and beam properties	
Extraction energy / voltage	2.5 keV/u (nominal) / maximum 25 kV
Extraction	By acceleration field, one gap
Operation mode	Pulsed, optimised for afterglow
Useful beam length, extracted pulse	~ 1 ms
Beam currents	Total 2-3 mA (main pulse) Analysed 80-100 μA Pb^{27+}

References

References P1 to P16 are found in the List of Publications

1. 9th International Conference on the Physics of Highly Charged Ions - HCI 98, Bensheim, Germany, ed. P. H. Mokler et al., Phys. Scr. Top. Issues **T80** (1999) p.1-564.
2. G. Bollen, *"Radioactive ion beams and Penning traps"*, Nucl. Phys. **A616** no.1-2 (1997) p.457c-468c.
3. K. Hermanspahn, W. Quint, S. Stahl, M. Toenges, G. Bollen, H-J. Kluge, R. Ley, R. Mann, G. N. Werth, *"Measurement of the g_j factor of hydrogenic ions: a sensitive test of bound state QED"*, Hyperfine Interactions **99** (1996) p.91-95.
4. E.D. Donets, *"Electron Beam Ion Sources"*, chapter 12 in *"The physics and Technology of ion Sources"*, ed. I. G. Brown, New York, John Wiley & Son, 1989.
5. R. Becker, *"Electron beam ion source/trap"*, chapter 2/section 11 in *"Handbook of Ion Sources"*, ed. B. H. Wolf, CRC Press Inc. 1995.
6. R. Geller, *"Electron cyclotron resonance ion sources and ECR plasmas"*, IOP Publishing, Bristol, 1996.
7. B. H. Wolf, *"ECR ion source >2.4 GHz"*, chapter 2/section 9 in *"Handbook of Ion Sources"*, ed. B. H. Wolf, CRC Press Inc. 1995.
8. F. Wenander, *"REXEBIS – an Electron Beam Ion Source for the REX-ISOLDE Project*", Licentiate thesis, Chalmers University of Technology, Göteborg 1998.
9. E. Kugler, D. Fiander, B. Jonson, H. Haas, A. Przewloka, H. L. Ravn, D. J. Simon, K. Zimmer, *"The new CERN-ISOLDE on-line mass-separator facility at the PS-Booster"*, Nucl. Instr. Meth. **B70** (1992) p.5-9.
10. B. Jonson, A. Richter, *"More than three decades of ISOLDE physics*", Hyperfine Interaction **129** no.1-4, (2000) p.1-22.
11. C. Hill, K. Langbein, *"Pulsed ECR Source in Afterglow Operation at CERN"*, Rev. Sci. Instr. **67** no.3 (1996) p.1328-1330.
12. P. Sortais, "*ECR ion source development at GANIL*", Nucl. Phys. News **6** no.4 (1996) p.6-8.
13. H. Haseroth, "*Pb injector at CERN"*, 18th International Linear Accelerator Conference - Linac '96, ed. C. Hill et al., Geneva, Switzerland, (1996) p.283-287.
14. N. Angert et al., "*CERN Heavy-Ion Facility Design Report*", CERN 93-01, ed. D. Warner, CERN, Switzerland.
15. L. R. Evans, *"LHC Accelerator Physics and Technology Challenges"*, Proc. of the 1999 Particle Accelerator Conference, ed. A. Luccio et al., New York, (1999) p.21-25.
16. *Radioactive beam experiment at ISOLDE: "Coulomb excitation and neutron transfer reactions of exotic nuclei"*, proposal to the ISOLDE committee, CERN-ISC94-25, Nov 1994, CERN, Switzerland.
17. D. Habs, O. Kester, T. Sieber, A. Kolbe, J. Ott, G. Bollen, F. Ames, D. Schwalm, R. von Hahn, R. Repnow, H. Podlech, A. Schempp, U. Ratzinger, L. Liljeby, K-G. Rensfelt, F. Wenander, B. Jonson, G. Nyman, P. van Duppen, M. Hyuse, A. Richter, G. Schrieder, G. Walter, and the REX-ISOLDE collaboration, *"The REX-ISOLDE Project"*, Nucl. Instr. Meth. **B139** no.1-4 (1998) p.128-35.
18. D. Habs, O. Kester, T. Sieber, H. Bongers, S. Emhofer, P. Reiter, P.G. Thirolf, G. Bollen, J. Äystö, O. Forstner, H. Ravn, T. Nilsson, M. Oinonen, H. Simon, J. Cederkäll, F. Ames, P. Schmidt, G. Huber, L. Liljeby, Ö. Skeppstedt, K-G. Rensfelt, F. Wenander, B. Jonson, G. Nyman, R. von Hahn, H. Podlech, R. Repnow, C. Gund, D. Schwalm, A. Schempp, K.-U. Kühnel, C. Welsch, U. Ratzinger, G. Walter, A. Huck, K. Kruglov, M. Huyse, P. Van den Bergh, P. van Duppen, L. Weissman, A.C. Shotter, A.N. Ostrowski, T. Davinson, P.J. Woods, J. Cub, A. Richter and G. Schrieder , *"The REX-ISOLDE project"*, Hyperfine Interactions **129** no.1-4 (2000) p.43-66.
19. http://fy.chalmers.se/subatom/f2bfw/rexposter.html
20. H. Raimbault-Hartmann, D. Beck, G. Bollen, M. König, H-J. Kluge, E. Schark, J. Stein, S. Schwarz, J. Szerypo, *"A cylindrical Penning trap for capture, mass selective cooling, and bunching of radioactive ion beams"*, Nucl. Instr. Meth. **B126** (1997) p.378-382.
21. F. Ames, G. Bollen, G. Huber, P. Schmidt and the REX-ISOLDE Collaboration, "*REXTRAP, an Ion Buncher for REX-ISOLDE*", Proc. of the 2nd International Conference on Exotic Nuclei and Atomic Masses (ENAM98), Bellaire, Michigan USA. AIP conference proceedings 455, (1998) p.927-932.
22. P. Schmidt, "*REXTRAP – Ion Accumulation, Cooling, and Bunching for REX-ISOLDE*", Doctoral Thesis, der Johannes Gutenberg-Universität in Mainz, Germany (2001).

23. R. Rao, O. Kester, T. Sieber, D. Habs, K. Rudolph and the REX-ISOLDE collaboration, "*Beam optics design of the REX-ISOLDE q/m-separator*", Nucl. Instr and Meth. **A427** (1999) p.170-176.
24. T. Sieber, O. Kester, D. Habs, A. Schempp, *"Design and status of the RFQ for REX-ISOLDE"*, Proc. of the 19th International LINAC Conference, ed. C. E. Eyberger et al., Argonne National Laboratory, Chicago, **2** (1999) p.777-779.
25. T. Sieber, O.Kester, D. Habs, S. Emhofer, A. Schempp, "*Design and development of the frontpart of the REX-ISOLDE LINAC"*, Proc. of the 5th Radioactive Nuclear Beam conference, ed. J. Lettry et al., Divonne, France (2000). To appear in Nucl. Phys. A.
26. O. Kester, D. Habs, R. Rao, K. Rudolph, T. Sieber, H. Bongers, R. von Hahn, H. Podlech, R. Repnow, D. Schwalm, A. Schempp, U. Ratzinger, *"The REX-ISOLDE LINAC"*, Proc. of the 6th European Accelerator Conference, ed. S. Myer et al., Institute of Physics Publishing, London, (1998) p.728-730.
27. H. Podlech, M. Grieser, R. von Hahn, S. Papureanu, R. Repnow, D. Schwalm, *"The 7-gap-resonator-accelerator for the REX-ISOLDE-experiment at CERN*", Nucl. Instr. Meth. **B139** (1998) p.447-450.
28. H. Podlech, R. von Hahn, R. Repnow, D. Schwalm, *"The 7-gap-resonator-accelerator for the REX-ISOLDE-Project at CERN"*, Proc. of the 5th Radioactive Nuclear Beam conference, ed. J. Lettry et al., Divonne, France (2000). To appear in Nucl. Phys. A.
29. R. W. Schmieder, Physics of the EBIS and its ions, *"Physics of highly-ionised atoms"*, Plenum, New York, (1989) p.321-376.
30. P. Schmidt, F. Ames, G. Huber, G. Bollen, O. Forstner, and the REX-ISOLDE, "*Bunching and cooling of radioactive ions with REXTRAP*", Proc. of the 5th Radioactive Nuclear Beam conference, ed. J. Lettry et al., Divonne, France (2000). To appear in Nucl. Phys. A.
31. G. Bollen, R. B. Moore, G. Savard, H. Stolzenberg, "*The accuracy of heavy-ion mass measurements using time of flight-ion cyclotron resonance in a Penning trap*", J. Appl. Phys. **68** no.9 (1990) p.4355-4374.
32. L. Brillouin, *"A theorem of Larmor and its importance for electrons in magnetic fields"*, Phys. Rev. **67** no.7-8 (1945) p.260-266.
33. D. Dubin, T. O'Neil, *"Trapped nonneutral plasmas, liquids, and crystals (the thermal equilibrium states)"*, Rev. Modern Phys., **71** no.1 (1999) p.87-172.
34. Oxford Instruments Superconductivity, Tubney Woods, Oxford, UK. http://www.oxfordinstruments.com/superconductivity/
35. J. H. Billen and L. M. Young, *"POISSON/SUPERFISH on PC Compatibles"*, Proc. of the 1993 Particle Accelerator Conference, ed. S. T. Corneliussen, Washington DC, US, **2** p.790-792.
36. W. B. Herrmannsfeldt, *"Electron Trajectory Program SLAC 266"*, Linear Accelerator Center, Stanford, 1979.
37. FEI Company, Beam Technology Division. http:// http://www.feibeamtech.com/
38. TREK, Inc. US. http://www.trekinc.com/
39. F.u.G. Elektronik GmbH, Rosenheim, Germany. http://www.fug-elektronik.de/
40. http://www.pfeiffer-vacuum.com/
41. SAES Getters, S.p.A., Milan, Italy. http://www.saesgetters.com/
42. PROFIBUS information homepage, http://www.profibus.com/
43. W. Heinze, R. Maccaferri, *"An inexpensive analog function generator in VME standard"*, Nucl. Instr. Meth. **A352** (1994) p.147-149.
44. http://www.simatic.de/
45. D. A. Dahl, J. E. Delmore, A. D. Appelhaus, *"SIMION PC/PS2 electrostatic lens design program"*, Rev. Sci. Instr. **61** (1990) p.607-609.
46. E. Beebe, L. Liljeby, Å. Engström, M. Björkhage, *"The Stockholm electron beam ion source"*, Phy. Scr. **47** (1993) p.470-474.
47. J. L. Hagedoorn, J. I. M. Botman, *"On the motions of ions in a cylindrically symmetrical magnetic field"*, Internal report GSI-90-29, GSI, Germany.
48. C. Benvenuti, P. Chiggiato, P. Costa Pinto, A. Escudeiro Santana, T. Hedley, A. Mongelluzzo, V. Ruzinov, I. Wevers, "*Vacuum properties of TiZrV non-evaporable getter films*", Vacuum **60** (2001) p.57-65.
49. C. Scheuerlein, B. Henrist, N. Hilleret, M. Taborelli, *"The secondary electron yield of TiZr and TiZrV non evaporable getter thin film coatings"*, CERN-EST-2000-007-SM, Geneva, Switzerland.

50. E. Beebe, J. Alessi, A. Kponou, A. Pikin, K. Prelec, *"Heavy ion extraction from the BNL high current EBIS teststand"*, Proc. of the 7th European Particle Accelerator Conference - EPAC 2000, ed. W. Mitaroff et al., Vienna, Austria, (2000) p.1589-1591.

51. S. Humphries Jr., *"Measurement of emittance"*, chapter 3.3. in *"Charged particle beams"*, John Wiley & Sons Inc, New York, (1990).

52. F. Ames, CERN, Switzerland (2000). Private communication.

53. Lead programme, *"Experiments at CERN in 1999 (Grey Book)"*, ed. B. W. Powell, Geneva, Switzerland (1999).

54. G. Shirkov, *"Improvement of highly charged ion production in the ECR source of heavy ions"*, Proc. International Conference on Ion Sources, Whistler, 1995. Rev. Sci. Instr. **67** (1996) p.1158-1160.

55. C. E. Hill, K. Langbein, *"Experiments on a 14.5 GHz ECR source"*, Proc. of the 18th International Linear Accelerator Conference - Linac '96, Geneva, Switzerland, ed. C. E. Hill et al., (1996) p.366-368.

56. C. E. Hill, K. Langbein, *"Experiments on a 14.5 GHz ECR source"*, Proc. of the 7th International Conference on Ion Sources - ICIS '97, ed. G. Ciavola et al., Taormina, Italy, Rev. Sci. Instr. **69** no.2 (1998) p.643-645.

57. K. Langbein, *"Experimental investigation of the afterglow of the pulsed ECR discharge"*, Proc. of the 12th International Workshop on ECR Ion Sources, ed. M. Skiguchi et al., Saitma, Japan (1995) p.198-202.

58. G. Melin, *"ECR ion sources: Present status and prospects"*, Phys. Scr. **T71** (1997) p.14-22.

59. T. Consoli, Ann. NY Acad. Sci. part.IV (1974) p.334-335.

60. Z. Q. Xie, C. M. Lyneis, *"Plasma potentials and performance of the advanced electron cyclotron resonance ion source"*, Rev. Sci. Instr. **65**, no.9 (1994) p.2947-2952.

61. G. Melin, F. Bourg, P. Briand, J. Debernardi, M. Delaunay, R. Geller, B. Jacquot, P. Ludwig, T. K. Nguyen, L. Pin, M. Pontonnier, J. C. Rocco, F. Zadworny, *"Some particular aspects of the physics of the ECR sources for multicharged ions"*, Proc. of the 3rd International Conference on Ion Sources, Berkely, Califonia, ed. I. G. Brown Rev. Sci. Instr. **61** no.1 part.II (1990) p.236-238.

62. P. Briand, R. Geller, G. Melin, *"A newly designed ECR source for the lead injector of CERN"*, Nucl. Instr. Meth. **A294** (1990) p.673.

63. R. Geller, *"ECRIS: the electron cyclotron resonance ion sources"*, Proc. of the 5th International Conference of Highly Charged Ions, Giessen, ed. E. Salzborn et al., Berlin: Springer Verlag (1990) p.117-121.

64. H. I. West, Jr., *"Calculation of ion charge-state distribution in ECR ion sources"*, Lawrence Livermore National Laboratory, US (1982) Report ECRL-53391.

65. T. Nakagawa, T. Kageyama, A. Goto, M. Kase, Y. Kanai, Y. Nakai, Y. Yano, *"Plasma cathode method for RIKEN 10 GHz ECRIS"*, Proc. of the 11th Int. Workshop on ECR Ion Sources, Groningen, ed. A. Drentje, KVI Report 996 (1993) p.208-212.

66. G. Melin, F. Bourg, P. Briand, J. Debernardi, M. Delaunay, R. Geller, B. Jacquot, P. Ludwig, T. K. Nguyen, L. Pin, M. Pontonnier, J. C. Rocco, F. Zadworny, Proc. of the 10th International Workshop on ECR Ion Sources, Oak Ridge, ed. F. W. Meyer et al., (1991) ORNL Conf. 9011136 p.1.

67. G. Melin, F. Bourg, P. Briand, M. Delaunay, G. Gaudart, A. Girard, D. Hitz, J. P. Klein, P. Ludwig, T. K. Nguyen, M. Pontonnier, Y. Su, *"Status of development of ECR ion sources at Grenoble"*, Proc. of the 5th International Conference in Ion Sources, Beijin, ed. C. Erg, Rev. Sci. Instr. **65** no.4 part.II p.1051-1056.

68. A. G. Drentje, *"Anomalous charge state distribution in ECRIS for oxygen isotopes"*, Proc. of the 4th International Conference on Ion Sources, Bensheim, ed. B. H. Wolf, Rev. Sci. Instr. **63** no.4 part.II (1992) p.2875-2877.

69. B. Jacquot, M. Pontonnier, *"Compact multiply charged 10 GHz ion source CAPRICE for all metallic and gaseous elements"*, Nucl. Instr. Meth. **A254** (1990) p.13-21.

70. P. Briand, R. Geller, H. Haseroth, C. Hill, K. Langbein, *"Utilizing the ECR Afterglow to Increase the Intensity of Highly Charged Ions in the CERN Accelerator Complex"*, Proc. of the 11th Int. Workshop on ECR Ion Sources, Groningen, ed. A. Drentje, KVI Report 996 (1993) p.135-137.

71. S. Runkel, K. E. Stiebing, O. Hohnl, V. Mironov, G. Shirkov, A. Schempp, H. Schmidt-Boecking, *"Time-resolved measurements of the Biased-Disk Effect at the Frankfurt 14 GHz Electron-Cyclotron-Resonance-Ion-Source"*, Proc. of the 14th International Workshop ECR Sources – ECRIS99, Geneva, Switzerland (1999) p.183-186.

72. K. E. Stiebing, O. Hohn, S. Runkel, L. Schmidt, H. Schmidt-Boecking, V. Mironov, G. Shirkov, *"Time resolved measurements of the biased disk effect at an Electron Cyclotron Resonance Ion Source"*, Phys. Rev. ST Accel. Beams, **2** (1999) 123501.

73. T. Nakagawa, S. Biri, T. Chiba, A. Goto, M. Hemmi, E. Ikezawa, N. Inabe, T. Kageyama, O. Kamigaito, M. Kase, M. Kidera, Y. Miyazawa, Y. Yano, "*Further development of RIKEN 18 GHz ECRIS"*, Proc. 6th European Part. Accelerator Conf., Stockholm (1998) p.1418-1421.

74. T. Nakagawa, Y. Higurashi, M. Kidera, A. Efremov, V. Mironov, G. Shirkov, *"The RIKEN 18 GHz electron cyclotron resonance ion source: Time-resolved study of operation"*, Proc. of PIBHI, ed. S. Gammino, Catania, Italy (2000), Conference Proceedings of SIF (Italian Society of Physics). In press.

75. Behlke Electronic GmbH, Germany.

76. A. T. Forrester, *"Large Ion Beams"*, John Wiley & Sons New York, 1988.

77. P. Spädtke, K. Tinschert, *"2D and 3D simulation of ion beam extraction from an ECR source"*, Proc. of the 14th International Workshop ECR Sources – ECRIS99, CERN, Switzerland (1999) p.143-146.

78. M. P. Bougarel, C. E. Hill, H. Haseroth, K. Langbein, E. Tanke, *"Performance of the ECR ion source of CERN's heavy ion injector"*, CERN-PS 96-021-HI, Geneva, Switzerland.

79. Z. Q. Xie, C. M. Lyneis, *"Improvements on the LBL AECR source"*, Proc. of the 12th International Workshop on ECR sources, RIKEN, Japan (1995) p.24-28.

80. J. E. Boers, Thunderbird Simulations. http://home.earthlink.net/~jeboers/PBGUNS.HTML

81. C. Muehle, U. Ratzinger, G. Jost, K. Lieble, S. Schennach, B. H. Wolf, *" PUMA-ECR ion source operation"*, Proc. of the 6th International Conference on ion sources, Whistler Canada 1995, Rev. Sci. Instr. **67** (1996) p.1331-1333.

82. P. Spädtke, *"Simulation of ion beam extraction"*, Rev. Sci. Instr. **65** no.4 (1994) p.1419-1422.

83. R. Becker, W. B. Herrmannsfeldt, *"IGUN – A program for the simulation of positive ion extraction including magnetic field"*, Rev. Sci. Instr. **63** no.4 (1992) p.2756-2758.

84. M. Harrison, "*The Commissioning Status of RHIC*", Proc. of the 1999 Particle Accelerator Conference, ed. A. Luccio et al., New York, US (2000) p.6-10.

85. E. Beebe, J. Alessi, A. Hershcovitch, A. Kponou, K. Prelec, R. W. Schmieder, *"Development of an electron-beam ion source for a relativistic heavy-ion collider preinjector"*, Rev. Sci. Instr. **67** no.3 (1996) p.878-880.

86. E. Beebe, J. Alessi, A. Hershcovitch, A. Kponou, A. Pikin, K. Prelec, P. Stein, R. W. Schmieder, *"Experimental results from the Brookhaven National Laboratory test electron beam ion source"*, Rev. Sci. Instr. **69** no.2 (1998) p.640-642.

87. F. Wenander, PS/HP/Note 99-09, CERN, Switzerland, (1999).

88. P. Giubellino, E. Crescio, ALICE Collaboration, "*The ALICE experiment at LHC: physics prospects and detector design*", Proc. of the 9th International Conference on Nuclear Reaction Mechanisms, ed. E. Gadioli, Varenna, Italy, (2000). In press.

89. J. Bosser, C. Carli, M. Chanel, R. Maccaferri, G. Molinari, S. Maury, D. Möhl, G. Tranquille, *"The production of dense lead-ion beams for CERN LHC"*, Nucl. Instr. Meth **A441** (2000) p.116-122.

90. J. Bosser, C. Carli, M. Chanel, C.E. Hill, A. Lombardi, R. Maccaferri, S. Maury, D. Möhl, G. Molinari, S. Rossi, E. Tanke, G. Tranquille, M. Vretenar, *"Experimental Investigation of Electron Cooling and Stacking of Lead Ions in a Low Energy Accumulation Ring"*, CERN/PS 99-033 (DI) (1999) Geneva, Switzerland.

91. N. Angert et al., "*High current, high frequency ECRIS development program for LHC heavy ion beam application"*, Proc. of the 14th Int. Workshop on ECR Ion Sources – ECRIS99, CERN, Switzerland (1999) p.220-223.

92. P. Fournier et al., *"CERN PS Laser Ion Source Development"*, Proc. of the 1999 Particle Accelerator Conference, ed. A. Luccio et al., New York, US (2000) p.103-105.

93. H. Haseroth, K. Prelec, "*Possible application of an EBIS in preinjectors for large heavy ions colliders",* Phy. Scr. **T71** (1997) p.23-27.

94. K. G. Dyall, I. P. Grant, C. T. Johnson, F. A. Parpia, E. P. Plummer, "*GRASP: a general-purpose relativistic atomic structure program"*, Computer-Physics-Communications **55** no.3 (1989) p.425-456.

95. A. Müller, E. Salzborn, "*Scaling of cross sections for multiple electron transfer to highly charged ions colliding with atoms and molecules"*, Phys. Lett. **62A**, 6 (1977) p.391-394.

96. R. Becker, O. Brinzanescu, Th. Stöhlker, *"Limitation of EBIS/T ion yield by radiative recombination"*, Proc. of the 8th International Symposium on Electron Beam Ion Sources and Traps and their Applications, Brookhaven National Laboratory, Nov 6-8, 2000. To appear in AIP Conference Proceedings Series.

97. Y. S. Kim, R. H. Pratt, "*Direct radiative recombination of electrons with atomic ions: Cross sections and rate coefficients"*, Phys. Rev. **A27** no.6 (1983) p.2913-2924.

98. B. H. Wolf, *"Vacuum arc ion sources"*, chapter 2/section 12 in *"Handbook of Ion Sources"*, edited by B. H. Wolf, CRC Press Inc. 1995.

99. H. Höltermann, R. Becker, M. Kleinod, *"Fast Ion Extraction from Intense Electron Beams*", Proc. of the 8th International Symposium on Electron Beam Ion Sources and Traps and their Applications, Brookhaven National Laboratory, (2000). To appear in AIP Conference Proceedings Series.

100. J. Alessi, Brookhaven National Laboratory, USA (2000). Private communication.

101. R. Becker, H. Höltermann, A. Pikin, Th. Stöhlker, *"Fast extraction of high currents from an EBIS"*, Proc. of the Workshop on the Production of Intense Beams of Highly charged Ions, ed. S. Gammino, Catania, Italy, (2000). To appear in Conference Proceedings of SIF.

102. K. N. Leung, *"Multicusp ("Bucket type") ion source"*, chapter 2/section 6 in *"Handbook of Ion Sources"*, ed. B. H. Wolf, CRC Press Inc. 1995.

103. I. Bergström, M. Björkhage, H. Danared, H. Cederquist, T. Fritioff, L. Liljeby, R. Schuch, *"Present status of the Stockholm electron beam ion source and its scientific program"*, Proc. of the 8th International Symposium on Electron Beam Ion Sources and Traps and their Applications, Brookhaven National Laboratory, (2000). To appear in AIP Conference Proceedings Series.

104. F. Herfurth, J. Dilling, A. Kellerbauer, B. Bollen, S. Henry, H-J. Kluge, E. Lamour, D. Lunney, R. B. Moore, C. Scheidenberger, S. Schwarz, G. Sikler, J. Szerypo, *"A linear radiofrequency ion trap for accumulation, bunching, and emittance improvement of radioactive beams"*, Nucl. Instr. Meth. (2000). Submitted for publication.

105. A. Nieminen, J. Huikari, A. Jokinen, J. Äystö, P. Campbell, E.C.A. Cochrane and the EXOTRAPS collaboration, *"Beam cooler for low-energy radioactive ions"*, Nucl. Instr. Meth. A (2001). In press.

106. F. Ames, P. Schmidt, O. Forstner, G. Bollen, O. Engels, D. Habs, G. Huber and the REX-ISOLDE collaboration, *"Space-charge effects with REXTRAP"*, Atomic Physics at Accelerators – Mass spectroscopy, Corsica, France, (2000). In press.

107. E. D. Donets, D. E. Donets, E. E. Donets, V. V. Salnikov, V. B. Shutov, E. M. Syresin, M. Björkhage, P. Carlé, L. Liljeby, K-G. Rensfelt, R. Becker, M. Kleinod, O. K. Kultashev, *"A study of electron strings and their use for efficient production of highly charged ions"*, Rev. Sci. Instr. **71** no.2 (2000) p.896-898.

108. T. Lamy, ISN Grenoble, France (2001). Private communication.

109. H. Kugler, CERN, Switzerland (2001). Private communication.

PAPER 1

REXEBIS – a charge state breeder for the REX-ISOLDE post accelerator

Authors:
J. Axelsson, M. Björkhage, P. Carlé, L. Liljeby, K-G. Rensfelt, B. Jonson, G. Nyman and F. Wenander

Published in:
Proc. of the 6th European Particle Accelerator Conference, Stockholm, Sweden, IOP Bristol, 1999, p.1412-1414.

REXEBIS – A CHARGE BREEDER FOR THE REX-ISOLDE POST ACCELERATOR

J. Axelsson, M. Björkhage, P. Carlé, L. Liljeby, K-G. Rensfelt, MSL, Stockholm, Sweden
B. Jonson, G. Nyman, F. Wenander, Chalmers University of Technology, Göteborg, Sweden
The REX-ISOLDE Collaboration, CERN, Geneva, Switzerland

Abstract

The REXEBIS is an electron-beam ion source developed to trap and further ionise the sometimes rare and short-lived isotopes that are produced in ISOLDE for the Radioactive EXperiment at ISOLDE (REX-ISOLDE). A 0.5 A electron beam is produced in a magnetic field of 0.2 T, and is compressed by a 2 T solenoidal field to a current density of >200 A/cm2. The 2 T magnetic field is provided by a warm-bore superconducting solenoid, thus giving easy accessibility but no cryogenic pumping. The EBIS is switched between 60 kV (ion injection) and ~20 kV (ion extraction). The EBIS design focused on high injection and extraction efficiencies to the surrounding Penning trap and RFQ in the REX-ISOLDE post accelerator. The design, which required simulation of a complete injection, breeding and extraction cycle, proved viable. Calculations of the back flow of Ar cooling gas from the Penning trap as well as effects of residual gas from the warm-bore vacuum chamber certified that possible outnumbering of the low number of radioactive ions by Ar and residual gas can be handled.

1 INTRODUCTION

The construction of REXEBIS, an Electron Beam Ion Source (EBIS), is part of a larger project, the so-called REX-ISOLDE project [1,2,3], which is an upgrading of the already existing ISOLDE (Isotope Separator On-Line) [4] facility at CERN.

Nuclear physics is now turning its attention to the regions far away from nuclear stability, to the neutron and proton drip-lines, and to physics with radioactive ions. To reach these extreme regions in the nuclear chart innovative accelerator concepts have to be used, and the ISOLDE community has chosen to add a post accelerator to the isotope on-line separator. This will give the physicists access to the already large number of isotopes produced at ISOLDE at higher energies.

The REX-ISOLDE is a pilot project with the aim to demonstrate an efficient scheme for post acceleration of radioactive beams, produced by an on-line mass separator, to energies somewhat below the Coulomb barrier. The ions are first accumulated and cooled in a Penning trap, then charge bred in an EBIS, and finally accelerated in a short linear accelerator to energies between 0.8 and 2.2 MeV/u.

An EBIS charge breeds ions by bombarding initially singly charged ions with high-energy electrons [5]. The bombarding electrons collide with electrons bound to ions, thus further ionising these ions. After a few milliseconds, the ion has been ionised to a higher charged state.

By introducing an EBIS into the post accelerator chain, the singly-charged ions are ionised to a q/A-value of ~1/4.5, and the length of the succeeding LINAC can be considerably reduced. For the low beam energies delivered by an on-line separator, an EBIS is in principle the only effective alternative. The REXEBIS has features similar to CRYSIS [6], the Stockholm EBIS, but there are some major differences and design challenges that we would like to emphasise in this article. A more extensive article describing the REXEBIS project is foreseen for this autumn.

2 REXEBIS SPECIFICATIONS

The specifications for the REX-ISOLDE post accelerator, together with the limits set by the Penning trap and the mass separator/LINAC, impose strict requirements on the REXEBIS design. The EBIS should be capable to charge-breed elements with mass A<50 to a charge-to-mass ratio of >1/4.5 within a confinement time of 20 ms. This short confinement time is set by the short life-time of the radioactive nuclei. For light elements, however, one has the possibility to use an even shorter cycle time. The number of ions injected per pulse may vary from a few ions to 10^7. The lower limit is set by the production yield at ISOLDE, whereas the space charge inside the Penning trap sets the upper limit. Due to few and costly produced radioactive ions the EBIS has to be efficient, i.e. the injection and extraction efficiency should be higher than 50% [7]. Due to the statistical nature of the ionisation process, the inherent breeding efficiency to a single charge state is less than 30%. Another reason for selecting an EBIS as part of this complex accelerator chain is that, this ion source has proved an excellent reliability record at MSL.

To fulfil the above requirements, we have chosen a design utilising a 5 keV electron beam with a current of 0.5 A. The current density is >200 A/cm^2, throughout a 0.8 m long trap region. With these parameters the REXEBIS trap can hold up to ~$6 \cdot 10^9$ charges at an electron beam charge-compensation of 10%. This large number of ions is more than ten times the maximum number of ions that due

to space charge limitations can conceivably be delivered from the Penning trap. Table 1 displays the most dominant charge states for some typical ions that are bred for 20 ms in the REXEBIS.

Table 1: Peak charge state at 20 ms breeding time.

Element	Charge-state
$_{8}$O	+7
$_{11}$Na	+9
$_{12}$Mg	+9
$_{18}$Ar	+11
$_{19}$K	+11
$_{20}$Ca	+12
$_{36}$Kr	+16
$_{37}$Rb	+18

3 SOLENOID

The superconducting magnet will provide a 2 T magnetic field, both for focusing of the electron beam and to facilitate trapping at ion injection. To optimise the performance of the EBIS, the magnetic field straightness, homogeneity, and stability must be carefully controlled. We have developed a simple method to verify the field straightness, and found the traced central field-line to be within a cylinder of radius 0.1 mm for the full EBIS length (-800<z<800 mm). The axial field has a specified homogeneity of 0.3% over ±400 mm, and we measured the homogeneity to be within 0.25%. The specified relative field stability is $5 \cdot 10^{-6}$ h^{-1}.

The REXEBIS has a warm bore, i.e. the inner cylinder containing the drift structure is held at room temperature, despite the cryogenic temperatures of the superconducting solenoid. We chose this concept to avoid the memory effect in which gases frozen to a cryogenic surface may re-enter the vacuum by the thermal load from the electron beam going astray. Furthermore, keeping the vacuum chamber at room temperature enhances the accessibility to the inner structure, and should allow good reliability. The main difficulty with this concept is to substitute the inherently efficient cryogenic pumping from a cold bore with NEG pumps and turbo-molecular pumps positioned at relatively poor conductance outside the solenoid.

4 ELECTRON GUN

The electron gun is of immersed type, positioned at 0.2 T. This design is uncomplicated, relatively in-sensitive to axial displacement, current and current-density is easy to control, and the design is well proved in EBIS constructions. Apart from a modest electron current compression, the main drawback is the unavoidable scalloping (periodical beam diameter variations along the beam propagation) which we have proved is insignificant for the working of the REXEBIS.

The electron gun will deliver a current of ~0.5 A at a cathode current density of 25 A/cm^2. The perveance of the gun is 0.87 μA/V$^{3/2}$. A 1.6 mm diameter LaB_6 cathode will be used. Figure 1 shows an EGUN simulation of the beam propagation in the gun region.

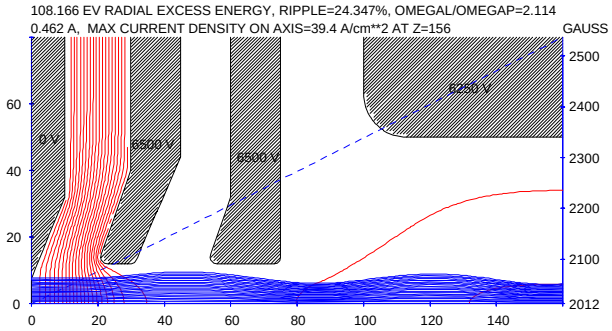

Figure 1. Cylindrical geometry simulation of the electron beam in the gun region. One unit of length corresponds to 0.1 mm.

4 INNER STRUCTURE

The inner structure consists of drift tubes, a support structure and NEG strips. All these elements are placed in UHV and close to room temperature (warm bore ~15 ºC). We have chosen to manufacture most of these details in titanium due to its gettering property. To further improve pumping efficiency, we have considered drilling holes radially in the drift tubes.

The drift tubes have a radius of 5 mm. The REXEBIS has three trapping tubes: 100, 230 and 464 mm long with 2 mm spacing, which can be combined to trap lengths of 100, 230, 332, 464, 696 and 798 mm. With a full length the charge trapping capacity for a 10% electron beam compensation amounts to $6 \cdot 10^9$ electrical charges.

The electron beam energy will be 5 keV, and the beam radius 0.25 mm. The potential depth of the electron beam will amount to 107 V, which is significantly larger than the potential ripple (±5 V) caused by beam scalloping. Ions are injected with a ~10 μs long pulse from the Penning trap, and are ejected by their inherent kinetic energy upon lowering the end-tube trap potential. Utilising this method, virtually no extra energy spread will be introduced.

5 ELECTRON COLLECTOR

A cylindrical iron shield surrounds the copper collector. The iron reduces the magnetic field drastically inside the collector, causing the electron beam to expand rapidly onto the collector surface. The design of the collector is tailored to the electron impact angle so that back-scattering is minimised (see Figure 2). Simulations show that the fraction of electrons that re-entered the trap region is about 0.25%. The collector has a large opening towards the combined injection/extraction beam optics. This minimises ion beam aberrations and increases pumping conductance.

The collector is placed at a +2000 V potential relative to the cathode, yielding that the 0.5 A electron current dissipates 1000 W at the collector surface. The power density in the affected region of the collector is below 8 mA/cm^2. Estimations of out-gassing caused by electron bombardment yields a rest gas pressure inside the collector of the order of 10^{-11} mbar.

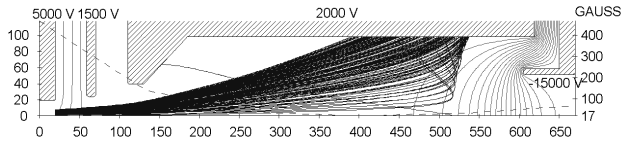

Figure 2. EGUN simulation of the absorbed electron beam. One unit of length corresponds to 0.25 mm. Only the upper cylindrical part of the collector region is shown.

6 HIGH VOLTAGE SWITCHING

The REXEBIS is situated at a 60 kV potential during injection, allowing captured of cooled 60 keV ions from the Penning trap. The potential is decreased to about 20 kV during the breeding time (figure 3). The RFQ is optimised for an ion energy of 5 keV/u, which with the EBIS output q/A~1/4.5 gives an ion extraction voltage of around 20 kV.

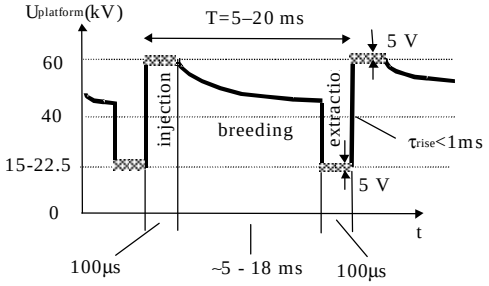

Figure 3. REXEBIS platform potential relative ground during two cycles.

7 VACUUM AND REST GAS SPECTRUM

The REXEBIS requires an extremely good residual gas pressure (10^{-11} mbar) inside the trap region to avoid a complete outnumbering of the few radioactive ions. The backbone in the pumping system is one turbo molecular pump on each side of the EBIS. These two pumps will together with a hexagonal pattern of NEG strips replace the needs for cryogenic pumping (traditionally used in cold bore EBIS).

The main vacuum concerns are out-gassing from the inner structure and gas load from the electron collector due to the impacting electrons. Moreover, there will be an argon gas load from the Penning trap, which has an argon buffer gas pressure of 10^{-3} mbar. A 7-stage differential pumping transfer line will provide an argon pressure of ~10^{-14} mbar inside the REXEBIS.

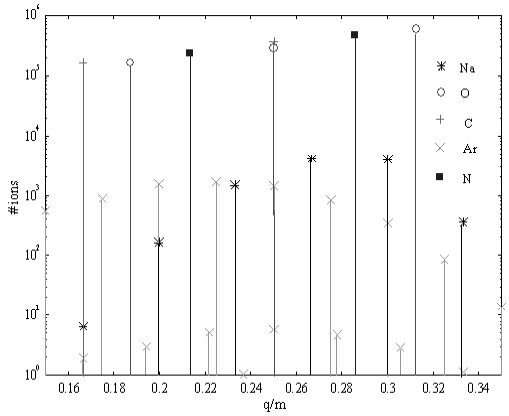

Figure 4. Calculated q/A spectrum showing the absolute number of extracted residual and radioactive ions per pulse. Breeding time 13 ms; 10 000 injected ^{30}Na ions.

Figure 4 shows a calculated q/A spectrum as produced from rest gas, gas from the collector and injected charge-bred ions. It is clear that the ions of interest may display a much lower intensity than nearby rest-gas peaks. To make a clean beam of the isotopes of interest, a mass separator is clearly needed.

Table 2 summarises the design properties of the REXEBIS.

Table 2: The REXEBIS design parameters.

Maximum central magnetic field	2.0 T
Electron gun type (Semi-immersed)	LaB_6
Electron beam current I_e	0.46 A
Electron beam current density	>200 A/cm^2
Electron beam energy E_e	5000 eV
Electron gun perveance P	0.87 A/V$^{3/2}$
Electrons re-entering the trap	<0.25%
Trap length	<0.8 m
Trap capacity (10% compensation)	~$6\cdot10^9$ C

REFERENCES

[1] Radioactive beam experiment at ISOLDE: Coulomb excitation and neutron transfer reactions of exotic nuclei, proposal to the ISOLDE committee, CERN-ISC94-25, Nov 1994

[2] D. Habs, O. Kester, K. Rudolph, P. Thirolf, G. Hinderer, E. Nolte, G. Bollen, H. Raimbault-Hartmann, H. Ravn, F. Ames, L. Liljeby, K-G. Rensfelt, D. Schwalm, R. von Hahn, R. Repnow, A. Schempp, U. Ratzinger, P. van Duppen, M. Huyse, G. Walter, Nucl. Instr. Meth. B vol.126 (1997) p.218-23

[3] D. Habs, O. Kester, G. Bollen, L. Liljeby, K.G. Rensfelt, D. Schwalm, R. von Hahn, G. Walter and P. Van Duppen, Nucl. Phys. A616 (1997) p.29c-38c

[4] B. Jonson, H. L. Ravn, G. Walter, Nucl. Phys. News vol.3 no.2 (1993) p.5

[5] E.D. Donets and V.I. Ilyushchenko, JINR R7-4124, 1968

[6] E. Beebe, L. Liljeby, Å. Engstöm, M. Björkhage, Physica Scripta, vol.47, (1993) p.470-474

[7] E. Beebe, L. Liljeby, A. Pikin, E. D. Donets, D. Habs, K. Janko, O. Tengblad, P. van Duppen, the ISOLDE collaboration, Nucl. Instr. Meth. B vol.93 (1994) p.378-381

PAPER 2

REXEBIS design and initial commissioning results

Authors:
F. Wenander, J. Cederkäll, B. Jonson, L. Liljeby, G. Nyman, K-G. Rensfelt, B. Wolf, Ö. Skeppstedt and the REX-ISOLDE collaboration.

Accepted for publication in:
Proc. of the 8th International Symposium on Electron Beam Ion Sources and Traps and their Applications, Brookhaven National Laboratory, Nov 6-8, 2000. AIP Conference Proceedings Series.

REXEBIS,
Design and Initial Commissioning Results

Fredrik Wenander[1], Joakim Cederkäll[2], Björn Jonson[1], Leif Liljeby[3], Göran Nyman[1], Karl-Gunnar Rensfelt[3], Örjan Skeppstedt[3],
Bernhard Wolf[2] and the REX-ISOLDE Collaboration

[1] *Chalmers University of Technology, SE-412 96 Göteborg, Sweden*
[2] *CERN, EP, CH-1211 Geneva 23, Switzerland*
[3] *Manne Siegbahn Laboratory, Frescativägen 24, SE-104 05 Stockholm, Sweden*

Abstract. The REXEBIS is an Electron Beam Ion Source (EBIS) developed particularly for charge breeding of rare and short-lived isotopes produced at ISOLDE for the REX-ISOLDE post accelerator. Bunches of singly charged radioactive ions are injected into the EBIS and charge bred to a charge-to-mass ratio of approximately ¼ and thereafter extracted and injected into a short LINAC. This novel concept, employing a Penning trap to bunch and cool the ions from an on-line mass separator prior to charge breeding in an EBIS, results in an efficient and compact system. In this article the final REXEBIS design is presented together with results from the first tests.

INTRODUCTION

The REXEBIS [1,2] is part of a larger pilot project, called REX-ISOLDE [3,4,5], see figure 1, which is a development of the already existing on-line mass separator ISOLDE at CERN. The aim is to demonstrate an efficient scheme for post-acceleration of radioactive ions [6]. Radioactive ions produced by ISOLDE are bunched and cooled in a Penning trap [7,8] prior to charge-state breeding in the REXEBIS. The highly charged ion beam is thereafter mass and charge separated in an achromatic separator [9] and subsequently accelerated in a three stage LINAC consisting of an RFQ [10], an IH-structure [11] and three 7-gap resonators [12]. This results in a final energy variable from 0.8 to 2.2 MeV/u, which is an energy range that allows for a wide number of experiments in the fields of nuclear spectroscopy, astrophysics and solid state physics.

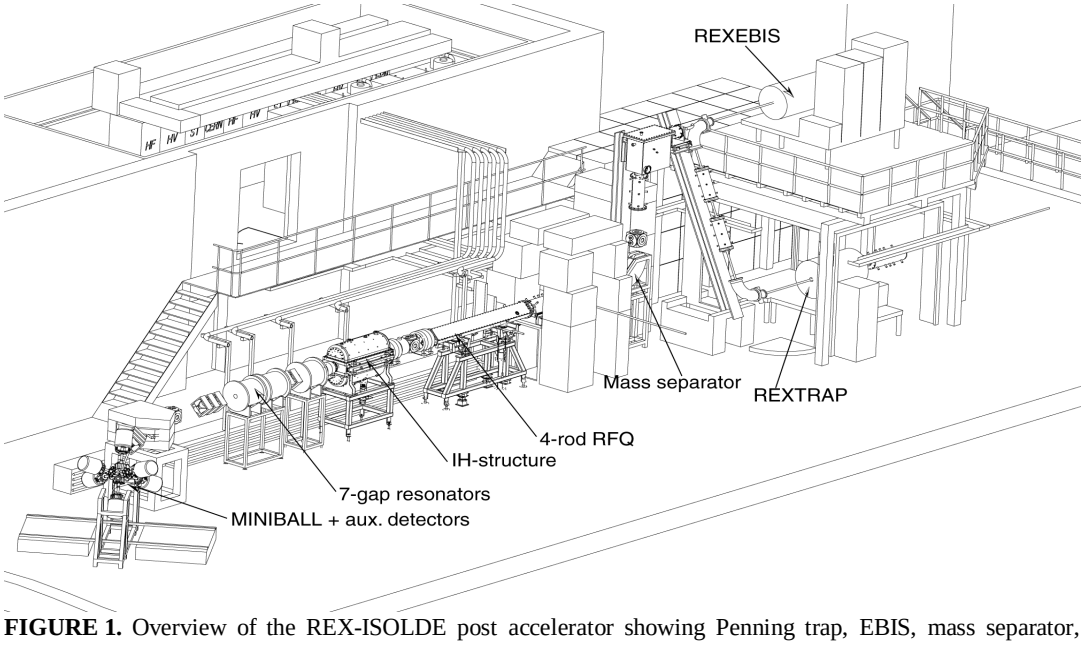

FIGURE 1. Overview of the REX-ISOLDE post accelerator showing Penning trap, EBIS, mass separator, LINAC and detectors.

The introduction of an EBIS into the post accelerator chain brings the singly charged ions delivered by ISOLDE to a Q/A-value of ~1/4.5 permitting the length of the succeeding LINAC to be considerably reduced. The use of an accumulating Penning trap for beam cooling and bunching in combination with a charge breeding EBIS is a completely new concept. Design studies promise a high efficiency for this scheme, which is of paramount importance when handling the rare exotic nuclei produced by ISOLDE. The complete REX-ISOLDE post-accelerator is expected to be operational in 2001.

REXEBIS SPECIFICATIONS

The planned performance of the REX-ISOLDE post accelerator, together with the strict limits set by the Penning trap and the following mass separator/LINAC had to be taken into account in the REXEBIS design. To begin with the following general constraints had to be satisfied:

- *Wide range of number of injected ions* – depending on the production yield from ISOLDE, the number of ions can vary between a few and 10^7 per pulse, where the upper limit is due to space charge limitations in the Penning trap.
- *High breeding efficiency* – the EBIS has to have a high injection and extraction efficiency (>50% [13]) in order to extend the operation to exotic ions with low production yields. The statistical nature of the ionisation process limits the number of ions in the dominant charge-state to around 30%.
- *Limited breeding time* – because of the short lifetimes for light radioactive nuclei the breeding time is restricted to <20 ms. An even shorter cycle time is possible for light elements.
- *High reliability* – the EBIS has to be reliable since it is part of a complex accelerator chain.
- *Moderate ion mass* – in a first stage experiments on nuclei with A<50 are planned.

Moreover, the Penning trap and the following mass separator/LINAC, imposes further requirements and restrictions on the REXEBIS design, for example the Penning trap delivers ions:

- with a transversal emittance $\varepsilon_x=\varepsilon_y<3$ π·mm·mrad at 60 kV assuming an ISOLDE emittance of 35 π·mm·mrad
- with a longitudinal emittance of ~5 μs·eV
- in bunches of a few to 10^7 ions, bunch length ~10 μs
- with a repetition rate of 50 Hz (optionally up to 100 Hz)

and the mass separator/LINAC requests:

- ions with Q/A > 1/4.5
- ions with 5 keV/u
- the delivered beam to fit within an emittance ellipse of 40 π·mm·mrad (4σ)
- an energy spread <50 eV/Q

To fulfil the above specifications, we have chosen a design based on a 5 keV electron beam with a current of 0.5 A. The current density is >200 A/cm^2 throughout a 0.8 m long trap region. With these parameters the REXEBIS trap can hold up to ~$6\cdot10^9$ charges at an electron beam charge-compensation of 10%. This is more than two orders of magnitude larger than the number of ions that can conceivably be delivered by the Penning trap due to its intrinsic space charge limitations. Figure 2 illustrates the breeding time versus charge-state for a selection of elements. To reach high charge states of heavier elements (A>50) either the breeding time or the current density has to be increased.

Several processes that compete with successive ionisation occur in an EBIS. Their influence is, however, predicted to be small for the REXEBIS due to the moderate charge-state breeding. During the ionisation process, elastic Coulomb scattering causes energy transfer from the electron beam to the ion population in the trap. It has been shown in ref. [14] that this heating mainly depends on the charge-state of a specific ion. Assuming that the ions are extracted immediately after reaching the desired charge-state, the REXEBIS heating voltages for $^{30}Na^{8+}$ ions are ΔU_{axial}=14 mV and ΔU_{radial}=0.4 V $\leftrightarrow$ ΔE_{axial}~0.1 eV and ΔE_{radial}~3 eV, which is much less than the radial trapping voltage of ~100 V inside the electron beam (non-compensated trap).

Another inherent heating process, unavoidable in a non-compensated trap, is the ionisation heating that occurs when the charge-state of an ion in a potential well is increased. At the moment of ionisation the position and kinetic energy of the ion are approximately unchanged, but the poten-

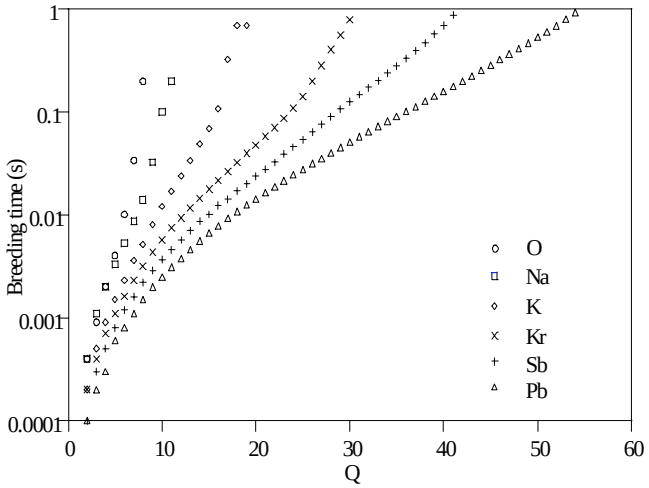

FIGURE 2. Charge-state evolution versus breeding time for a selection of elements, not all planned to be used in the REXEBIS in a first stage.

tial energy increases since the depth of the potential well increases. Thus, as the ion charge rises, so does its mean energy in the trap. This kind of heating does not directly lead to ion losses but contributes to the energy spread in the extracted beam.

SOLENOID

The REXEBIS magnet is an iron shielded, superconducting, 2 T solenoid manufactured by Oxford Instruments. The solenoid is 1200 mm long and has a 150 mm diameter room temperature bore. By employing correction coils at the ends of the winding it was possible to produce an 800 mm long constant field region with a homogeneity better than $5 \cdot 10^{-3}$. There were two main reasons in favour of a room temperature bore over the cold bore used in most EBISes. The release of condensed elements deposited during previous runs can be avoided and consequently memory effects are strongly suppressed. Secondly the out-gassing from electron beam loading on the drift tubes and other surfaces inside the bore is reduced.

The system has a specified holding time of >14 days for LqHe (~70 *l*) and LqN_2 (120 *l*), with the current leads connected. Two identical systems have been ordered. The second will be used for the twin ion source that is planned to be set-up as a test-bench at MSL.

ELECTRON OPTICS

The REXEBIS electron gun is of the so-called semi-immersed type, which means that the cathode is in a strong magnetic field and only magnetic beam compression is achieved. This means that the current density compression will be almost proportional to $B_{max}/B_{cathode}$.

The relatively low compression, ($j_{trap}/j_c \approx 11$) is compensated for by a larger cathode-current loading. A focussing electrode with Pierce geometry produces flat equipotential lines at the cathode and a uniform emission density from the cathode, as well as a laminar flow. The scalloping of the electron beam is, however, a drawback of this injection method. This can be suppressed by adding a post anode in the design. If it is positioned appropriately in the z-direction and a high potential is applied, it will reduce the beam blow-up after the anode and the ripple of the beam. On the other hand, a post anode at high potential in an axial magnetic field will act as a Penning trap for electrons. For this reason the post anode is an option that has to be practically evaluated before being implemented in the design.

Results of EGUN [15] simulations of the extracted electron beam, with and without post acceleration, are shown in figure 3. It can be concluded from these simulations that post acceleration results in a less scalloping beam, as expected. The effect is, however, not overwhelming for $U_{post\ anode} < 10\ 000$ V. With $U_{anode}=6500$ V the electron beam and the perveance is determined to be $I_e=0.46$ A and $P=0.87\ \mu A/V^{3/2}$, respectively. The cathode surface is positioned at a magnetic field $B_z=0.2$ T. The simulated beam profile r_{ebeam} equals ~0.24 mm in full field, which corresponds to a full-field electron current-density j_e(full field) of 250 A/cm^2, surpassing the design value of 200 A/cm^2.

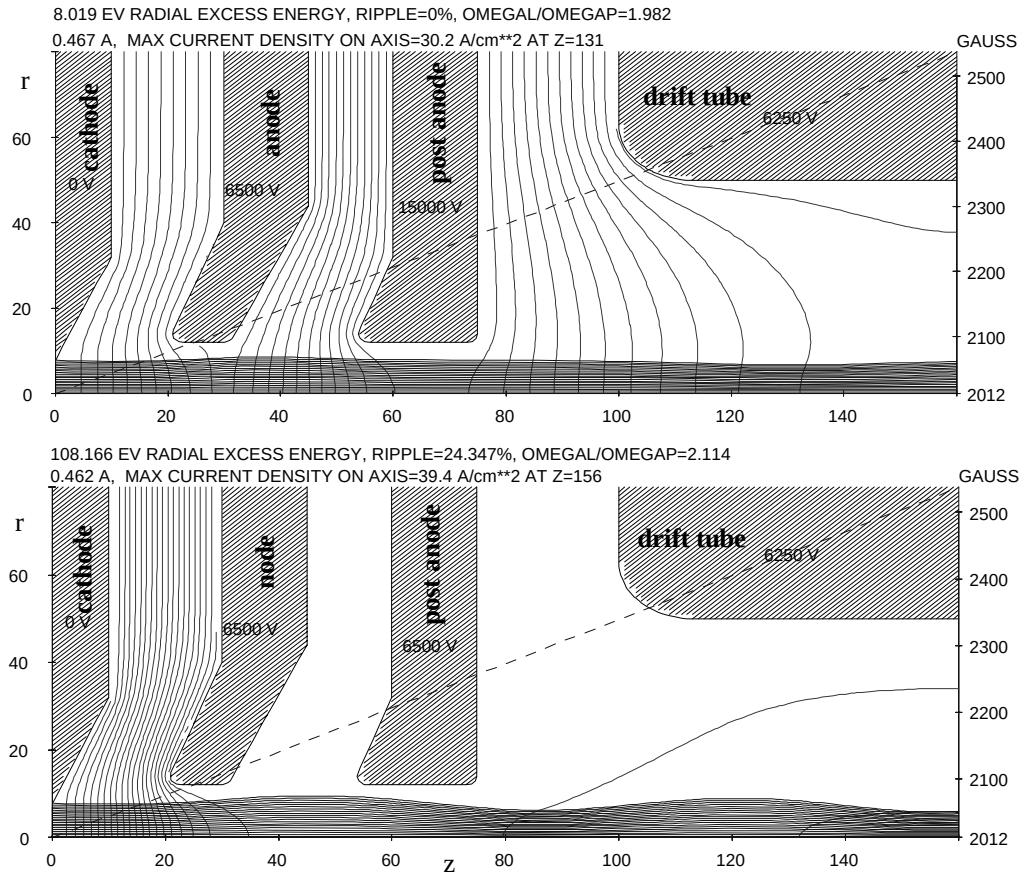

FIGURE 3. Simulation of the electron beam in the gun region with and without post acceleration. One unit of length corresponds to 0.1 mm.

The beam scalloping in full magnetic field is less than ±5 V. In ref. [16] Herrmann states that the scalloping will be largely suppressed by the higher frequencies of the motion of the electrons winding in and out of the beam if $B_c << B_{full}$.) The beam stiffness, defined as the ratio between the Larmor (ω_L) and the plasma (ω_p) frequencies, equals 5.1 in full field.

Mono crystalline lanthanum hexaboride (LaB_6, crystal orientation <310>), from FEI Company, is used as cathode material. The lifetime at T_c=1750 K, yielding a cathode current density j_c of 25 A/cm^2, is approximately 1 year if a surface degeneration of 100 µm is accepted.

The REXEBIS has three trapping tubes: 100, 230 and 464 mm long with 2 mm spacing, combinable to trap lengths of 100, 230, 332, 464, 696 and 798 mm. The theoretical trapping capacity for a 0.8 m trap is $6 \cdot 10^{10}$ elementary charges and the design value for the electron beam energy E_e is 5000 eV. The tube potentials are set by fast switching supplies of type TREK 50/750 (1500 V, 100 mA), with slew rates >125 V/µs.

The cross section of the inner structure is shown in figure 4. The inner structure is mounted in a 100 mm diameter stainless steel vacuum tube. The five drift tubes have an inner diameter of 10 mm, and are made of titanium. Titanium was chosen as material for the inner structure because of its low out-gassing and the conceivable sublimating properties of the material. The low electrical conductivity should reduce the risk for electron-beam resonance-phenomena in the structure. The tube ends are adjustable sideways in pairs by three insulating supports that are mounted on the support plates. The support plates are in turn fixed to the solenoid by three stainless steel support tubes.

The electron beam is separated from the ions in the collector and absorbed at its surface. Important properties for the collector design are e.g.: a high electron collecting efficiency; small ion beam influence; and a low out-gassing rate.

To minimise aberrations and increase pumping conductance the REXEBIS collector was designed with an open end. Ions are extracted from the collector region by a 28 mm diameter cylindrical extractor at -20 kV relative to the drift tubes. Simulations show that the ion beam fills less than 1/5 of the extractor diameter, and there are no indications of a distorted phase space.

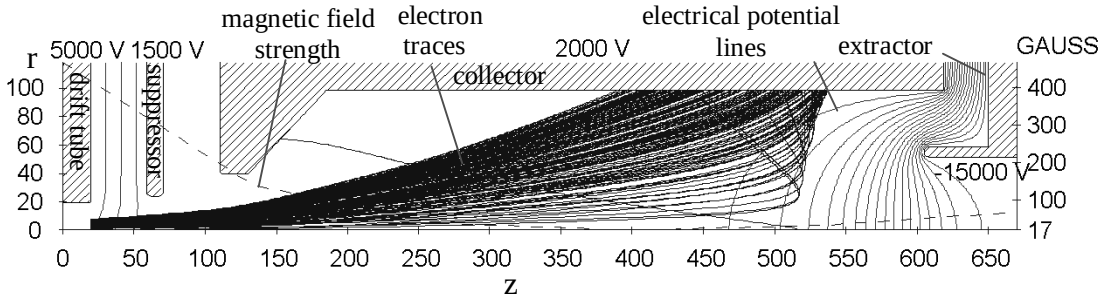

FIGURE 5. EGUN simulation of the absorbed electron beam. One unit of length corresponds to 0.25 mm. Each trajectory (in total 210) carries about the same current (~2.5 mA) and the trajectories have a thermal starting energy of 0.1 eV (⇔ 1100 K) at the cathode.

An EGUN simulation of the absorbed electron beam is shown in figure 5. The dashed line visible to the left in the picture indicates the magnetic field strength. The electron beam is dissipated over an area of ~65 cm^2, i.e. the average current load is <8 mA/cm^2.

A detailed simulation of the electron behaviour in the collector was made in order to determine the fraction of electrons that are reflected into the trap region [1]. The results showed that the back-scattering breaks down into <0.1% by direct reflection, <0.1% by inelastic back-scattering, and <0.05% by elastic back-scattering.

The collector is water cooled and made of OFHC copper. The complete collector structure is bakeable to 350 ºC. A cylindrical 5 mm mild steel screen around the collector reduces the magnetic field inside to less than 0.02 T.

INJECTION AND EXTRACTION OPTICS

The injection/extraction optics guide the ion beam from the transport line to the EBIS during injection and in the opposite direction to the mass separator during extraction. The REXEBIS optics section contains the following elements (see also Figure 6):

- Two 80 mm diameter cylindrical deflectors for steering. The deflectors are made of cylinders that have been sliced into four 90° sectors.
- Two 80 mm diameter einzel lenses for focusing.
- Optionally a differential pumping stage made of a 50 mm long and 10 mm wide tube.
- Retardation system (60 keV to 20 keV).

The lenses and reflectors are switched between injection and extraction settings since the injection and extraction voltages differ due to the design criteria discussed above. The switching voltages for the lenses and the steering plates are generated by TREK 20/20 (±20 kV, 20 mA) and TREK 601B (±500 V, 20 mA) supplies, respectively. The switching is performed in less than 1 ms.

The REXEBIS is located on a platform at ~60 kV potential during injection, allowing the cooled 60 keV ions extracted from the REXTRAP to be captured. During the breeding period, the potential is decreased to provide an ion beam with an energy of 5 keV/u for acceleration in the RFQ. This injection energy ensures an efficient, adiabatic bunching and small output emittance from the RFQ. The platform potential during injection and extraction is shown in figure 7. The platform voltage is generated by a switchable 60 kV/100 mA HV supply from FUG with rise and fall times, between 15 and 60 kV, of 1.1 ms for the 0.8 nF capacitive load generated by the platform itself. The voltage accuracy is better than 10^{-4}.

Two beam-diagnostics elements are implemented in order to assure correct conditions for injection and extraction. A Faraday cup registers higher beam currents and a CCD camera is used to image the beam profile and position for low intensity beams. These detectors are bi-directional, i.e. they either register the injected beam coming from REXTRAP or rest-gas beam going out from REXEBIS. These beam monitoring systems are installed at the EBIS beam focal point outside the outer einzel lens, and at the symmetry point in the transport line. A double-sided MCP diagnostics unit will also be introduced closer to the EBIS.

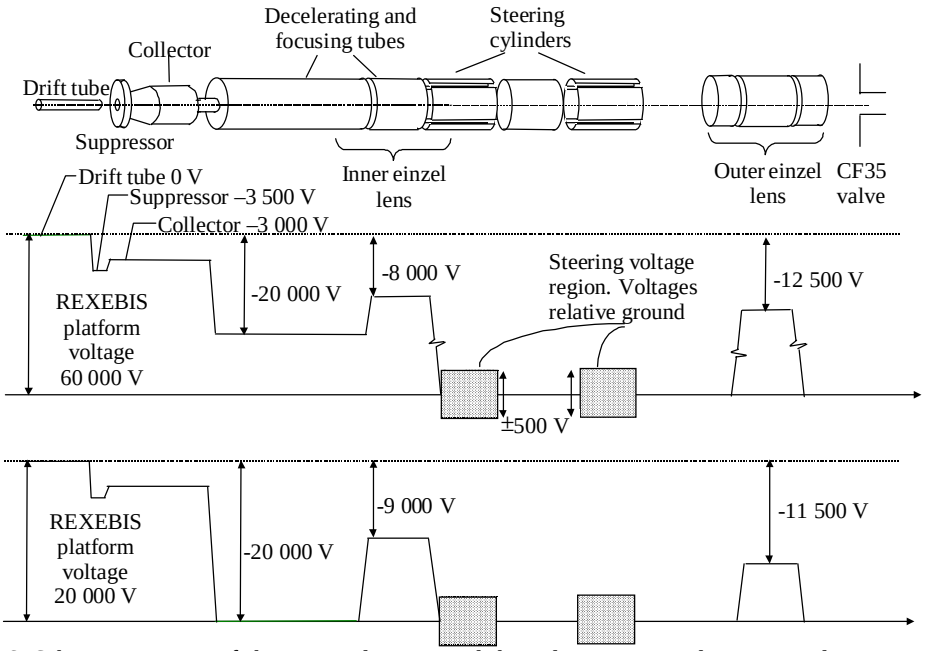

FIGURE 6. Schematic picture of the optics elements and the voltage settings during typical injection. The einzel lens voltages are switchable between +20 and –20 kV, the steering plates between +500 and -500 V.

CONTROL SYSTEM

The control system of the REXEBIS is presently based on a client server model where a task-dispatching server process runs on a VME based Motorola 68030 processor under OS/9. The dispatcher receives requests to start different control processes via TCP/IP packets transmitted from the client processes via the local network using socketing. The control hardware for the REXEBIS consists, on the one hand of ADCs and DACs connected to a PROFIBUS line that is controlled by a VME resident PROFIBUS controller and on the other hand by a set of functions generators, so-called GFASs [18] that also reside in VME. The PROFIBUS controlled ADCs and DACs are used for the control of static parameters such as e.g. lens voltages and electron beam control whereas the function generators drive devices that need to be dynamically controlled. The client processes can be started on a number of control consoles, which in the present concept of the ISOLDE control system, means that they may run on any PC that runs Windows95 or NT. At start-up the client process typically connects to a database located on a server to inquire about current settings for the hardware it intends to control. The user subsequently controls the equipment completely via a GUI.

Due to the potential differences between the three voltage platforms that the REXEBIS system comprises, the control signals for the PROFIBUS ADCs and DACs, as well as for the DACs connected to the function generators, are transmitted via fibre-optic links. The vacuum system is independently controlled via a PLC based (SIMATIC) control system that is connected to a second PROFIBUS line whose controlling process runs under NT.The REXEBIS control system is presently undergoing an upgrade in order to make it comply with the general control concept used for REX-ISOLDE as a whole.

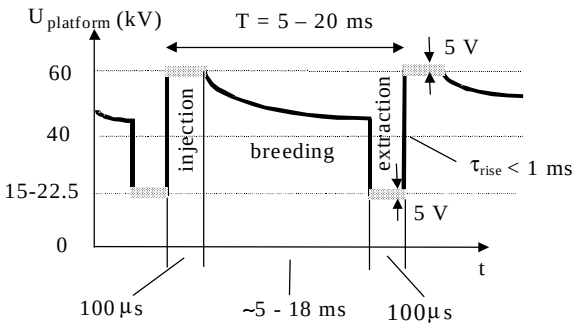

FIGURE 7. REXEBIS platform potential relative to ground potential during two cycles. (The internal REXEBIS voltages, for instance the barrier tube voltages, are related to this platform potential).

VACUUM COMPONENTS

The REXEBIS vacuum requirements are challenging. This is due to the absence of cryogenic pumping inside the warm-bore REXEBIS and the necessity of being able to charge breed ions without losses. A poor vacuum in the trapping region can result in such a considerable number of residual gas ions that the separation of the radioactive ions from the rest-gas ions is obstructed. The REXEBIS will be operated with low compensation of the electron beam space charge. For example, the residual gas pressure needed to cause 10% compensation, assuming 20 ms breeding time and H_2 as dominating residual gas, is about 10^{-8} torr.

Turbo and NEG pumps are used to create a high-quality vacuum. The backbone in the pumping system is two Pfeiffer TPU180 (180 *l*/s) turbo drag pumps, located on the gun and at the collector sides, respectively. The optics system following the EBIS is pumped by a Pfeiffer TPU260 turbo pump. These three pumps are backed by a small turbo on ground potential providing a fore vacuum better than 10^{-5} torr. The system provides a base pressure better than 10^{-11} torr inside the EBIS.

Non-evaporative getters (SAES St707), with a total getter area of 6000 cm^2, are mounted in an octagonal geometry around the inner structure in order to provide additional pumping in the ionisation region. The getter material has a very high pumping speed of 1 $l/cm^2 \cdot s$ for H_2 [19] while O_2, N_2 and CO are pumped with 65%, 15% and 40% of that speed. The hydrocarbon sorption efficiency is very low, and inert gases are not pumped at all. The complete vacuum system and the internal parts will be vacuum fired, the stainless steel parts at 950° C and the titanium at 700° C, to reduce the out-gassing of hydrogen. The whole vacuum system is baked at 350° C, which is also needed for activation of the NEG pumps.

As REXTRAP operates with an Ar (alternatively Ne or He) pressure of about $3 \cdot 10^{-3}$ mbar, five differential pumping stages are introduced along the transport line, with a turbo pump in each section. This is expected to give a partial Ar pressure at the EBIS optics tube of about 10^{-12} torr, which is acceptable for EBIS operation.

The partial pressures in the trap region have been estimated using a simplified REXEBIS vacuum model [1]. The absolute number of residual gas ions produced during a breeding period was estimated with help of this model and the resulting Q/A-distribution was deduced. The Q/A-spectrum, with 10 000 injected ^{30}Na ions, is given in figure 8 for a breeding time set to optimise charge-state 8^+. Since the N_2 partial pressure is uncertain, it was assumed to be same as for O_2. It is clear form the extraction spectrum that a mass selection system with a good resolution is needed after the REXEBIS, in order to separate the residual gas ions from the radioactive ions, as the number of rest-gas ions may exceed the number of radioactive ions by orders of magnitude. A high resolution achromatic mass analyzer, with a Q/A-resolution of approximately 150 [9], has therefore been constructed.

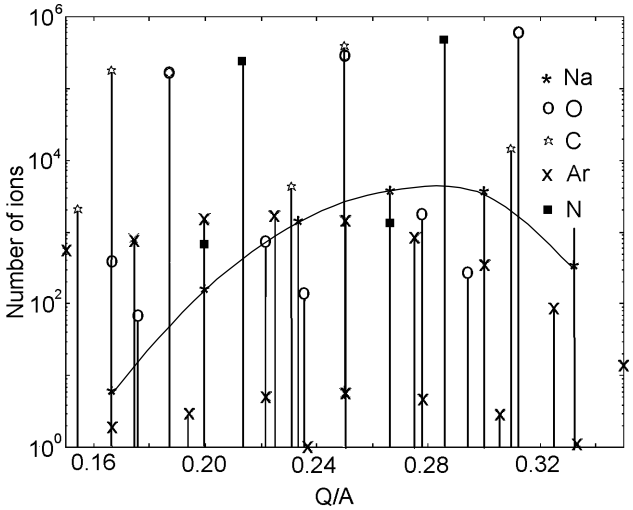

FIGURE 8. Calculated Q/A spectrum showing the absolute number of residual and radioactive ions. Breeding time 13 ms; 10 000 ^{30}Na ions; Ar diffusion from the REXTRAP (^{16,17,18}O, ^{12,13}C, ^{14,15}N, ^{36,38,40}Ar isotopes are present).

FIRST TEST RESULTS

The most important commissioning results from the four major test runs with the REXEBIS are presented in this section. The effort has, so far, concentrated on electron beam investigations and ion beam production from the rest-gas.

Vacuum

A vacuum better than 10^{-11} mbar has been reached after bake-out with the electron beam switched off. On the other hand the pressure in the gun and collector regions increased to between 2 and $20 \cdot 10^{-9}$ mbar with the electron beam on. Inside the trapping region the pressure has been estimated to between 2 and $5 \cdot 10^{-9}$ mbar. It has so far not been possible to perform an optimal bake-out. As a consequence, the electron beam tests carried out so far have suffered from a poor vacuum. In the future, after a complete vacuum firing of all inner parts and with a complete baking procedure, the vacuum with electron beam on should improve significantly.

Electron Beam

The initial tests showed that the electron beam was well-behaved and not critically sensitive neither to drift tube nor to suppressor or collector voltage settings. The loss current, I_{loss}, i.e. current going to EBIS ground potential instead of to the suppressor and the collector, was <0.5% for an electron current I_e=200 mA. It displayed a small variation during the breeding cycle and peaked for an uncompensated trap. At a higher electron current the loss increased exponentially, and with a power-supply limitation of 2.5 mA, a maximum current of 375 mA has been obtained. Less than 3% of the loss current reached the anode and the inner drift tube and not more than 1% was collected on the trapping tubes. On the other hand, the largest portion (50-70%) went to the drift tube closest to the suppressor. The rest of the loss current could not be accounted for. The excessive loss current could be due to a misalignment of the inner structure with respect to the magnetic field axis. An indication of this is that the loss current is very sensitive to small movements of the EBIS structure. A translation of about 0.2 mm of one end of the structure could occasionally increase the losses by as much as 50%. Another reason could be that the suppressor and collector unit was axially displaced by 5 to 8 mm. The poor vacuum in the collector region most likely contributed to the high loss current as well. It should, nevertheless, be stated that a high loss current is acceptable as the electrodes of REXEBIS are at room temperature.

The experimental gun perveance value, P_{gun}, was found to be 1.55 μP, which exceeds the value of 0.9 μP given by the EGUN simulation. A perveance that exceeds the design value may be favourable since it allows for a lower electron beam current and energy while maintaining a short breeding time. The beam energy will not restrict the ionisation possibilities at a moderate charge-to-mass ratio of ~1/4 and A<50. Moreover, the change in space charge capacity is small, and in any case only 10% of the total capacity is occupied by injected ions. At present, the maximum electron current in REXEBIS yields a calculated breeding time that is ~1.2 times longer than the design value and has 84% of nominal space-charge capacity.

It has been noted that large and rapid variations in the cathode filament heating caused the perveance to change. The perveance of the electron gun dropped abruptly, typically in steps of 0.1 to 0.2 μP, after each cool-down and warm-up cycle. This can most likely be attributed to an axial movement backwards of the cathode in its support clamps. With a considerably slower warming-up and cooling-down procedure one could possibly avoid this phenomenon. The electron beam tests have therefore been carried out with a gun perveance going from 1.55 down to 0.6 μP.

Extracted Ion Beam

The peak current of the extracted pulse varied between 20 and 300 μA depending on the selected breeding and/or extraction time. The latter time was varied by applying either a flat voltage distribution or a 300 V ramp over the trap tubes at extraction. The extracted DC component was approximately only 1 μA, but with an extraction duty factor of 1‰, it still dominants over the pulsed beam. By switching the beam with the steering plates in the optics line, clean pulses can be obtained for DC measurements. The extracted pulse shape for a ramped extraction is plotted in figure 9.

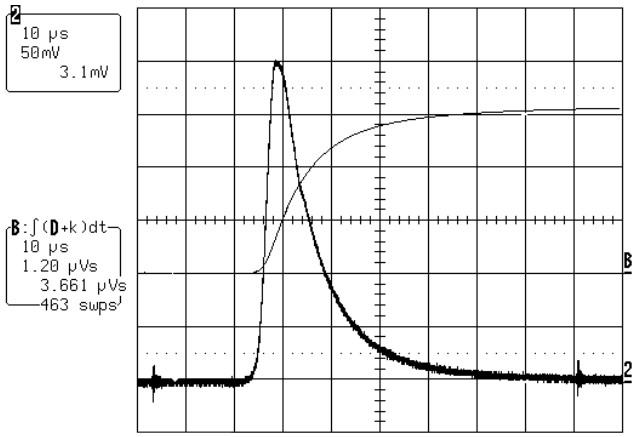

FIGURE 9. EBIS pulse (trace 2) recorded in a FC (1 kΩ load resistor) for non-ramped extraction. T_{period}=200 ms, $T_{breeding}$=150 ms, I_e=279 mA. Integrated charge (trace B) where 1 µVs ⇔ 1 nC.

The electron beam compensation time was investigated and it was found that the extracted charge saturated after 50 ms at a collector rest-gas pressure of approximately $1 \cdot 10^{-8}$ mbar, see figure 10. It is interesting to note that the extracted charge is not zero even for very short breeding times. This might be explained by a disturbance being induced in the electron beam when the potentials of the trap electrodes are switched. This may force the beam to hit parts of the inner structure and thus cause out-gassing from the surfaces. Theoretically, the EBIS trap can confine 5.4 nC, but only 2.5 nC was extracted in the first test. After tuning of the extraction optics the extracted charge increased to about 3.7 nC, i.e. to a compensation level of 68%. Further increase of the trap barrier height, with ramped as well as with non-ramped extraction, did not enhance the extracted charge, neither had the extraction time any significance on the amount of extracted charge.

It was found that the number of extracted ions was influenced by the cycle time also for a fixed confinement time (assuming an uncompensated trap). A longer period time resulted in fewer extracted ions per pulse. This suggests that frequent switching of the trap, and thereby a frequent change of the electron beam propagation, caused a higher release of rest-gas from the interior surfaces. For example, with $T_{breeding}$=45 ms and T_{period}=50 ms => 2.33 nC extracted charge, while for $T_{breeding}$=45 ms and T_{period}=200 ms => 1.80 nC extracted charge.

The extracted beam profiles were recorded using a multi-channel plate 0.5 m after the outer einzel lens. Optimal focusing resulted in a beam-spot size of 5 mm.

A typical rest-gas spectrum analysed in the REX-ISOLDE mass separator is shown in figure 11 (DC component gated away). The presence of oxygen and carbon, but also of some nitrogen is clear. The neon peaks appear since REXTRAP was operated with neon as buffer gas and the differential pumping system in the transport line was incomplete. The relatively low amount of detected H_2 is confusing, but could possibly have its explanation in the large emittance for low-charged hydrogen, which has poor transmission out of the EBIS and through the mass separator. Hydrogen may also be heated out of the trap by collisions with heavier elements. A j_e-value of 125 to 150 A/cm^2 was calculated (125 A/cm^2 expected). Due to the elevated filament heating, significant traces of lanthanum and boron were also seen in certain mass spectra.

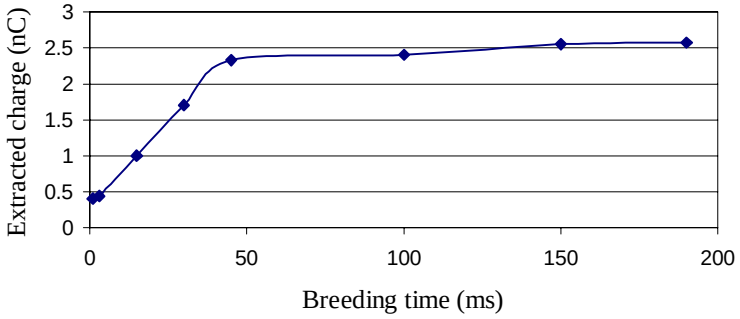

FIGURE 10. Extracted charge as function of breeding time, for I_e=282 mA and a cathode to trap voltage of 5800 V. The collector rest-gas pressure was $9 \cdot 10^{-9}$ mbar. The theoretical trapping capacity was 5.4 nC.

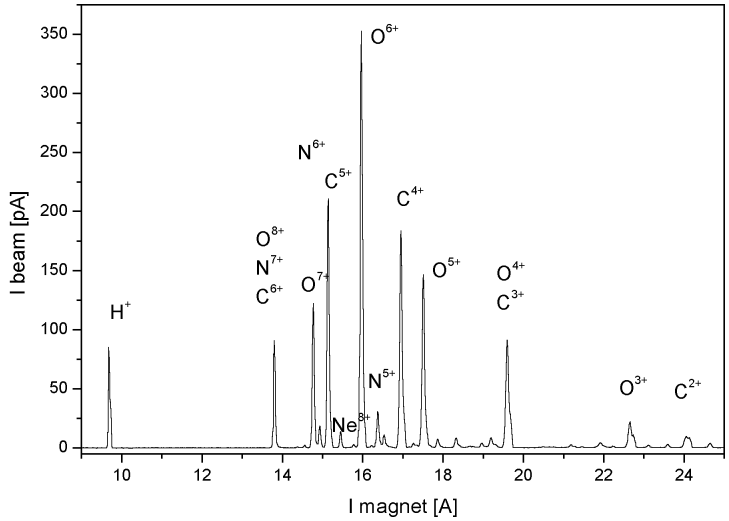

FIGURE 11. Mass-analysed residual gas spectrum from REXEBIS, with an estimated trapping region pressure of $5 \cdot 10^{-9}$ mbar. REXEBIS parameters: I_e=210 mA, U_{trap}=5440 V and $T_{breeding}$=20 ms.

Emittance Measurements

The emittance of the extracted and non-separated beam was measured at an extraction voltage of 20 kV using an emittance meter of the slit-grid type. The device was positioned either directly after the REXEBIS or in the mass separator line. The relatively weak average current, ~150 nA extracted out of the EBIS, resulted in a modest signal-to-noise ratio in the emittance meter (which in its present version has no gating possibilities). The determination of the background level, and consequently the measurement of the geometrical emittance, was therefore hampered. It was not possible to measure the emittance for separate charge states after the mass separator due to the too low current.

The effect of the breeding time on the emittance was investigated in a first set of measurements. With an increased breeding time, the geometrical emittance increased from 20 π·mm·mrad ($T_{breeding}$=1 ms) to over 60 π·mm·mrad ($T_{breeding}$=85 ms). The electron beam gradually became compensated with longer breeding times because of the poor vacuum inside the EBIS trap ($2\text{-}5 \cdot 10^{-9}$ mbar). Compensation of the electron beam generates a large emittance since it makes the ions move with larger radii inside the trapping region.

A difference in orientation of the horizontal and vertical phase spaces was recorded. The horizontal phase space had its beam waist at the emittance meter while the vertical phase space was significantly divergent. This effect is not expected as the EBIS and its extraction optics, except for the deflectors, have an axial symmetry. The source of this quadrupole component has not yet been determined, but might possibly be a misaligned solenoid field. The horizontal phase space showed signs of aberration, which also could be attributed to a misaligned solenoid field or to influence from the Penning gauge magnets.

A minor emittance decrease was recorded when the electron beam current was decreased from 240 to 82 mA, which leads to a more shallow electron beam well. A more exact value could not be arrived at due to the low signal-to-noise ratio for the lower current. The result nevertheless agrees with the general expression for the emittance $\varepsilon \propto C_1 B + \sqrt{C_2 B^2 + I_e}$, where B denotes magnetic field, and C_1 and C_2 are constants. No beam was seen at the emittance meter with a statically open trap (i.e. EBIS operated in TOF-mode) using steerer gating. This verifies that the measured signal originates in the trapping region and that no significant ion production takes place in the collector region. On the other hand, without gating, a detectable current was recorded, and a geometrical emittance of ~15-20 π·mm·mrad was measured. This case simulates an EBIS with very good vacuum, since the electron beam is completely non-compensated, and represents what can be expected for the REXEBIS operating at optimum vacuum conditions. The calculated geometrical emittance for low-charged (1^+ or 2^+) rest-gas ions is 19 π·mm·mrad, which is in good agreement with the measured value. The horizontal phase space for a breeding time of 1 ms is shown in figure 12.

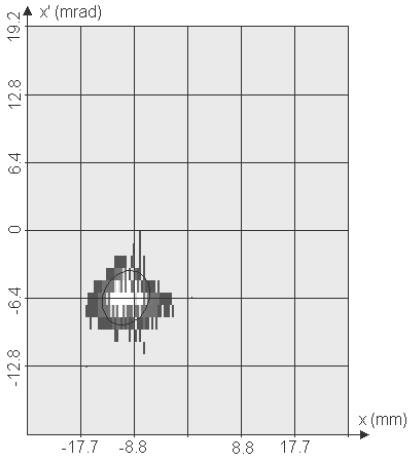

FIGURE 12. Horizontal phase space plot for 1 ms breeding time. The ellipse encloses an emittance of 9.9 π·mm·mrad. REXEBIS parameters: I_e=300 mA and U_{trap}=4960 V.

CONCLUSIONS AND OUTLOOK

After two years of installations the build-up phase of the REXEBIS at ISOLDE is nearly completed. Several important commissioning results have been achieved. Although the design values have not been fully reached so far, the results are promising.

In the immediate future, with the mass separator and the beam transport line from the Penning trap to the EBIS in place, a new series of studies will commence. On the agenda are: determination of the electron current-density and residual gas composition; emittance measurement of different charge states; and finally injection tests determining the overall efficiency for ions delivered by the Penning trap.

ACKNOWLEDGMENTS

This work is funded by the Knut and Alice Wallenberg Foundation, Sweden. We thank Oliver Kester for supplying the emittance meter and for his assistance during the emittance measurement.

REFERENCES

1. Wenander, F., Jonson, B., Liljeby, L., and Nyman, G., *CERN-OPEN-2000-300*, CERN, Switzerland, (2000).
2. Rao, R. and Wenander, F., *Nucl. Instr. Meth.* **A416**, p210 (1998).
3. Radioactive beam experiment at ISOLDE: "Coulomb excitation and neutron transfer reactions of exotic nuclei", proposal to the ISOLDE committee, *CERN-ISC94-25*, Nov 1994, CERN, Switzerland.
4. Habs, D. et al., *Nucl. Instr. Meth.* **B139**, p128 (1998).
5. O. Kester et al., *Hyperfine Interactions* **129**, p43 (2000).
6. Jonson, B. et al., *Nucl. Phys. News* vol.3 no.2, p5 (1993).
7. Raimbault-Hartmann, H. et al., *Nucl. Instr. and Meth.* **B126**, p378 (1997).
8. Ames, F, et al., Proc. 2nd Int. Conf. On Exotic Nuclei and Atomic Masses (ENAM98), 23 Nucl. Instr and Meth. **A427,** p170 (1999).
9. Rao, R., et al., *Nucl. Instr and Meth.* **A427** p170 (1999).
10. Sieber, T. et al., *Proceedings of of the XIX International LINAC Conference,* edited by C. E. Eyberger et al, Argonne National Laboratory, Chicago, Vol. 2, p777.
11. Kester, O. et al. *Proceedings of the 6th European Accelerator Conference,* edited by S. Myer et al, Institute of Physics Publishing, London, 1998, p728.
12. Podlech, H. et al., *Nucl. Instr. Meth.* **B139**, p447 (1998).
13. Beebe, E. et al., *Nucl. Instr. Meth.* **B93**, p378 (1994).
14. Becker, R., *Proc 3rd EBIS Workshop*, Ithaca, eds. Kostroun, V. and Schmieder, B. W., p185 (1985).
15. Herrmannsfeldt, W. B., *Electron Trajectory Program SLAC 266*, Linear Accelerator Center, Stanford, 1979.
16. Herrmann, G., *J. Appl. Phys.* **29**, p127, (1958).
17. Schmidt, P., Control system report, *Internal document ISOLDE*, CERN, Geneva, 1998.
18. Heinze, W., Maccaferri, R., *Nucl. Instr. Meth.* **A352,** p147 (1994).
19. Chiggiato. P, *Physica Scripta* **T3,** p9 (1997).

PAPER 3

EBIS as charge breeder for radioactive ion beam accelerators

Authors:
F. Wenander

Accepted for publication in:
Proc. of the 5th Radioactive Nuclear Beam conference, Divonne, France (2000). Nuclear Physics A.

EBIS AS CHARGE BREEDER FOR RADIOACTIVE ION BEAM ACCELERATORS

Fredrik Wenander[a]

[a]*Chalmers University of Technology, 412 96 Gothenburg, Sweden and PS/CERN, 1211 Geneva-23, Switzerland*

Abstract

The numerous forthcoming post accelerators for radioactive ions produced with the isotope separator on-line (ISOL) technique all have a need for an efficient method to accelerate the precious primary ions. By including an Electron Beam Ion Source (EBIS) as a charge breeder after the radioactive ion production stage, a short and compact linear accelerator can be employed as a result of the increased ion charge-to-mass ratio.

In view of the constraints on a post accelerator for radioactive beams, an EBIS appears to be an attractive solution. It is independent of the element injected, and an overall efficiency as high as 30% for the peak charge-state can be attained. The mean charge-state of the extracted ion beam is easily varied by changing the breeding time needed and the beam has excellent properties (time structure and emittance) from a LINAC point of view. Furthermore, the extraction of a bunched beam improves the signal-to-noise ratio for low-intensity beams. The good vacuum inside the source affords the possibility of suppressing residual gas contamination peaks from the extracted beam. With a high electron beam density, the breeding time can be kept short, so decay losses are minimised. To obtain a high efficiency for a charge breeding EBIS, it is advantageous if the beam from the primary production stage in an ISOL system is bunched and has its emittance reduced before injection. To achieve this a Penning trap can be introduced in front of the EBIS. The space-charge limit inside the Penning trap restricts the number of ions per bunch to a couple of orders of magnitude lower than the constraint set by the EBIS. A positive side effect though, is that a mass selection can take place inside the trap if desired.

In this article the above listed features will be discussed more thoroughly. As an example, the charge breeding system for the REX-ISOLDE post accelerator will be introduced. In addition, future possible developments of an EBIS leading to shorter breeding times, the acceptance of a continuous beam, and an increased number of charge-bred ions, will be discussed.

Keywords: charge breeding, EBIS, post accelerator, radioactive ion beam

1. Introduction and motivation

1.1 Higher energy calls for higher charge

One major trend in nuclear physics research is to map the unexplored energies that are not covered by traditional ISOL and Fragment Recoil Separator (FRS) facilities, that is the energy range between a few 100 keV and approximately 25 MeV/u. The bridging of this gap in energy will be accomplished by post-acceleration of ISOL beams. A high charge-to-mass ratio (q/A in the range between 1/9 to 1/4) is inevitable for injection into

a post accelerator, as the simplicity, efficiency and costs of the accelerator are directly related to the charge-state of the low energy ions.

The EBIS was invented more than 30 years ago by Donets [1], and altogether about 20 EBISs are presently in operation around the world. In general, EBISs are mainly associated with high charge-state ion-injection into storage rings, heavy ion injectors, or for atomic physics experiments [2,3,4]. Likewise, as will be shown in this article, it is well suited to charge breed 1^+ ions for an ISOL post-accelerator using a LINAC. In that case, the charge breeding will only be moderate and ion injection will be utilised instead of gas injection, thus slightly relaxing design specifications compared to extreme performing EBISs. Introductions to EBISs are found elsewhere [5].

1.2 Physics with highly charged ions

With an EBIS, one is, in principle, not limited to a charge-to-mass ratio of about 1/4, in fact, fully stripped ions are available up to uranium [6]. The high charge-state of the ions can itself be of physics interest, so instead of accelerating the ions in the post accelerator, they can be used for various physics experiments at an acceleration potential of some tens of kilovolts. For example, the accuracy in mass determination of short-lived nuclei using the Penning trap mass spectrometer technique [7] can be increased; the solid state physics community will profit from the higher ion energy in the form of deeper ion implantation; surface bombardment of highly charged radioactive ions is possible, and more precise tests of QED using heavy hydrogen-like ions are made conceivable.

2. EBIS properties and limitations

2.1 General properties

Because the ions are trapped within an electromagnetic trap without any contact with the walls, no surface chemistry is involved and it is equally easy to charge breed all elements. Furthermore, radioactive contamination of the breeder becomes small. Since no hold-up processes delays the fast charge breeding, decay losses are minimised. In addition, the charge-state distribution in an EBIS is narrow (approximately 30% in a single charge-state depending on element mass), making the ionisation very efficient. Because of the mono-energetic electron beam, even higher peak concentrations (up to 100%) can be reached if shell effects are exploited [8]. Simply by adjusting the confinement time appropriately, the centroid of the charge-state distribution can be chosen so it corresponds to the desired *q/A*-value, and so it does not interfere with rest-gas peaks. Light polarised injected nuclei will remain polarised since the magnetic field inside the EBIS is strong enough to decouple the nuclear and electronic spins, so depolarisation is avoided during breeding [9]. In general, the operation of an EBIS has a high level of reliability, and running periods of several weeks without interruption are regular.

2.2 Ionisation time and attainable charge-state

The main characteristic entity describing an EBIS is the ionisation factor, the product of the electron beam current density j_e and the breeding time τ, which determines the reachable mean charge-state. Due to the statistical behaviour of the ionisation process, the charge of the extracted ions will be distributed between several charge-states. The extracted charge distribution is a balance between the step-by-step ionisation and losses. Nevertheless, the loss phenomena are negligible in a non-compensated EBIS (the electron beam space-charge is not compensated by the ion

charge) intended for charge breeding. Firstly, radiative and dielectric recombination processes are insignificant inside an EBIS [10]. Secondly, a low residual gas pressure results in a minuscule chance for electron pick-up from rest-gas (a fraction of a percent [11]). Elastic Coulomb scattering, by which heat is transferred to the ion population in the trap [12], can induce escape from the electrostatic trap, and thereby limit the attainable charge-state. By adding cool light ions to the beam, the highly charged and hot ions are cooled [13] and maintained for a longer period inside the electron beam. Nevertheless, inside a charge breeder the ion population is only bred to a moderate charge-state, and therefore the heating effect is minor (radial holding voltage less than 1 V). Naturally, a low electron beam energy can in itself be limiting for the highest obtainable charge-state, but already with a very modest electron beam energy of 5 keV, elements up to at least Z=82 can be charge-bred to a charge-to-mass ratio of 1/4.

2.3 Charge breeding capacity

Electron beam compensation is an important concept and denotes the degree of electron beam space-charge compensation caused by the positively charged ions. When the compensation increases, the potential well depth (the radial holding voltage) decreases, and energetic ions may leave the trap. The potential well depth ΔU with a compensation degree k ($0<k<1$) can be expressed as $\Delta U = \frac{1}{4\pi\delta\varepsilon_0}\frac{I_e}{\sqrt{2\frac{e}{m_e}U_e}}(1-k)$, where U_e (V) and I_e (A) are the electron beam acceleration voltage and current, e (C) and m_e (kg) the charge and mass of an electron. Typical radial holding voltage values for k=0.5 lie between 20 and 100 V, and should be put in comparison with the above stated heating values. The attainable compensation degree increases with electron current, and at least 77% compensation has been achieved [14].

The maximal current for certain electron beam energy is determined by the perveance limit, $P = I_e / U_e^{3/2}$. An electron beam exceeding this current is reflected by its own space-charge; this is called the 'virtual cathode' situation. Electron beams with a perveance between 5 and 10 μP are practically realisable. The absolute trapping capacity equals the electron beam space-charge and, with an allowed compensation degree k, it can be expressed as $n = 1.05 \cdot 10^{13} P U_e L_{trap} k$ number of elementary charges, where L_{trap} (m) is the trap length. Representative values for existing EBISs are L_{trap}=1 m, I_e=1 A, U_e=10 kV and k=0.5, which yields $5 \cdot 10^{10}$ charges.

2.4 Longitudinal acceptance and emittance

Bunched injection into the EBIS results in a higher trapping efficiency (59% [15]) than continuous injection. A conservative estimate of the longitudinal acceptance for pulsed injection amounts to 20 μs·30 eV, depending on trap compensation and element mass. Using self-extraction (ions leaving the trap by their own kinetic energy) bunch-lengths between 50 and 100 μs are normal, which are perfectly adapted for injection into a LINAC. The energy spread from an EBIS was measured for instance at CRYSIS, but then with a highly compensated trap. The obtained result was an energy spread of 57 eV/q for a 300 mA electron beam at 17.4 keV [16]. For a trap with a low degree of compensation, as for the REXEBIS, an energy spread of about 15 eV/q is anticipated. The extraction time can be shortened by applying a field gradient within the trap, however, the energy spread will then become larger (up to several hundred eV/q). Also a longer extraction time than 50 to 100 μs is attainable, with an even lower energy spread as a consequence. A pulsed beam structure allows the LINAC to work at a

favourable low duty factor, and increases the signal-to-noise ratio in the experiments, which is advantageous for low-intensity beams.

2.5 Transverse acceptance

The transverse non-normalised acceptance for ions that are fully trapped inside a non-compensated electron beam in an EBIS is [11]:

$$\alpha = \pi \frac{r_{ebeam}}{\sqrt{2U_{ext}}} \cdot \left(Br_{ebeam} \sqrt{\frac{q}{m}} + \sqrt{\frac{qB^2 r_{ebeam}^2}{4m} + \frac{\rho_l}{2\pi\varepsilon_0}} \right) \pi\cdot\text{mm}\cdot\text{mrad}$$

where r_{ebeam}, U_{ext}, q, m and ρ_{l} represent electron beam radius (m), ion injection potential (V), ion charge (C), ion mass (kg) and electron-beam charge per meter (C/m). Inserting representative EBIS parameters yields a 1^+ ion acceptance of the order of 10 π·mm·mrad for 60 kV injection voltage. With increasing compensation the acceptance value decreases. By increasing either the electron beam radius or current, or the magnetic field, a larger acceptance is obtained (a good overlap between electron beam and injected ion beam is necessary for a high efficiency). For example, the Århus EBIS with r_{ebeam}=0.5 mm, B=0.1 T and I_{e}=250 mA, should have an acceptance of about 15 π·mm·mrad.

2.6 Transverse emittance

An EBIS has an excellent transverse emittance, typically smaller than 5 π·mm·mrad at 60 kV extraction voltage, which in general shrinks with increasing charge-state of the extracted ions as long as ion heating effects are not dominating. The fact that the emittance is smaller than the acceptance is due to the radial redistribution of the ions during ionisation. One should emphasise that the emittance is strongly correlated to the acceptance, since no phase space cooling takes place inside the EBIS. The small emittance has a favourable impact on a RNB post-accelerator. For example, beam losses and radioactive contamination are kept low, the resolving power of a mass separator is improved, and RNBs could be focused to micron-size spots.

2.7 Extracted spectrum

An EBIS is a UHV device that has to work at a vacuum better than 10^{-9} mbar to be efficient. The risk of compensating the electron beam by the production of ions from residual gases is not the main reason (a 10% compensation of the beam is reached after 20 ms breeding in a 5 keV electron beam assuming H_2 as the dominating residual gas with a partial pressure of 10^{-8} mbar). It is rather that a poor vacuum inside the trapping region can result in such a considerable number of residual gas ions being created that the separation from the radioactive ions in the mass separator is obstructed.

3. The REX-ISOLDE bunching and breeding system

3.1. Penning trap - EBIS concept

Due to the strong correlation between emittance and acceptance, one finds that a requested beam emittance out of the EBIS of less than 10 π·mm·mrad is impossible to achieve with an acceptance adequately large to enclose the ISOL beam emittance. By introducing a Penning trap [7] in front of the EBIS, which accumulates, bunches and phase space cools the semi-continuous beam, a considerably higher injection and trapping efficiency into the EBIS is obtained and ISOL emittances up to 50 π·mm·mrad can be accepted. Moreover, the mass selectivity (in ideal cases exceeding 10^5 [7]) of the

side-band cooling technique in a Penning trap could be employed for a further purification of the incoming beam. The extracted pulse length from the trap is in the order of 10 μs and has an energy spread of some eV, thus the ions can be easily injected into an EBIS. It is transferred to the EBIS via a transport line, and because of the buffer gas, several stages of differential pumping has to be built in the transport line to ensure a high vacuum inside the EBIS. The trapping losses should be overcompensated by the improved capture in the EBIS. Cooling of the ions to room temperature takes a few ms [17]. The Brillouin constraint states that the space-charge density in a Penning trap is roughly limited to 10^6 mm^{-3}. Hence ~10^8 can be accumulated and cooled per bunch in a large trap. Even though the element indifference remains in principle, the cooling efficiency has to be optimised with the choice of different cooling gases (e.g. He and Ar).

3.2 The REXEBIS

Presently, an EBIS intended to work as charge breeder for radioactive ions is being commissioned, the REXEBIS [11,18] at the REX-ISOLDE [9,19] post-accelerator at CERN. The main design properties of the REXEBIS are listed in Table I.

Table I. REXEBIS design parameters.

Electron beam I_e=0.5 A
Electron beam energy U_e=5 keV
Full electron current density j_e~250 A/cm^2
Maximum trap length L_{trap}=0.8 m
Maximum solenoidal field strength B=2 T
Trapping capacity (10% compensation) 6·10^9 charges

Preliminary electron beam tests show a well-behaved beam, with small losses and no critical settings. The source has so far been operated with an electron current of 250 mA and 4 keV, and a beam of rest-gas ions has been extracted. Extensive simulations have shown that the ion injection and extraction efficiency should exceed 90%. A maximum transverse acceptance of 10 π·mm·mrad at 60 keV is expected, and the emittance for $^{30}Na^{7+}$ is predicted to approximately 10 π·mm·mrad at 20 kV extraction voltage. The extracted pulse should be shorter than 100 μs, and an energy

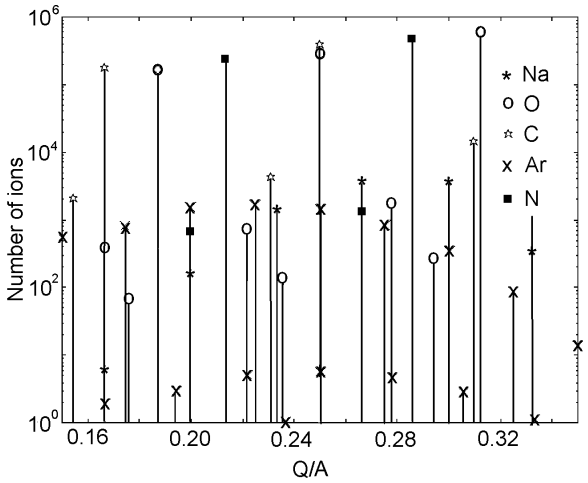

Fig. 1. Calculated *q/A* spectrum showing the absolute number of residual and radioactive ions. Breeding time 13 ms; 10 000 ^{30}Na ions; Ar diffusion from the REXTRAP (^{16,17,18}O, ^{12,13}C, ^{14,15}N, ^{36,38,40}Ar isotopes are present).

spread of less than 15 eV/q (1σ) is anticipated. The charge bred ions should have a charge-to-mass ratio of about 1/4.5 at an energy of 5 keV/u. To achieve a mass separation of 150, the ions are to be delivered within an emittance ellipse of 10 π·mm·mrad (2σ), 20 kV, with an energy spread of less than 50 eV/q. (The RFQ requirement is more relaxed with an acceptance of 180 π·mm·mrad (2σ).) With the LINAC running at <10% duty factor, the extraction must be pulsed. In an initial phase, the investigated nuclei masses are limited to A<50, and the cycle time is <20 ms.

Of great interest is the extracted q/A-spectrum. Figure 1 shows a prediction of radioactive ions between residual gas peaks. It is clear that the ions of interest may display a much lower intensity than nearby rest-gas peaks, and maximum suppression of these by a ultra-high vacuum and an efficient mass separator is necessary to obtain a clean beam. In Table 2 the mean charge-state after 20 ms of breeding is listed for a number of elements. The overall performances for the REXTRAP[17]/REXEBIS is a conservative efficiency estimation of 10% [9] in the major charge-state (decay losses excluded), and a total hold-up time of 20 to 40 ms.

Table II. Peak charge-state for a selection of elements after 20 ms breeding in the REXEBIS.

Element	Charge-state
$_{8}$O	7^{+}
$_{11}$Na	9^{+}
$_{18}$Ar	11^{+}
$_{19}$K	11^{+}
$_{36}$Kr	16^{+}
$_{37}$Rb	18^{+}
$_{51}$Sb	19^{+}
$_{82}$Pb	22^{+}
$_{92}$U	22^{+}

4. Operation of a TRAP-EBIS system

The difficulty with the low beam intensities is avoided by the use of a so-called pilot beam (an intensive, in most cases non-radioactive, beam from the primary source or a separate 1^{+} ion source) during the beam set-up. Another vital trick to ensure correct injection conditions into the EBIS is to match the forward beam parameters in the transfer line with the ones obtained by extracting a lowly charged beam of residual gas ions from the EBIS in the direction of the Penning trap. Two-way beam diagnostics along the transfer line are necessary for such an operation.

5. Conclusions and future prospects

In this article it has been shown that an EBIS is well adapted as a charge breeder for the first generation of radioactive beam post accelerators. The fast breeding (some tens of milliseconds), the high breeding efficiency, the absence of any dependence on the ion species (hydrogen to superheavy elements), the exceptional beam properties (transverse and longitudinal emittance), the low beam contamination (possible with a few ions per pulse) and the well-proven technique (Saclay [15], MSL [16], KSU [4], BNL [20]) among other things make it unrivalled for these conditions. Although, the question remains of how can one go on and improve its performance, and adapt it to the higher yield that is expected from the 2nd generation RNB facilities?

5.1. Shorter breeding time

A shortened breeding time yields higher efficiency for short-lived species, but to retain an unchanged extracted ion charge, the electron beam current density j_e has to be increased correspondingly. The current density can either be boosted by stronger beam compression in the solenoidal field, or by higher cathode current density. A beam compression of a factor of 100 is straightforward by means of Brillouin injection (compare with a factor of 10 for REXEBIS). With cathode materials as IrCe, LaB_6 and

CeB_6, cathode current densities of 100 A/cm^2 and 1 year of operation time are feasible (compare with 25 A/cm^2 for REXEBIS). On the whole, breeding fully stripped Be or Na^{9+} in the order of 5 ms are within reach with existing EBIS technology, thus short-lived nuclei as ^{35}Na ($t_{1/2}$=1.5 ms) can be accelerated.

5.2 Continuous ion injection

Instead of pulsed injection into the EBIS as described above, the possibility of injecting a continuous beam exists. In case of a small ISOL beam emittance the need for the bunching Penning trap would disappear and the space-charge restrictions set by it. Nonetheless, so far the continuous injection mode has shown a very poor efficiency. Unavoidably, the charge spectrum distribution becomes broader, and the trapping probability inside the electron beam potential well can not reach 100% with ordinary EBIS electron current densities. Most important is a decreased transverse beam acceptance compared to pulsed injection conditions (a factor 5 to 10, i.e. to a few π·mm·mrad). Measurements were carried out on the Dioné EBIS at Saclay [15] and total efficiency values below 0.1% were reported for continuous injection. CRYSIS in Stockholm [16] uses the mode regularly and, with a set-up not especially optimised for continuous injection, total efficiency values for Pb^{55+} and Ar^{18+} of 0.5 and 2% have been obtained [21]. To improve the injection efficiency a gas-filled RFQ can be used to shrink the emittance by at least a factor 10 (in each phase plane) on a single pass-single-pass through the ion guide [22]. Transmission up to 80% has been measured, and energy spread less than 0.2 eV has been obtained [23]. Since no bunching takes place, the space-charge limitation is relaxed compared with a Penning trap.

5.3 Increased breeding capacity

A direct action to increase the turnover of ions in a Penning trap/EBIS system is to raise the repetition rate. Cooling times down to 5 ms are in accordance with manageable breeding times inside the EBIS. The possibility to extend the Penning trap radius and length always remains, but the implications on the transverse and longitudinal emittances have to be investigated.

Various evolutions of the EBIS open up opportunities for higher beam intensities. For example, the new generation of EBIS to be used as an injector for RHIC (presently under development) will have a 10 A and 20 keV electron beam, an electron current density higher than 400 A/cm^2, and an estimated trap capacity of $5 \cdot 10^{11}$ charges (50% compensation) [20]. Another high performing EBIS is a proposed modified version of the REXEBIS that could work as ion injector for the heavy ion project at LHC [8]. Just by running the EBIS at a higher degree of compensation, at 50% instead of 10% as intended for the REXEBIS, a factor five could be gained in charge capacity. Furthermore, a factor three is gained if the electron beam current is increased from 0.5 to a feasible 1.5 A. In total $1 \cdot 10^{11}$ charges per pulse are within reach, and if the high repetition rate is considered (100 Hz for j_e>400 A/cm^2), that means up to $1 \cdot 10^{13}$ charges can be charge bred per second. Yet another project under development is the investigation of the reflex mode EBIS (RefEBIS [24]), where the electron beam is reflected multiple times (several hundred) inside the EBIS. Thus, a high electron current (i.e. charge capacity) and current density can be produced by a moderate EBIS construction.

6. References

1. E.D. Donets and V.I. Ilyushchenko, JINR R7-4124, 1968
2. C. J. Herrlander, International Symposium on Electron Beam Ion Sources and Their Applications, AIP Conf. Proc. No. 138, Upton, New York, 1988, p.27
3. V. P. Ovsiannikov, Physica Scripta T71, (1997) p.147
4. M. P. Stöckli, C. L. Cocke, P. Richard, Rev. Sci. Instr. 61 (1990) p.242
5. E.D. Donets, 'Electron Beam Ion Sources', chapter 12 in 'The physics and Technology of ion Sources', New York, John Wiley & Son, 1989, p.245-279
6. D. A. Knapp, R. E. Marrs, S. R. Elliot, E. W. Magee, R. Zasadzinski, Nucl. Instr. Meth. A334, (1993), p.305
7. G. Bollen, Nucl. Phys. A616 no.1-2 (1997) p.457c-468c
8. Design proposal for an EBIS as lead ion source for the LHC, F. Wenander, PS/HP/Note 99-09, June 16 (1999)
9. Radioactive beam experiment at ISOLDE: Coulomb excitation and neutron transfer reactions of exotic nuclei, proposal to the ISOLDE committee, CERN-ISC94-25, Nov 1994
10. V. Kalagin, V. P. Ovsyannikov, JINR preprint E9-96-I28 (1996)
11. REXEBIS – a charge breeder for the REX-ISOLDE project, F. Wenander, Licentiate thesis, Chalmers University of Technology, Gothenburg, Sweden (1998)
12. R. Becker, Proc 3rd EBIS Workshop 1985, Ithaca, eds. V. Kostroun and B.W. Schmieder, p.185
13. E. D. Donets, Rev. Sci. Instr. 61 (1990) p.225
14. E. Beebe, J. Alessi, A. Hershcovitch, A. Kponou, A. Pikin, K. Prelec, P. Stein, R. W. Schmieder, Rev. Sci. Instr. 69 no.2 (1998) p.640
15. B. Visentin, P. van Duppen, P.A. Leroy, F. Harrault, R. Gobin, the Isolde collaboration, Nucl. Instr. Meth. B101 (1995) p.275-279
16. R. Rao, M. Björkhage, P. Carlé, Å. Engström, L. Liljeby, G. Rouleau, F. Wenander**,** Hyperfine Interactions 108 (1997) p.307-317
17. F. Ames, G. Bollen, G. Huber, P. Schmidt, the REX-ISOLDE collaboration, Proc. 2nd Int. Conf. on Exotic Nuclei. and Atomic Masses (ENAM98), 1998, Bellaire, Michigan USA, AIP conf. Proc. 455 (1998) p.927
18. J. Axelsson, M. Björkhage, P. Carlé, L. Liljeby, K-G. Rensfelt, B. Jonson, G. Nyman, F. Wenander, Proc. of the 6th European Particle Accelerator Conference, Stockholm, Sweden (1998) p.1412-1414
19. D. Habs, O. Kester, T. Sieber, A. Kolbe, J. Ott, G. Bollen, F. Ames, D. Schwalm, R. von Hahn, R. Repnow, H. Podlech, A. Schempp, U. Ratzinger, L. Liljeby, K-G. Rensfelt, F. Wenander, B. Jonson, G. Nyman, P. van Duppen, M. Hyuse, A. Richter, G. Schrieder, G. Walter, and the REX-ISOLDE collaboration, Nucl. Instr. Meth. B139 no.1-4 (1998) p.128-135
20. E. Beebe, J. Alessi, S. Bellavia, A. Hershcovitch, A. Kponou, R. Lockey, A. Pikin, K. Prelec, P. Stein, G. Kuznetsov, M. Tiunov, Proc. of 8th Int. Conf. on Ion Sources (ICIS'99), Kyoto, Japan, 6-10 Sept. 1999, Rev. Sci. Instr. 71, no.2, (2000) p.893-895
21. M. Björkhage, Manne Siegbahn Laboratory, Stockholm, Sweden, private communication
22. M. D. Lunney, R. B. Moore, Int. J. Mass Spec. 190/191 (1999) p.153
23. T. Kim, Ph.D. thesis, McGill University, Montreal (1997), unpublished
24. E. D. Donets, D. E. Donets, E. E. Donets, V. V. Salnikov, V. B. Shutov, and E. M. Syresin, M. Björkhage, P. Carlé, L. Liljeby, K.-G. Rensfelt, R. Becker, M. Kleinod, O. K. Kultashev, Rev. Sci. Instr. 71, no.2 (2000) p.896

PAPER 4

Experiments on the pulsed afterglow operation of an ECR ion source

Authors:
C.E. Hill and F. Wenander

Published in:
Proc. of the 14th International ECRIS Workshop, ECRIS99, Geneva, Switzerland (1999) p.187-190.

Experiments on the Pulsed Afterglow Operation of an ECR Ion Source

C. E. Hill and F. Wenander
PS Division, CERN, 1211 Geneva 23
Switzerland

Abstract

Various experiments have been performed on the 14.5 GHz ECR4 in order to improve the beam yield. The source operates in pulsed "afterglow" mode, and provides currents >120 eμA of Pb^{27+} to the Heavy Ion Facility on an operational basis. In the search for higher beam intensities, the effects of a pulsed biased disk on axis at the injection side were investigated with different pulse timing and voltage settings. Different plasma electrode geometries were also tested, including running the source without a plasma electrode. The use of CF_4 as mixing gas was investigated, and high secondary electron emission materials, such as LaB_6 and Al_2O_3, were inserted inside the plasma chamber in an attempt to increase the cold electron density.

No proof for higher intensities was seen for any of the tested modifications. On the contrary, several of the modifications resulted in lower source performance, and less stability. Although the source has previously proved to have very stable modes of operation, during the last physics run, after the above tests, the stability decreased and the source settings were very different from the normal operation values.

Introduction

The CERN Heavy Ion Accelerating Facility [1] has now completed five periods of operation, and has become a reliable system for the first stage acceleration of lead ions used for the heavy ion physics experiments. Each year, the ion intensity and the integrated number of ions delivered to the physics targets have increased (Fig. 1). The increase is partly due to a performance enhancement of the Electron Cyclotron Resonance Ion Source (ECRIS, Fig. 2), which utilises the afterglow phenomenon [2] to produce short pulses (500-1500 μs suitable for synchrotron operation) of high charge state ions (Pb^{27+}) that are injected into the heavy ion linac (Linac3). Even though the linac runs at 1 Hz, the source is pulsed with 10 Hz to obtain a higher pulse to pulse stability. So far, the maximum intensity obtained from the source in an exceptionally stable afterglow mode of operation is more than 120 eμA of Pb^{27+}, extracted at an energy of 2.5 keV/u

Nevertheless, the search for higher beam intensities continues. Present physics experiments have a constant call for more particles, and when the LHC project goes into operation with heavy ions, the lead ion production has to be increased almost an order of magnitude compared to present values to fulfil the specifications set by the experiments. For this reason, several months of 1998 were

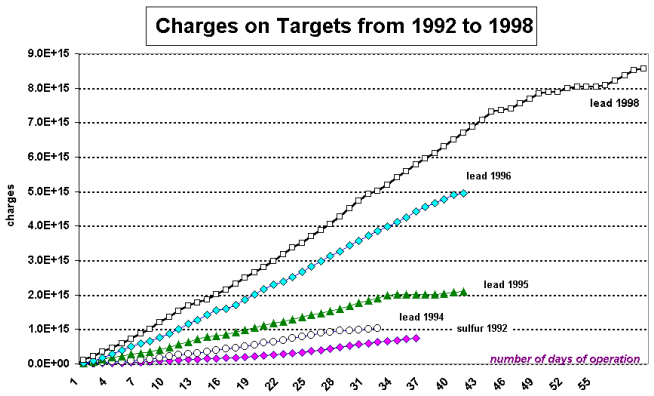

Figure 1. Integrated charges delivered to physics target.

dedicated to a continuation of the yield improvement experiments on the ECR ion source. Two different approaches were tried: either to increase the total number of ions inside the plasma, or to extract the available ions within a shorter period of time (presently the extracted pulse length from the ECR exceeds the typical 400 μs accepted by the synchrotron). The requirements of a high pulse to pulse stability and a flat pulse top were not relinquished.

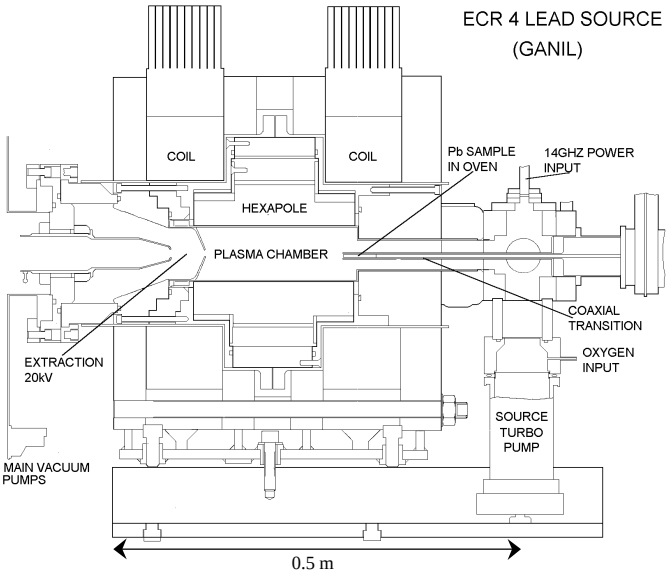

Fig. 2. Cross-section of the ECR4 ion source used at the heavy ion linac at CERN.

Experimental tests

The general test procedure was to first optimise the source before introducing the modification, and thereby obtain an

yield reference value. Thereafter the change was carried out, and the source was once again re-tuned to an optimal performance, which was compared with the reference value and the record notation of 120 eμA.

Biased axial electrode

It is usually claimed that a negatively biased electrode, positioned on axis near the plasma at the injection side, may reduce the electron losses out of the magnetic bottle and/or influence the electron density positively due to the injection of cold (secondary) electrons created by bombardment of the electrode with loss electrons and ions. Recent investigations, on the other hand, suggest that the yield increase is solely due to improved extraction conditions [3] or a plasma potential optimisation [4].

It has previously been shown in an ECRIS for sulphur ions that the presence of a biased electrode in the vicinity of the plasma improves the performance and stabilises the afterglow [5]. On the CERN ECR4, biasing tests of the inner conductor of the co-axial transition, which contains the sample oven and which penetrates 8 mm inside the maximum field peak from the injection solenoid in the plasma chamber (see Fig. 3), were performed without any gain in current [6]. A more advanced biasing with a pulsed voltage has now been tested, using a Behlke HTS31 switch. The intensity of Pb^{27+} was measured at Faraday cup positioned after the mass selection and the following acceleration in the RFQ. During normal non-biasing operation the electrode and the plasma chamber are at the same potential.

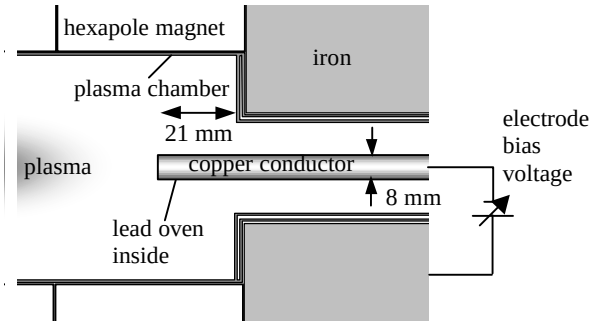

Fig. 3. Schematic drawing of the lead oven arrangement acting as a biased electrode.

With a negative static voltage applied on the electrode, a yield optimum (4% increase) was found for –20 V. Voltages more negative than –50 V quenched the current, and at a maximum voltage of –300 V sparking occurred. After removing the bias the current recovered. The 4% current gain could later be regained solely with tuning efforts and without any bias. A positive static voltage degraded the ion current severely.

Pulsing of the biased electrode was tried, with the opportunity to vary both the voltage, the pulse length and the timing of the pulse relative to the end of the RF pulse. A wide variety of time and voltage settings were investigated. For example, to prevent the electrons from escaping the magnetic bottle a negative bias was applied to the electrode during the breeding phase. With a pulsed bias of -75 V, 1.2 ms long extending 300 μs after RF off flank, a 2% percent current increase was obtained. A negative pulse, active only during the extraction of the beam gave a 3% current increase for a bias voltage of –35 V, while a more negative voltage quenched the beam. The yield increase must have been due to improved extraction conditions, and not due to an increased electron density.

In a similar way positive bias pulsing was investigated. A positive pulse, with a voltage varying between 0 and 100 V, was applied after the RF off flank and different time settings were tried. The purpose was to facilitate the extraction of the electrons from the plasma, and to repel the positive plasma towards the extraction side, but no significant enhancement of the ion current was detected. In addition, a positive pulse before the RF off flank was applied, but this resulted only in a yield reduction.

The O^{2+} peak (from the O_2 mixing gas) was measured in a Faraday cup before the RFQ for a 1.2 ms long pulse extending 300 μs after RF off flank. When increasing the negative voltage from 0 to about –30 V, the O^{2+} afterglow peak was extinguished completely, while the current intensity in the end of the main pulse increased with 30%. This could be interpreted as a sign of increased cold electron density.

To conclude, no major current increase was noticed for the different arrangements of a biased electrode. A slight enhancement may have been detected for a voltage of about -30 V, which corresponds to the potential that a floating electrode near the plasma would acquire. The electrode size might have been too small to have an effect for certain of the above-described experiments.

Alternative mixing gas

Under normal operation oxygen is used as mixing gas for the ECR4 source at CERN. Other gas combinations have been tried out in the past, without any major improvement [6]. The yield increasing effect by a mixing gas, dominant with respect to the main element and always lighter, has various interpretations: the gas increases the electron density and/or performs cooling of the lead ions by ion-ion collisions.

As an alternative to oxygen, CF_4 was tried as mixing gas (without any pre-calculations and a bit hesitatingly due to the poor reputation of fluorine inside other ion sources), mainly for two reasons:

- F has similar properties as O (mass, electro-negativity).
- The CF_4 molecules (if not immediately dissociated) has several metastable states in the region of 10 to 20 eV that could be excited by lead collisions and act as cooling on the lead.

During the experiment both O_2 and CF_4 were connected as mixing gases. The source was first optimised using exclusively oxygen, and thereafter CF_4 was introduced into the source in varying quantities. For each level of CF_4 gas flow, the oxygen in-flow was varied. A clear correlation between the injected amount of CF_4 gas and the extracted Pb^{27+} current was found: the more injected gas, the less extracted current. The Pb^{27+} current decreased to about a tenth of its nominal value for a

CF_4 gas pressure in the same region as an optimal oxygen pressure. At a higher CF_4 pressure, the source was almost entirely quenched. When going back to the original source settings, i.e. using oxygen as mixing gas again and with no CF_4 gas present, it was very difficult to make the source performing well. In the end, the lead oven had to be turned off, and the source was run only with oxygen for one day until it finally could be re-tuned to reach its pre-test current.

The experiment showed a much poorer yield than expected, and the reasons for this are not fully clear. In the case of non-dissociated CF_4 molecules, large charge-exchange cross-section between the molecule and the multiply charged lead ions may have impeded the production of highly charged ions. An inhibiting compound at the oven could also have been created. It is interesting to note the strong yield quenching effect by the addition of the CF_4. Even after the gas was disconnected, and a good source vacuum had been obtained, it was still almost impossible to keep the plasma ignited. It is suspected that a surface coating on the plasma chamber wall had been created, which produced this "memory effect". Since the yield was quenched only after a combination of CF_4 and RF had been applied[1], it is believed that the memory effect was due to the fluoride and not the CF_4 since the latter should dissociate when the plasma is ignited.

Insertion of internal electron donors

The supply of cold electrons to the ECRIS magnetic trap is necessary to have a large electron density and thereby obtain an efficient ionisation. Plasma chamber coatings with high secondary emission have been tested in several CW ECRIS with a positive effect on the ion current. A chamber liner of aluminium has previously been inserted in the CERN ECR4, but no improvement in the Pb^{27+} current was noticed. This time a slab of Al_2O_3 ($40*10*4$ mm^3) was inserted in the chamber at the pole tip of the hexapole magnet to be bombarded by plasma particles. Unfortunately, the RF power could not be increased to its nominal value due to heavy discharging and source runaways. The Al_2O_3 being melted by the plasma caused this misbehaviour, which started a violent outgassing and vacuum perturbations.

The next step was to place a small sample of LaB_6 (~50 mm^2) just behind the plasma electrode, but the result from this test was not extraordinary. After one day of adjustments we reached 93% of the record intensity for this set-up. Moreover, we had to start up the source fairly slowly in order to avoid discharges and a high load current. Possibly a better result could be obtained with a larger piece of LaB_6 positioned further into the plasma chamber where the plasma particle bombardment rate is higher.

[1] The source performed normally after the CF_4 gas pressure calibration, which was carried out without the RF on.

Plasma electrode variations

Different plasma electrode apertures were tested, including the complete removal of the plasma electrode. The ECR4 source was originally designed with a 6 mm diameter extraction hole, but is normally operated with a 16 mm hole because of its higher performance.

After a stable run of >40 days, the 16 mm plasma electrode was exchanged for the smaller with a 6 mm opening. The source showed an extremely poor yield, a factor 1/75 compared to the unmodified set-up, while simulations predicted a current of 1/10. In spite of tuning, the low current persisted, so the experiment was abandoned and the plasma electrode changed back. Nevertheless, the yield still remained low and spontaneous runaways occurred. Possible explanations for this behaviour could be a malfunctioning oven or too high outgassing, and therefore no direct conclusions can be drawn from this test.

Following an idea of Geller in ref. [7], the plasma electrode was completely removed. Without a plasma electrode the plasma should be confined by the magnetic field lines from the hexapole magnet. When tested, Penning discharges occurred in the extraction, and the nominal extraction voltage could not be reached. It is believed that since the differential pumping usually obtained by the small plasma electrode hole did not exist anymore, the gas pressure in the extraction region became too high. The only way to stop the discharges was to go down with the gas pressure.

Conclusions

Similar tests as described in this report have resulted in a current improvement for ECR ion sources operating in pulsed or CW mode. For the CERN ECR4 source operating in afterglow mode, no significant current increase was noticed in connection with these experiments, neither with previously carried out tests [6,8]. Instead, when introducing the changes the source demonstrates a less stable behaviour; only a minor current increase that can often later be regained by fine-tuning the source without the modification; and in most cases a decrease in the desired Pb^{27+} ion current. Consequently, the experience gained from CW sources seems not to be directly applicable on an ECR source running in afterglow mode.

The source performance might already be optimised, i.e. an enhanced production of highly charged ions, or a more rapid extraction of the ions, only result in worse beam extraction conditions. Even though the beam extraction should not be space charge limited for the present intensities, ion extraction simulations suggest that the plasma meniscus becomes distorted and the extraction conditions degrades for higher ion currents.

Future tests

In a near future, experiments with a larger (20 mm diameter) biased electrode will take place. Electrode materials with different secondary electron emission coefficients (Cu, Ta, Al_2O_3 and stainless steel) will be tested to investigate if a possible current gain is due to a higher electron density or a plasma potential optimisation. An axially moveable puller has

recently been designed to allow a continuous variation of the plasma electrode to puller distance without opening up the source. A current increase is expected for larger distances than have been tested so far [8]. A recently purchased x-ray diagnostics system will give information about the characteristic x-rays of the ions and bremsstrahlung of the electrons emitted from the ECR plasma. The wide energy-range for the detector (500 eV to ~500 keV) allows determination of the energies for both the cold and hot electrons. Since the measurement will be time-resolved, the plasma build-up and release can be studied, and hopefully contribute to the understanding of the processes in the plasma and the release of electrons and ions.

References

1. H. D. Haseroth, Proc 1995 Particle Accelerator Conference, Dallas, IEEE, V1 (1996) p.411
2. G. Melin, F. Bourg, P. Briand, J. Debernardi, M. Delaunay, R. Geller, B.Jacquot, P. Ludwig, T. K. N'Guyn, L. Pin, M. Pontonnier, J. C. Rocco and F. Zadworny, "Some Particular Aspects of the Physics of the ECR Source for Multicharged Ions", Rev. Sci. Inst. **61** (1990) p.236
3. S. Runkel, K. E. Stiebing, O. Hohn1, V. Mironov, G. Shirkov, A. Schempp and H. Schmidt-Boecking., "Time-resolved measurements of the Biased-Disk Effect at the Frankfurt 14 GHz Electron-Cyclotron-Resonance-Ion-Source", this workshop
4. T. Nakagawa, S. Biri, T. Chiba, A. Goto, M. Hemmi, E. Ikezawa, N. Inabe, T.Kageyama, O. Kamigaito, M. Kase, M. Kidera, Y. Miyazawa and Y. Yano, "Further development of RIKEN 18 GHz ECRIS", Proc. 6th European Part. Acc. Conf., 1998, Stockholm, p.1418-14210
5. P. Briand, R.Geller, H. Haseroth, C. Hill and K. Langbein, "Utilising the ECR Afterglow to Increase the Intensity of Highly Charged Ions in the CERN Accelerator Complex", Proc. 11th Int. Workshop on ECR Ion Sources, Groningen, 1993, KVI Report 996 (1993) p.132
6. C. E. Hill and K. Langbein, "Experiments on a 14.5 GHz ECR source", 7th Int. Conf. on Ion Sources, Taormina Italy, 1997
7. R. Geller, "Electron cyclotron resonance ion sources and ECR plasmas", IOP Publishing, Bristol, 1996
8. C. E. Hill and K. Langbein, "Experiments on a 14.5 GHz ECR source", 18th Int. Linac Conf., Geneva, 1996

PAPER 5

Effect of a biased probe on the afterglow operation of an ECR4 ion source

Authors:
C.E. Hill, D. Küchler, F. Wenander and B. H. Wolf

Published in:
Proc. of the 8th International Conference on Ion Sources, ICIS99, Kyoto, Japan, Rev. Sci. Inst. **71** no.2 (2000) p.863-865.

Effect of a biased probe on the afterglow operation of an ECR4 ion source

C. E. Hill,[a] D. Küchler, F. Wenander, and B. H. Wolf
PS Division, CERN, 1211 Geneva 23, Switzerland

(Presented on 7 September 1999)

Various experiments have been performed on a 14.5 GHz ECR4 in order to improve the ion yield. The source runs in pulsed afterglow mode, and provides currents ~120 eμA of Pb^{27+} to the CERN Heavy Ion Facility on an operational basis. In the search for higher beam intensities, the effects of a pulsed biased disk on axis at the injection side were investigated with different pulse timing and voltage settings. No proof for absolute higher intensities was seen for any of these modifications. However, the yield from a poorly tuned/low-performing source could be improved and the extracted pulse was less noisy with bias voltage applied. The fast response on the bias implies that increases/decreases are not due to ionization processes. A good tune for high yield of high charge states during the afterglow coincides with a high plasma potential. © *2000 American Institute of Physics.* [S0034-6748(00)59702-0]

I. INTRODUCTION

The CERN Heavy Ion Accelerating Facility,[1] after five periods of operation, has become a reliable injector for the lead ions used by the heavy ion physics experiments. An electron cyclotron resonance ion source (ECR4) operates in the afterglow mode[2] to produce short pulses (500–1500 μs) of highly charged ions (Pb^{27+}) that are accelerated in the heavy ion linac (Linac 3). The maximum intensity obtained from the source, in an exceptionally stable afterglow mode of operation, was more than 120 eμA of Pb^{27+}, extracted at an energy of 2.5 keV/u. The search for higher beam intensities continues as the LHC project[3] requires a pulse current at least an order of magnitude higher. Two different approaches are being tried: either to increase the total number of ions in the plasma, or to extract the available ions in a shorter pulse.

II. TESTS AND RESULTS WITH BIASED AXIAL ELECTRODE

It is often claimed that a negatively biased electrode, positioned on axis in the plasma at the injection side, may reduce the electron losses out of the magnetic bottle and/or influence the electron density positively due to the injection of cold electrons created by bombardment of the electrode with loss electrons and ions. Recent investigations, on the other hand, suggest that the ion yield increase be mainly due to improved extraction conditions[4] or plasma potential optimization.[5]

It has previously been shown in an ECR for sulphur ions (a MiniMafios with off axis microwave coupling) that the presence of a biased electrode in the vicinity of the plasma improved the performance and stabilized the afterglow.[6] On the ECR4, (microwave coupling on axis) a bias could be applied to the inner conductor of the coaxial transition which contains the sample oven (Fig. 1), but no gain in current could be observed[7] at the time.

The ion intensity was measured in Faraday cups either before (FC1) or after mass selection (FC2) or after acceleration in the RFQ (FC3). FC1 and 2 show the full ion beam pulse while FC3 shows just the portion accelerated by the RFQ (600 μs). The total ion current at FC1 is about 1.5 mA during the main pulse (rf on) and increases (over about 300 μs) to about 8 mA after the rf is switched off. Depending on the mode of the afterglow[8] and on the tuning of the source, the current either decreases exponentially over more than 10 ms or ends in a sharp breakdown after 1–2 ms. The time structure of the FC2 current is very similar to FC1 for the higher lead charge states, but shows no afterglow increase for the O^{2+}($+Pb^{26+}$).

During normal operation the electrode and the plasma chamber are at the same potential and sparking occurs above 300 V due to insulation problems. Pulsing of the electrode was also tried, with variation of the voltage, the pulse length, and the timing of the bias relative to the end of the rf pulse. The response to a change of the bias voltage was, within some μs, too short to change the charge state distribution in the ECR plasma (Fig. 2). The yield increase must, therefore, be due to improved extraction conditions or an increased electron density, and not due to additional ion production (except possibly for O^{+}).

In addition to negative bias voltages, a positive pulse of up to +300 V, was applied after the rf-off flank and for

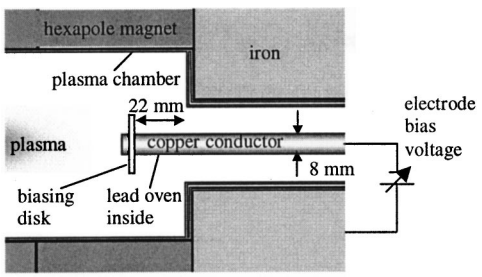

FIG. 1. Schematic drawing of the lead oven arrangement acting as a biased electrode. (The biasing disk was not used in all experiments.)

[a]Electronic mail: charles.hill@cern.ch

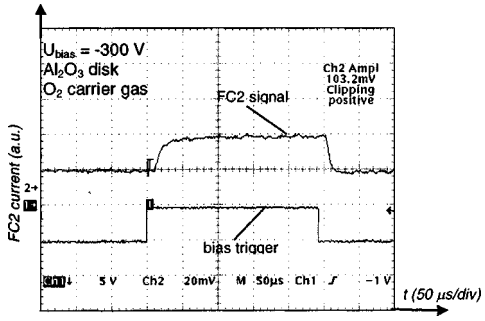

FIG. 2. Time response to bias pulse in the main pulse region.

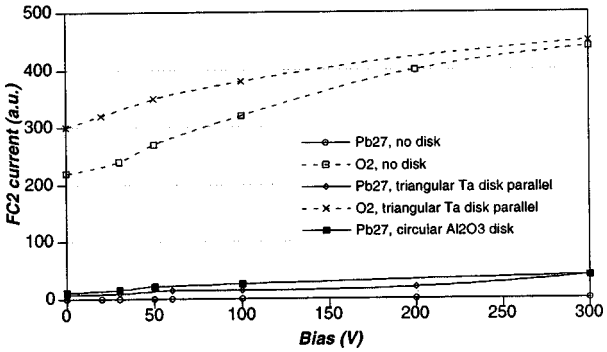

FIG. 4. Ion yields during main pulse with bias voltage.

different times. The idea was to facilitate the ejection of the electrons from the plasma, and to repel the positive plasma towards the extraction. No significant enhancement of the ion current was seen either with or without a metallic or insulating (Al_2O_3) disk (just a small noise reduction).

While these bias tests were under way, the floating potential of the source was measured with a high impedance probe while under full rf power and with the extraction voltage off. Figure 3 shows that after the plasma ignites, the coaxial electrode rapidly rises to around 400 V with respect to the plasma chamber and continues rising during the heating phase to 500 V. This potential collapses almost instantaneously, with the removal of the rf heating (1300 W), to a few volts during the afterglow pulse.

With the floating potential, an average electron temperature of 80–100 eV[9] can be calculated. The Bohm energy is assumed to be about one half of the electron temperature, i.e., about 50 V, a value which would influence the emittance of the source in a positive way.[10]

With normal extraction (20 kV), the floating potential of the biased probe was ~100 V. A resistor of <1 kΩ was necessary to keep the probe potential below ~1 V during the microwave pulse or to discharge the (ion) current of about 1.5 mA (equivalent to the total extracted ion current). Larger resistors would create a bias voltage.[11]

It was considered that the electrode used in the first tests[11] was possibly too small. The electrode surface was increased by the addition of metallic or dielectric disks to the coaxial line. Without a disk and zero bias the maximum Pb^{27+} ion current after the RFQ (FC3) was 94 μA, at the beginning of these tests.

(1) A 20-mm-diam Ta disk was mounted at the end of the tube. This made the conditioning and operation of the ion source very difficult and the rf tuning had to be adjusted for a high reflected power of about 150 W. Obviously the disk interfered with the propagation of the rf into the cavity. All settings of the source parameters were very sharp and the Pb^{27+} ion current (FC3) was <60 μA.

(2) The disk was replaced by one made from pure Al_2O_3. Conditioning was accompanied by gas bursts from the disk and needed much more time than usual, but the final operation of the source was similar to without the disk. At zero bias, the maximum Pb^{27+} current in FC3 was 75 μA.

(3) A triangular shaped Ta disk was mounted oriented either parallel or in opposition to the hexapole loss lines. Tuning was much easier compared to the full disk, but, at zero bias, the maximum Pb^{27+} current was 84 μA (parallel), or 64 μA (opposite).

(4) Finally the source was run without disk and zero bias, but the maximum Pb^{27+} current was only 74 μA after intensive optimization (compared to 94 μA at the start of the experiments). A rebuilt and cleaned standard source could be trained after one week to 83 μA.

For all geometries a similar reaction to the timing of the bias voltage pulse was found:

If the bias pulse is active only during the rf pulse, there is a gain in ion current for the O^{2+}+Pb^{26+} for all cases. Pb^{27+}, improved for the Al_2O_3, had an unstable gain for both orientations of a triangular Ta disk and no gain at all without the disk (Fig. 4). The gain during the main pulse had no influence on the afterglow if the biasing pulse was switched off before or with the rf.

If the bias pulse is both on the main and the afterglow region, it tends to destabilize the rising of the afterglow, creates a prepulse or a faster rising of the afterglow, but is then slower increasing to the maximum of the Pb^{27+} current.

If the bias pulse is on only during the afterglow it changes the current only during the applied time, depending on the applied voltage. In some cases a nice long stable afterglow pulse could be achieved (Fig. 5).

In Fig. 6 the afterglow current in FC2 is shown depending on the bias voltage for the different geometries. Usually the ion current increases by <10% at around −15 V (depending on the disk) and decreases to a minimum at about −30 V. Afterwards the Pb^{27+} current increases again, usually to values above the 0 V bias one (beyond the highest

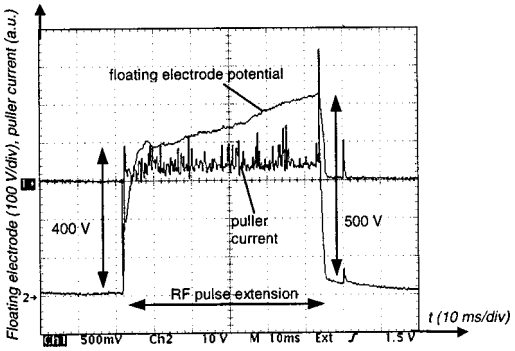

FIG. 3. Change of floating potential with rf pulse.

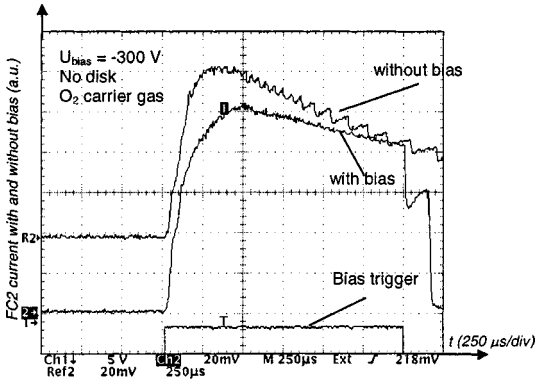

FIG. 5. Afterglow pulse of Pb^{27+} on FC2. The yield increase is evident, and the pulse less noisy.

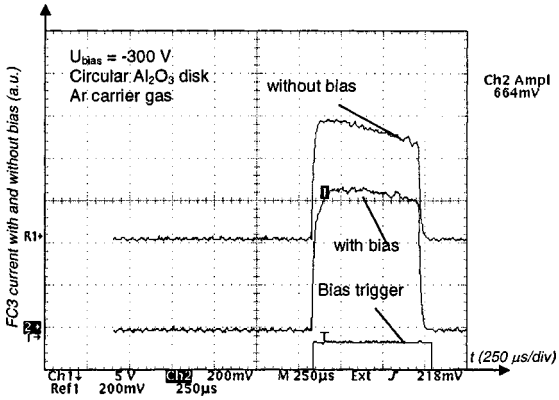

FIG. 7. Pb^{27+} current (FC3) for argon support gas and −300 V bias. The current increases from 57 to 66 μA.

available voltage of −300 V). The same behavior can be seen for the $O^{2+}+Pb^{26+}$ afterglow yield.

FC3 showed similar trends as FC2, but was more sensitive, and sometimes beam line readjustments were necessary, i.e., a change in the source emittance occurred during the bias voltage pulse. (The solenoids after the source and in front of the RFQ had to be changed and a small adjustment of the extraction voltage (<50 V) was necessary for best yield.) For Al_2O_3 a 10% increase for −300 V bias to 82 μA was found, for the triangular one from 64 to 78 μA (opposite) or from 84 to 90 μA (parallel).

Other support gases, Ar and He, were also tried. Both gave lower yields of Pb^{27+} ions (57 and 9 μA, respectively). For argon the increase was about 15% to 66 μA (see Fig. 7).

III. CONCLUSIONS AND DISCUSSION

Similar tests to those described in this article have resulted in ion current improvements for ECR ion sources operating in pulsed or cw mode.[4,5] For the CERN cw source operating in afterglow mode, no significant current increases have been observed in any of these or previous experiments.[7,8,11] Instead, changes to the source usually result in a less stable behavior. Any relative current increase does not improve the optimum found in the original configuration following fine tuning of the source. There seems to be an absolute maximum Pb^{27+} ion current under stable operation conditions. The source performance may already be optimized, i.e., an enhanced production of highly charged ions, or a more rapid extraction of the ions, only result in instabilities or breakdown of the afterglow reservoir. Consequently, the experience gained from CW sources seems not to be directly applicable to an ECR source running in afterglow mode.

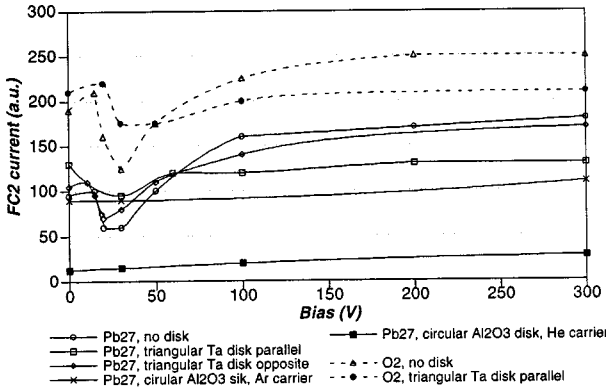

FIG. 6. Afterglow yield for Pb^{27+} and $O^{2+}+Pb^{26+}$ with bias voltage for various disk and gas combinations.

There is no possibility to extract a higher ion pulse in a shorter time by applying electric potentials inside the ECR source. The only promising way is the PuMa method of a fast pulsed magnetic field,[12] but this would imply a totally new source design.

Could higher afterglow currents be extracted from out of the next generation of ECR sources with higher rf frequency and/or magnetic field? Fuller understanding of the afterglow performance of an ECR ion source is needed.

[1] H. D. Haseroth, *Proceedings of the 1995 Particle Accelerator Conference, Dallas* (IEEE, 1996), Vol. 1, p. 411.
[2] G. Melin, *et al.*, Rev. Sci. Instrum. **61**, 236 (1990).
[3] L. R. Evans, Proceedings of the 1999 Particle Accelerator Conference, New York, 1999, p. 21.
[4] S. Runkel, K. E. Stiebing, O. Hohnl, V. Mironov, G. Shirkov, A.Schempp, and H. Schmidt-Boecking, *Proceedings of the 14th ECR Workshop, Geneva, 1999* (CERN/PS 99-052 (HP) Geneva 1999), p. 183.
[5] T. Nakagawa, S. Biri, T. Chiba, A. Goto, M. Hemmi, E. Ikezawa, N. Inabe, T. Kageyama, O. Kamigaito, M. Kase, M. Kidera, Y. Miyazawa, and Y. Yano, Proceedings of the 6th European Particle Accelerator Conference, 1998, Stockholm, pp. 1418–1421.
[6] P. Briand, R. Geller, H. Haseroth, C. Hill, and K. Langbein, Proceedings of the 11th International Workshop on ECR Ion Sources, Groningen, The Netherlands 1993; KVI Report No. 996, 1993, p. 132.
[7] C. E. Hill and K. Langbein, Proceedings of the 7th International Conference on Ion Sources, Taormina, Italy, 1997; Rev. Sci. Instrum. **69**, 643 (1998).
[8] C. E. Hill and K. Langbein, Proceedings of 18th International Linac Conference, Geneva, 1996; CERN 96-07, Geneva 1996, p. 366.
[9] A. T. Forrester, *Large Ion Beams* (Wiley, New York, 1988), p. 64.
[10] P. Spaedtke, in Ref. 4, p. 143.
[11] C. E. Hill and F. Wenander, in Ref. 4, p. 187.
[12] C. Muehle, U. Ratzinger, G. Jost, K. Leible, S. Schennach, and B. H. Wolf, Proceedings of the 6th International Conference On Ion Sources, Whistler, Canada 1995; Rev. Sci. Instrum. **67**, 1331 (1996).

PAPER 6

An EBIS as heavy ion source for the LHC pre-injector

Authors:
F. Wenander

Accepted for publication in:
Proc. of the 8th International Symposium on Electron Beam Ion Sources and Traps and their Applications, Brookhaven National Laboratory, Nov 6-8, 2000. AIP Conference Proceedings Series.

An EBIS as Heavy Ion Source for the LHC Pre-injector

Fredrik Wenander

Chalmers University of Technology, 412 96 Göteborg, Sweden

Abstract. A design proposal for an Electron Beam Ion Source (EBIS) for the ion pre-injector for the Large Hadron Collider (LHC) is presented. The LHCEBIS would produce lead ions, as well as lighter ions, that are directly injected into and further accelerated in an RFQ/LINAC arrangement. The source would operate with a repetition rate of 0.8 Hz, and the extracted yield is estimated to $1.6 \cdot 10^9$ Pb^{54+} per pulse. Using fast extraction, the extraction time can be less than 10 μs, possibly allowing single-turn injection into the PS Booster.

INTRODUCTION

The use of an EBIS [1] as ion source for large heavy-ion collider projects such as LHC or RHIC is by no means new; in fact the RHIC project is experimentally investigating the possibility [2]. However, this study, which is an update and revision of a previous proposal [3], has a different design approach. Instead of the development of a high electron energy and current EBIS, a moderate concept is proposed and its realisation feasibility is discussed within this article. Compared to a high performance ECR ion source [4,5], the LHCEBIS will provide a faster ion expulsion from the source, and the need for the first stripper foil is avoided. In addition, the need for tuning when changing between different elements is minimal for an EBIS compared to an ECR ion source.

The main challenge when using an EBIS as an ion source for a large heavy-ion injector is to create sufficient negative space charge to confine the large positively charged ion-cloud. So far, the suggested solution to the space charge problem has been to increase the electron beam, which has required the development of a new EBIS generation. The idea behind this proposal is to make use of the high space charge capacity, C, of the trap at low electron beam energies, demonstrated by:

$$C = \frac{1.05 \cdot 10^{13} \cdot I_e L}{\sqrt{E}} f \quad \text{elementary charges} \qquad (1)$$

where L (m) is the trap length, f the compensation degree ($0<f<1$), I_e (A) and E (eV) the electron current and energy, respectively. As seen from the formula, one way to increase the negative charge is to decrease the electron beam energy E (the lower limit for a specific I_e is set by the perveance). A low electron beam energy is adequate in the proposed EBIS since the lead ions have not to be fully stripped. The second idea is to make use of the so called closed shell effect, that means boosting the fraction of ions in the desired charge state from about 20% (normal breeding) to at least 50%, by choosing the electron beam energy just below the ionisation energy of the principal charge state. Operation with a closed shell effect breeding leads to a more effective use of the confining negative space charge (i.e. the electron current), which can therefore be decreased by a factor of two.

Keeping the electron beam current low has several advantages, for instance: the convenience of lower voltages inside the EBIS; easier electron beam handling; the need for intense cooling of the electron collector disappears; the risk for RF generated beam instabilities is reduced. The main advantage of the LHCEBIS compared to a high current EBIS is that its function is founded on performances not far away from those already obtained in existing EBISes. Nevertheless, the design involves some new and unexplored areas and the difficulties involved are discussed below.

GENERAL DESIGN ASPECTS AND THEORY

The proposed EBIS has a design very similar to the REXEBIS [6,7], which will be used at the REX-ISOLDE project. The constructional changes that are needed to adapt an REXEBIS to LHCEBIS performances concern mainly the electron gun, which will have to deliver 1.5 A instead

of 0.5 A, the drift tube structure that should allow for fast extraction, and the ion extraction system that should be capable of handling high currents (see Fig. 1). Even if the LHCEBIS is to be used for a completely different purpose (the REXEBIS charge breeds a small number of ions to a moderate Q/A with a very high efficiency), one can benefit from the experience gained from the construction of the REXEBIS.

The design parameters for the EBIS are determined by the goals of the physics carried out at the heavy ion collider LHC. By using the B-scenario outlined in ref. [8], the EBIS/LINAC has to deliver $1.24 \cdot 10^9$ ppp (pulse rate ~0.8 Hz) to the PS Booster for the LHC luminosity requirement to be fulfilled.

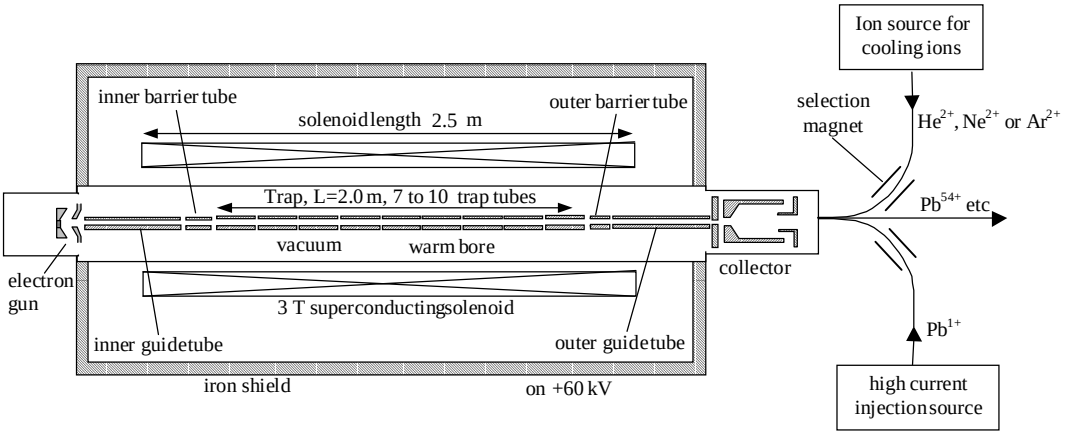

Figure 1. Schematic drawing of the LHCEBIS showing the most important elements described within this proposal. (Not to scale.)

CHARGE STATE

The proposed EBIS would deliver lead ions with charge state 54^+, meaning that the first stripper stage at 4.2 MeV/u after the CERN heavy ion linac (LINAC3) becomes obsolete. To breed lead ions to charge state 82^+ in large numbers within the EBIS, and in that way avoid the final stripper, is not realistic since it would require an extreme $j_e\tau$-value (with ion cooling problems etc as consequences) and an electron beam energy exceeding 90 keV.

For lead 53^+ and 54^+ ions the ionisation potential to attain the next higher charge state increases significantly from about 3.3 keV to 5.4 keV (multiconfiguration Dirac-Fock calculated [9]) because of the transition from n- to m-shell. By operating the EBIS at an electron beam energy below 5.4 keV, most ions will end up as Pb^{54+} after some time of breeding. The large difference in ionisation potential between the two charge states is convenient since all beam electrons do not propagate with the same velocity (the radial potential causes kinetic energy variations). If the ionisation potentials were close, the spread of the electron beam velocity would cause a distribution between two or more charge states instead of a single one.

The charge state development for lead ions bombarded with 5 keV electrons is shown below (Fig. 2). Note that the calculation in the left plot does not include any recombination processes, neither ion loss effects due to ion heating by electron Coulomb scattering. The dielectronic recombination with the electron beam will be negligible (the recombination rate with secondary electrons, however, is not fully clear) in the LHCEBIS. The charge exchange probability between a neutral gas (residual gas pressure 10^{-11} torr) and a Pb^{54+} ion is about 2% according to Müller and Salzborn's formula for electron transfer from atoms or molecules to highly charged ions [10]. The narrow charge state distribution for the lead ion population leads to a very small charge exchange rate between lead-lead. It will later be shown that the ion losses due to heating and subsequent radial escape can also be kept small. Nevertheless, the radiative recombination seems to be non-negligible [11] and the cross-section ratio $\sigma_{ion}/\sigma_{radiative}$ for electron beam energies close to the next charge state (55^+) is approximately 2, based on radiative recombination cross-sections described in ref. [12]. When taking the radiative recombination into account, the charge state evolution is modified as shown in the right plot (Fig. 2). One has to keep in mind that both the ionisation and recombination cross sections are based on theoretical calculations, meaning that the real number of obtained Pb^{54+} ions may be larger or smaller.

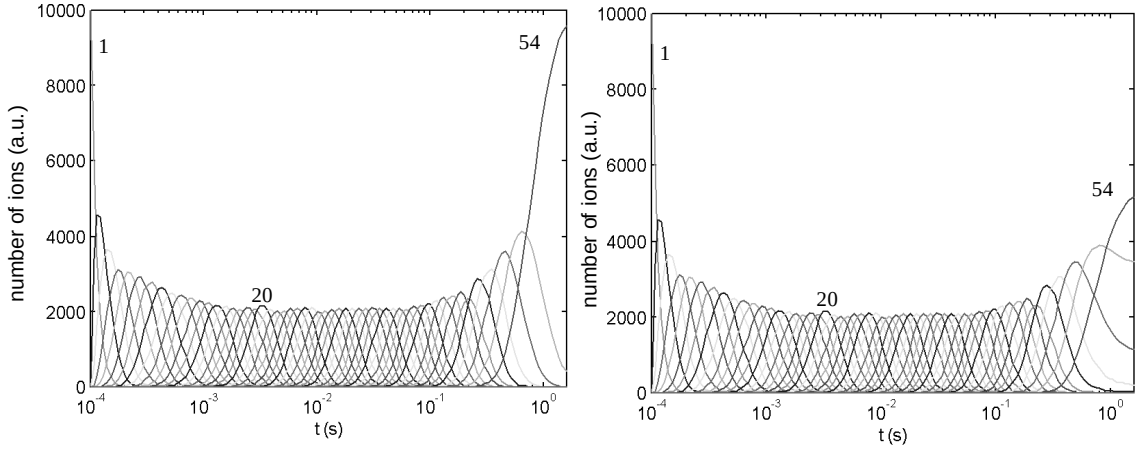

Figure 2. Relative charge state abundance for Pb stepwise ionised by a 5 keV electron beam (radiative recombination excluded and included in the left and right plot, respectively).

SPACE CHARGE

The negative space charge, constituted by the electrons, will be provided by the single pass electron beam. The proposed LHCEBIS has a total trap capacity of 70 nC and, assuming a maximal trap compensation of 50% (>60% reached at the REXEBIS, see also ref. [13]), the useful space charge will be ~35 nC. From the charge evolution graph in Fig. 2 (including radiative recombination) it is clear that the relative abundance of Pb^{54+} ions can be at least 50%, which equals an effective trap capacity of ~$2 \cdot 10^9$ Pb^{54+} ions.

If cooling ions have to be added, a fairly light element (e.g. He^{2+}) would be preferable to avoid undesirable occupation of the negative space charge and to eliminate the possible charge exchange process between the lead and the not fully ionised cooling ions, even though the heavier Ne or Ar alternatives might be more efficient from a cooling point-of-view. The quantity of cooling ions, and therefore the amount of occupied negative space charge, is not known and has to be investigated experimentally.

Residual gases are also ionised and trapped within the electron beam. A total residual gas pressure of 10^{-11} torr should be achievable inside the trap region and that yields a space charge compensation of less than 5% for a 1 s breeding period. A positive side effect of the residual gas is its evaporative cooling effect on the hot lead ions.

An EBIS is virtually indifferent to the ion species that are injected for breeding. Thus, the EBIS is also capable of breeding for example O, Ca and Nb as shown in Table 1.

Table 1. Ion yield per pulse for the proposed LHCEBIS assuming 50% compensation and j_e = 400 A/cm^2. Closed shell effects used in all cases except for Pb^{27+} and Nb^{31+}; the former is presented as a comparison.

Ion	Peak charge	Breeding time	Abundance	Ions per pulse
Lead (Pb)	54^+	1 s	50%	$2 \cdot 10^9$
Lead (Pb)	27^+	0.01	20%	$8 \cdot 10^8$
Oxygen (O)	8^+	0.1 s	50%	$1.7 \cdot 10^{10}$
Calcium (Ca)	18^+	0.5 s	50%	$7 \cdot 10^9$
Niobium (Nb)	31^+	0.3 s	50%	$4 \cdot 10^9$

DESCRIPTION OF A BREEDING CYCLE

Injection

The lead is introduced into the trap region by external ion injection, i.e. 1^+ Pb ions are produced in a high-current external ion source (for example a RF-source) and then injected into the EBIS. This type of injection scheme is, for instance, used at CRYSIS in Stockholm where also Pb, Ge, and Cr amongst other elements have been successfully injected [14].

In principle, two different injection scenarios are possible. The first implies pulsed injection of ~15 μA for 50 μs, corresponding to a total number of ~$4.7 \cdot 10^9$ 1^+ Pb ions; a little more than the

amount of lead ions needed for LHC, thus, very little boiling-off during the breeding phase is allowed. To ensure a minimal degree of boiling-off and radial heating, evaporative ion cooling can be used. In addition, the 1^+ ions should be injected into the very bottom of the electron beam potential[1]. It then follows that the ions are completely trapped inside the electron beam, and they have a low initial temperature.

The alternative method is to completely fill the trap with 1^+ Pb ions, i.e. to compensate it already at injection. Since the external ion sources are limited in current, slow injection has to be used, that means a 2.5 μA beam is injected over an already raised outer barrier for some ten milliseconds[2]. The temperature of these ions inside the trap is higher than in the previous alternative, and during breeding most of the Pb ions are boiled-off, so only a fraction of the initial number of ions remains when the Pb^{54+} ions are extracted.

A shortcoming of the first method is the need for lowering the trap tube potential as the breeding progresses and the electron beam space charge becomes neutralised by the ions, in order to keep the electron beam energy at 5 keV. On the other hand, if the trap is compensated at injection, the trap tube voltage should be fixed during breeding. Experimental tests have to decide which of the methods (or a mixture of both) provides the highest number of Pb^{54+} after the breeding has finished.

It is essential that the ions pass the outer guide tube with a high velocity during injection and therefore not have time to be ionised, since an ionisation outside of the trap results in ion rejection at the trap entrance and thereby a low injection efficiency. Hence, the injection energy should be such that the ions pass the outer guide tube with ~2000 eV and, thus, the trap tube potential is raised during injection to allow the ions to be trapped within the electron-beam potential well. Directly after injection, the trap tube potential is decreased so an electron beam energy of 5 keV is obtained inside the trap, see Fig. 3. Note that it is not possible to simply lower the potential of the outer guide during injection due to the perveance limit.

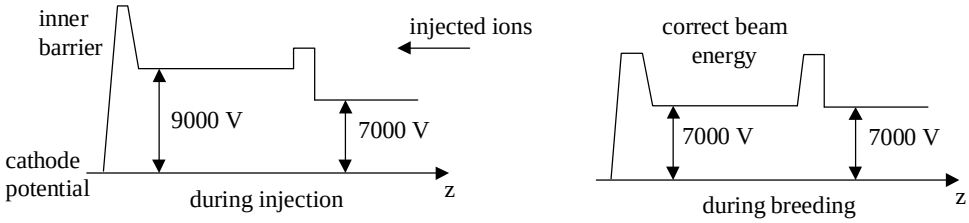

Figure 3. Necessary drift tube voltage alterations during injection to avoid pre-ionisation outside the trap.

Breeding

As was shown in Fig. 2, a breeding time of ~1 s is needed to reach Pb^{54+} at a current density of 400 A/cm^2. Thus, the EBIS can work with a repetition rate of almost 1 Hz if one assumes complete trapping within the electron beam since the extra time required for injection, extraction and cleaning is negligible.

While the ions are trapped inside the confinement region they are heated (mainly in radial direction) by the electron beam. Heat is transferred from the electrons to the ion population by elastic small-angle Coulomb scattering, and may cause radial boil-off of the highly charged lead ions. According to ref. [15], the radial holding voltage, i.e. the radial voltage needed to prevent the Pb^{54+} ions from escaping, is in the order of 20 V, which is much less than the radial voltage from the electron beam well. Thus, there is little danger from an ion loss perspective. However, since the ions may not be perfectly injected into the bottom of the potential well of the electron beam, that is to say if the injection energy inside the trap is larger than 160 eV, a certain fraction will have the energy to leave the electron beam potential well, with or without heating. This has to be compensated for by an increase in confinement time or electron current density. In fact, the 1.2 s confinement requirement is based on an electron density of 400 A/cm^2, but in reality one can expect a density of 450 A/cm^2 from the design, and that would to a certain extent compensate for the non-complete capture within the electron beam. Although, an even higher current density might be necessary.

[1] Due to the small acceptance for ion injection at the bottom of the electron beam potential [7], the injection current might have to be larger than 15 μA if the emittance of the external ion source is poor.

[2] With an injection time of 15 ms, the needed injection current has to be 2.5 μA to fill the trap to 50% (~35 nC), however, due to a low efficiency for continuous injection, the injection current may have to be two orders of magnitude larger.

To reduce the heating of the lead ions the use of evaporative ion cooling is suggested. The cooling ions could either be introduced into the trapping region via ordinary gas injection, or by slow external ion injection. Using the latter method one would gain control over the exact amount of injected coolant, as well as the timing for cooling. Nevertheless, for this method to be successful, the cooling ions have to be injected into the trapping region with a very low energy.

Extraction

After breeding, the ions are extracted from the trap region by so-called fast extraction. That means, an axial electric field gradient extending over the whole trapping region is applied during the extraction phase to push out the ions and, by doing so, single turn injection into the Booster is achievable. Experiments with fast extraction have already proven that it is possible to reach very short extraction times, e.g. 10 µs FWHM for Xe ions from a 750 mm long trap [16]. In case the goal of 5 µs is unreachable for practical reasons, and the transverse emittance is sufficiently low, one could consider 2 to 4 turn injection into the Booster.

Immediately before the opening of the outer barrier, the trap and barrier potentials are simultaneously elevated by ~1000 V to allow the ions to overcome the energy threshold caused by the expanding electron beam in the outer guide tube. The consequence of an increased trap potential is higher electron beam energy, and therefore the risk for ionisation to a higher charge state, however, since the trap potential is elevated for only some 100 µs, that risk is negligible.

A supplementing concept, the so called accelerated potential wall has been suggested in ref. [17] and, if successfully used at the LHCEBIS, all ions may be extracted with the same low radial energy dispersion of the 50% neutralised beam. The effectiveness of this has not yet been proven experimentally.

The injection energy into the present RFQ in LINAC3 is 2.6 keV/u, resulting in a low extraction voltage of 10 kV for Pb^{54+}. A more convenient extraction voltage, from a space charge and energy spread point-of-view, would be 50-60 kV. The extraction efficiency out of the EBIS should exceed 80%.

MECHANICAL DESIGN

Solenoid

For electron beam focusing and ion confinement in the trap region, a 3 T field from a superconducting magnet is used. The solenoid, with a full field length of 2.0 m (total length 2.5 m), is shielded, and it has a “warm bore”, i.e. the inner cylinder is at room temperature. This means: it is easy to open up since the solenoid has not to be warmed up to room temperature; the out-gassing caused by spurious electron beam load is low; finally, the drift tubes do not condense gases and thus do not have a “memory effect”. However, the latter only of importance if different ion species are used consecutively in a run.

Electron gun

The electron beam is generated in a semi-immersed gun, i.e. a gun configuration with a flat cathode that is immersed in the fringe field (~0.2 T) of the solenoid. The cathode, a LaB_6 with 310-crystal orientation, can have a high emission density (~30 A/cm^2) with a lifetime of approximately 1 year. As an alternative cathode material, with similar performances, IrCe could be used. With an anode voltage of 10 000 V the gun perveance becomes a moderate 1.5 microperv for a 1.5 A electron beam. After the emission from the electron gun, the beam is compressed by the increasing magnetic field strength (approximately linearly to B) when entering the solenoid, resulting in an electron current density of >400 A/cm^2 in full magnetic field. First at the axial position corresponding to a field strength of about 1 T, the electron beam energy is decreased from 10 to 5 keV, and thereby the perveance increased to a relatively high value of 4.2 microperv.

Drift tube structure

The system of drift tubes defines the extension of the trap in longitudinal direction and the electron beam energy. The drift tubes can be divided into three types: guide, barrier and trap tubes (Fig. 1). The drift tube structure will be mounted in vacuum inside the room temperature bore of the

solenoid. To reach the UHV (10^{-11} torr) inside the EBIS, turbopumps on each side of the solenoid, and NEG strips or other getter pumping inside the trapping region are necessary.

With a large drift tube radius, or more correctly, tube to electron beam radius ratio, the radial ion losses are kept low because of the considerable potential well. When the electron beam becomes compensated by the ions and the radial potential therefore decreases, the ions may have sufficient energy to leave the electron beam radially. If the trajectory radius, in spite of the precessing motion in the magnetic field, becomes larger than the drift tube radius, the ions are lost at the walls. To keep this radial ion loss as low as possible, and to minimise beam instabilities, it is desirable to have a large tube radius. On the other hand, the perveance limits the tube radius to maximum 4 mm.

A non-compensated electron beam of 1.5 A has a potential well (electron beam edge to beam axis potential difference) of 320 V, and a total potential well of 2100 V for 0.25 mm and 4 mm electron beam and tube radii, respectively. Even with a 50% trap compensation, the radial holding voltage is ~1000 V, which exceeds the radial heating by far (in the order of 20 V). Thus, the ion losses in radial direction are expected to be low, and can be made very small in longitudinal direction if the barrier potentials are high enough.

Because of the axial electric field gradient necessary to obtain a fast extraction, 7 to 10 trapping tubes are required to create the field. Additionally two barrier tubes and inner and outer guide tubes close to the anode and collector, respectively, are needed, in total 11 to 14 tubes. The number of tubes should be kept low to avoid risks of self-induced RF generation. Instead of several separated cylindrical tubes, the same field gradient effect can be obtained by a few electrodes, which azimuthally penetrate into each other like non-touching cogwheels [18].

Electron collector

At the electron collector the electron beam is separated from the extracted ions, and the electrons are absorbed at the collector surface. With a collector potential of +3 kV relative to the cathode, the deposited effect on the collector surface, which has to be cooled away by water, is 4.5 kW. Compared to many other EBISes, the collector end has an open design with a large diameter extractor peeking into the collector, see Fig. 4. A large, open end ensures that the ion beam aberrations are kept small.

Given that the collector is bakeable, and the design has an open end, a good vacuum inside the collector is obtained. No extra bucking or transverse magnet correcting coils are foreseen, however, the collector is surrounded by an iron cylinder to decrease the magnetic field inside the collector region, and thereby improve the electron beam expansion and absorption.

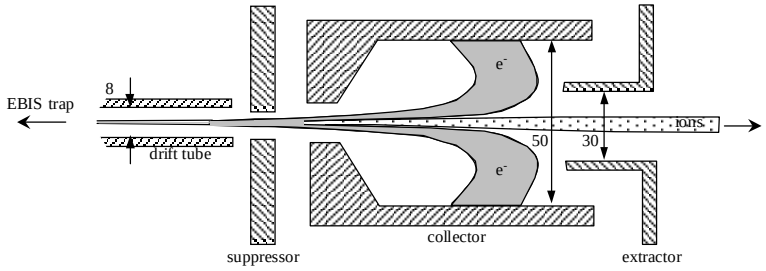

Figure 4. Schematic drawing of the electron collector. Note the open collector end and the large extractor diameter. (Not to scale. Typical dimensions and beams shapes indicated.)

BEAM PROPERTIES

The optimal transverse emittance for the LHCEBIS at an extraction voltage of 60 kV is estimated to 4 π mm mrad (2σ) [7]. This very small emittance presumes a full compensation of the electron beam in the active trapping region during the whole extraction cycle, which is unmanageable to attain, and ions fully trapped within the radius of the electron beam. With only 50% compensation the emittance may increase to a more realistic 40 π mm mrad (2σ) (ε_n = 0.06 μm). In any case, the accelerated wall concept is essential to keep the compensation level high throughout the extraction phase. Even so, in the collector region where the ions are separated from the electrons and still move with a relatively low velocity, space charge blow-up may occur, which could enlarge the emittance severely unless precaution is taken.

Ions extracted from an EBIS in general have a finite energy spread caused by: finite injection energy; ion heating due to elastic electron-ion collisions; ion heating due to ionisation at different radii (i.e. different electrostatic potentials); trap potential decrease during the extraction phase; and linear axial electrical field gradient inside the trap to acquire fast extraction. When utilising fast extraction the latter is completely dominating, that means an energy spread of approximately ±500*Q eV and ±2000*Q eV for t_{ext} = 10 μs and 5 μs, respectively. Thus, the analysing magnets in the present LEBT at LINAC3 can not be employed, but instead the beam, mainly containing Pb^{54+}, should be injected directly into an RFQ with a high energy-spread acceptance. Simulations have shown that a very high transmission through an RFQ, >95%, can be obtained for an energy spread as high as 20% [19].

Due to the short extraction time, the ion peak current becomes as high as 4 mA; therefore the EBIS to RFQ distance should be minimised to avoid space charge blow-up. Moreover, a short distance reduces the charge-exchange losses with the residual gas, even if the losses should be negligible for a pressure better than 10^{-9} mbar (a pressure necessary to reach the intended good vacuum inside the EBIS).

CONCLUSIONS

It has been shown that an EBIS, as the one proposed in this article, can meet the requirements set by the LHC ion injector if direct injection into the PS Booster is to be used instead of accumulation in the LEIR. Table 2 shows an estimation of the ion balance for the LHCEBIS concept, with a pulse yield after the LINAC3 exceeding the constraint of $1.25 \cdot 10^9$ Pb^{54+} ions required for single-turn injection into the Booster. Using fast extraction, the extracted ion pulse could possibly fit within the time-window of 5.5 μs set by the revolution time in the Booster, however, the energy spread becomes lower if a somewhat longer (10 μs) extraction time is tolerated. The emittance is estimated to 40 π mm mrad (2σ) for 60 kV extraction voltage (ε_n = 0.06 μm), i.e. within the 0.07 μm specified after the ion source. With an effective electron current density of >400 A/cm^2, the pulse period can be 1.2 s. Other ion types can be produced in the LHCEBIS as well.

This proposal has shown that it is theoretically possible to design an EBIS that meets the LHC specifications for lead ion production without having to develop and exploit a high current and high energy EBIS, nor to use four separate EBISes (one for each Booster ring). Instead, an alternative route with a design similar to the REXEBIS can be taken, which makes use of an electron beam with relatively low current and energy, and utilises the closed shell effect. Table 3 summaries its design properties.

Nevertheless, the LHCEBIS design has a few uncertainties that need further investigation before one can confidently claim that the concept will fulfil its promises. The electron beam has a high perveance that can make the propagation through the drift tubes difficult. Besides, the relatively small drift tube radius can possibly cause alignment problems and excessive ions losses. It is not clear what fraction of the available negative space charge will be occupied by cooling gas ions and, most important, it remains to experimentally examine how the radiative recombination will effect the abundance of Pb^{54+}. The latter test could most likely be performed at the REXEBIS at ISOLDE when it is fully operational. Finally, the fast extraction brings about a high space charge in the collector region before the ions are accelerated to 60*Q keV, which could cause emittance enlargement. The high peak current has to be transported to and injected efficiently into an RFQ with a high transmission for a large energy spread.

If the overall efficiency of the LHCEBIS should turn out to be worse than predicted, the electron current has to be increased or a longer trap utilised. It is however difficult to intensify the electron current much higher than 2 A for a 5 keV electron energy due to the perveance limit, and the present practical upper trap length is around 2 m (set by superconducting solenoid and extraction time limitations). If a shorter breeding time is requested, either the current density extracted from the cathode or the magnetic compression has to be increased.

Table 2. Space charge use and number of ions for the different steps in the LHCEBIS concept.

Total available space charge	$4.4 \cdot 10^{11}$ elementary charges
50% attainable space charge compensation	$2.2 \cdot 10^{11}$ elementary charges
50% Pb^{54+} abundance (RR, rest-gas, cooling gas etc)	$2.0 \cdot 10^{9}$ Pb^{54+} ions
80% EBIS extraction efficiency	$1.6 \cdot 10^{9}$ Pb^{54+} ions
80% LINAC transmission (Pb^{54+} after LINAC)	$1.3 \cdot 10^{9}$ Pb^{54+} ions

Table 3. Design parameters for the proposed EBIS for the LHC lead ion pre-injector.

Electron voltage (gun) / (trap)	10 keV / 5 keV
Electron current	1.5 A
Electron current density	>400 A/cm^2
Extracted ion energy spread	±0.15 to ±1.5 keV/u
Trap length	2.0 m
Full magnetic field	3 T
Total charge capacity	$4.4 \cdot 10^{11}$ elementary charges
Yield Pb^{54+}	$1.6 \cdot 10^{9}$ ions
Normalised transverse emittance	0.06 μm
Ion extraction energy	~15.6 keV/u

REFERENCES

1. Donets, E. D., and Ilyushchenko, V. I., JINR R7-4124, Dubna, Russia, 1968.
2. Beebe, E., Alessi, J., Hershcovitch, A., Kponou, A., Prelec, K., and Schmieder, R. W., *Rev. Sci. Instr*. **67,** no.3, 878-880 (1996).
3. Wenander, F., PS/HP/Note 99-09, CERN, Switzerland, (1999).
4. Geller, R., *Electron cyclotron resonance ion sources and ECR plasmas*, IOP Publishing Ltd, London, 1996.
5. Angert, N., et al., "High current, high frequency ECRIS development program for LHC heavy ion beam application", in *Proceedings of the 14th Int. Workshop on ECR Ion Sources*, CERN, Switzerland, 1999, pp.220-223.
6. Wenander, F., Axelsson, J., Björkhage, M., Carlé, P., Rensfelt, K-G., Jonson, B., and Nyman, G., "REXEBIS – A charge breeder for the REXISOLDE post accelerator", in *Proceedings of the 6th European Particle Accelerator Conference*, edited by S. Myers et al., Stockholm, Sweden, IOP Bristol, 1999, pp.1412-1414.
7. Wenander, F., Jonson, B., Liljeby, L., and Nyman, G., CERN-OPEN-2000-320, CERN, Switzerland, (2000).
8. Haseroth, H., and Prelec, K., *Physica Scripta* **T71** 23-27 (1997).
9. Dyall, K. G., Grant, I. P., Johnson, C. T., Parpia, F. A., and Plummer, E.P., *Computer-Physics-Communications* **55**, no.3 425-456 (1989).
10. Müller, A., and Salzborn, E., *Phys. Lett.* **62A**, 6 391-394 (1977).
11. Becker, R., Brinzanescu, O., and Stöhlker, Th., these proceedings.
12. Kim, Y. S., and Pratt, R. H., *Phys. Rev.* **A27**, no.6, 2913-2924 (1983).
13. Beebe, E., Alessi, J., Hershcovitch, A., Kponou, A., Pikin, A., Prelec, K., Stein, P., and Schmieder, R. W., *Rev. Sci. Instr*. **69**, no.2, 640-642 (1998).
14. Axelsson, J., Björkhage, M., Carlé, P., Engström, Å., Liljeby, L., and Wenander, F., "Sputtered and gaseous ions into CRYSIS", *Annual Report 1997*, Manne Siegbahn Laboratory, Stockholm Sweden, pp.11-12.
15. R. Becker, "Electron beam ion source / trap", in *Handbook of ion sources*, edited by B. H. Wolf, CRC Press Inc., Boca Raton, 1995, chapter 2/section 11.
16. Beebe, E., Alessi, J., Kponou, A., Pikin, A., and Prelec, K., "Heavy ion extraction from the BNL high current EBIS teststand", in *Proceedings of the 7th European Particle Accelerator Conference*, edited by W. Mitaroff et al., Vienna, Austria, 2000, pp.1589-1591.
17. Höltermann, H., these proceedings.
18. Becker, R. Höltermann, H., Pikin, A., and Stöhlker, Th., "Fast extraction of high currents from an EBIS", in *Proceedings of the Workshop on the Production of Intense Beams of Highly charged Ions*, edited by S. Gammino, Catania, Italy, 2000.
19. Alessi, J., Brookhaven National Laboratory, New York, USA, private communication.

PAPER 7

REXEBIS – the electron beam ion source for the REX-ISOLDE project

Authors:
F. Wenander, B. Jonson, L. Liljeby and G. Nyman

Published in CERN open series:
CERN-OPEN-2000-320, CERN, Switzerland.

REXEBIS

the Electron Beam Ion Source for the REX-ISOLDE Project

Design and Simulations

F. Wenander[1], B. Jonson[1], L. Liljeby[2], G. Nyman[1]
and the REX-ISOLDE collaboration

1. Experimental physics
Chalmers University of Technology
and Göteborg University

in collaboration with

2. Manne Siegbahn Laboratory
Stockholm University
Stockholm

CERN 1999

Abstract

The REXEBIS is an Electron Beam Ion Source (EBIS) developed especially to trap and further ionise the sometimes rare and short-lived isotopes that are produced in the ISOLDE separator for the Radioactive beam EXperiment at ISOLDE (REX-ISOLDE). By promoting the single-charged ions to a high charge-state the ions are more efficiently accelerated in the following linear accelerator. The EBIS uses an electron gun capable of producing a 0.5 A electron beam. The electron gun is immersed in a magnetic field of 0.2 T, and the electron beam is compressed to a current density of >200 A/cm^2 inside a 2 T superconducting solenoid. The EBIS is situated on a high voltage (HV) platform with an initial electric potential of 60 kV allowing cooled and bunched 60 keV ions extracted from a Penning trap to be captured. After a period of confinement in the electron beam (<20 ms), the single-charged ions have been ionised to a charge-to-mass ratio of approximately ¼. During this confinement period, the platform potential is decreased to about 20 kV, and an axial potential barrier is lowered to allow the now highly charged ions to be extracted from the EBIS at an energy matching the requirement of the Radio Frequency Quadrupole (RFQ).

Several different topics are presented in this report, all connected with the design and construction of an EBIS. Old 'truths' have also been scrutinised, for instance alignment tolerances. A large part is devoted to the description of a novel EBIS simulation implementation.

A complete injection, breeding and extraction cycle has been simulated to certify high injection and extraction efficiencies. The entire EBIS was modelled in an ion-tracing program called SIMION, and the accepted and emitted phase spaces were determined. Beam optics parameters such as lens positions, voltages, accepted beam-tilt and displacement tolerances at the focal points were also settled using SIMION. An analytically derived acceptance formula was verified with simulations, and general conclusions on acceptance, emittance and energy spread of an EBIS are presented in this report. Any possible correlation between the two transverse emittance phase spaces was shown to be insignificant. Furthermore, continuous injection, and maximal obtainable efficiency for such an injection mode were studied theoretically.

The electron reflection and back-scattering in the collector was simulated using a combination of EGUN and SIMION. The result showed that a much lower degree of electron back-scattering may be obtained with this design as compared to previously published estimations. Furthermore, the Penning trapping of electrons at the trap barrier (or the post anode) was addressed, and techniques to avoid it were evaluated.

Vacuum considerations for residual gas in the warm-bore magnet chamber, and the back-flow of Ar cooling gas from the Penning trap, have also been addressed since there is a risk of outnumbering the small number of radioactive ions. Simulated extraction spectra for different pressure scenarios are presented.

All different REXEBIS elements (magnet, electron gun, inner structure, collector etc) are described from a design and performance perspective, and preliminary investigations of the platform high voltage switching and the beam diagnostics are included as well. A very elegant and simple method to align the solenoid within the iron yoke was developed and used.

The high experimental emittance value obtained for electron beam ion source at MSL in Stockholm (4 times larger than the absolute upper theoretical value) was reproduced in simulations and could be justified by aberrations in the small einzel lens following the collector. The result of this simulation also verified the validity of the developed EBIS code.

Keywords: REXEBIS, REX-ISOLDE, EBIS design, beam simulations, SIMION, ion injection, continuous injection, acceptance, emittance, phase space correlation, electron back-scattering, CRYSIS, radioactive ions

REXEBIS

the Electron Beam Ion Source for the REX-ISOLDE Project

Design and Simulations

PART I – THE REX-ISOLDE PROJECT

PART II – THE REXEBIS DESIGN

PART III – SIMION SIMULATIONS

PART IV – CONCLUSIONS

Foreword

The construction of REXEBIS, an Electron Beam Ion Source (EBIS), is part of a larger project, the so-called REX-ISOLDE project [1,2,3,4,5,6], which is a post accelerator connected to the ISOLDE (Isotope Separator On-Line) [7,8] facility at CERN. The nuclear physics community is now turning its attention to the regions far away from nuclear stability, to the neutron and proton drip-lines and the physics with radioactive ions. There, exciting new phenomena may be found, such as changed magic numbers, halo shells etc. To reach these extreme regions in the nuclear chart innovative accelerator concepts have to be used. The ISOLDE community has chosen to add a post accelerator to the isotope on-line separator. By doing so, the physicists will have access to the large number of isotopes produced at ISOLDE, and make use of the long experience in radioactive ion production at ISOLDE, but now at higher energies.

The post acceleration of radioactive ions is a novel concept and the REX-ISOLDE is a pilot project aiming at demonstrating an efficient scheme for post acceleration of radioactive beams produced by an on-line mass separator (ISOLDE) to energies somewhat below the Coulomb barrier. The ions are first accumulated in a Penning trap, thereafter charge bred in an EBIS, and finally accelerated in a short linear accelerator to energies between 0.8 and 2.2 MeV/u. The first experiments planned for the REX-ISOLDE involve studies of the nuclear structure of medium-light neutron-rich nuclei by Coulomb excitation and neutron transfer reactions.

An EBIS is a device that charge breeds ions by bombarding single-charged ions with high energy electrons [9]. These electrons knock out electrons from the ions, and after a few ms the ions have been ionised to a higher charge state. By introducing an EBIS into the post accelerator chain, the 1^+ ions are ionised to a Q/A-value of about ¼ in our case, thus the length of the succeeding LINAC can be reduced considerably. For the low beam energies delivered by an on-line separator, an EBIS is an effective alternative. The actual REXEBIS has features similar to CRYSIS [10], and will be installed after a Penning trap [11,12] and in front of a three stage LINAC in the REX-ISOLDE accelerator. Design and construction of the REXEBIS are carried out at the Manne Siegbahn Laboratory in Stockholm in collaboration with the Chalmers University of Technology with economical support from the Knut and Alice Wallenberg foundation.

This report summarises the last three years work done on the REXEBIS, and is a modified version of the Licentiate thesis of Fredrik Wenander. The motivation has been to write a report that should act as REXEBIS documentation in which the source design is described and motivated. Also some results from theoretical investigations of EBISs in general are discussed. The report begins with a brief overview of the REX-ISOLDE project, where the concept of the post accelerator design and the new physics are explained. In the second and major part, the different REXEBIS components are discussed in separate sections. The third part contains theoretical simulation results applicable for EBISs in general. In the last part Conclusions, Outlook, Appendices, etc are collected.

Part I – The REX-ISOLDE project

1.1 What is REX-ISOLDE?

One of the most exciting and foremost frontiers in nuclear physics today is physics with energetic radioactive beams. That is confirmed by the number of conference proceedings and workshops [13,14,15,16] discussing the design of such facilities and the new physics which can be carried out. Going for nuclear physics further away from the valley of stability is also advocated in two reports from the "Nuclear Physics European Collaboration Committee" (NuPECC) [17,18].

REX-ISOLDE - Radioactive beam EXperiment at ISOLDE – is one of the first steps into this new physics arena: a pilot experiment testing a new concept of post acceleration of radioactive ions. It is placed at an already existing isotope separator facility – the ISOLDE at CERN, Geneva – and makes use of the vast experience and availability of low-energy radioactive 1^+ ion beams from about 70 chemical elements. REX-ISOLDE employs a new concept to bunch, charge-multiply and post accelerate the single-charged ions from 60 keV to 2.2 MeV/u. The main initial aims of the experiment were [1]:

- to demonstrate an efficient way to post accelerate low energy radioactive beams from ISOL-facilities
- to study very neutron-rich nuclei around the neutron shell closures (N=20, N=28) by Coulomb excitation and neutron transfer reactions using a highly efficient γ- and particle-detector array

For a start, REX-ISOLDE will deliver ions with a maximum final energy of 2.2 MeV/u, though options for extension to higher and lower beam energies are on hand, which open up a wide field of physics including Coulomb barrier penetration experiments. The project involves a dozen universities from all around Europe, and the initial experiments are scheduled for late 2000.

1.2 REX-ISOLDE physics

To start with very neutron-rich nuclei in the vicinity of the closed neutron shells N=20 and N=28, corresponding to isotopes of Na, Mg, K and Ca, will be investigated. Level schemes, B(Eλ)-values and quadrupole moments will be obtained, and provide key information for the theoretical description of the nuclei in the shell model context in a wide range of isospin values. The intention is to use the accelerated beam for studying dynamical properties and deduce the shapes of very neutron-rich nuclei close to semi-magic shells by Coulomb excitation and neutron transfer reactions.

A new facility like REX-ISOLDE will of course address a great deal of new physics, and some questions that it should answer are listed below, as well as proposals (P) or the letters of intent (LoI) addressing these questions. In ref. [19,20] more information on the REX-ISOLDE and MINIBALL physics can be found. In the future, after it has been demonstrated that the accelerator concept works, an optional energy boost to ~5-10 MeV/u can come into question.

Nuclear structure topics

- How are level schemes, B(Eλ)-values and quadrupole deformations changed in a region close to the drip-line?
- What is the most appropriate nuclear model far away from stability?
- Do there exist new regions with extreme nuclear deformation?
- Are new collective modes to be found with stable octupole, oblate or triaxial nuclear shapes?
- Neutron halo nuclei: how abundant are they and do more forms exist?

P Investigation of the single particle structure of the neutron-rich sodium isotopes $^{27\text{-}31}$Na [21].
P Investigations of neutron-rich nuclei at the dripline through their analogue states: The cases of ^{10}Li-^{10}Be (T=2) and ^{17}C-^{17}N (T=5/2) [22].
P Study of the unbound nuclei ^{10}Li and ^{7}He at REX ISOLDE [23].
P Structure features of ^{6}He from direct reactions on light target nuclei [24].
LoI Study of neutron dripline nuclei using post accelerated ion-beams [25].
LoI Dipole Coulomb polarizability in the scattering of halo nuclei [26].

LoI A post-accelerator for ISOLDE [27].

Nuclear astrophysics topics

- The nucleosynthesis during the early universe: how did the process continue through the bottlenecks, e.g. through the ^{35}Ar(p,γ) reaction?
- What is the magnitude of the astrophysical S factor, and how can the solar neutrino problem be solved?

LoI A radioactive-ion beam experiment for the study of the astrophysical rp-process at CERN-ISOLDE [28].
LoI Measurement of the ^{7}Be(p,γ)^{8}B absolute cross-section in inverse kinematics [29].

Atomic and fundamental physics

- Is there parity non-conservation in heavy ions or atoms (Ba^+ [30], Ra^+ and Fr [31])?
- What are the exact masses of short-lived medium mass and heavy isotopes?

LoI Search for new physics in β-neutrino correlations using trapped ions and a retardation spectrometer [32].

Solid state physics

- How will radioactive implantation, creating point defects and impurities on a deep level in the semiconductor, affect its properties?

LoI Energetic radioactive ion beam studies of hydrogen in semiconductors [33].
LoI Defects studies in high-energy ion implanted semiconductors [34].
LoI Diffusion in highly immiscible systems [35].

1.3 Accelerator concepts

1.3.1 Accelerators world-wide

Physics with radioactive ions is a hot and expanding topic that until now has been technically too challenging. Though, the latest accelerator achievements have prepared the way, and several Radioactive Ion Beam (RIB) facilities are at the planning stage or under construction, and will start running around year 2000 [36]. They can be divided into two types: the in-flight (E_{ion}>25 MeV/u) and the ISOL-technique (E_{ion}<25 MeV/u). See further Figure 1 for explanation of each type. A list of a few ISOL-based facilities follows below.

- Louvain-la-Neuve, Belgium, is an accelerator operating an intense low-energy proton driver (30 MeV, 500 mA) and a CYCLONE 44 post-accelerating cyclotron. An upgraded version is under commissioning and it will produce secondary beams close to stability, in the energy range for nuclear astrophysics [36,37].
- The SPIRAL facility at GANIL, France, is ready to start. The existing GANIL will be used as "driver" accelerator that allows a great variety of production reactions. The exotic elements, including nuclei far from stability, are accelerated in the newly constructed K=265 cyclotron to a wide energy range (2-25 MeV/u) [36,38,39,40].
- At TRIUMF in Canada, a 100 mA, 500 MeV proton beam bombards a target and produces a variety of very intense beams of nuclei far from stability. After mass separation the beams can be directed into two different experimental areas: one has 60 keV energy and in the second the beam is post accelerated to 0.15-1.50 MeV/u [41,42].
- The HRIBF, Oak Ridge Laboratory USA, is devoted to low-energy nuclear structure and astrophysics research. Radioactive ions are produced when intense hydrogen or helium beams accelerated by the K=105 cyclotron are directed onto thick, refractory targets. The radioactive elements diffuse out of the target, are ionised, and mass selected for injection into the 25 MV Tandem Accelerator producing beams of 0.1-10 MeV/u for light nuclei and up to 5 MeV/u for mass 80 nuclei [43,44].

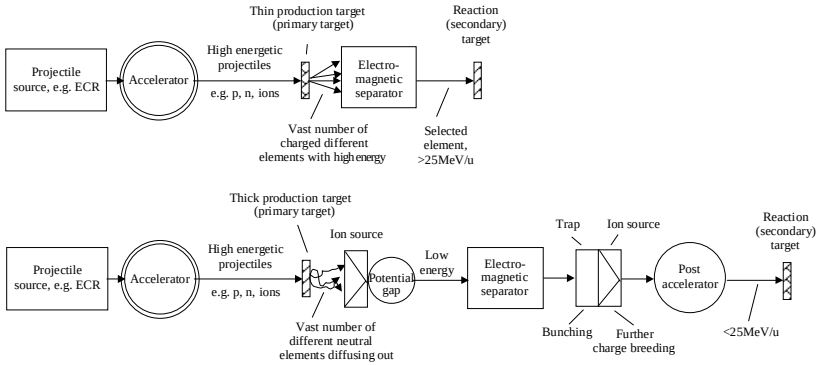

Figure 1. *In-flight and ISOL-technique (including post acceleration) production of radioactive ions. The major difference between the two methods is the production of elements in the production target, which in the case of the ISOL-technique calls for post acceleration.*

1.4 The REX-ISOLDE post accelerator

Like the accelerators listed above, the REX-ISOLDE is of on-line mass separator type and uses the long experience gathered at ISOLDE for the production of beams far from stability. The radioactive species produced at ISOLDE are bunched and cooled in a Penning trap prior to charge-state breeding in an EBIS. The highly charged ion beam is thereafter mass analysed and accelerated in a three stage LINAC consisting of an RFQ, an IH-structure and three 7-gap resonators to reach an energy of 0.8-2.2 MeV/u. It is also foreseen to redirect the highly charged ions to the ordinary ISOLDE experimental area without any post acceleration. An overview of the concept is shown in Figure 2, and progress reports are found in ref. [2,3,4]. This concept, utilising an accumulation device with buffer gas cooling and bunching, and a charge breeder, is the first of its kind. It should have a high efficiency, which is important when handling valuable and rare exotic nuclei. REX-ISOLDE is expected to be operational in year 2000.

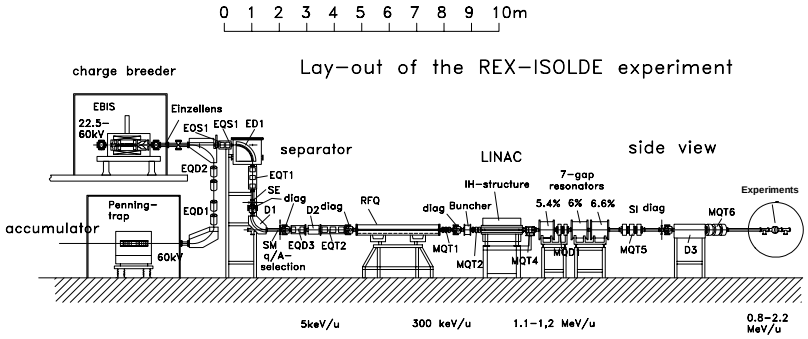

Figure 2. *Overview of the REX-ISOLDE beam line [45].*

1.4.1 ISOLDE

ISOLDE is an on-line separator, located at the PS Booster at CERN. It produces a wide variety of radioactive nuclides [7,8]; around 600 isotopes of about 70 different elements.

An on-line separator (ISOL) can principally be divided into four stages: (i) element production by particle induced nuclear reactions in a primary target; (ii) ionisation; (iii) acceleration; (iv) mass analysis. From the PS-Booster (a stack of four small synchrotrons that accelerates protons delivered by the proton LINAC to 1 or 1.4 GeV) about $3 \cdot 10^{13}$ protons impinge the primary target every second. The target [46] is rather thick, <230 g/cm^2, and in the form of metal foils, molten metal, oxide or carbide. At the proton impact a vast number of different elements and isotopes are produced by spallation, fission and fragmentation processes. The reaction products diffuse out from the heated target to an ion source of surface, plasma or laser type. In the ion source the elements are ionised to mainly 1^+ charge-state, and then accelerated over a potential gap of 60 kV. This means that the ions have an energy of 60 keV – the ISOLDE energy – when they enter the experimental hall. The desired mass number is selected in an electrostatic isotope separator. Two different separators are available at ISOLDE (Figure 3) – the General Purpose Separator (GPS) and the High Resolution Separator (HRS) with resolutions m/Δm of 2400 and ~10 000, respectively.

From the PS-Booster a proton pulse is delivered every 1.2 s, and on average every second pulse is delivered to ISOLDE. The pulse length is approximately 2.4 μs, but the diffusion time out of the primary target is much longer. Time constants down to some tenths of a second can be reached for the fastest targets and this fact sets the lower life-time limit typically to some 10 ms. Since the yields drop very fast when approaching the drip-lines and half-lives of the nuclides decrease, a highly efficient acceleration method is prerequisite for successful experiments with exotic nuclei.

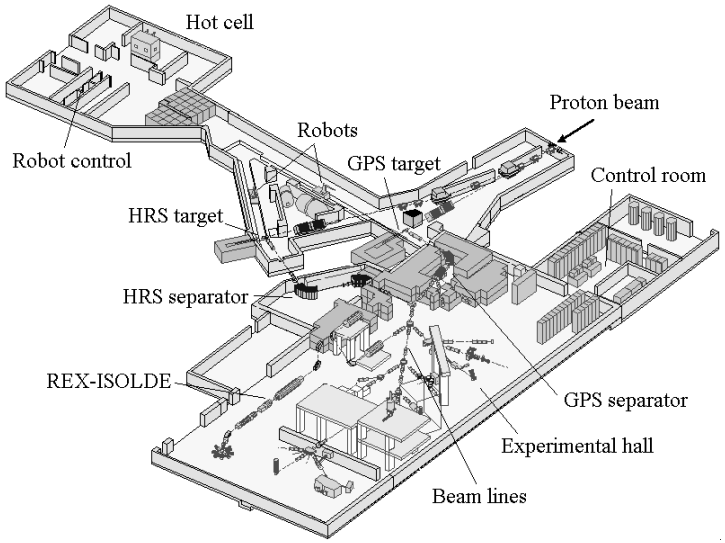

Figure 3. *Schematic picture of the ISOLDE targets, the beam lines with already existing experiments, and the coming REX-ISOLDE.*

1.4.2 The Penning trap

A Penning trap – the REXTRAP [11,12] – is introduced as the first step in the accelerator scheme to accumulate and bunch the almost continuously injected beam from ISOLDE. Besides, the ions are cooled so that smaller longitudinal and transverse emittances (see sec. 3.3 for definition) are obtained. The

reasons for introducing a trap in the system are that an EBIS has optimum injection efficiency for a pulsed beam with small emittance, and the LINAC operates with a duty factor of about 10%. Moreover, a bunched beam also improves the signal to background ratio for the measurements.

The REXTRAP is located close to 60 kV potential so that the semi-continuous 60 keV ISOLDE ions just enter the trap. The ions are trapped in a combination of a solenoidal magnetic field created by a superconducting magnet, and an electric field from cylindrical electrodes (see Figure 4). Inside the trap the ions perform mainly three different motions: axial, cyclotron and magnetron eigenmotions as illustrated in Figure 5. To reduce the eigenmotions, and thereby improve the emittances, the ions are cooled by buffer gas collisions [48]. To achieve this the trap is filled with a buffer gas (e.g. Ar, Ne or He), and by long range Coulomb collisions energy is transferred from the ions to the buffer gas, so the axial as well as the cyclotron motion amplitudes decrease exponentially with time. The magnetron motion, however, is unstable, i.e. the amplitude increases exponentially under influence of any dissipative force. To avoid this, the ion motion is driven at the frequency $\omega_c+\omega_+$ so the magnetron (ω_-) and the cyclotron (ω_+) motions couple [49] in such a way, that the friction force due to the buffer gas now decreases the amplitude of the magnetron motion.

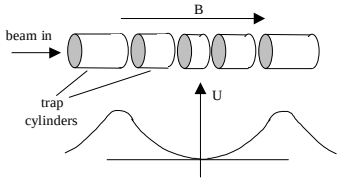

Figure 4. *Solenoidal magnetic field B and cylindrical electrostatic surfaces in a Penning trap.*

This frequency coupling is used in the so-called sideband cooling technique [50] where the ion cloud in the trap is purified from unwanted ion species contaminating the ion beam. In this mode all ions are first driven within a few ms to magnetron orbits larger than the diameter of the extraction hole of the trap. Subsequently only the desired species are re-centred by sideband excitation and thus enabling extraction.

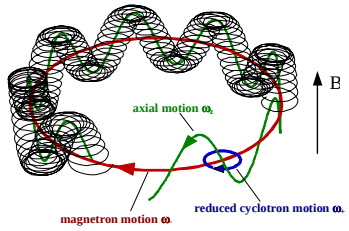

Figure 5. *Ion eigenmotions in a Penning trap: magnetron, cyclotron and axial motion; $\omega_c=q\cdot B/m=\omega_++\omega_-$=true cyclotron frequency.*

The energy loss, ΔE, in the buffer gas during a single oscillation in a trap has to be larger than the energy spread of the ISOLDE beam (effectively 100 eV) for the ions to be trapped. With a trap length of 0.9 m and an argon gas pressure of $1\cdot10^{-3}$ mbar, the aim to accumulate 100% of the injected ions should be reached. The cooling time for this fast cooling is in the range 10-20 ms. The magnetic field strength B created by the superconducting coil equals 3 T. In a future larger trap version 10^7-10^8 ions can be accumulated, but with stringent emittance and time structure requirements, a maximum ion current of 10^7 ions/s for 100 Hz repetition rate is realistic. At the end of the cycle the ions are extracted in a bunch and transported to the EBIS with 60 keV kinetic energy.

1.4.3 The Electron Beam Ion Source (EBIS)

Inside the REXEBIS the ions are charge bred to a higher charge-state. An EBIS is a device for production of multiply charged ions with capabilities for:

- Producing an axially extended electron beam of given energy and current density.
- Creating an electrostatic ion trap along the beam.
- Receiving a certain number of low-charged ions of the working substance into the EBIS trap during a defined pre-set period of time.
- Confining the ions in the electron beam for a period of time sufficient for the ions to reach the desired charge-state.
- Extracting the produced highly charged ions from the EBIS trap along the electron beam and simultaneously prepare for the next cycle.

The EBIS, Figure 6, uses a dense mono-energetic electron beam from an electron gun to further ionise the ions [9]. The electron beam is focused and compressed by a strong magnetic field created by a surrounding solenoid. Ions injected into the EBIS are confined radially by the electrostatic forces from the negative electron beam and the magnetic field, and longitudinally by potential barriers, established by cylindrical electrodes surrounding the beam. Inside the trapping region the high-energy electrons collide with ions, which are stepwise ionised, until they finally are extracted by raising the trapping potential and lowering the extraction barrier simultaneously. The ion motion inside the trap is a combination of radial oscillation in the electrostatic field of the beam with a superimposed azimuthal cyclotron motion around the magnetic field lines, and a relatively independent bouncing between the end barriers [51].

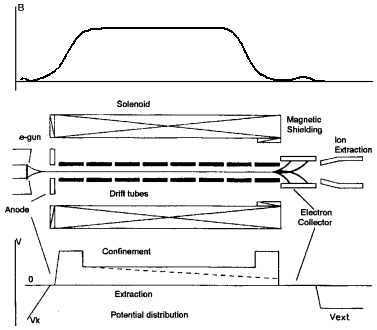

Figure 6. *Scheme of EBIS and corresponding axial potential function and axial magnetic field [52].*

The main characteristic entity describing an EBIS is the product $j_e\tau$, the ionisation factor, of the electron-beam current-density j_e and the breeding time τ. The probability for transition of an ion from charge-state q to q+1 is $P_{q\to q+1}=\sigma_{q\to q+1}\cdot j_e\cdot\tau/e$, where e is the elementary charge. Thus, on the average, all ions of charge-state q transform to q+1 ions when $j_e\tau=e/\sigma_{q\to q+1}$. This means that to reach ions of mean charge k from singly charge ions with stepwise ionisation, the ionisation factor $j_e\tau$ has to be:

$$j_e\tau=\sum_{q=1}^{k-1}\frac{e}{\sigma_{q\to q+1}} \qquad \textbf{(8)}$$

The REXEBIS is designed for a current density j_e~200 A/cm^2 (see sec. 2.6.3 for comments) and a current I_e=0.5 A. An electron kinetic energy of 5 keV enables ionisation to Q/A>1/4.5 for almost all elements. The limited lifetime of the radioactive nuclides restricts the breeding cycle time to about 20 ms, with option to go to shorter time-periods for lighter elements. To reach the required charge-to-mass ratio for ^{30}Na ($T_{1/2}$=54 ms) and ^{51}K ($T_{1/2}$=365 ms), breeding times of 13 and 19 ms are needed, respectively. Table 1 lists the peak charge-states for different elements at a breeding time of 20 ms, and Figure 7 illustrates the breeding time versus charge-state for a selection of elements. To reach high charge states of heavier elements either the breeding time or the current density has to be increased.

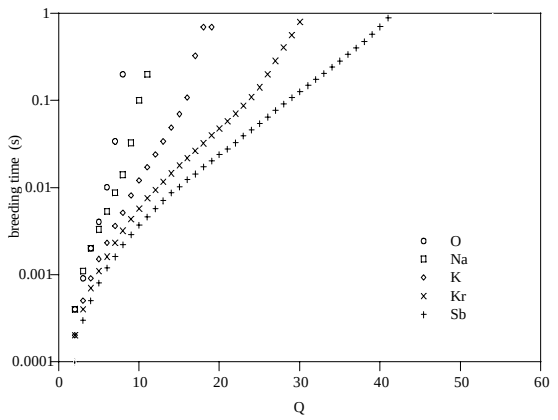

Figure 7. *Breeding time versus charge-state for the REXEBIS design parameters.*

The solenoid has a length of 1.2 m, with a trap length of 0.8 m where the magnetic field equals 2 T. The REXEBIS trap can hold ~$5\cdot10^9$ C for an electron-beam charge-compen-

sation of 10%, i.e. $6 \cdot 10^8$ Na^{8+}. This is approximately one order of magnitude more ions than the REXTRAP can accumulate. Since only one specific charge-state is selected from the total charge distribution by the mass analyser, a maximum breeding efficiency $q_i/\Sigma q_i$ of about 30% is expected.

To obtain an efficient charge breeding the overlap between the ion trajectories and the electron beam has to be complete and the injection into the EBIS exact. A low extraction emittance of 3 π·mm·mrad from the Penning trap (60 kV) is required, and the following mass analyser accepts at most an emittance of 5·8 π·mm·mrad (4σ) at 20 kV extraction voltage. While the voltage of the trap platform is fixed to 60 kV to decelerate the ions from ISOLDE, the platform of the EBIS will be pulsed between 60 kV (injection) and ~20 kV (extraction). The low extraction voltage results in a low RFQ injection energy and thus an efficient, adiabatic bunching providing better output emittance of the RFQ.

Element	Charge-state
$_{8}O$	7^+
$_{11}Na$	9^+
$_{12}Mg$	9^+
$_{18}Ar$	11^+
$_{19}K$	11^+
$_{20}Ca$	12^+
$_{36}Kr$	16^+
$_{37}Rb$	18^+
$_{51}Sb$	19^+
$_{54}Xe$	21^+

Table 1. *Peak charge-state after 20 ms breeding time.*

Inside the REXTRAP the buffer gas pressure is 10^{-3} mbar, while the REXEBIS requires an extremely good residual gas pressure (10^{-11} torr) to avoid completely outnumbering of the radioactive ions. A 7-stage differential pumping transfer line will provide an argon pressure of ~10^{-14} torr inside the REXEBIS, which yields an Ar ion production of the same magnitude as 5000 injected Na ions.

1.4.4 The mass separator

From the REXEBIS a wide variety of ions emerges, not only highly charged ions of the desired isotope that was injected. This is due to residual gas contamination inside the REXEBIS that is also ionised in the electron beam. As the intensity of the radioactive ions can be much smaller than the residual gas intensity, a mass separator is required.

Due to the potential depression of the REXEBIS electron-beam space-charge, the extracted ions will have an energy spread (<100 eV/charge, see sec. 3.3.6 for further comments), that limits the Q/A-resolution of an ordinary magnetic achromat with two 90° dipoles separator to Q/A<200. However, to suppress the residual gas spectrum from the EBIS a Q/A-resolution of approximately 150 is needed, and hence a Nier-spectrometer [53] will be used as mass selector. A Nier-spectrometer consists of an electrostatic 90° cylinder deflector and a 90° magnetic bender arranged in a vertical S-shape (Figure 8). The electrostatic deflector separates the ions according to their energies irrespective of their masses to a focal plane (SE). The correct charge-to-mass ratio is selected in the focal plane of the bending magnet (SM). Assuming a 40 π·mm·mrad (4σ) emittance and an energy spread <50 eV/charge from the REXEBIS, a resolution of 150 is expected.

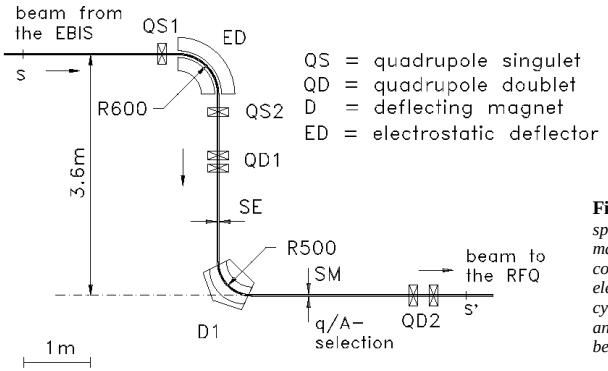

Figure 8. *Nier-spectrometer for mass separation consisting of an electrostatic 90° cylinder deflector and a 90° magnetic bender [45].*

1.4.5 The LINAC

The linear accelerator consists of three separate stages: RFQ, IH-structure and 7-gap resonators, all operating at a resonance frequency of 101.28 MHz and with a duty factor of 10%. The macrostructure of the accelerated ions will have a typical pulse width of 100 µs and a pulse separation of 20 ms. The microstructure has pulse widths between 2.4 and 13 ns, depending on energy. The time between the micro-pulses will be 10 ns. The overall beam transmission is calculated to ~90% [1].

1.4.5.1 The RFQ

The use of a Radio Frequency Quadrupole (RFQ) [54,55,56] is favourable for low energetic beams owing to its good efficiency. In principle an RFQ can be divided into four sections: the radial matching section, the shaper, the buncher, and the accelerator section. The 4-rod RFQ consists of four electrodes (see Figure 9), on which an alternating voltage field is applied. The RF quadrupole field provides transverse focusing for the low energy ions while a modulation of the spatial length of the four rods performs smooth bunching of the injected dc-beam and acceleration. The 3 m long 4-rod RFQ accelerates the radioactive ions with a charge-to-mass ratio larger than 1/4.5 from 5 keV/u to 300 keV/u. Due to a conservative layout, it should be possible to go to even lower Q/A, such as 1/6.5 for the maximum voltage between the rods, a fact which is important when heavier ions shall be used in future experiments.

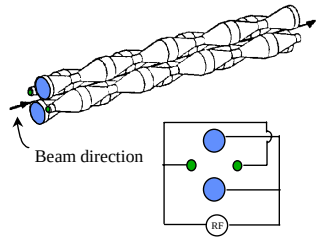

Figure 9. *Schematic picture of a 4-rod RFQ.*

1.4.5.2 The IH-structure

The second acceleration stage, the Interdigital H-type (IH)-structure, is an efficient drift tube structure with special beam dynamics [57]. Inside the resonator tank cylindrical cavity drift tubes of varying length (matching the ion velocity) are mounted alternating on opposite sides (Figure 10). The magnetic field lines are parallel to the beam axis and the induced currents flow azimuthally on the wall, creating electric fields of alternating direction between the drift tubes. This field forces the ions forward. After a first accelerating section the beam is transversally focused in a quadrupole triplet. Thereafter the beam is rebunched in the first three gaps behind the triplet, followed by a second accelerating stage. The IH-structure has 20 gaps and a total length of 1.5 m. A tuning of the final energy between 1.1 and 1.2 MeV/u can be achieved by adjusting the gap-voltage distribution via two capacitive plungers and adjusting the RF-power level in the resonator.

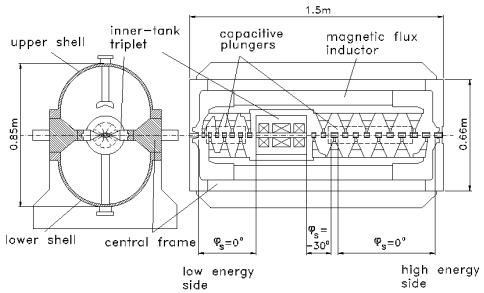

Figure 10. *End and side view of an IH-structure [45].*

1.4.5.3 The 7-gap resonators

The last acceleration section consists of three 7-gap resonators [58,59]. These special types of split ring resonators are designed and optimised for synchronous particle velocities of β=v/c=5.4%, 6.0% and 6.6%. The resonator has a single resonance structure, which consists of a copper half-shell and three arms attached to both sides of the shell. Between the first and second resonator there is an additional doublet for transverse focusing. The final ion energy can easily be adjusted between 0.8 and 2.2 MeV/u by tuning the RF power and phase of the three active resonators.

1.4.6 The experimental area

In the dipole magnet after the 7-gap resonators the beam is momentum analysed and directed to a target in one of the two experimental beam lines. One of the targets is surrounded by a highly efficient detector system for γ-rays (MINIBALL [19,60]), and inside the target chamber a position sensitive silicon detector [61] for Doppler shift corrections of the scattered ions (or the recoiling target nuclei) can be found (see Figure 11 and 12). The second beam line will be used for experiments which do not require the MINIBALL γ-detection array.

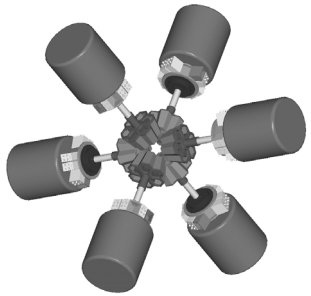

Figure 11. *The MINIBALL – a Ge-array consisting of six clusters. The six cryostats are included in the illustration.*

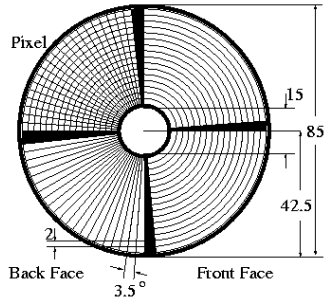

Figure 12. *Double Sided Silicon Strip Detector of CD type used as particle detector.*

Part II – The REXEBIS design

2.1 REXEBIS introduction

An Electron Beam Ion Source (EBIS) is a special type of ion source, with the ability to produce highly charged ions. There exist other ion source types [62], but despite of the complexity and the expensive price tag of an EBIS, the advantages such as:

- highest charge-states
- excellent beam quality
- variable pulse length from μs to DC
- no life-time limitations
- UHV-compatible

outbalance the difficulties for many applications. An ECR ion source produces higher currents but with poorer beam quality and not such high charge-state [63]; a PIG ion source is much less complicated [64], but is limited to low charge-states (see Figure 13).

The EBIS can also be used as a pure charge breeder – low-charged ions are produced externally, injected into the EBIS and charge-multiplied to the desired charge-state. The REXEBIS will operate after this already tested working principle [10]. The novelty is to place the EBIS after a Penning trap and to inject radioactive ions into it. The EBIS will be in the middle of an accelerator chain, and not as more commonly, constitute the initial stage. The introduction of a charge-breeding EBIS will lead to a compact and efficient accelerating system, compared with acceleration of 1^+ ions or the use of stripping foils.

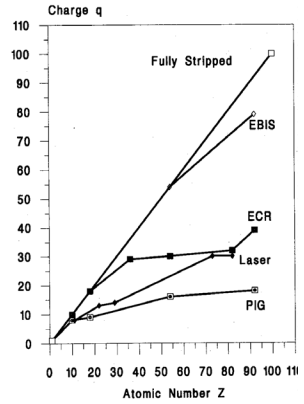

Figure 13. *Charge-states available from EBIS, ECR, laser and PIG sources [65].*

2.2 General EBIS theory

The very basic EBIS theory was covered in the first part, sec. 1.4.3 and only complementary short sections on ionisation, ion heating and cooling will follow here below. The EBIS is not a new device; it was invented 30 years ago by Donets [9], and several comprehensive reviews of the machine and its physics exist [66,67,68] and we refer to these for a theory compilation. Instead we prefer to introduce the necessary theory in connection with each treated section.

2.2.1 The ionisation process

The main objective of an EBIS is to produce highly charged ions by electron impact, and since the probability for multiple ionisation is low, the high charge-state is predominantly reached by sequential ionisation (i.e. only one electron is removed at each collision) and therefore several electron-ion collisions are required.

A compilation of processes in an EBIS could be:

- electron-impact ionisation of ions
- radiative recombination of ions
- charge-exchange between ions and neutral atoms or between ions and ions
- ion heating by the electron beam
- ion-ion energy exchange
- ion confinement in, and escape from, the trap

but since the cross-sections for many of the processes are very uncertain, but nevertheless small, most often only the electron impact ionisation is included when calculating required breeding parameters to reach a certain charge-state.

The transition probability from charge-state q to q+1 for a short breeding time τ is:

$$P_{q\to q+1} = \frac{\sigma_{q\to q+1} j_e \tau}{e} \qquad \textbf{(9)}$$

where the deciding parameters are the electron beam current density j_e, the breeding time τ and the effective cross-section $\sigma_{q\to q+1}$ for ionisation of an ion with charge-state q by electron impact. Thus, the average ionisation factor $j_e\tau$ needed for all ions with charge-state q to reach q+1 is $j_e\tau = e/\sigma_{q\to q+1}$, which when extended to ionisation from q=1 to q=k give an ionisation factor:

$$j_e\tau = \sum_{q=1}^{k-1} \frac{e}{\sigma_{q\to q+1}} \qquad \textbf{(10)}$$

From the equation it is clear that to reach high charge-states, either one has to go for a high electron beam current density, or for long breeding times. The effective ionisation cross-section for an electron energy E_e is calculated using Lotz's semi-empirical formula:

$$\sigma_{q-1\to q} \approx 4.5\cdot 10^{-14} \sum_{nl} \frac{\ln\left(E_e / E_{q,nl}\right)}{E_e E_{q,nl}} \qquad \textbf{(11)}$$

where $E_{q,nl}$ is the binding energy and the summation extends over all removable electrons in orbitals nl [69,70]. Even if the ionisation probability is largest for the outer electrons, this expression includes inner electron ionisation as a possibility. The cross-sections also show that approximately 90% of the breeding time is spent on removing the K-shell electrons. Several correction terms can be added (e.g. Carlson's correction [71] of the binding energies assuming a spherical electrostatic model of the atom/ion), but they are not included in any of the first-order charge evolution plots presented in this report. The set of coupled differential equations governing the charge-state abundance in an EBIS using ion injection, with the ionisation frequencies $\nu_{q\to q+1} = j_e/e\cdot\sigma_{q\to q+1}$, are [68]:

$$\begin{aligned}
\frac{dn_1}{dt} &= a_{inj} - \upsilon_{1\to 2} n_1 \\
\frac{dn_i}{dt} &= \upsilon_{i-1\to i} n_{i-1} - \upsilon_{i\to i+1} n_i \qquad \text{i = 2...m - 1} \\
\frac{dn_m}{dt} &= \upsilon_{m-1\to m} n_{m-1} \qquad \text{m = max charge}
\end{aligned} \qquad \textbf{(12)}$$

where a_{inj} is the number of injected ions per unit time. Recombination, charge exchange and heating processes can be included in the differential equations and an attempt to do this is found in ref. [72].

The peak cross-section is obtained for an electron beam energy E_e typically 2-3 times the ionisation threshold energy. Recombination with the electron beam electrons can be described by the Kim and Pratt formula [73], but for an EBIS with normal electron beam energy parameters radiative recombination processes are negligible [72]. Of course, recombination with the secondary electrons may not be excluded completely, but the magnitude of the effect is difficult to calculate. The charge-exchange with the residual gas can on the other hand be a more severe problem, as well as charge-exchange with low-charged ions. Therefore, the residual gas pressure has to be controlled; more about this in sec. 2.10. The charge exchange cross-section is calculated using the Müller and Salzborn formula [74]:

$$\sigma_{q-q-1} = 1.43\cdot 10^{-12} Z_q^{+1.17} P_0^{-2.76} \qquad (= 10^{-14}\ \text{cm}^2 \text{ for } Z=8^+ \text{ and } P_0=10 \text{ eV}) \qquad \textbf{(13)}$$

where Z_q is the ion charge and P_0 the ionisation potential of the neutral atom/molecule. With a residual gas pressure of 10^{-11} torr, the probability for charge exchange during a 20 ms breeding period is <0.02%, i.e. also this process is negligible.

2.2.2 Ion heating and cooling

Two competing processes of major importance in a high charge-state EBIS are the ion heating and cooling. The former increases the ion energy and can even cause the ions to leave the trap. For this reason a light cooling gas can be introduced to cool the ions.

In ref. [75] Becker describes how the electrons performing inelastic ionisation collisions with ions also cause elastic Coulomb scattering, by which heat is transferred to the ion population in the trap. It has been shown that the heating is mainly dependent on the charge-state of a specific ion and can be expressed as:

$$\begin{aligned}
\Delta U_{axial}[V] &= \frac{0.22}{QA\cdot E_e}\left[e\sum_{\xi=1}^{\xi_{max}} \frac{\xi^2}{\sigma_\xi} + j_e \cdot \xi_{\max}^2 \Delta t \right] \\
\Delta U_{radial}[V] &= \frac{6.2}{QA\cdot E_e}\left[e\sum_{\xi=1}^{\xi_{max}} \frac{\xi^2}{\sigma_\xi} + j_e \cdot \xi_{\max}^2 \Delta t \right]
\end{aligned} \qquad \textbf{(14)}$$

where Q and A are the ion charge and mass numbers; j_e and E_e the electron beam current density and energy in A/cm^2 and keV, respectively; ξ_{max} the extraction charge of the ion; σ_ξ the ionisation cross-section for charge-state ξ; and Δt the breeding time in the last charge-state ξ_{max}. Assuming that the ions are extracted immediately after reaching the desired charge-state, i.e. Δt=0, the REXEBIS heating voltages for $^{30}Na^{8+}$ ions become ΔU_{axial}=14 mV and ΔU_{radial}=0.4 V $\leftrightarrow$ ΔE_{axial}~0.1 eV and ΔE_{radial}~3 eV, which is much less than the radial trapping voltage.

Another heating estimation was formulated by Landau-Spitzer [76], and this gives an even smaller heating value. RF-heating of the ions is difficult to calculate, and has not been confirmed unambiguously in experiments. From the above values we can first conclude that there will certainly occur no ion loss from the trap region due to electron-ion collision heating. Secondly, that a single-ion model such as the one used in the SIMION simulations (see sec. 3.1), which assumes no electron-ion and ion-ion interaction (apart from ionisation by electron impact) most probably is valid. This implies that the ions "remember" their injection conditions when they are extracted, and apart from the random ionisation, the process is deterministic.

Moreover, these estimates suggest that there is no need for ion cooling, which otherwise could be obtained by introducing a light cooling gas to the trap region (compare with mixing gas in an ECR [77,78]). Further reading about ion heating can be found in ref. [79,80].

Another inherent heating process, unavoidable in a non-compensated trap, is the ionisation heating that occurs when the charge-state of an ion in a potential well is increased. At the ionisation moment the position and kinetic energy of the ion are unchanged, but the potential energy increases since the depth of the potential well increases. Thus, as the ion charge rises, so does its mean energy in the trap. This kind of heating does not directly lead to loss from the beam (as long as no ion-ion collisions occur), since the ions are confined even more tightly as their charge increases (see also sec. 3.3.4).

2.3 REXEBIS specifications

The expected performance of the REX-ISOLDE post accelerator, together with the limits set by the Penning trap and the following Mass separator/LINAC, impose strict requirements and restrictions on the REXEBIS design. Here follows a list of parameters that the REXEBIS must fulfil.

The Penning trap delivers ions:

- with a transverse emittance $\varepsilon_x = \varepsilon_y < 3$ π·mm·mrad at 60 kV, assuming an ISOLDE emittance of 100 π·mm·mrad
- with a longitudinal emittance of ~5 μs·eV
- in bunches of a few to 10^7 ions, bunch length ~10 μs
- with a repetition rate of 50 Hz (optionally up to 100 Hz)

The Mass separator/LINAC request:

- ions with Q/A~1/4.5
- ions with 5 keV/u
- the delivered beam to fit within an emittance ellipse of 40 π·mm·mrad (99.99% confidence)
- an axial energy spread <50 eV/Q

Due to the low intensity of the most exotic radioactive ions produced at ISOLDE the EBIS has to be efficient, i.e. the combined injection and extraction efficiency should be higher than 50% [81]. (The inherent breeding efficiency is limited to ~30% since only one specific charge-state is selected from the total charge distribution in the mass analyser.) Furthermore the EBIS has to be reliable since it is part of a complex accelerator chain.

2.4 The solenoid

2.4.1 General magnet properties

The magnet constitutes the largest individual part of the EBIS system both when it comes to weight and cost. The purpose of the solenoidal field is to compress the electron beam from the gun cathode to the trap region. The CRYSIS magnet [10,82,83,84] was used as a starting point for the REXEBIS magnet design: an iron-shielded 5 T superconducting magnet with a cold bore. The REXEBIS magnet is shielded as well, with a cylinder of iron bars. In contrast to all existing high performance EBISs, the REXEBIS has a warm bore, i.e. the inner cylinder containing the drift structure is kept at room temperature by thermally decoupling the cryostat from the ionisation volume. Using this concept we will:

+ strongly reduce the memory effects, i.e. avoid release of frozen in elements from previous runs
+ minimise the out-gassing from electron beam loading
+ improve reliability; no build-up of cryosorbed gas layers
+ minimise the interruption time in case of urgent inner structure changes

The disadvantages with a warm bore are the difficulties to:

– arrange efficient pumping for noble gases due to poor pumping speed of inert gases
– arrange efficient differential pumping between the gas injection and ionisation regions (not a problem for REXEBIS since only ion injection will be used)

When injecting as few as 10^4 ions, a very short (<1 μm) trap is sufficient to contain the ions without compensating the electron beam space-charge, though a certain trap length, L_{trap}, is required to capture the injected ion pulse (typically >0.1 m). The REXEBIS will have a trap length of 0.8 m, optionally shorter.

The solenoid, manufactured by Oxford Instruments, is of superconducting type and therefore needs less power than ordinary non-superconducting magnets. The basic solenoid and iron shielding shapes were calculated using POISSON [85] and are described in ref. [86]. Even if it intentionally was designed for the use of a Pierce-type gun situated in low magnetic field, it is well suited for an immersed gun. In this

Central magnetic field at 4.2 K	variable between 0.1 and 2.0 T
Current for full 4.2 K field	116.115 A
Field homogeneity over ±400 mm on axis	0.25% (measured), 0.3% (specified)
Field straightness	$r_{central}$<0.1 mm over –800<z<800 mm (measured) $r_{central}$<0.5 mm over –825<z<825 mm (specified)
Relative field decay	$13 \cdot 10^{-6}$ h^{-1} (measured), $5 \cdot 10^{-6}$ h^{-1} (specified)
Bore diameter	150 mm
Nominal inductance	8.292 H
Superconducting solenoid length	1200 mm
Stored energy	56 kJ

Table 3. *Solenoid data*

configuration the magnetic field compresses the electron beam from a current density of 25 A/cm^2 to >200 A/cm^2. As superconducting winding material NbTi of single wire type is utilised. It has a critical magnetic field (B_{crit}=3.25 T) well above the needed field, and its transition temperature is ~7 K.

In June 97, the two solenoids were delivered from Oxford Instruments to Stockholm. The solenoids are identical, and one will be used for the twin ion source that is planned to be set-up as a test-bench at MSL. During the Oxford initialisation of the two magnets, one of the solenoids developed a short-cut to ground (the test-bench magnet), and had to be returned to the manufacturer. The other (the REXEBIS magnet) was tested during the autumn. Due to not fulfilled specifications, it was later sent back to Oxford, and was thereafter shipped directly from England to CERN after repair.

2.4.2 Magnet cooling

The main inconvenience with a superconducting magnet is the need for cooling to 4.2 K to achieve the superconducting properties of the coil. This calls for extensive tricks to construct a compact system with long refilling period, namely:

- eccentric helium reservoir containing the magnet
- surrounding He cooled radiation shields
- superisolation

The coil is situated in a cryostat with an effective volume of 70-75 *l* filled with LqHe, see Appendix 1. To make better use of the He, the cryostat is eccentric. Outside the cryostat an intermediate-temperature radiation shielding is fitted and cooled using the entalphy of the exhaust He gas. A ~120 *l* LqN_2 cryostat cools the outer parts of the magnet to 77 K. Multi-layer superisolation reduces the convection heating, and vacuum (10^{-5} torr) between the He and N_2 reservoirs and surrounding room temperature provides thermal conduction isolation. Support rods extending from room temperature to the He cryostat are made of low thermal conductivity materials. To further extend the operating period the current leads are removable. The hold times for LqHe and LqN_2 were measured for the test-bench solenoid and are presented in Table 4. From the table it is clear that the LqN_2 specifications are violated, while the LqHe hold time is within specifications. Oxford has been obliged to modify the REXEBIS solenoid so it also fulfils the LqN_2 specifications before finally delivering to ISOLDE[1].

	Specified hold time	Measured hold time (days)
LqHe	14 days for 70 *l* without refilling and with current leads connected	19 days without current leads connected
LN_2	>14 days and LqN_2 consumption <7 *l*/day	11 days and LqN_2 consumption 11 *l*/day

Table 4. *Specified and measured LqHe and LN_2 hold times for the test-bench solenoid.*

2.4.3 Solenoid construction

The solenoid is surrounded by passive iron shielding (iron yoke) for two reasons. Firstly, when the magnet was ordered, the intention was to be use a Pierce-type electron gun positioned in low axial magnetic field. This required an iron shield to shape the field. Secondly, to reduce the stray fields so not close-by beam lines or personnel are affected. The REXEBIS is therefore surrounded by a ring of passive iron bars of 25 mm thickness forming a cylinder similar to a water heater. Additional compensation coils are added that improve the homogeneity at the centre of the field by reducing the rate at which the field drops at the ends of the coils (due to finite winding length effects). These are indicated in Appendix 1. No extra shims or cancellation coils, nor extra iron field clamps are added.

2.4.4 Magnetic field

The magnet field straightness, the homogeneity and the stability are three parameters of importance for the application of the magnet. They will be defined in the following sections together with expected requirements.

[1] After the latest repair the REXEBIS solenoid seems to withstand provoked quenches, and the LqN_2 consumption is within specifications, however, the LqHe consumption in violated with a hold-time of about 9 days.

2.4.4.1 Field straightness

The field straightness should not be confused with the field homogeneity, and specifies the maximal radial deviation from the geometrical axis of the central field line. This is of importance since the electron beam follows the field lines, and a shift from the tube axis alters the potential inside the tube. The electric potential from the space-charge of a cylindrical electron beam passing inside a drift tube with a definite potential, can be expressed as follows [87]:

$$U(r,\theta) = U_t - \frac{1}{4\pi\varepsilon_0}\cdot\frac{I_e}{\sqrt{2\frac{e}{m_e}U_e}}\cdot\ln\left(\frac{r_t^2 - 2a_{disp}r\cos\theta + a_{disp}^2\frac{r^2}{r_t^2}}{r^2 - 2a_{disp}r\cos\theta + a_{disp}^2}\right) \qquad r>r_{ebeam} \qquad \textbf{(15)}$$

$$U(r,\theta) = U_t - \frac{1}{4\pi\varepsilon_0}\cdot\frac{I_e}{\sqrt{2\frac{e}{m_e}U_e}}\cdot \cdot\left\{\ln\left(r_t^2 - 2a_{disp}r\cos\theta + a_{disp}^2 r^2/r_t^2\right) - \left(\frac{r^2 - 2a_{disp}r\cos\theta + a_{disp}^2}{r_{ebeam}^2}\right) - \ln r_{ebeam}^2 + 1\right\} \qquad r<r_{ebeam} \qquad \textbf{(16)}$$

U_t = drift tube potential relative to cathode potential
U_e = electron beam potential relative to cathode
r_t = inner radius of the drift tube
a_{disp} = distance between beam axes and drift tube
r_{ebeam} = electron beam envelope
r and θ = cylindrical coordinates

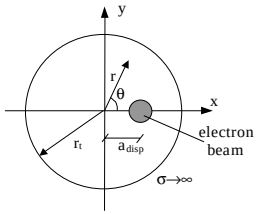

Figure 14. *Geometry and notations for a displaced electron beam inside a highly conducting tube.*

In the case of axial symmetry, then:

$$U(r,\theta) = U_t - \frac{2}{4\pi\varepsilon_0}\cdot\frac{I_e}{\sqrt{2\frac{e}{m_e}U_e}}\cdot\ln\left(\frac{r_t}{r}\right) \qquad r>r_{ebeam} \qquad \textbf{(17)}$$

$$U(r,\theta) = U_t - \frac{1}{4\pi\varepsilon_0}\cdot\frac{I_e}{\sqrt{2\frac{e}{m_e}U_e}}\cdot\left[2\ln\left(\frac{r_t}{r_{ebeam}}\right) + 1 - \frac{r^2}{r_{ebeam}^2}\right] \qquad r<r_{ebeam} \qquad \textbf{(18)}$$

Note that eq. 15 and 16 are just approximate expressions, since second order terms occur due to not pure Brillouin flow, non-circular beam shape and a change in electron beam energy occur when the beam is displaced. Anyhow, they can be used for an estimation of the potentials. Inserting REXEBIS parameters and comparing the beam axis potential to tube potential $U_{a\text{-}t}$ and the beam potential depth ΔU (see sec. 2.7.1) for a non-shifted beam with a 1 mm displaced beam, gives results as listed in Table 5.

a_{disp} (mm)	ΔU (V)	$U_{a\text{-}t}$ (V)
0	107	-750
1	107	-741

Table 5. *Beam axis relative tube potential $U_{a\text{-}t}$ and beam potential depth ΔU for 0 and 1 mm radial electron-beam displacement in the REXEBIS (tube radius 5 mm).*

From the table we can conclude that a displaced beam results in a shallower potential depression $U_{a\text{-}t}$, i.e. ions with injection energy exactly adapted for a central beam may have too little kinetic energy to climb the potential hill. The change in potential depth ΔU is insignificant, but a displaced beam may have non-symmetric acceptance and emittance phase spaces. Calculations of the latter effect have not been carried out. Schmieder claims that the beam displacement should not exceed a fraction of the beam diameter [67].

For the REXEBIS case that means <0.1 mm, however, from the arguments above we would say a displacement of even 1 mm in a 5 mm radius tube is tolerable.

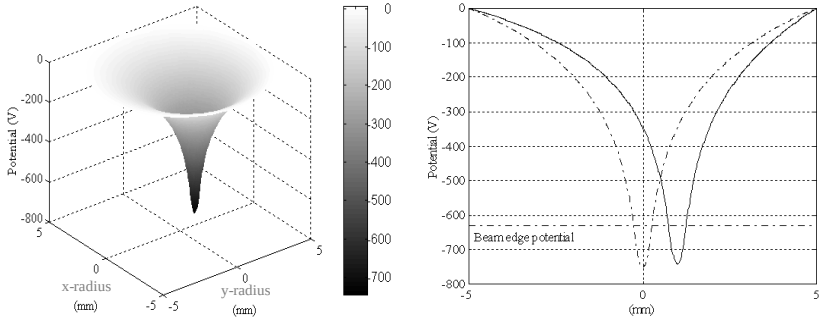

Figure 15. *Calculated electron beam potential plots inside the REXEBIS drift tubes with the beam displaced 1 mm. The dash-dotted curve represents a non-displaced beam.*

Since Oxford Instruments claimed that they could not verify the straightness, we measured it ourselves by inserting a Hall element probing the magnetic field components in horizontal and vertical directions. By integrating the transverse field components along the z-axis, the central field line was traced[2], (Figure 16). Twelve position knobs adjusted the position and alignment of the solenoid within the iron shielding. The field mapping procedure is described in Box 1, and is similar to the method presented in ref. [88,89]. The advantage of this method is the cancellation of possible non-straightness of the tube holding the Hall probe. Such bending can affect the result more than the sag caused by the tube weight, which was compensated for by an awkward arrangement in ref. [90]. We determine the tube sag afterwards by optical measurements.

To optimise the field straightness and to find the magnetic axis, the following procedure was used:

1. The solenoid cryostat was positioned inside the iron yoke while most of the iron bars covering the side were removed.
2. Using the cryostat as a reference, the iron end flanges were adjusted until they became parallel to the cryostat and each other.[3]
3. By attaching a mirror to the end flanges and using the telescope, the parallelism was determined.
4. The solenoid was then centred radially with respect to the 150 mm holes in the iron shield.
5. The transverse field was mapped using the method described in Box 1.
6. The position of the cryostat inside the iron yoke was adjusted using knobs and micrometer gauges and (5) and (6) were repeated until the traced field line fell within a cylinder of specified radius.

After (2) the iron end flanges were measured to be parallel relative each other within 0.75±0.2 mrad. The solenoid was radially centred (4) within ±0.2 mm. The final result after a few iterations of adjustment is presented in Figure 18 (the sag is not eliminated and adds a convex shape to the y-curve), and we find the traced central field line to be within a 0.1 mm radius cylinder concentric with the geometrical axis for -800<z<800 mm. The specification required the central field line to be within a cylinder of radius 0.5 mm over –825<z<825 mm.

[2] In fact, we measured the transverse field components at a number of positions along the geometrical axis of the magnet, but since the radial variation in the field is small, the integrated path will be approximately the same as a field line beginning at the integration starting point. This integrated path is what we refer to as the central field line.
[3] We were later told by Oxford Instruments that the cryostat only have a precision of 1 mm, so the cryostat is not perfect as a reference for parallel adjustment of the iron end flanges.

Box 1. Magnetic field mapping method.

1. At the two 150 mm holes in the iron flanges, a fixed axi-symmetrical end plate with a hole for a brass tube was mounted.
2. A brass tube was inserted through these end plates. The tube was azimuthally rotateable and axially moveable.
3. Inside the brass tube a Hall element, which probed the transverse field, was inserted. The Hall element was fixed at a known position inside the brass tube.
4. The Hall probe was then moved to a z-position by moving the brass tube. The brass tube was rotated in steps of 90º and the B_{x+}, B_{y+}, B_{x-}, B_{y-} fields were measured. Thereafter the tube was moved 2 cm axially, and new transverse values recorded etc.
5. By taking the average $B_x(z)=(B_{x+}-B_{x-})/2$ and $B_y(z)=(B_{y+}-B_{y-})/2$, possible tube bending was cancelled.
6. The central field line (see footnote 1 on previous page) was traced by integrating B_x/B_z and B_y/B_z.
7. The weight of the tube created a sag that was superimposed on the result. The sag was optically measured with a telescope (see Figure 17).

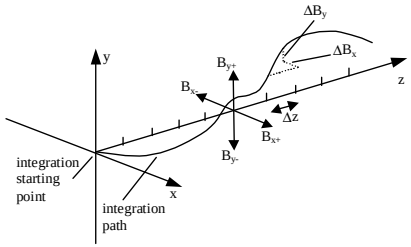

Figure 16. *Field mapping method.*

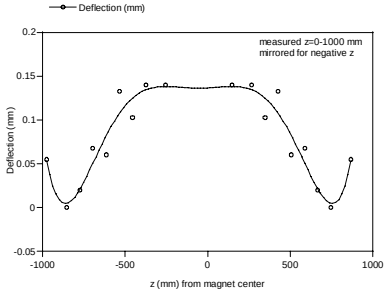

Figure 17. *Measured sag of the brass tube holding the Hall probe (positive value corresponds to bending down).*

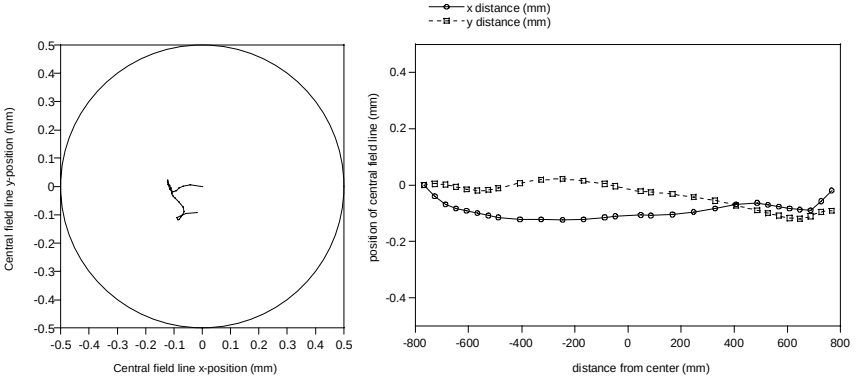

Figure 18. *x-y plot of the central field line trace (left); x-z (solid) and y-z (dashed) plots of the central field line trace (right).*

2.4.4.2 Field homogeneity

The second magnetic field parameter of importance is the field homogeneity, i.e. the longitudinal field strength variation. A field strength that fluctuates with the z-position leads to a varying beam radius, which in turn modulates the beam potential. The relation governing the electron beam radius r_{ebeam} is:

$$r_{ebeam} = r_{cathode}\sqrt{\frac{B_{cathode}}{B_{full}}} \qquad \textbf{(19)}$$

where B_{full} and $B_{cathode}$ are the magnetic field strengths in the trap and at the cathode. From eq. 18 the axial potential (relative to the drift tube) in the case of axial symmetry is given as:

$$U_{axis} = -\frac{1}{4\pi\varepsilon_0}\cdot\frac{I_e}{\sqrt{2\frac{e}{m_e}U_a}}\left[2\ln\left(\frac{r_t}{r_{ebeam}}\right)+1\right] \qquad \textbf{(20)}$$

Differentiation yields:

$$\frac{\Delta U_{axis}}{U_{axis}} = \frac{\Delta B_{full}}{B_{full}}\cdot\frac{1}{2\ln\left(\frac{r_t}{r_{ebeam}}\right)+1} \qquad \textbf{(21)}$$

Now assume that U_{axis}=-750 V as for the REXEBIS (see also sec. 2.7.1), and allow a potential variation ΔU_{axis}<5 V (approximately the potential variation created by the beam ripple, see sec. 2.7.2). Then the $\Delta B_{full}/ B_{full}$ must be less than 5%. This limit is far more relaxed than the rule of thumb of 0.1% given in ref. [67].

The axial full field inside the REXEBIS is 2 T with a specified field homogeneity of 0.3% over ±400 mm on axis. The measured homogeneity falls within 0.25% (see Figure 19).

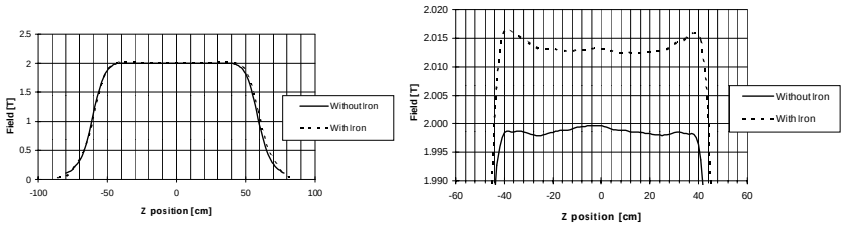

Figure 19. *Axial B_z plot and detail for the REXEBIS solenoid. Measured by Oxford Instruments.*

2.4.4.3 Field decay

The field has to be stable in time since a decreasing field changes the beam injection conditions. Even though the electron beam potential remains basically constant with a varying absolute magnetic field strength (both the cathode and the trap field decrease with the same factor and therefore the electron beam compression remains), the magnetic part in the Lorentz force will vary with in time. The effect of this is not evident and requires simulations.

Oxford Instruments quoted a relative field stability of $5\cdot10^{-6}$ h^{-1}, but the actually measured stability for the REXEBIS solenoid is worse, about $13\cdot10^{-6}$ h^{-1}, measured with a NMR-probe.

2.4.5 Magnet operation

One of the main advantages of a superconducting magnet is its ability to operate in persistent mode, i.e. when current has been injected into the solenoid the power supply can be removed. The superconducting circuit is closed and forms a continuous loop, the power supply is switched off and disconnected, and the solenoid is left at field. In this state, the current can run for a year without interference, however, the EBIS parameters will of course be affected due to the slow, but non-negligible, field decrease.

Persistent mode operation is achieved using a superconducting switch that is fitted to the magnet in parallel with the main winding (see Figure 20). When energising the magnet, the superconducting switch is heated to a non-superconducting state with a few ohms resistance. Although the resistance is low, almost all current flows through the magnet coil when the power supply is switched on. Soon after the magnet reaches the desired field, the induced voltage across the switch drops to zero, and the switch can be closed and returned to a superconducting state by switching off the heater. Now the current in the magnet leads is slowly reduced by running down the power supply, and as the current in the leads drops, the current flowing through the switch increases gradually, until it carries the full current of the magnet. The procedure is opposite when the solenoid is de-energised.

For different reasons, some part of the magnet winding might go normal (i.e. resistive), and the current passing through it will cause ohmic heating. In turn this heating will extend the resistive zone, and if the disturbance is unstoppable (usually the case unless the disturbance is very small), the complete coil may become resistive and heated. All stored energy in the magnet is dissipated rapidly, causing the liquid helium to boil off very quickly and often warming the magnet to a temperature significantly above 4.2 K. This technical hitch is called a quench. To cause quenches a very small amount of energy is required, even microscopic movements of the wires in the coil may be sufficient as triggers.

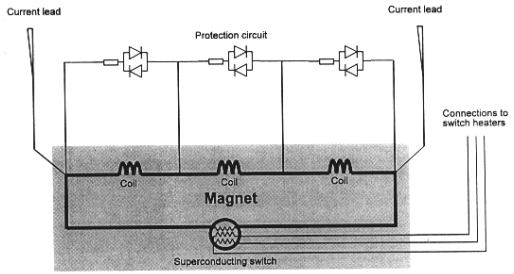

Figure 20. *Schematic circuit showing the solenoid, the switch and the protection circuits [91].*

A magnet protection circuit is used automatically in the event of a quench:

- to dissipate the energy stored in the magnet
- to make sure that high voltages are not produced

Protection resistors and diodes are provided for all magnet sections. The diodes are used in the protection circuit to ensure that all the current passes through the magnet under normal operating conditions, but in the case of a quench, the barrier voltage of the diodes is exceeded and the protection comes into operation automatically. The current then passes the protection resistors that dissipate the stored energy.

2.5 EGUN simulations

To simulate the electron beam propagation from the electron gun cathode to the collector, two different programs were utilised: a modified version of EGUN [92] and OPERA 2D [93]. Both programs assume axi-symmetrical geometry, and the former uses the finite difference method, while the latter is a Finite Element Methode program. Both programs have limitations, mainly convergence and boundary problems, and after some time of evaluation we concentrated on calculations with EGUN. This program has been used in many EBIS designs, but due to the maximum number of mesh points (101 000), we were not able to simulate the complete system in one run. Instead the geometry was divided into 17 sections, and the solutions were spliced. This resulted in problems for the program to determine the potential at the boundaries, with energy non-conservation as a consequence, which had to be handled manually.

2.6 The electron gun

2.6.1 Gun theory

The electron beam that confines and ionises the ions in an EBIS is created at the electron gun cathode and accelerated by the anode potential. Several different gun concepts exist, which utilise pure thermal or pure field emission from the cathode, or a combination of the two. Important properties of the extracted electron beam are the current, current density, energy, beam radius and shape. Involved forces are the Lorentz, the space-charge and the centrifugal force.

For a space-charge limited cathode the current I_e and the anode voltage U_{anode} are related as:

$$I_e = PU_{anode}^{3/2} \qquad \textbf{(22)}$$

where P is the perveance (unit $A/V^{3/2}$) that determines the current yield from a specific gun geometry. One should note that the perveance is *only* dependent on the gun geometry. The current density is connected to the compression of the electron beam, and the two distinct designs types are:

1. Immersed flow gun
The gun is positioned in full magnetic field and there is no compression of the electron beam. A simple method where the electrons tend to follow (spiral around) the individual lines of magnetic flux, so perturbations in beam diameter can be made arbitrarily small merely by increasing the magnitude of the B-field. The current density is limited to the cathode density.

2. Brillouin flow gun
A way to create high-density beams by the use of magnetic fields. The cathode is placed in a B-field free region, and when the beam enters the magnetic field the current density is compressed adiabatically as B^2. The three forces listed above acting on the electrons are made to balance and produce a smooth beam, a so-called space-charged balanced flow. To obtain this the whole electron beam has to be set in rotation with half of the cyclotron frequency – the Larmor frequency ω_L.

For the REXEBIS we have chosen a slightly modified immersed gun design – a semi-immersed gun with compression proportional to B^n (n>1). Since n is only slightly larger than unity, the beam behaviour is similar to that of an immersed, and we will therefore briefly touch upon the theory that governs the immersed gun. A laminar-flow beam is assumed (no electron trajectory crossing), which leads to comfortable calculations and the need to only consider the outermost electron to determine the beam shape. While this is a severe idealisation, this hypothesis does in fact yield results that agree well with observed first-order beam characteristics.

The radial space-charge field acting on an electron at radius r in an electron beam with radius r_{ebeam} is:

$$E_r = \frac{I_e}{2\pi\varepsilon_0 v_e} \cdot \frac{r}{r_{ebeam}^2} \qquad \textbf{(23)}$$

Busch's theorem expresses the angular velocity v_θ. Let the magnetic flux threading a circle of radius r be denoted by Φ, and index c indicating cathode. Then Busch's theorem is written as [94]:

$$\dot{\theta} = \frac{e}{2\pi r^2 m_e}(\Phi - \Phi_c) + \frac{r_c^2}{r^2}\dot{\theta}_c \qquad \textbf{(24)}$$

We conclude that the angular velocity of a charged particle in a magnetic field only depends on the terminal radii of the trajectory and the values of total enclosed magnetic flux, not on the trajectory details between these two points. To a good approximation $\dot{\theta}_c$ may be considered zero, and with a constant magnetic field B_0 in which the emitting surface and the beam are immersed, eq. 24 is reduced to:

$$\dot{\theta} = \frac{eB_0}{2m_e}\left(1 - \frac{r_c^2}{r^2}\right) \qquad \textbf{(25)}$$

Here r_c is the radius at which the peripheral electron leaves the emitting surface. With the magnetic field normal to the cathode the electron will start to move radially outwards governed by eq. 23. It is then affected by the Lorentz force $r\dot{\theta}_c B_0 e$, which bends the trajectory, and forces the electron inwards again. Thus, perturbation in the electron beam diameter is an inherent property of immersed guns. One can show that the beam expansion beyond r_c is larger the contraction below r_c, resulting in a larger average beam radius than the cathode radius.

Moreover, from eq. 24 we see that $\dot{\theta}_c$ reverses sign when the electron crosses r_c, which means that the electrons do not encircle the stream but rotate more or less around radius r_c. An important factor describing the trajectories is the beam stiffness $\frac{\omega_L}{\omega_p} = \frac{(eB_0/2m_e)}{\sqrt{\frac{j_e}{\varepsilon_0}\sqrt{e/2U_e m_e}}}$. For the REXEBIS the ω_L/ω_p-value is 5.1 (compare with $\omega_L/\omega_p = 1/\sqrt{2}$ for Brillioun flow), that means we have a rather stiff beam strongly connected to the magnetic field lines. Typical beam behaviour is shown in Figure 21. The beam diameter fluctuation, or scalloping, is highly undesirable since it causes beam potential variations which can act as local ion traps inside the large EBIS trap. For large ω_L/ω_p-values and moderate scalloping the normalised radius equation is:

$$R_{max} \approx 1 + \frac{1}{\left(\omega_L/\omega_p\right)^2} + \frac{R_0'}{\omega_L/\omega_p} \qquad \textbf{(26)}$$

where R'_0 is proportional to the beam envelope slope after the anode. It is clear that either the magnetic field has to be increased, or the initial R'_0 reduced, to minimise the beam oscillations. To control R'_0 suitable electron-optical methods can be used, such as converging-beam gun, post anode or magnetic field gradient. In ref. [95] Herrmann claims that the scalloping will be largely suppressed by the higher frequencies of the motion of the electron's winding in and out of the beam if $B_c << B_{full\ field}$.

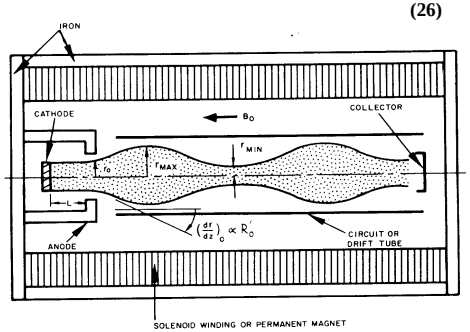

Figure 21. *Beam behaviour in immersed flow [94].*

2.6.2 Electron gun design concept

The REXEBIS electron gun is as already mentioned of so-called semi-immersed type, with the cathode not in full magnetic field. In that way a current density compression almost proportional to B is obtained when the beam enters full field. Such a design has several positive features as compared to a high compressing Pierce-type gun [94] that we first intended to use:

- uncomplicated and well proved in EBIS constructions
- less sensitive to axial displacement
- I_e and j_e adjustable by changing the anode voltage and the gun position in the magnetic field, respectively

The relative low compression, ($j_{trap}/j_c \approx 10$) is compensated for by a larger cathode-current loading. Pierce electrodes with an angle of 67.5° to the cathode surface produce flat equipotential lines at the cathode, and a uniform emission density from the cathode as well as a laminar flow. As a drawback the scalloping of the electron beam should be mentioned, nevertheless, this can be suppressed by adding a post anode in the design. If it is positioned appropriately in z-direction, and a high potential is applied, the beam blow-up after the anode is decreased and a less rippling beam is obtained. However, a post anode at high potential in an axial magnetic field will act as a Penning trap for electrons (see sec. 2.6.4), so therefore the post anode is just optional and has to be practically evaluated.

2.6.3 Electron beam simulations

The electron extraction from the cathode is governed by Child's law, i.e. it is space-charge limited and in principle not dependent on the cathode temperature. The cathode heating is anyway specified in the simulations to give the electrons a thermal starting energy (1750 K ↔ 0.15 eV). EGUN simulations of the extracted electron beam, with and without post acceleration, are shown in Figure 22. From the figures we conclude that a post acceleration results in a less scalloping beam as expected, but for $U_{post\ anode}$<10 000 V, the effect is not overwhelming. With U_{anode}=6500 V the electron beam I_e=0.46 A, and the perveance is determined to P=0.87 μA/V$^{3/2}$. The cathode surface is positioned at z=-738 mm relative to the magnet centre, at a magnetic field B_z=0.2 T. The cathode loading and a phase space plot at z=-722 mm are displayed in Figure 23.

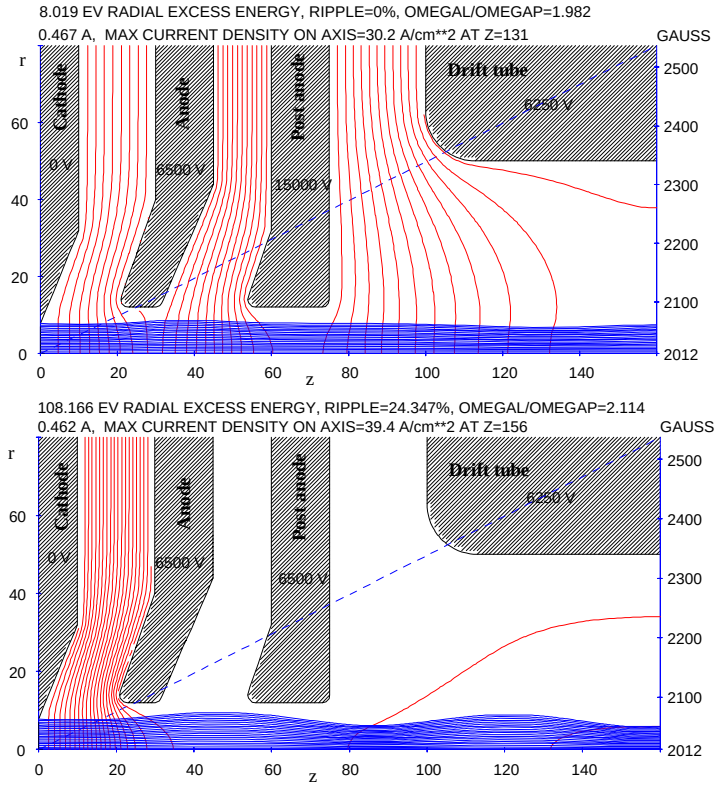

Figure 22. *Simulation of the electron beam in the gun region with and without post acceleration. One unit of length corresponds to 0.1 mm. Only the upper cylindrical part of the gun region is shown.*

The simulated beam profile r_{ebeam} equals ~0.25 mm in full field, corresponding to a full field electron current density j_e(full field)=250 A/cm^2. Thus, the compression is:

$$\text{Compression} = \frac{j_e(\text{full field})}{j_e(\text{cathode})} \approx \frac{250}{25} = 10 \qquad \textbf{(27)}$$

and we confirm that the compression is nearly proportional to B_z(full field)/B_z(cathode).

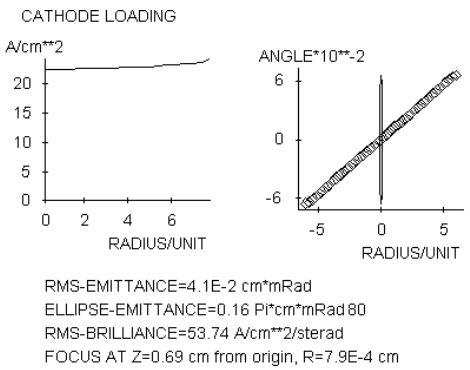

Figure 23. *Simulated cathode loading and radial phase space plot of the electron beam at z=-722 mm for the gun without post anode voltage.*

The full field beam current density is higher than the specified 200 A/cm^2. We have chosen this cause of action to have some marginal since the simulation program is not always exactly reliable.

According to ref. [67] it is important to use laminar beams in order to avoid ion losses. The high field gradients connected with non-laminarity, together with the possibility of instabilities, could cause ion heating. The beam tracing simulations indicate laminar beam behaviour.

2.6.4 Electron trapping

So far, secondary electrons created in the ionisation process have been neglected. These can influence the self-consistent field, and cause space-charge build-up along the line of electron beam propagation, that in worst case reflects the beam. After the creation at a point with potential U_0 the secondary electron with kinetic energy E_0^{kin} moves in complicated trajectories in the region with potential $U>U_0+E_0^{kin}$. The possibility for escape from the beam in radial direction is small because of the strong magnetic field – the electrons are trapped in a Penning trap. Not even the space-charge from the primary electrons is strong enough to eject the electrons radially due to the magnetic field. Instead they start to drift, either by their initial kinetic energy or due to Coulomb interactions with the beam electrons, until they reach the longitudinal trap barriers with their high potential (or to the anode/post anode if such exists and has higher potential). If the secondary electrons are not caught here, their motion is oscillatory within the trap region.

The production rate of secondary electrons from the ionisation process in an EBIS with REXEBIS properties is $<5\cdot10^{10}$ s^{-1}. The energy spread of the secondary electrons is very narrow, and has a distribution as shown in Figure 24 (calculated in Box 2).

To remove the electrons there are in principle three different causes of action:

- apply a strong radial field that pulls out the electrons
- apply an asymmetric electrical field along one of the perpendicular directions to the magnetic field and let them drift out [66]
- let them be heated by repeated Coulomb collisions until they gain enough energy to leave the trap

Box 2. Calculation of the energy distribution of secondary electrons.

The secondary electrons are kicked loose from the atoms or ions by Coulomb collisions by the beam electrons. The energy transfer ΔE in a Coulomb collision between two electrons is [96]:

$$\Delta E = E\sin^2\left(\frac{1}{2}\Theta_{scattering}\right) \qquad \textbf{(28)}$$

where E is the electron beam energy and $\Theta_{scattering}$ the scattering angle between the electrons in the centre-of-mass system. The impact parameter s is related to the scattering angle $\Theta_{scattering}$ as:

$$s = \frac{e^2}{8\pi\varepsilon_0 E}\cot\left(\frac{\Theta_{scattering}}{2}\right) \qquad \textbf{(29)}$$

Hence, the energy transfer as function of impact parameter s is:

$$\Delta E(s) = E\sin^2\left(arc\cot\left(s\frac{8\pi\varepsilon_0 E}{e^2}\right)\right) \qquad s_{min}<s<s_{max} \qquad \textbf{(30)}$$

where s_{min} is the lower limit taken to be the classical distance of closest approach defined by $s_{min}\sim e^2/E_e$ [63], and s_{max} is the maximum impact parameter determined by the ionisation energy of the atom/ion, ~10 eV. (If the impact parameter is larger, the energy transfer will be too small to kick out an electron. The Debye length (sec. 3.2.2) is not limiting in this case.) From eq. 28 and 29, s_{max} is determined to $\sim3\cdot10^{-12}$ m. Furthermore, the Coulomb cross-section $\sigma\propto s^2$, and when inserting a s-distribution like that in eq. 30, a secondary electron distribution as the one in Figure 24 is obtained. We note that most of the electrons have a low energy <100 eV, compared to the 5 keV of the primary electrons.

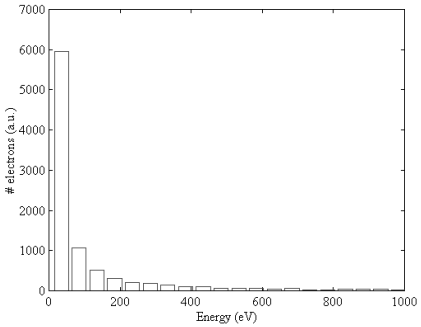

Figure 24. *Energy distribution of secondary electrons just after they have been kicked loose form the atoms/ions.*

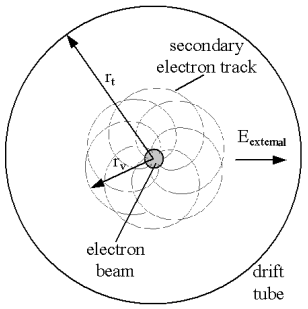

Figure 25. *Schematic electron trajectory in the r-θ plane at the potential barrier or post anode.*

Let us first investigate how strong the radial electrical field must be for the electrons to leave the electron beam and to hit the potential barrier or post anode. We have a situation as illustrated in Figure 25. Insertion of a thin positive drift tube between two negative tubes can create the radial electric field.

The radial electric field is assumed to be radially invariant, i.e. $E_r(r)=E_{external}$. One of two conserved quantities is the energy W:

$$W = \frac{1}{2}m_e\left(\dot{r}^2 + r^2\omega_\theta^2\right) + qU(r) \qquad \textbf{(31)}$$

where $U(r)=U_{external}+U_e(r)$ is the electrostatic potential defined as:

$$U(r) = U_{external} + U_e(r) = U_{external} - \begin{cases} \frac{\rho_l}{4\pi\varepsilon_0}\left[\left(\frac{r}{r_{ebeam}}\right)^2 - 1 + 2\ln\left(\frac{r_{ebeam}}{r_t}\right)\right] & r < r_{ebeam} \\ \frac{2\rho_l}{4\pi\varepsilon_0}\ln\left(\frac{r}{r_t}\right) & r > r_{ebeam} \end{cases} \quad (32)$$

and ρ_l=-I_e/v_e (<0) denotes the linear charge density. The following equation, relating the enclosed magnetic flux Φ(r) with the angular momentum is also constant:

$$mr\omega_\theta + \frac{e}{2\pi r}\Phi(r) = C \quad (33)$$

The constant C is determined from the starting condition and ω_θ can then be solved for varying r. Insert the value of ω_θ in the energy expression and use the conservation of energy to determine the turning radius r_v for the electron. Demanding r_v to be equal to the drift tube or the post anode radius, the radial electrical field can be determined. This has been done for two cases: at the drift tube and at the post anode, see Table 6. The electrons started at the beam centre with no kinetic energy. Such high radial electrical fields as $450\cdot10^6$ and $95\cdot10^3$ V/m are unrealistic to create, therefore a radial field is no solution for secondary electron removal.

Position	Parameters	Required $E_{external}$
Drift tube	B_z=2 T, r_{ebeam}=0.25 mm, r_t=5 mm, E_e=5000 eV	$450\cdot10^6$ V/m
Post anode	B_z=0.2 T, r_{ebeam}=1 mm, r_t=1.2 mm, E_e=8000 eV	$95\cdot10^3$ V/m

Table 6. *Required radial electrical field to remove secondary electrons from the beam.*

The second method involves an asymmetric electrostatic field (e.g. a split drift tube with opposite potentials on each side) that makes the electrons drift towards the drift tubes as shown in Figure 26. (An asymmetric post anode arrangement is probably not appropriate due to primary beam disturbance in the sensitive gun region.). The applied voltage required to remove secondary electrons from the barrier region (B~2 T, r_{ebeam}~0.25 mm), starting at the beam centre with no kinetic energy, amounts 2000 V. The removal time is in the order of 10-20 µs. Donets alleges in ref. [66] that even small misalignments (<0.5 mm) of the drift tubes may cause electron removal without any extra applied asymmetric voltage, but we do not see this in the simulations. For that to happen, the ions must also be heated by collisions.

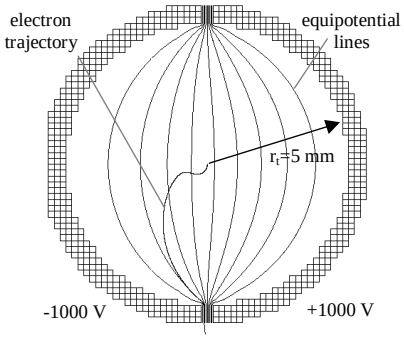

Figure 26. *Secondary electron removal at B~2 T and r_{ebeam}~0.25 mm by asymmetric voltage on drift tubes.*

Thirdly, the secondary electrons can be transported away from the electron beam by Coulomb heating. As seen in sec. 2.2.2 the most frequent collisions are the long-range encounters, the Spitzer collisions [66], that can have a large-angle scattering net effect (well described in ref. [63]). The characteristic Spitzer frequency for 90° electron-electron scattering is [97]:

$$\upsilon_{90}^{ee} = \frac{3.2\cdot10^{-40} n_e \ln\Lambda}{E^{3/2}} \approx \begin{cases} 1000\,\text{Hz in trap region} \\ 4\,\text{Hz at post anode} \end{cases} \quad (34)$$

where n_e (m^{-3}) and E_e (J) are the density and energy of the electron beam, respectively, and lnΛ the Coulomb logarithm. Moreover, the small-angle collisions that produce a 90° deflection will cause a change in energy. For identical-particle collisions they result in a transfer of about half of the initial energy in the same time as a 90° deflection. Thus, secondary electrons in full magnetic field with low initial energy will have an energy of a few thousand eV within 1 ms after they were kicked loose from the ions/atoms, while secondary electrons in the post anode region need almost one second to reach the same energy. (Naturally, after some heating, the electrons have gained energy so they can move between

different places (potentials) within the trap, and are therefore not fixed to the post anode for instance.) Electrons with a radial velocity corresponding to 5000 eV will only escape ~0.25 and ~2.5 mm radially from the beam axis in 2 and 0.2 T magnetic field, respectively, and thus not collide with the post anode, nor the barrier tube. However, due to the Spitzer heating they have now gained enough energy to have the energetic ability to reach the anode or the collector where they can be absorbed. All that is needed is a close collision to redirect the transverse momentum of the electron into longitudinal momentum.

To conclude the discussion, secondary electrons have always been a mystery in EBIS, and we might have to be observant on Penning trap phenomena at the anode or post anode in the REXEBIS since these are the regions with highest potential in the present design.

2.6.5 Mechanical design

The dimensions of the gun are of millimetre size and with kilovolt applied, this calls for high manufacturing accuracy and clever design solutions. Figure 27 contains a commented drawing of the electron gun.

As cathode material lanthanum hexaboride (LaB_6) produced by FEI Co [98] is used. The work function for the 310-crystal direction is 2.41 eV, and inserted in the Richardson equation:

$$j_c = \frac{4\pi m_e e k^2 T^2}{h^3}\exp\left(-\frac{e\phi}{kT}\right) \quad (35)$$

we conclude that a cathode temperature of T_c~1750 K is enough to yield a cathode current density j_c of 25 A/cm^2 which is needed in our design.
The lifetime with T_c=1750 K is approximately 1 year if a surface degeneration of 100 µm is accepted (Figure 28). To calculate the heating power needed to reach the desired cathode temperature, one must observe both the radiative and the emissive cooling; the former governed by Stefan-Boltzmann's law and the latter equals the energy the emitted electrons carry away when leaving the cathode. The average electron energy can be approximated with the work function ϕ_{work}.

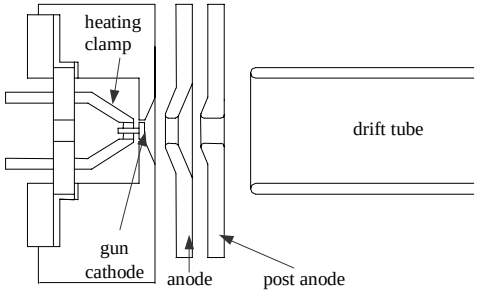

Figure 27. *Electron gun for the REXEBIS.*

Thus, the heating power for a cathode geometry as illustrated in Figure 27 is:

$$P_{heating} = P_{radiation} + P_{emissive} = \sigma T^4 A_{radiation} + \frac{I_e}{e}\phi_{work} = \sigma\cdot1750^4\cdot10\cdot10^{-6} + 0.5\cdot2.41 = 6.5\,\text{W} \quad (36)$$

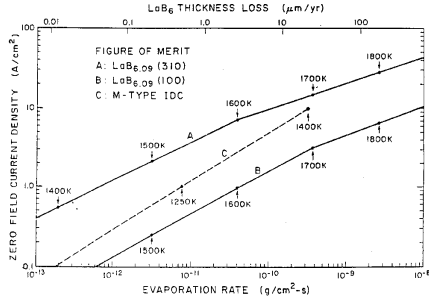

Figure 28. *Evaporation rate for three thermionic cathodes. The LaB_6(310) at j_c=25 A/cm^2 that we use has a loss rate of <100 µm/year at 1750 K.*

2.6.6 Gun alignment

Injecting charged particles successfully into a magnetic solenoid field sets limitations on the alignment of the source to the magnetic field axis. The particle, e.g. an electron, will enter a magnetic region if the angular orientation β of the velocity to the magnetic field line meets the following condition [63]:

$$\beta < \mathrm{acrsin}\left(\sqrt{\frac{B_{outside}}{B_{inside}}}\right) \qquad \textbf{(37)}$$

A theoretical investigation of the electron-gun alignment requirements is presented in ref. [99]. The outcome was that a steep axial magnetic-field gradient leads to a small radial positioning error tolerance and a large angular tolerance and vice versa. Using data of a typical EBIS (B_{full}=3 T, B_c=1.5 T, field rise over 0.5 m, E_e=5 keV), the tolerances were estimated to be:

$$\Delta r_c \leq 1.3 \text{ mm} \qquad \Delta(dr/dz) \leq 4 \text{ mrad} \qquad \textbf{(38)}$$

The parameters for the REXEBIS are similar, and we should expect tolerances of the same order. The tolerated axial displacement of the gun to the magnetic field is estimated from the EGUN simulations to be at least Δz=±5 mm, but naturally with a change in electron current-density at full field. The electron propagation in a displaced tube geometry was treated in the sec. 2.4.4.1.

Gun type	Semi-immersed
Cathode material	LaB_6 310 crystal orientation
Cathode temperature T_c	1750 K
Cathode life-time	1 year
Cathode current density j_c	25 A/cm^2
Cathode diameter	1.6 mm
Magnetic field at cathode B_c	0.2 T
Electron beam current I_e	0.46 A
Anode voltage U_{anode}	6500 V
Perveance P	0.87 A/V$^{3/2}$
Post anode voltage $U_{post\ anode}$	~10 000 V
Compression	from 25 to >200 A/cm^2 (~250 A/cm^2)
ω_L/ω_p in full field	5.1
Radial gun misalignment Δr_c	<1.3 mm
Gun tilt $\Delta(dr/dz)_c$	<4 mrad
Axial gun misalignment Δz_c	<±5 mm

Table 7. *Electron gun parameters.*

2.7 The inner structure

To the inner structure belong the drift tubes, the support structure and the NEG strips. All these elements are in UHV, and at low room temperature (warm bore ~15 ºC). The drift tubes (inner radius r_t=5 mm) can be categorised in transport, barrier and trapping tubes. The potential along the axis is varied by applying different tube voltages, for instance high potentials at the barrier tubes to define the trap size and force the ions to be reflected longitudinally between the barriers. The potential of the trapping tubes relative to the gun cathode determines the electron beam energy E_e. The REXEBIS has three trapping tubes: 100, 230 and 464 mm long with 2 mm spacing, combinable to various trap lengths of 100, 230, 332, 464, 696 and 798 mm. These trapping tubes are all immersed in full magnetic field.

2.7.1 Potentials

It is easy to be fooled and to create unwanted ion traps when setting the tube voltages. This section therefore contains an analysis of the drift tube potential situation. We start with the trap potential, and keep in mind that the desired beam energy E_e=5000 eV. Using the expression for the space-charge potential depression given in eq. 20, we obtain the following equation for the beam axis potential U(r=0):

$$U(r=0) = U_t - \frac{I_e}{4\pi\varepsilon_0\sqrt{2\frac{e}{m_e}U_e}}\left(2\ln\left(\frac{r_t}{r_{ebeam}}\right)+1\right) \qquad \textbf{(39)}$$

where U_t represents the tube potential (relative to the cathode) as before, and U_e the electron beam energy. Note that U(r=0) should equal U_e, and we want to find a tube potential U_t that gives a beam energy E_e=e·U_e=5000 eV. For REXEBIS conditions eq. 39 then yields U_t~5750 V. The electron beam potential depth ΔU (i.e. potential difference between electron beam edge and axis) is calculated using eq. 18:

$$\Delta U = U(r=r_{ebeam}) - U(r=0) = \frac{1}{4\pi\varepsilon_0}\cdot\frac{I_e}{\sqrt{2\frac{e}{m_e}U_e}} \approx 107 \text{ V} \qquad \textbf{(40)}$$

Thus, if one intends to trap 60 keV ions within the electron beam potential, the REXEBIS potential ($U_{platfrom}$) should be between 59 900 and 60 000 V with a trap potential of 750 V relative to the REXEBIS potential. Alternatively, one can decrease the trap tube potential to 650 V, and keep the REXEBIS potential at 60 kV. More about this in sec. 3.3.3. The inner barrier (closest to the gun) is fixed at +1250 V relative to the REXEBIS potential, while the outer barrier is pulsed. At injection the outer barrier is at same potential as the outer drift tubes, i.e. at 0 V relative to the REXEBIS potential. During breeding it is raised 500 V higher than the trapping tube potential, i.e. to 1250 V. At extraction, the outer barrier is again lowered to 0 V, simultaneously as the trap potential is raised to 1000 V. In Figure 29 the tube potentials for injection, confinement and passive extraction are illustrated. One should note that if the REXEBIS should be run fully compensated, the barrier potentials must be ΔU·[1+2·ln(r_t/r_{ebeam})]≈750 V higher than the trapping potential. Note that the tubes have approximately the same potential as the surrounding stainless steel tube; in that way Penning discharges are avoided. After extraction an extra cleaning phase may be added. That involves applying a potential slope on the tubes to make sure that the trap is cleaned from ions. The probability for ionisation before entering the trap at injection is <10%, that means a loss of the same order is expected. (Higher trap tube voltages can decrease this loss if needed.)

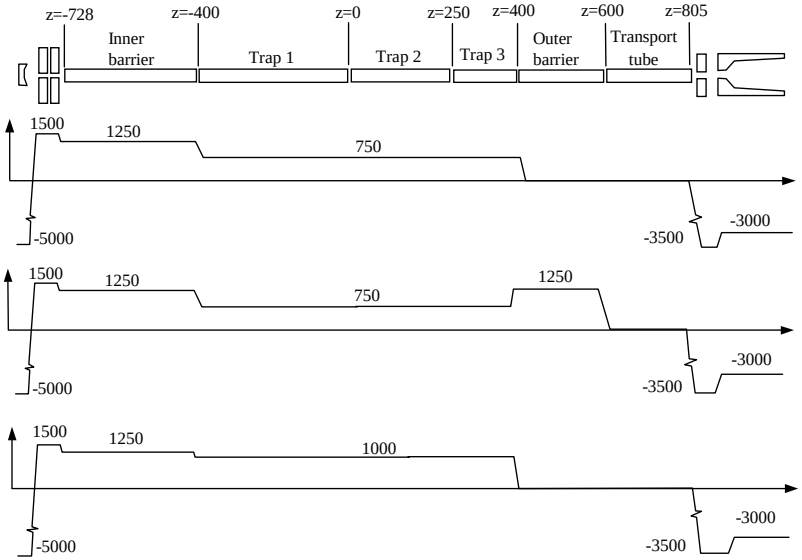

Figure 29. *Axial dimensions of the inner structure. The potential settings (relative REXEBIS potential $U_{platform}$) for injection, confinement and extraction are plotted beneath the structure. (Note that the voltages are not to scale, nor the structure sketch. The gun and collector regions are enlarged. Anode and post anode are at same potential, and cathode at negative potential.)*

The theoretical trapping capacity, for a L_{trap}=0.8 m trap, equals the electron space-charge, and for the REXEBIS it amounts (expressed in number of elementary charges):

$$N^- = \frac{\rho_l L_{trap}}{e} = \frac{I_e}{e v_e} L_{trap} = \frac{I_e}{e\sqrt{2\frac{e}{m_e}U_e}} L_{trap} = \frac{0.5}{e\sqrt{2\frac{e}{m_e}5000}} \cdot 0.8 = 6 \cdot 10^{10} \qquad \textbf{(41)}$$

2.7.2 Potential well distortion

The desired alignment accuracy of the drift tubes is strongly related to the tolerated axial displacement of the electron beam. This was treated in sec. 2.4.4.1, and the old rule-of-thumb (a very conservative estimation) states a tolerance of 0.1 mm. The alignment of the drift tubes, carried out optically, for the REXEBIS will be within the 0.1 mm tolerance. In sec. 2.6.3 we noticed that the electron beam has a ripple. Defining a scalloping measure as:

$$Ripple = \frac{r_{\max} - r_{\min}}{r_{average}} \qquad \textbf{(42)}$$

the EGUN simulations gave a full field ripple of 0.7%, corresponding to a potential variation of ±5 V. Compared with the total electron beam potential depth ΔU=107 V, the scalloping effect is unimportant. Moreover, the thermal mix-up with the rippling paraxial beam may produce a Gaussian beam without ripples after a large number of ripple periods [94].

2.7.3 Extraction scenarios

We have chosen to use passive extraction, which means that the outer barrier is lowered to let the previously confined ions move out by their own kinetic energy. (The axial field gradient from the lowered barrier does not penetrate far into the trap, just some centimetre.) Typical extraction times will be ~100 μs, and the maximal longitudinal energy spread $<q_{ion}\cdot\Delta U$ due to the low electron beam compensation degree. Results from simulated longitudinal energy spread are presented in sec. 3.3.6.

Other types of extraction modes are illustrated in Figure 30. The leaky mode gives a slower extraction, but a more well-defined energy, while fast extraction has opposite properties. Stöckli [100] has also tested multi-trap solutions with specific breeding and extraction properties.

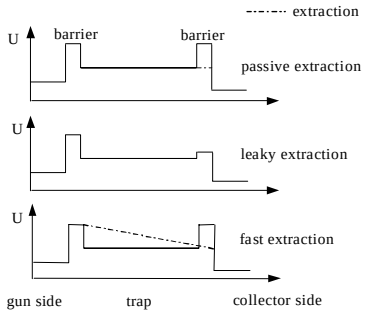

Figure 30. *Different modes of ion extraction from an EBIS: passive, leaky and fast extraction. The first type will be used for the REXEBIS.*

2.7.4 RF generation by the electron beam

The inner structure of an EBIS has considerable similarities with a Travelling Wave Tube amplifier (TWT). A high amplification factor for beam instabilities may develop due to the interaction of the electron beam with the drift tube structure of an EBIS, and the broad band amplification can cause dangerous (from an electron beam stability point of view) RF generation if accidentally modulated [101,102].

In an EBIS the danger for unwanted RF interaction with the beam is a priori not very high since no transverse deviations exist in the basic drift tube structure, nevertheless, the connections to the HV supplies may change the picture [103]. According to ref. [104] RF-feedback circuits with many eigenfrequencies are formed by: the connecting wires; the drift tubes ending in axial gaps; the impedance step at the transition of the connecting wires to the support structure, and these may start generating RF if a certain construction-dependent electron-current is reached.

Different ways to suppress the RF-feedback are proposed in ref. [103], for example to use constructing materials with high loss factors such as stainless steel. The connecting leads should be rudimentary screened, and the lengths of the drift tubes relative to the beam wavelength chosen such that their frequencies of maximum beam interaction are well outside the bandpass of the overall structure. Capacitive shunts (overlapping ends) decrease the coupling between the drift tubes so the bandpass bandwidth is kept low. The precautions taken to avoid self-excitation in the REXEBIS are the use of titanium as drift and supporting tubes (high loss factor) and few drift tubes (6 in total). Optionally drift tubes with overlapping ends can be used, but then the pumping conductance to the NEG strips will be limited.

During the summer of 1997, RF measurements were carried out on CRYSIS in Stockholm. These could not confirm the hypothesis of RF-induced instabilities [103], and our conclusion is that the instabilities seen are due to other effects.

2.7.5 Mechanical design

The two drawings in Figure 31 show side and end views of the inner structure. The inner structure is confined under vacuum in a 75 mm radius stainless steel tube. The six drift tubes have an inner and an outer radius of 5 and 6 mm, respectively, and are made of titanium. The choice of titanium is due to the conceivable sublimating properties of the material, and the moderate electrical conductivity ($2.4\cdot10^6$ S/m [105]) should reduce the ability for electron beam resonance phenomena in the structure. In the future, we have the option to drill radial holes in the drift tubes to improve the pumping speed from the NEG strips that are mounted in an octagonal shape at a radius of 40 mm.

There are no coupling/damping sleeves at the ends of the drift tubes due to pumping reasons, only a 2 mm insulation distance between the flat front faces of the tubes. It is feasible to add sleeves if it turns out to be necessary. The tube ends are adjustable sideways in pairs by three insulating supports, which are mounted on the support plates. The support plates are in turn fixed to the solenoid by three support tubes of titanium.

Gravitational deformation of the structure can be compensated by an extra support from the vacuum stainless steel tube to the inner structure, and by individual adjustment of the drift tubes in vertical direction. With only two supports at the ends the maximal deflection is ~0.15 mm, but with a third support at the centre it can be reduced to 0.02 mm (see Box 3). (If the clamping of the ends should not be perfect, the deflection will be a factor five larger.)

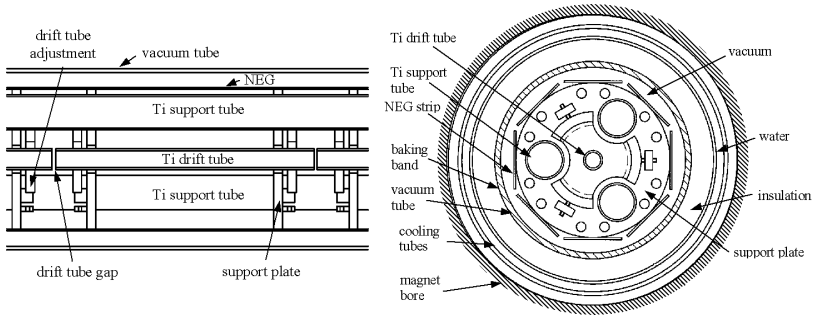

Figure 31. *Side and end view drawings of the inner structure.*

Outside the stainless steel tube two heating bands of each 700 W are wound in spiral (see Figure 32). Four layers of 2 mm ceramic paper (Plisulate, λ=0.07 W/m·K [106]) heat-insulates the tube (350 °C during baking) from the cooling water tube (15 °C). The water tube consists of two concentric stainless steel tubes, between which the water is forced by two barrier walls to flow forth and back along the tube axis. The water flow is ~4-5 *l*/min, and with a water temperature increase of 5 °C, the water has a maximum cooling effect of 1600 W (implies turbulent flow). This is well below the tolerated 40 °C that

the magnet bore can withstand for a 12 h baking period. Due to the high voltage, the water transferred to the platform has to be de-ionised. The ISOLDE de-mineralised water has a conductivity of ~50 µS/m.

Box 3. Inner structure deflection.

The support structure consists of 3 titanium tubes, each with a moment of inertia:

$$I_{tube} = \frac{\pi}{4}\left(r_{outer}^4 - r_{inner}^4\right) = \frac{\pi}{4}\left(\left(6\cdot10^{-3}\right)^4 - \left(5\cdot10^{-3}\right)^4\right) = 5.3\cdot10^{-10}\ \mathrm{m}^4 \quad \textbf{(43)}$$

The total weight per meter w<3 kg, and Young's modulus E for titanium equals $1.1\cdot10^{11}$ Pa.

Maximum deflection for the structure is then [107]:

clamped at both ends $$d_{\max} = \frac{wL^3}{384E\cdot 3I_{tube}} = 0.15\,\mathrm{mm} \quad \textbf{(44)}$$

clamped at both ends with an extra support in the middle $$d_{\max} = \frac{w(L/2)^3}{384E\cdot 3I_{tube}} = 0.02\,\mathrm{mm} \quad \textbf{(45)}$$

The abundance of residual gas should be enough for breeding and extraction tests (see sec. 2.10.6), so no extra feed-through for gas injection is foreseen. Due to the warm bore construction, pulsed injection is difficult to control and had to be arranged by a pulsed needle valve.

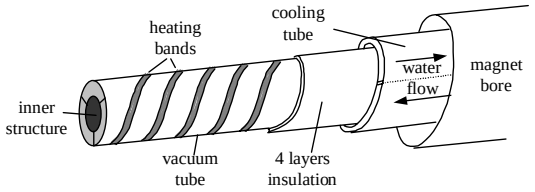

Figure 32. *Schematic 3D picture of inner structure, heating band, insulation and cooling water tube.*

The drift tubes are electrically connected to the power supplies via glass-insulated wires and feed-throughs at the magnet ends.

Trap length	100, 230, 332, 464, 696 or 798 mm
Trap capacity	$6\cdot10^{10}$ charges (for 798 mm length)
Number of drift tubes	6
Drift tube inner diameter	10 mm
Electron beam energy	5 keV
Electron beam diameter	0.5 mm
Electron current density at full field	>200 A/cm^2 (~250 A/cm^2)
Electron beam well depth	107 V
Beam ripple	±5 V
Drift tube material	titanium

Table 8. *Inner structure parameters.*

2.8 The collector

In the collector the electron beam is separated from the extracted ions, and the electrons are absorbed at the collector surface. Important properties for the collector design are among others: a high electron collecting efficiency; small ion beam influence and a low out-gassing rate. In addition, the design must also be realistic and feasible to manufacture in a workshop.

2.8.1 General collector design ideas

An EBIS has an axis-symmetrical geometry and the tradition has been to make also the collector axis-symmetrical, although we considered alternative solutions similar to the ones used in electron coolers (a deflecting magnetic field that guides the electron beam away from the ions so it can be absorbed in a very efficient way).

To avoid virtual cathodes, the collector radius should not increase too much in comparison to the electron-beam radius-expansion, but approximately follow the electron beam envelope. In our design we have relinquished this condition, and we use a collector with a cylindrical instead of conical form in the absorbing region (see Figure 33). From the EGUN simulations we do not experience any virtual cathodes due to this modification.

Usually, the residual axial magnetic field keeps the electron beam together, and prevents it from diverging out to the absorbing collector surfaces. To counteract this, we reduce the magnetic field drastically inside the collector by adding a cylindrical iron screen around the collector. The electron beam then has the opportunity to expand by space-charge and Busch's theorem.

The REXEBIS collector has been designed with a very unclosed end. By having this large extraction hole, we expect to minimise the ion beam aberrations; besides the pumping conductance increases.

2.8.2 Electron absorption and ion extraction

To extract the ions from the collector region, a cylindrical extractor (-20 000 V relative to the drift tubes) with a 14 mm radius is positioned at the end of the collector. The large radius ensures small aberrations, and from the SIMION simulations we concluded that the ion beam fills less than 1/5 of the extractor diameter. There were no indications of a distorted phase space either. The extractor acts as a strong lens (due to the electrical field), and creates a focus inside the extractor. This is not a problem from a space-charge point of view, since the focal size is large, ~2 mm (compare with sec. 3.2).

Figure 33 shows an EGUN simulation of the absorbed electron beam. The dashed line visible to the left in the picture indicates the magnetic field strength. One unit of length corresponds to 0.25 mm. Each trajectory (in total 210) carries about the same current (~2.5 mA) and the trajectories have a thermal starting energy of 0.1 eV at the cathode. The electron beam is dissipated over an area of ~65 cm^2, i.e. the average current load is <8 mA/cm^2.

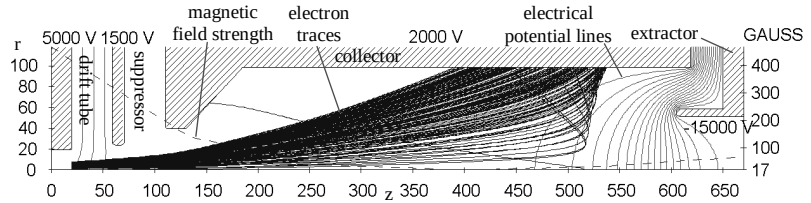

Figure 33. *EGUN simulation of the absorbed electron beam. One unit of length corresponds to 0.25 mm. Only the upper cylindrical part of the collector region is shown.*

2.8.3 Electron reflection and back-scattering in the collector

Electrons entering the collector have a certain probability to re-enter the trap region, either by direct reflection due to the negative extractor potential (directly reflected electrons), or after back-scattering off the collector surface (back-scattered electrons), or by kicking out low-energetic electrons from the surface (secondary electrons[4]). These back-streaming electrons may lead instabilities [108,109] and anode heating [110], and the problem has previously been addressed by Hershcovitch et al. in ref. [110]. Due to certain limitations in their modelling, we preferred to repeat and improve the simulation.

[4] These secondary electrons should be distinguished from the secondary electrons created in the ionisation process (sec. 2.6.4)

Both reflected and back-scattered electrons are in our design avoided by an extra low magnetic field inside the collector creating a strong magnetic mirror effect that prevents most of the electrons to re-enter. The slow secondary electrons are hindered by the suppressor, which is on -500 V relative to the collector potential, in combination with the electrostatic depression caused by the space-charge of the electron beam. Electrons created in residual gas ionisation processes in the collector region are also low-energetic, and will not enter the trap region for the same reasons.

2.8.3.1 Basic considerations and theory

Secondary electrons are low-energetic with energies about 20 eV [111,112], and the secondary electron emission coefficient is smaller than 25% for electrons incident on copper with an energy E_0<5 keV [113]. Owing to the suppressor and the electron-beam space-charge, the secondary electrons are energetically disqualified to re-enter the trap region. On the other hand, electrons with impact energies E_0 of a few hundred electronvolts to 2 keV incident normally on copper have a 38% back-scattering coefficient and an average energy of 80% of the incident energy when they leave the surface. This can be enough to promote re-entering of the electrons into the trap provided that the electrons enter the EBIS trap within the "loss cone" of the magnetic mirror. The amount of directly reflected electrons re-entering the trap is solely governed by the loss cone condition, eq. 37.

The back-scattering coefficient η is dependent on the deviation from normal incidence on the collector surface, and the following expression is suggested in ref. [114] to include the angular dependence:

$$\eta_\alpha = C\left(\frac{\eta_0}{C}\right)^{\cos\alpha} \qquad \textbf{(46)}$$

where α is the angle of incidence, η_0 and η_α are the back-scattering coefficients for α=0 and $\alpha\neq0$, respectively, and C=0.891 is a fitted constant [115]. As already stated, η_0~38% on copper for electrons with energy E_0<2 keV.

The energy spectrum for the back-scattered electrons has been measured by Darlington [116], and a plot for a 3 keV beam is found in Figure 34. For lower impact energies there is little data available, but the energy distribution of the back-scattered electrons broadens with decreasing incident energy [110]. In the simulations, the distribution was approximated with:

$$\frac{d\eta}{dE} = \begin{cases} 0 & E/E_0 < 0.4 \\ -2/3 + 5/3 \cdot E/E_0 & E/E_0 > 0.4 \end{cases} \qquad \textbf{(47)}$$

over the whole incident energy spectrum (a few hundred eV up to 2 keV). This approximation generates back-scattered electrons with slightly overvalued energy, especially for the low-energy impact electrons, which probably resulted in an overestimation of the number of electrons that were reflected into the trap region.

A major complication for the modelling is the angular distribution of the back-scattered electrons. At low energies (<10 keV), no data regarding angular distributions were found, but it is known that angular effects of inelastic scattering become significant [116]. For this reason, plus the fact that the fraction of electrons that undergo pure elastic scattering is uncertain [110,117], we chose to simulate two extreme cases in a similar way as was done in ref. [110]. In the first, the inelastic case, all electrons were completely randomly scattered over a solid angle of 2π, while in the second, the elastic case, all electrons had a cosine distribution about the most probable starting angle (i.e. the reflection angle); in both cases with an energy distribution governed by eq. 47. The angular distribution of elastically back-scattered electrons do obey the Lambert cosine distribution with reasonable accuracy [114,118,119].

The presumably dominant drawback in the simulations was the exclusion of the space-charge that is created by the reflected electrons, i.e. the reflected electrons did not interact with other electrons reflected inside the collector. Yet another minor simplification was to sort out and not further trace the electrons that hit the conical part of the collector, but this fraction of events was only ~1%.

2.8.3.2 Simulation description

To generate the primary electrons, a beam of 40 electron trajectories from EGUN was used. The electrons were started on equally distant radial positions, thus each trajectory had to be multiplied with its current

weight factor ($\propto r_{start}/r_{ebeam}$), and a total number of 1500 electrons were obtained. EGUN traced the electrons to the collector surface. The reflection probability for each electron was then decided using eq. 46. For the elastic case, the angular reflection direction was weighted by a factor $\cos(\varphi)/N$, where φ is the angle between the actual take-off and the most probable take-off direction (equals the incident angle α), and N is a normalisation constant. The inelastic electrons on the other hand had a complete random angular distribution over the free 2π solid angle. Both the inelastic and the elastic electrons received an energy distribution according to eq. 47. Thereafter the electrons were traced, using SIMION, in 3-dimensions in a collector with the following features:

- potential surfaces of collector, suppressor, drift tubes and extractor
- primary electron beam space-charge
- magnetic field

Note that all electrons were started at θ=90° (Figure 35 and 36), just to simplify the reflection direction calculations. It is of no real limitation since the geometry is cylindrically symmetrical. The electrons could then either re-enter the trap region in which case they were not further traced, or they could hit the collector surface once again. If the latter happened, then the same reflection and trace procedures were performed until only ~10 very low energetic electrons remained wandering around in the collector region (all others had either re-enter the trap region, or become absorbed at the collector surface).

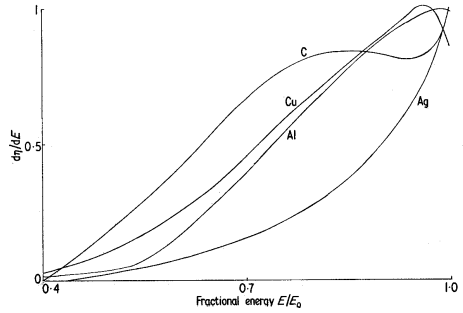

Figure 34. *Reflected energy spectra dη/dE for an incident E_0=3 keV electron beam energy. Note that dη/dE is negligible for E/E_0<0.4.*

2.8.3.3 Electron back-streaming results

EGUN simulations of the electron beam behaviour inside the collector showed that a fraction <0.1% was direct reflected. The number of back-scattered electrons were ~0.1% (inelastic) and ~0.05% (elastic), which is significantly lower than the result (8% inelastic and 0.6% elastic) from a comparable simulation [110]. The shortcomings of the model in ref. [110] as compared to the one used here were:

- a two-dimensional simulation
- possible uncertainties in the current weight factor for the trajectories from the EGUN simulation[5]

These features have been corrected for in our simulation. Moreover we have an open collector design with a large, strongly negative extractor reaching into the collector region, which seems to quench most of the re-entering attempts (Figure 35 and Figure 36).

The back-scattered electrons build up an extra space-charge in the collector region. The magnitude of this can be estimated by a simple reasoning. With an average reflection coefficient $n_\alpha \approx 0.5$ for each collector surface collision, each back-scattered electron will survive $n_\alpha + n_\alpha^2 + n_\alpha^3 + \ldots \approx 1$ reflections. The mean distance between consecutive collector collisions is of the order 5 cm. Assuming an average energy of 1000 eV, each electron will wander about in the collector region for approximately $1 \cdot 0.05/\sqrt{2 \cdot 1000 \cdot e/m_e}$ ~3 ns. Thus, the back-scattered electron space-charge from a 0.5 A incident electron beam amounts $0.5 \cdot 3 \cdot 10^{-9}$=1.5 nC, which should be compared with the primary beam space-charge of ~2 nC. As seen in Figure 35 and Figure 36 quite a few of the back-scattered electrons are concentrated at the surface of the collector, and this sheath will affect the absorption of the primary electrons; how is not fully clear.

[5] The author of ref. [110] recalls having problems with the weighting factor in certain simulations.

2.8.3.4 Conclusions

To conclude, only a minuscule part of the electrons are reflected back into the trap region: <0.1% by direct reflection, 0.1% by inelastic back-scattering, and 0.05% by elastic back-scattering. The high extractor voltage seems to quench most of the re-entering attempts. Still remains to investigate the lifetime of the back-scattered electrons inside the collector, and the space-charge build-up.

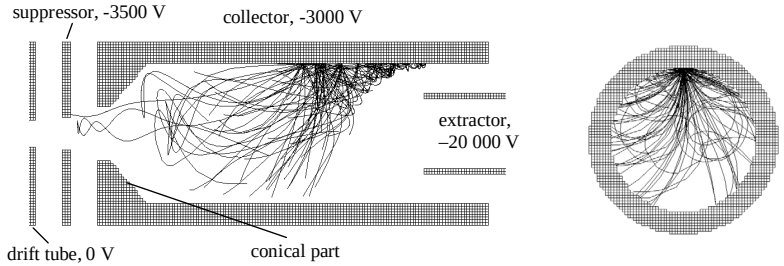

Figure 35. *Simulated electron back-scattering from the collector for the inelastic case. The plots show a few back-scattered trajectories from the primary beam impact until they hit the collector again. Side and end views. (The geometry of the model differs somewhat from the actual collector in the extractor region, but this should not affect the results significantly.)*

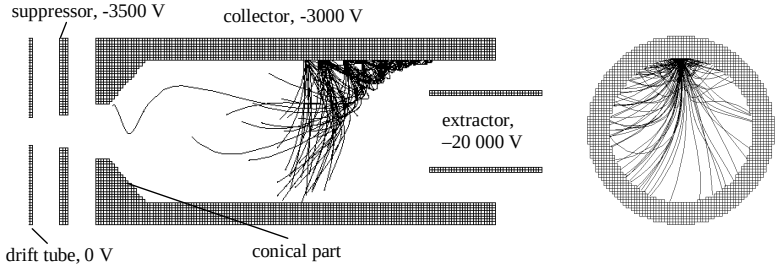

Figure 36. *Similar as previous figure, but for the elastic case.*

2.8.4 Mechanical design

The collector is made of oxygen free high conductive (OFHC) copper. The absence of oxygen ensures an oxide free formation when the outer cylinder is attached to the inner (see Figure 37). The whole collector structure is bakeable to 350 ºC. In between the two cylinders a two-way spiralling water canal for cooling is housed. The total length L of the water canal is 1.6 m. Approximating the 3·6 mm^2 cross-section with a circle of diameter d_{canal}=4 mm, the flow will be turbulent (Re~7000) if the flow velocity v_{flow}=2 m/s. The pressure drop Δp is given by [120]:

$$\Delta p = \rho_{H_2O}\xi(turbulent)\frac{Lv_{flow}^2}{2d_{canal}} = \quad (48)$$

$$= \left[\xi(turbulent) \approx 0.32\,\mathrm{Re}^{-1/4} \text{ for } \mathrm{Re} < 3\cdot 10^5\right] = 1000 \cdot 3.5 \cdot 10^{-2}\,\frac{1.6 \cdot 2^2}{2 \cdot 4 \cdot 10^{-3}} \approx 0.3\,\text{bar}$$

This, together with the low water pressure for the drift tube cooling, implies that no special pressure arrangement for the cooling water is necessary. A FEM calculation of the collector heating due to the electron impact was carried out using Matlab PDE toolbox [121], and the temperature rise from the electron beam load is expected to be less than a few degrees (see Box 4).

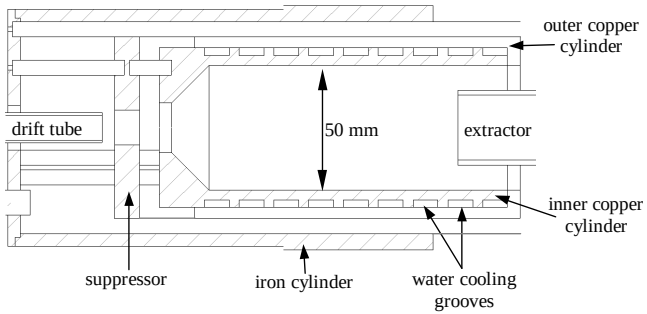

Figure 37. *Cross-section of the collector.*

Box 4. Temperature distribution in the collector at electron impact.

The following assumptions were used for calculating the electron-beam heat effect on the collector.

- The cylindrical collector was approximated by a two dimensional slab of copper. (In the figure only the upper half of it is shown.)
- We allow the 15 ºC cooling water to be heated 10 ºC, and the worst case assumption is then a 25 ºC water cooling temperature at the upper boundary. The water flow must be >1.5 *l*/min.
- No convection was included in the model, and isolating Neumann boundary conditions on all non-marked sides assumed.

From the heat distribution plot (Figure 38) we conclude that the heating is very small, less than a few degrees.

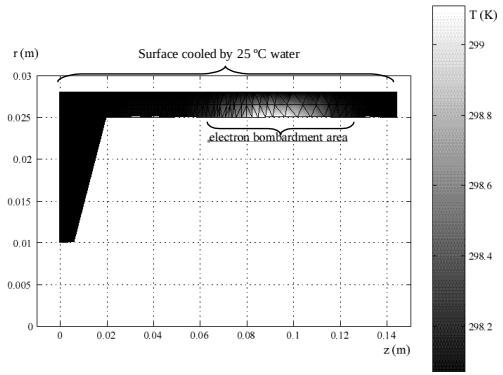

Figure 38. *Temperature distribution in the collector at 1000 W electron beam bombardment and with 25 ºC cooling water. (Note the non-proportional length scales.)*

With a cylindrical 5 mm screen of Armco iron (μ_{rm}=250) surrounding the collector, the magnetic field inside the collector is reduced to <0.02 T. Due to misalignment of the collector, or a deviation between the central magnetic field line and the geometrical axis, a non-symmetrical situation can occur. This may lead to a higher fraction of reflected electrons, and affect the direction of the extracted ion beam. Even though the latter effect is easily adjusted for by the steering plates after the extractor, the electron reflection is both hard to determine and to adjust for. A conservative estimation indicates that a collector displacement Δr<0.5 mm and a tilt Δα<10 mrad should not affect the performance seriously.

Collector voltage relative to cathode	2000 V
Suppressor voltage relative to cathode	1500 V
Extractor voltage relative to collector	-17 000 V
Power dissipation	1000 W
Material	OHFC
Current density	<8 mA/cm^2
Temperature increase due to electron load	<2 K
Cooling water flow	>1.5 *l*/min
Direct reflected, back-scattered and secondary electrons	<0.1%, 0.1%, 0.05%

Table 9. *REXEBIS collector data.*

2.9 Injection and extraction optics

2.9.1 Transport line

After bunching and cooling in the Penning trap, the ions are extracted to ground potential (i.e. 60 keV) and transferred to the REXEBIS via the transport line. It has a symmetric design, and consists of two 7.5º kickers, two 82.5º spherical benders and two electrostatic quadrupole triplet on each side of the symmetry point (see Figure 39). The kicker close to the 2nd bender focus is only active during injection; at extraction the beam goes straight through to the mass analyser. To improve the differential pumping of argon between the trap and the EBIS, orifices are positioned at the 1st and 2nd bender focus, and at the mirror point of the line. The radii of these are not fixed for the moment (see also sec. 2.10.4).

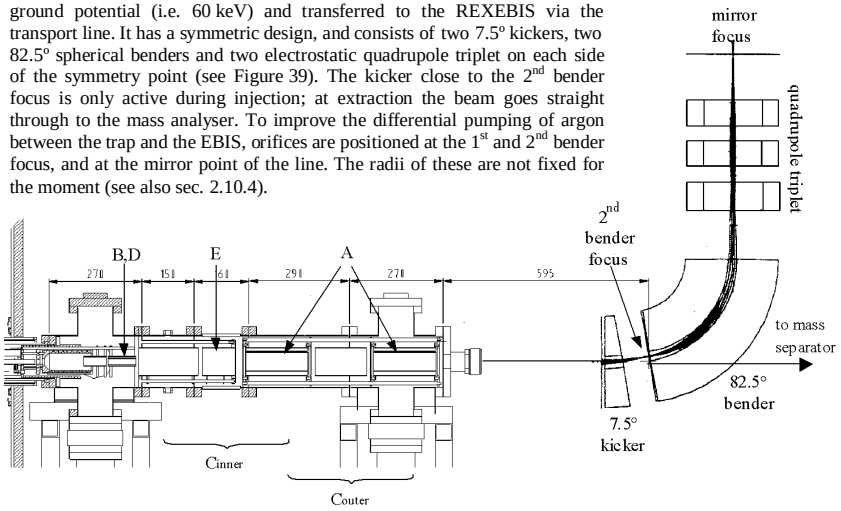

Figure 39. *Drawing of the REXEBIS beam optics with part of the transport line indicated (interface is not included). Note the insulating ceramic beam tube enclosing the retarding element E.*

2.9.2 Optical elements

The hardware interface between the transport line and the REXEBIS consists of flange and a bellow after the 2nd 7.5º kicker. Concerning the beam transport, we take over the beam at the 2nd bender focus and deliver it at same longitudinal position, but slightly radially shifted due to the inactive 2nd kicker at extraction. Inside the REXEBIS optics section the following elements are contained:

A. Two 80 mm diameter cylindrical deflectors for steering. The deflector is a cylinder that has been sliced along the longitudinal axis into four 90º sectors, and then rotated 45º to the horizontal plane. Aberrations from a deflector of this type are less than from ordinary flat plate deflectors.

B. A small cylindrical deflector close to the collector.

C. Two 80 mm diameter einzel lenses for focusing.

D. A differential pumping stage made of a 50 mm long and 10 mm diameter tube.

E. Retarder from 60 keV to 20 keV.

Since the ion injection energy is 60 keV and the extraction voltage is variable between 15 and 22.5 keV (the RFQ injection energy should be 5 keV/u), the lenses and the retarder have to be switched between injection and extraction. The einzel lens voltages are switchable between +20 kV and -20 kV, which guarantees a wide extraction voltage range. In Figure 40 typical voltage settings are found.

The REXTRAP will deliver a 60 keV ion bunch with a 3 π·mm·mrad focus at the 2nd bender. The tolerated beam tilt and transversal displacement, which are correctable by the deflectors, have been calculated using SIMION: tilt±0.3º, displacement ±5 mm. After charge breeding the ions are extracted from the EBIS with a voltage varying between 15 and 22.5 kV (depending on the Q/A-value). To obtain a Q/A resolution of 150, the ions emitted at 20 kV extraction voltage must fit in a phase space ellipse with the dimensions 5·8 π·mm·mrad (4σ). With the steering elements the beam tilt and focus position at the delivering point can be shifted (tilt ±1º, displacement ±20 mm). A summary of the beam properties at the 2nd bender with tolerances are presented in Table 10 (the acceptance and emittance are treated in sec. 3.3). The beam profile and phase space at the 2nd bender for injection and extraction are plotted in Appendix 2.

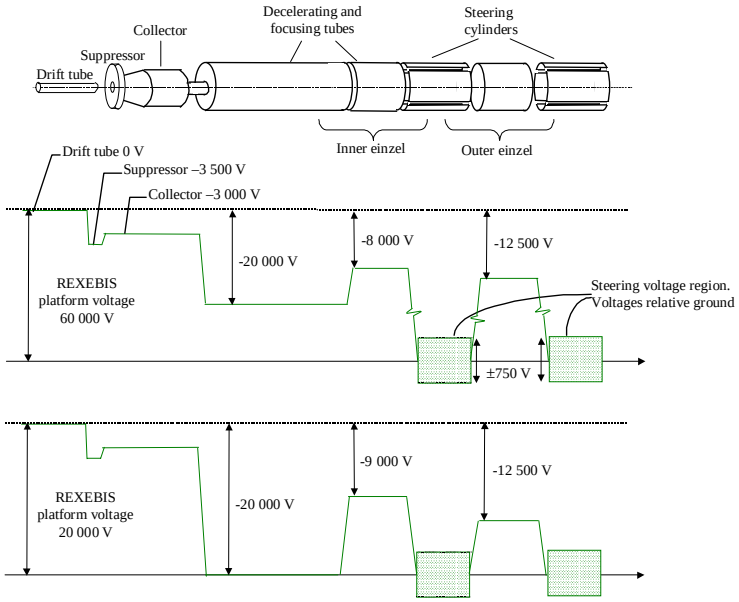

Figure 40. *Schematic picture of the optics elements and the voltage settings for typical injection and extraction. The einzel lens voltages are switchable between +20 kV and -20 kV.*

	Injection	Extraction
Maximum tilt	±0.3°	±1°
Maximum transversal displacement	±5 mm	±20 mm
Specified geometrical acceptance	3 π·mm·mrad (60 kV)	
Maximum geometrical acceptance	11 π·mm·mrad (60 kV)	
Geometrical emittance		<19 π·mm·mrad (20 kV)

Table 10. *Beam properties at 2nd bender. The emittance and acceptance values are stated for ions completely within the electron beam.*

2.10 Vacuum

2.10.1 Specifications and requirements

A good vacuum is of vital importance for an EBIS since residual gases may compensate the trap and cause a large beam radius with an increased emittance as a consequence. For the REXEBIS this problem should not occur, due to the low degree of compensation (<10%). For instance, the compensation pressure (assuming 20 ms breeding time and H_2 as dominating residual gas) is[6]:

$$p(H_2)_{10\%} = \frac{kT}{\tau_{breed} v_e \sigma_{H_2}} \cdot 0.1 \approx 10^{-8} \text{ torr} \quad \textbf{(49)}$$

which is several orders higher than the pressure we aim for (<10^{-11} torr). We do not have to worry about ion heating either since for such low Q/A-values as ~¼, the heating mechanism is negligible (see sec. 2.2.2) and therefore no ions will be kicked out of the well. Instead, the low number of injected ions is the main problem, since they can be outnumbered by the residual gases by orders of magnitude, even for very good UHV.

Moreover a good vacuum is needed to avoid Penning discharges in the structure, that may heat-up the system and lead to more out-gassing. This is probably of no danger for the REXEBIS design, since the stainless steel tube is at approximately the same potential as the drift tubes.

Three sources for poor vacuum are:

- High vapour pressure from the constructing materials. Though, in the case of stainless steel and titanium as the main construction materials for the inner structure, the vapour pressures are in the region of 10^{-20} torr, which is way below our objectives, and they can therefore be neglected.
- Desorption from the surfaces, mainly H_2, CO, O_2, N_2 and H_2O. For vacuum fired stainless steel H_2 is the main contributor with a desorption rate $Q_{desp} \sim \exp(-E_d/2RT) \cdot t^{-0.5}$, where E_d is the energy of activation for the diffusion process, R the molar gas constant, T the temperature and t the time since the sample was put under vacuum. Due to uncertainties in for instance E_d, the desorption rate for H_2 is difficult to calculate, but it is estimated to $5 \cdot 10^{-13}$ torr·*l*/cm^2·s [122]. Hydrocarbons, such as CH_4, are produced at the surface from H diffusing out of the bulk and reacting with C in the steel, as well as on the hot cathode area. The desorption rate is estimated to $5 \cdot 10^{-16}$ torr·*l*/cm^2·s [122]. Other contributors are CO, CO_2 and H_2O that cover the system surface after exposure to air, and have an estimated contribution of $1 \cdot 10^{-16}$ torr·*l*/cm^2·s each.
- Permeation – diffusion through the confining material. The permeation Q_{perm} through metals can only occur for gases that are soluble, that excludes inert gases, and it varies as:

$$Q_{perm} = \frac{AK}{d_{wall}} \left(\sqrt{p_2} - \sqrt{p_1} \right) \quad \textbf{(50)}$$

where p_1 and p_2 (Pa) are the partial gas pressures at each side of a wall of thickness d_{wall} (m), and K (m^2·Pa$^{1/2}$·s^{-1}) is the permeation constant. For the stainless steel vacuum tube in the REXEBIS with d_{wall}=2 mm, $p_1 = 5 \cdot 10^{-2}$ Pa (H_2 partial pressure in air), $p_2 \sim 0$ Pa, $K = 1 \cdot 10^{-14}$ m^{2}Pa$^{1/2}$s^{-1} (extrapolation of hydrogen permeation constant from ref. [123]), the hydrogen permeation $q_{perm}(H_2)$ is $1.5 \cdot 10^{-16}$ torr·*l*/cm^2·s. This is much less than the desorption $q_{desp}(H_2) = 5 \cdot 10^{-13}$ torr·*l*/cm^2·s, thus, we can safely neglect the influence from permeation. (Also true for heavier gases due to their much smaller permeation constants.)

Apart from the gases listed above, we also have Ar diffusing from the REXTRAP. This is handled by differential pumping, sec. 2.10.4. At the filament of the electron gun, as well as at the electron collector, the desorption rates are strongly amplified due to a high temperature and electron bombardment, respectively.

[6] One should observe that the compensation time is independent on the j_e, therefore the current density should be increased and the current decreased if one wants to avoid compensation problems.

All high performance EBISs have so far been designed with a cold bore (apart from a warm EBIS at Sacley that was never finished), and thereby have a cryogenic pumping mechanism in the drift structure. The REXEBIS, however, has a warm bore, which calls for other pumping techniques described below.

2.10.2 Pumping systems

2.10.2.1 Turbo pumps

The backbone in the pumping system consists of two 180 *l*/s and one 260 *l*/s 2-stage turbo molecular pumps from Balzers (further data in Table 11). The two 180 *l*/s pumps are positioned at the high voltage platform on each side of the EBIS, and the 260 *l*/s pump at ground potential near the 2nd bender in the transport system (see Figure 41). As backing pump a small turbo at ground potential is used, connected via a plastic hose to the main turbos. The turbo pumping of the trap region is conductance limited.

	180 *l*/s pump	260 *l*/s pump
Pumping speed (*l*/s)	180	260
Compression	N_2 >$1 \cdot 10^{12}$, He $2 \cdot 10^8$, H_2 $5 \cdot 10^5$ (heavier elements → higher compression)	N_2 >$1 \cdot 10^9$, He $3 \cdot 10^5$, H_2 $1.3 \cdot 10^4$ (heavier elements → higher compression)
Lower pressure (torr)	<$1 \cdot 10^{-12}$	<$1 \cdot 10^{-11}$

Table 11. *Turbo pump characteristics.*

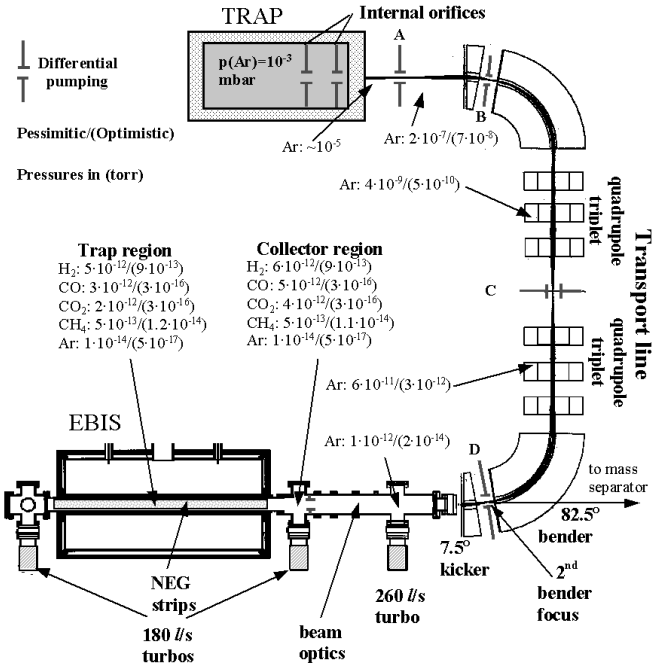

Figure 41. *Vacuum picture of the REXEBIS system. Three different pumping devices exist: three turbo molecular pumps that pump all gas types with high compression; NEG strips with high pumping speed especially for H_2; drift and supporting tubes of titanium with gettering properties. In the transport line between the REXTRAP and the REXEBIS there are differential pumping stages (pumps not shown). Calculated partial pressures in the system are also included (values from Table 13 and sec. 2.10.4).*

2.10.2.2 NEG pumps

Around the inner structure, non-evaporable getter strips are mounted in a octagonal geometry. These non-evaporable getters, St707 produced by SAES Getters S.P.A [124], are made of a Zr(70%)-V(24.6%)-Fe(5.4%) alloy, and have a very high pumping speed for H_2.

In the getter material active gases such as O_2, CO and N_2 are permanently kept by strong chemical bonds to the Zr with the exception of H_2 and its isotopes, which form a solid solution in the alloy and can thus be reversibly sorbed, according to Sieverts' law (with parameters specific for St 707):

$$\ln\left(p(H_2)\right) = 4.8 + 2\ln\left(\Gamma_{conc}\right) - \frac{6116}{T} \qquad \textbf{(51)}$$

where $p(H_2)$ is the H_2 equilibrium pressure in torr, Γ_{conc} the concentration of H_2 within the alloy in torr·l/g (valid for Γ_{conc}<10 torr·l/g) and T the temperature in K.

We conclude that a lower temperature results in a better partial pressure $p(H_2)$ (hydrogen solubility decreases with increasing temperature), and since the hydrogen atoms diffuse quickly into the bulk even at low temperatures, the complete NEG strip body can be used for H_2 pumping. On the other hand, for O_2, CO and N_2 that are chemisorbed on the surface the accumulation of adsorbed species can form a passive layer at low temperatures, retarding the sorption process. Therefore the diffusion process should be promoted by increasing the NEG operating temperature to 200 to 250 ºC. Such a high temperature should be possible to keep at the inner structure by the heating bands surrounding the vacuum tube, without affecting the operation of the magnet. The optimal temperature has to be tested and it depends on the relative residual gas pressures of H_2 and O_2, CO, N_2. The operating temperature will probably be at room temperature to maximise the H_2 pumping speed, and when the other gases have built up passive layer, the NEG is reactivated (this operation procedure is also recommended by the manufacturer). At room temperature the H_2 pumping speed amounts ~0.5 $l/cm^2 \cdot s$, while O_2, N_2 and CO are pumped with 65%, 15% and 40% speed with respect to H_2.

Reactivation means that the NEG is heated to around 350 ºC under vacuum (<$1\cdot10^{-3}$ torr) for about 20 h, and the NEG pumping speed should thereafter return to 100% efficiency. The reversible hydrogen diffuses out of the material, while O_2, CO and N_2 that are strongly bond, migrate into the bulk. This means that after some, typically 20-30, reactivation occasions, the getter is saturated with O_2, CO and N_2 and only pumps H_2. Using dry nitrogen instead of air when venting results in less reduction of the pumping speed.

To determine the reactivation period, we solve for $\Gamma_{conc\ limit}$ in Sievert's law.

$$\exp\left(\frac{\ln\left(p(H_2)\right) - 4.8 + 6116/T}{2}\right) < \Gamma_{conc\ limit} \qquad \textbf{(52)}$$

and with a maximum tolerated hydrogen residual gas pressure of let us say $1\cdot10^{-14}$ torr, the limiting $\Gamma_{conc\ limit}$ in the getter should not exceed $3\cdot10^{-4}$ torr·l/g. Estimating the gassing area to ~1 m^2, the total H_2 desorption is $10\,000\cdot5\cdot10^{-15}$ torr·l/s. This gas load is absorbed by eight 27 mm wide and double-sided NEG strips, with a total length of 12 m and a weight of 240 g, and the concentration limit is reached after a pumping time $t_{reactivation}$:

$$t_{reactivation} = \frac{\Gamma_{conc\ limit} \cdot m_{getter}}{q_{gas\ load}} = \frac{3\cdot10^{-4}\cdot240}{5\cdot10^{-11}} \approx 46\ \text{years} \qquad \textbf{(53)}$$

i.e. practically unlimited pumping time for H_2 desorption. The passivisation rate of the surface at low temperatures due to O_2, CO and N_2 is hard to estimate but should not be limiting at these pressures.

The chemical bonds of water vapour are cracked on the surface of the getter material, and the hydrogen and oxygen are then absorbed as explained before. The hydrocarbon sorption efficiency at temperatures below 500 ºC is very small. Inert gases are not pumped at all.

H_2 pumping speed	0.5 $l/cm^2 \cdot s$
O_2, N_2 and CO pumping speed relative H_2	65%, 15% and 40%
Hydrocarbon sorption efficiency relative H_2	<0.1%
Maximum number of reactivation cycles	20-30
Reactivation conditions	350 ºC, p<$1\cdot10^{-3}$ torr, 100% efficiency after 8 h
NEG melting point	1300-1500 ºC
Flammability point of the powder	200 ºC in air
Resistivity for a 27 mm wide strip	1.6 Ω/m

Table 12. *NEG data.*

2.10.2.3 Gettering material

To further enhance the pumping capacity of the system the drift and supporting tubes are made of titanium that has gettering properties and forms pseudo-hydrides with hydrogen. The pumping speed for H_2 is of the order of 1 $l/cm^2 \cdot s$ [122].

2.10.3 Vacuum firing and baking

The main cause for bad vacuum is not gas leaks but gas desorption from components and vacuum tubes. To minimise the gas desorption, the material is heated in two different processes: during vacuum firing and baking.

2.10.3.1 Vacuum firing

Before the parts are assembled we vacuum fire the stainless steel components. The parts are then heated to the highest temperature possible without melting the material, which is typically ~900-1000 ºC for stainless steel. The high temperature is desired since the diffusion of residual gases out of the material (the desorption) is exponentially proportional to the temperature. The vacuum firing is carried out in vacuum ($1\cdot10^{-5}$<p<$1\cdot10^{-4}$ torr), for a period of 8-12 hours. Before the material is vacuum fired it has been chemically cleaned to remove surface oxide or other containment layers, and degreased to remove oil. After finished firing the material must not be touched, but the parts can be stored in atmosphere pressure since the re-adsorption is a fairly slow process. The main objective with the vacuum firing is to remove H_2 from the bulk and oxide layers.

2.10.3.2 Baking

After the parts have been assembled, the system is put under vacuum, and then heated to ~350 ºC for 16-24 hours. This process is called bakeout, and aims to remove water vapour (easily done) and gases that were adsorbed after vacuum firing (a slower process).

In our case the parts are heated by specially designed heat jackets and wound heating bands. The temperature is surveyed by a microprocessor-controlled system. When baking, heat sensitive equipment as turbos, vacumeters and valves have to be protected.

2.10.4 Differential pumping calculations

To restrict the Ar flow from the REXTRAP (Ar pressure inside the TRAP is <$1\cdot10^{-3}$ mbar) to the REXEBIS, five differential pumping stages are introduced along the transport line with a turbo pump in each section, see Figure 41. Moreover, there are two orifices inside the trap, so the Ar pressure immediately outside the trap will be ~10^{-5} torr. For the moment, the transport line is not finally designed, and only an approximate estimation of the final partial Ar pressure at the EBIS is possible. Assuming four transport line orifices (A, B, C and D, radius=5 mm) situated as shown in Figure 41, and four pumps with pumping speed S=400 l/s, the pressure in the EBIS optics tube will be 10^{-12} torr. The two 90º bends of the structure is overseen which will decrease the conductance and improve the vacuum values.

The fifth differential pumping stage into the collector consists of a 50 mm long tube with 5 mm radius. At the collector the Ar pressure is down at 10^{-14} torr. No further pressure decrease caused by differential pumping into the trap will occur since the NEG strips do not pump Ar. If needed, shrinking the radius of the orifices to 3 mm will improve the vacuum almost 3 orders of magnitude ($5\cdot10^{-17}$ torr at the collector).

2.10.5 Gas desorption from the collector

Residual gases can originate from desorption caused by electron bombardment of the collector surface. This phenomenon has been investigated in many publications [125,126], and the results do not always harmonise (see e.g. [127]). In ref. [128] the gas evolution at continuous bombardment of copper surfaces was studied at current densities up to 4 mA/cm^2 with electron energies in the range of 0-3 keV (beyond 200-300 eV electron energy, the desorption yields only increase very slowly with energy [125,126]). The material had been baked out at 200 ºC for 6 hours, and the measurement was done at a base pressure of $2\cdot10^{-10}$ torr. The partial desorption efficiencies η (number of desorbed molecules per electron impact) were determined to be:

$\eta(H_2)=7\cdot10^{-6}$, $\eta(CO)=3\cdot10^{-6}$, $\eta(CO_2)=2\cdot10^{-6}$, $\eta(CH_4)=5\cdot10^{-8}$ molecules/electron

A higher current density load (~8 mA/cm^2 for the REXEBIS collector) leads to less desorption [125,126], and the combination of higher bakeout temperature and longer baking time, should lead to maybe one order of magnitude smaller desorption coefficients, i.e.

$\eta(H_2)=7\cdot10^{-7}$, $\eta(CO)=3\cdot10^{-7}$, $\eta(CO_2)=2\cdot10^{-7}$, $\eta(CH_4)=5\cdot10^{-9}$ molecules/electron

Thus, with I_e=0.5 A the gas load is:

$Q_{coll}(H_2)=1\cdot10^{-8}$, $Q_{coll}(CO)=5\cdot10^{-9}$, $Q_{coll}(CO_2)= 3\cdot10^{-9}$, $Q_{coll}(CH_4)=8\cdot10^{-11}$ torr·*l*/s

The pressure increase Δp(gas) for each gas is given by:

$$\Delta p(gas) = \frac{\eta(gas) I_e kT}{eS} \qquad \textbf{(54)}$$

With only the 180 *l*/s turbo pump connected, the partial gas pressures in the collector region will be:

$p(H_2)\sim 1\cdot10^{-10}$, $p(CO)\sim 3\cdot10^{-11}$, $p(CO_2)\sim 2\cdot10^{-11}$, $p(CH_4)\sim 8\cdot10^{-13}$ torr

In addition, differential pumping in the solenoid bore (accomplished by the three support plates at z=400, 600 and 775 mm and the NEG surfaces) will improve the vacuum for collector out-gassed H_2, CO and CO_2. Only CH_4 is unaffected by the NEG pumping. Before a run the collector can be cleaned by sweeping the electron beam over the collector surface. As a final remark, one should point out that the experience from the electron collector at the electron cooler at MSL suggests that out-gassing problems are of minor importance [129].

2.10.6 Overall vacuum calculations

Due to the large uncertainties in out-gassing constants, very detailed vacuum calculations are pointless, and approximate models give reasonable vacuum estimations. We have implemented a very rudimentary model including:

- the collector
- the three supporting plates (conductance limiting) between the collector and the trap centre
- the turbo pumps, the NEG strips and the sorbing titanium
- the collector gas desorption
- the out-gassing from the inner structure

and calculated the trap pressure for different scenarios. The results are presented in Table 13, and the most likely values lie probably somewhat closer to the higher estimation 'Out-gassing from inner structure and collector' than the more wishful 'Out-gassing only from inner structure'.

(torr)	H_2	CO	CO_2	CH_4
Trap region				
Out-gassing from inner structure + collector	$5\cdot10^{-12}$	$3\cdot10^{-12}$	$2\cdot10^{-12}$	$5\cdot10^{-13}$
Out-gassing only from inner structure	$9\cdot10^{-13}$	$3\cdot10^{-16}$	$3\cdot10^{-16}$	$1.2\cdot10^{-14}$
Collector region				
Out-gassing from inner structure + collector	$6\cdot10^{-12}$	$5\cdot10^{-12}$	$4\cdot10^{-12}$	$5\cdot10^{-13}$
Out-gassing only from inner structure	$9\cdot10^{-13}$	$3\cdot10^{-16}$	$3\cdot10^{-16}$	$1.1\cdot10^{-14}$

Table 13. *Vacuum estimations. The pressures are based on the following inner structure out-gassing rates: $q_{desp}(H_2)=5\cdot10^{-13}$, $q_{desp}(CO)=1\cdot10^{-16}$, $q_{desp}(CO_2)= 1\cdot10^{-16}$, $q_{desp}(CH_4)= 5\cdot10^{-16}$ torr·l/cm^2·s, and a collector gas desorption of $Q_{desp}(H_2)= 1\cdot10^{-8}$, $Q_{desp}(CO)= 5\cdot10^{-9}$, $Q_{desp}(CO_2)=3\cdot10^{-9}$, $Q_{desp}(CH_4)=8\cdot10^{-11}$ torr·l/s.*

2.10.7 Ion extraction spectrum

We are now able to make an absolute prediction of the number of residual gas ions produced during one breeding period, i.e. to decide the residual gas contamination of the extraction spectrum. Spectra for the two extreme cases:

- inner structure + collector out-gassing + high argon diffusion from the trap
- inner structure out-gassing + low argon diffusion from the trap

are plotted in Figures 42 and 43. Included is also the charge distribution for a typical radioactive ion: 10 000 ^{30}Na ions. The breeding time is set to optimise charge-state 8^+. Since the N_2 pressure is uncertain, it is assumed to have the same partial pressure as O_2 (In reality probably lower, which should give an overestimation of the N_2 peaks.) The calculations of the breeding spectra do not include the spherical correction of binding energies [71].

From the extraction spectra it is clear that a mass selection system with a good resolution is needed after the REXEBIS to separate the residual gas peaks from the radioactive peaks, since the number of rest-gas ions can exceed the radioactive ions with several magnitudes of orders. The Mass separator has a Q/A-resolution of ~150.

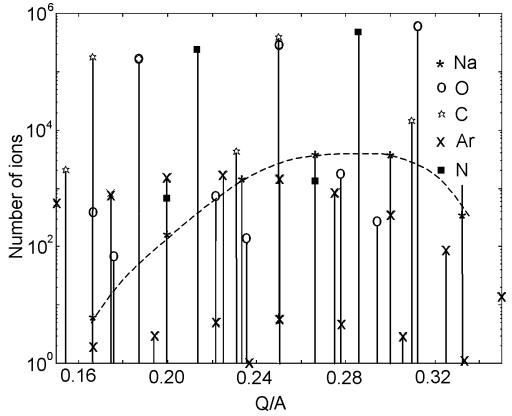

Figure 42. *Calculated Q/A spectrum showing the absolute number of residual and radioactive ions. Breeding time 13 ms; 10 000 ^{40}Na ions; collector out-gassing included; high Ar diffusion from the REXTRAP (^{16,17,18}O, ^{12,13}C, ^{14,15}N, ^{36,38,40}Ar isotopes are present).*

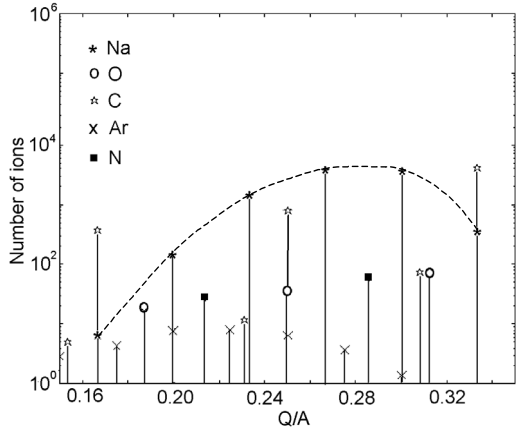

Figure 43. *Calculated Q/A spectrum showing the absolute number of residual and radioactive ions. Breeding time 13 ms; 10 000 ^{30}Na ions; collector out-gassing not included; low Ar diffusion from the REXTRAP (^{16,17,18}O, ^{12,13}C, ^{14,15}N, ^{36,38,40}Ar isotopes are present).*

2.11 Beam diagnostics

A major dilemma is to guide the ion beam into the trap region of the EBIS, and after breeding extract it in an efficient way to the Mass separator (Figure 8). We are dealing with extremely low beam intensities, and it is practically impossible to insert any kind of detector inside the trapping region to confirm a correct injection. Here follows a description of the beam diagnostics that we have considered so far.

2.11.1 Emittance meter

It is important to measure the EBIS emittance for beam transport and mass analyser design reasons. Different methods exist, and most commonly a narrow slit is swept over the beam profile to determine the angular beam spread in one dimension for each slice of the beam [131,132]. A one-dimensional transverse emittance measure is then obtained.

A more sophisticated device involves a so-called pepperpot (see Figure 44). The beam passes through a plate (thickness δ) that is penetrated with a two-dimensional array of small holes (radius d). After a free-space propagation D, the beam hits a detector, in our case a fluorescent plate, and the beam spots are recorded by a CCD camera [132,133,134]. From the sizes and positions of the beam spots, a variety of information is obtained, e.g.:

- relative current density of the beam
- if the beam is converging or diverging
- complete four-dimensional phase space distributions
- horizontal and vertical phase space plots if the motions are separable in x and y

A few important design details to keep in mind are that the plate thickness δ should be small to avoid vignetting, i.e.:

$$\delta\Delta\theta << d \qquad \textbf{(55)}$$

and that the width of the particle profile at the detector must be large as compared to the dimension of the aperture, in other words:

$$D\Delta\theta >> d \qquad \textbf{(56)}$$

Our emittance meter has a design as is shown in Figure 45. The exact distances have to be settled after tests since they are dependent on the actual beam divergence and focal spot size.

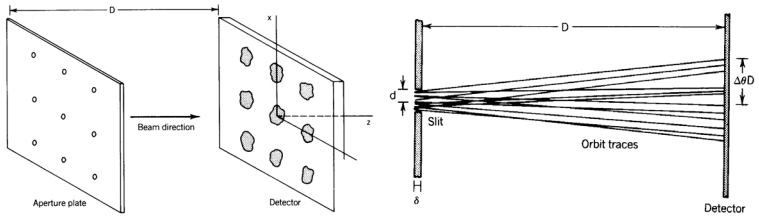

Figure 44. *Principle of the pepperpot emittance diagnostics [130].*

During the autumn 1997 we carried out pre-tests on such a device to determine a suitable fluorescent plate material and found that a scintillator screen of YAG:Ce (commercial name P46) has a higher light intensity than CsI:Ti (usually used for low energetic ion beam detection), see Table 14. The transverse resolution (estimated to ~0.1 mm) seems also to be better due to a thinner active layer, and since the fluorescence material is evaporated on a glass substrate it facilitates observation from the back. The tests appear very promising, and we hope to assemble a system in the near future. Though, one has to keep in mind that the REX-ISOLDE intensities are very low. The CRYSIS tests were performed with a total output charge of ~1 nC at the beam line Faraday cup, with approximately 25% transmission from the Faraday cup to the pepperpot. The beam focus at the pepperpot was estimated to 4·4 mm^2, and the

pepperpot hole diameter was 0.15 mm. Under these conditions the fluorescent spots on a P46 plate mounted directly behind the pepperpot were clearly visible both with a naked eye and with an ordinary, non-cooled and non-integrating, CCD camera. However, typical output charges for the REXEBIS (including residual gas) will be ~0.0001 nC; the beam-spot size ought to be at least 10·10 mm^2; the beam transmission is >90%; the pepperpot hole diameter 0.1 mm; the distance between the pepperpot and the fluorescent plate ~100 mm. Taking all these facts into considerations, it is easy to realise that the detection will be a bit of a challenge. Furthermore, since the fluorescence response is not linear with respect to the impinging ion intensity it is difficult to judge how large the beam spots are, and thereby to obtain a quantitative value of the emittance.

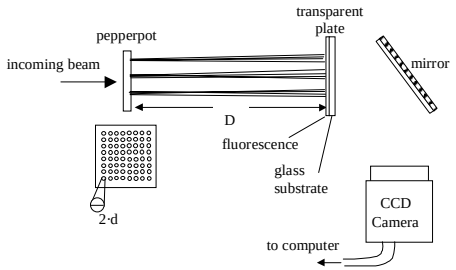

Figure 45. *Possible emittance meter design for the REXEBIS based on the 'pepperpot fluorescent-plate CCD-camera' method.*

P46	CsI:Ti
3 mg/cm^2 YAG:Ce as phosphor	~0.5 mm thick fluorescence, non-transparent
2 mm thick float glass substrate	Slightly hygroscopic
Covered with 5 nm Al layer reflector	No conducting covering layer
Yellow green emission colour, 560 nm	550 nm emission wavelength
100 ns decay time to 10%	900 ns decay constant

Table 14. *Fluorescent material properties.*

2.11.2 Other beam diagnostic devices

Apart from an emittance meter a current quadrant detector may be installed in connection with the inner differential pumping tube. Such a device is able to detect misalignments of an injected pilot-beam (a test beam that has higher intensity than the ordinary radioactive beam) with a total pulse charge below pC [135], which is at the limit of the 10^7 ions the Penning trap can bunch and cool. However, the use of a pilot-beam may produce slightly faulty settings since it is claimed that the trap performances will change when going from a space-charge compensated trap (pilot beam case) to few ions (real radioactive beam case).

Another possible injection-optimising action is to extract a single-charged beam from the REXEBIS and guide it backward into the transport line between the REXEBIS and the REXTRAP. At the symmetry point of the transport line a two-way detector could be placed, which would be of guidance when setting the extraction parameters of the Penning trap and the transport line.

It has also been suggested to mount a MCP at the 2nd bender focus to check the injection focal position and spot size.

2.12 Platform HV switching

The REXEBIS is situated at 60 kV potential during injection[7], allowing the cooled 60 keV ions extracted from the REXTRAP to be captured. During the breeding period, the potential is decreased to about 20 kV. A low extraction voltage results in a low RFQ injection energy, thus an efficient, adiabatic bunching and small output emittance from the RFQ. The RFQ is optimised for an ion energy of 5 keV/u,

[7] Actually, the ions are extracted from the REXTRAP with an energy of ~59 700 eV. This is a more correct potential value the REXEBIS will be at during injection, even if a value of 60 kV is stated throughout this report.

and since 1/4.5<Q/A<1/3, the extraction voltage U_{ext} should be variable between 15 and 22.5 kV. Figure 46 illustrates the platform potential function.

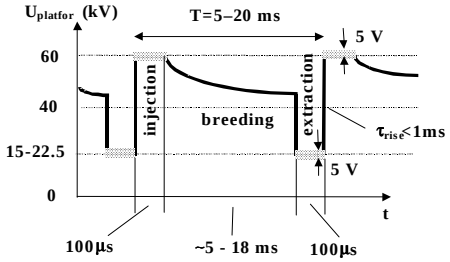

Figure 46. *REXEBIS platform potential relative to ground potential during two cycles. (The internal REXEBIS voltages, for instance the barrier tube voltages, are related to this platform potential).*

2.12.1 Design proposals for HV switching

Two different angles to attack the HV switching problem have been considered. The first involves a static REXEBIS platform at 20 kV and a drift tube arrangement to retard the beam during injection, see Figure 47. Its properties are summarised below, and one can conclude that the solution is not very attracting.

- a long drift tube is required: ~2 m
- lenses are needed inside the drift tube
- focusing difficulties: large beam radius and beam aberrations
- maximum Penning trap extraction time has to be short: <1 µs
- short switching time: ~0.5 µs between 40 kV and 0 V

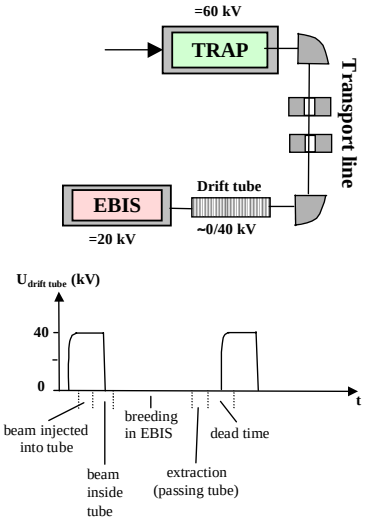

Figure 47. *Drift tube arrangement to retard the 60 keV beam. At injection the tube is at 40 kV (relative to ground potential) so the ions move with 20 keV inside. Before they leave the tube to enter the REXEBIS, the tube potential is decreased to 0 V, and since the EBIS is at 20 kV, the ions have just enough energy to climb the EBIS potential, and consequently they are trapped inside the EBIS. During extraction the tube is still at ground potential until the ions have reached the Mass separator, and then it is immediately raised to 40 kV to be prepared for a new cycle.*

An alternative to the drift tube is to switch the complete EBIS between 60 kV (at injection) and 20 kV (at extraction). This has some advantages, e.g. a longer switching time can be allowed. On the other hand, the capacitance to switch is larger (~1 nF).

+ a compact system
+ allows longer Penning trap extraction time (<100 µs); now limited by the EBIS trap design
- difficult to switch the REXEBIS between 20 and 60 kV

Several different circuit layouts for switching of the complete REXEBIS have been put forward by Paal [136], and we will here present one based on two semiconducting switches [137] (electrical scheme in Figure 48). A switching cycle is described here.

1. Assume the REXEBIS platform to be at 20 kV.
2. Open Switch2 and close Switch1. The REXEBIS, represented by C_2=1 nF, will be charged up to 60 kV by the 60 kV power supply in combination with capacitor C_1. The manoeuvre takes a little more than 1 µs (1.4 µs for $U_{platform}$ to reach 59 800 V; thereafter a linear increase to 60 000 V within 5 ms). A quick charge-up is important since we do not want to loose breeding time due to slow switching. In principle, we can allow charging-up times <1 ms.
3. $U_{platform}$ stays at 60 000±5 V during the 100 µs long injection period.
4. Then Switch1 is opened while Switch2 still is unclosed. The REXEBIS capacitance will slowly (τ=40 ms) discharge to 40 kV.
5. Just before extraction Switch2 is closed, and the REXEBIS is discharged to 20 kV within about 15 µs. In this way the breeding time is variable between 5 and 20 ms depending on the required charge-state. The platform charge is taken care of by the large capacitor C_3. The voltage stability should be 20 000±5 V for the extraction period.

When realising this circuit one has to be aware of not overloading the switches, and therefore build in miscellaneous security mechanisms, and not run it with too short period time. Inherent inductances in the circuit may cause unacceptable ripples, and this has to be investigated in practice.

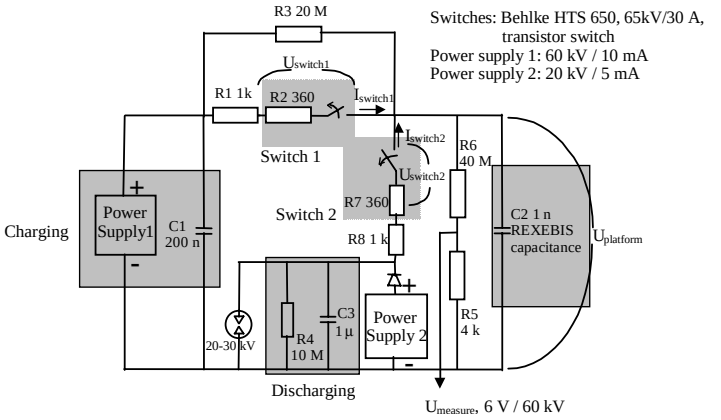

Figure 48. *Proposal for REXEBIS platform switching based on two semiconducting switches.*

Other imaginable schemes we have looked into comprise a current generator, a high voltage tube amplifier or a commercially designed power supply. The latter solution was chosen in the end. Since it is preferable, from the power supply point of view, to keep the voltage swing below 40 kV, the ISOLDE separator could be run at a lower energy than 60 keV, perhaps 55 keV. Then a 40 kV switching supply could reach the required 15 kV which is needed for Q/A=1/3.

2.12.2 Platform power

The power needed on the REXEBIS platform is delivered by a motor-generator arrangement. A transformer would be a less awkward solution, but the higher capacitance of such a device makes the switching more problematic. The motor is positioned on the mechanical platform and grounded, while the generator is electrically insulated and impelled by an insulating rod. The generator is physically separated from the REXEBIS platform, but is electrically connected with it, i.e. situated on 20/60 kV.

Motor	Generator
3-phase	3-phase
15 kW	15 kVA
380/660 V Δ/Y	400 V
31.5/18 A	21.7 A

Table 15. *Motor-generator data.*

2.13 Electronics

Most of the electronics is physically situated in the racks on the REXEBIS platform. One of the racks, containing the electron gun, the suppressor and the collector supplies, is on -5 kV relative to the REXEBIS platform. This has been arranged by insulating the inner shelves from the rack cabinet, so the rack can be placed directly on the platform without electrical insulation. The power to the rack is delivered by a 5 kVA transformer. The other two racks, containing the magnet supply, pump controls, power supplies etc, are on REXEBIS potential. Furthermore, there will be one rack on ground potential for beam optics supplies, pump controls etc.

2.13.1 Power supplies

There are in total 17 power supplies (+2 optional) for the REXEBIS. The power supplies can be divided into DC type, slow beam optics supplies (ms), and fast switching trap supplies (μs). A VME-computer at ground potential controls the power supplies, either directly, or via function generators situated on the platform.

2.13.2 Control parameters

The parameters that have to be controlled can in principle be divided into the following groups:

- Vacuum – turbo pumps, vacuum gauges and valves
- Magnet – magnet current, magnet field, LqHe and LqN_2 levels
- Beam diagnostics – Faraday cup, channel plate and TOF
- Power supplies – trap electrodes, beam optics, gun, collector etc
- Baking system

Some signals are read/write, but most of them are only write. See further Appendix 3 for a complete list of control parameters.

2.13.3 Control system

A number of EBIS voltages have to be synchronised in time for the system to work; not only to each other but also to the REXTRAP and the following LINAC. A convenient solution is to integrate the control systems for the REXTRAP and the REXEBIS, and such a system has been development by the two groups. In total there are three high voltage platforms plus the ground potential. On ground potential, a VME-computer running OS9 as operative system is situated. This controls the on-line working and the synchronisation of the Penning trap and the EBIS. As user-interface to the VME-computer an ordinary PC is used, communicating with the former via the ISOLDE Ethernet. Due to the potential difference between the three platforms all data have to be transmitted via optical fibre links (TTL and PROFIBUS [138]). The microsecond switching of the drift tubes is done by Simple Analog Function Generator (GFAS) [139]

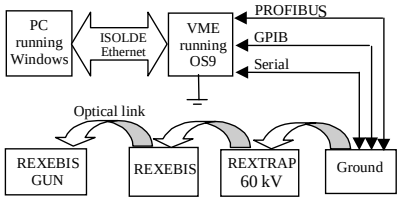

Figure 49. *The principle of the REXTRAP and REXEBIS control system [140]. (NB! The optical links are two-way.)*

placed on ground and connected via optical fibres to 14-bit precision General DAC for GFAS (GFAD) [139] situated on the HV platform. In an identical way the two beam optics lenses are controlled even if the switching times are more relaxed (~1 ms). The control of the supply for the platform HV switching calls for high accuracy and stability, which can not be fulfilled by a 14-bit DAC, and therefore a 16-bit precision GFAD with a low temperature drift coefficient is used. Figure 49 shows the layout of the control system.

2.14 Mechanical platform

The complete REXEBIS apparatus is placed on a mechanical platform (to be distinguished from the REXEBIS high voltage platform) diagonally above the REXTRAP, approximately 3.5 meter above the floor level (see Figure 2). Space restriction in the hall is the motivation for positioning the EBIS one level above the TRAP and the LINAC. The platform is made of steel and is supported by 7 stands to the floor. On this mechanical platform the REXEBIS high voltage platform is positioned, including the EBIS and three electronics rack. It is insulated by 300 mm insulators from Siemens made of epoxy to allow the REXEBIS platform to jump between 20 and 60 kV. The motor-generator has been recuperated from old ISOLDE, and the motor and generator are mounted on a common frame, with the generator electrically insulated from ground. It is foreseen to have the motor-generator situated on the same mechanical platform as the EBIS, since the result from a vibration investigation implies that they are tolerable by the EBIS and the transport beam line. A maximum weight distribution is shown in Figure 50. For security reasons the entire apparatus is surrounded by a high-voltage cage, which is semi-transparent to allow supervision of the instruments in the racks.

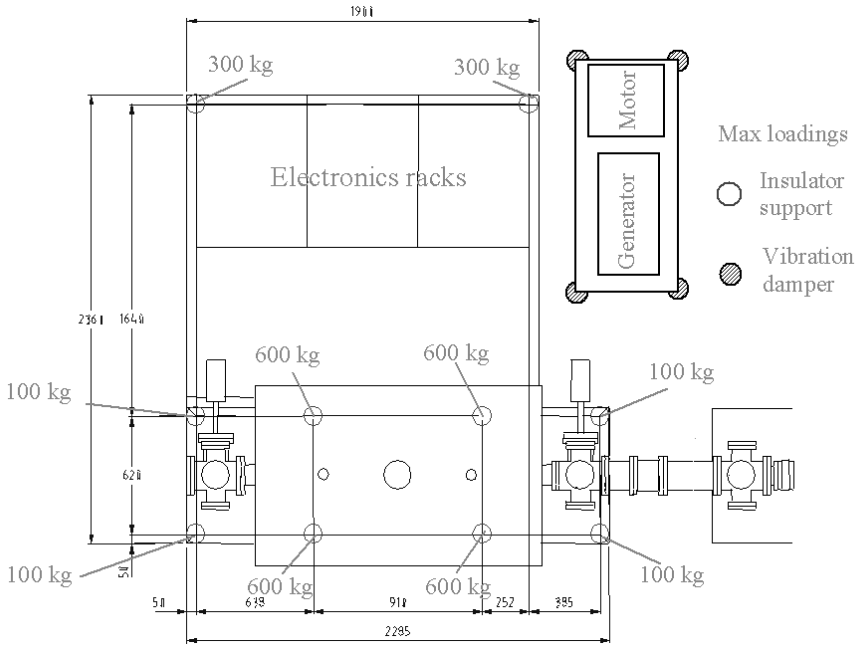

Figure 50. *Top view of the layout with worst case weight distribution on the mechanical platform.*

Part III – SIMION simulations

3.1 Implementation of an EBIS model in SIMION

3.1.1 SIMION 3D

SIMION 3D 6.0 [141] is a simulation program that models ion optical problems in 3D asymmetrical electrostatic and magnetic potential arrays. It traces the charged particles and displays them together with the electrostatic/magnetic structure. SIMION 6.0 incorporates user programming – a feature that allows the user to include any required function.

3.1.2 The physical model

The implementation of the physical EBIS model followed the basic structure used by Axelsson [142] in the investigation of CRYSIS, but the model was refined and extended to comprise a complete injection, breeding and extraction cycle. The SIMION model included the following features:

- Time-varying electric potentials produced by the switched tubes and optics elements
- Magnet field from the solenoid
- Space-charge potential from the electron beam
- Charge multiplication within the electron beam

Not included in the model were:

- Heating, i.e. momentum transfer in ion-ion or electron-ion interactions
- Ion-ion or ion-atom interactions leading to electron transfer (charge exchange processes)
- Space-charge effects from the ions

The model was of so-called zero order, that is no momentum transfer from electron-ion or ion-ion Coulomb collisions were included, nor recombination or charge exchange events. The electron-ion mixture was simply not regarded as a plasma, instead the tracked ion moved as a single particle in the electric and the magnetic fields. The main justifications for this simplification are the low desired Q/A-value (gives little time for heating) and the low residual gas pressure (minuscule chance for electron pick-up from rest-gas).

3.1.2.1 Electrical field

The REXEBIS structure was modelled with its transport, trap and barrier tubes, the suppressor and collector, the extractor and the injection/extraction optics. Due to the switching of the platform potential and the varying drift tube voltages, the structure potentials were changed between injection and extraction.

As a consequence of the electron beam space-charge – the second electrical force contribution – the positive ions are trapped radially along the EBIS axis by the radial field given as:

$$E_r = \begin{cases} \dfrac{\rho_l}{2\pi\varepsilon_0}\dfrac{r}{r_{ebeam}^2} & r < r_{ebeam} \\ \dfrac{\rho_l}{2\pi\varepsilon_0}\dfrac{1}{r} & r_{ebeam} < r \end{cases} \qquad \textbf{(57)}$$

where ρ_l is the electron beam charge per unit length and r_{ebeam} the electron beam radius. The attenuation of ρ_l in the collector (due to electron absorption) was incorporated by multiplying ρ_l with $(r_{surface}(z)/r_{ebeam}(z))^2$ and, by so doing, determine the fraction of electron beam found inside the radius of the limiting potential surface, $r_{surface}(z)$, (the trap tubes, the extraction tubes, the suppressor and obviously the collector). The variable $r_{surface}(z)$ was approximated by:

$$r_{surface}(z) = r_{tube} + \frac{r_{collector} - r_{tube}}{1 + exp(-C_1(z - z_{collector}))} \qquad \textbf{(58)}$$

where $r_{collector}$ and $z_{collector}$ denote the radius and position of the collector, respectively, and C_1 is a positive constant. An approximation of the axial field E_z was derived from the potential ($V(r,z) = -\int E_r(r,z)dr$) by the derivative ($E_z = -\partial V/\partial z$), resulting in:

$$E_z \approx \begin{cases} -\dfrac{\rho_l}{2\pi\varepsilon_0}\left(\dfrac{r^2}{r_{ebeam}^3}\dfrac{\partial r_{ebeam}}{\partial z} + \dfrac{r_{ebeam}r_{surface}\dfrac{\partial r_{surface}}{\partial z} - r_{surface}^2\dfrac{\partial r_{ebeam}}{\partial z}}{r_{ebeam}^3}\right) & r < r_{surface} < r_{ebeam} \\ \dfrac{\rho_l}{2\pi\varepsilon_0}\left(\left(\dfrac{1}{r_{ebeam}} - \dfrac{r^2}{r_{ebeam}^3}\right)\dfrac{\partial r_{ebeam}}{\partial z} - \dfrac{1}{r_{surface}}\dfrac{\partial r_{surface}}{\partial z}\right) & r < r_{ebeam} < r_{surface} \\ -\dfrac{\rho_l}{2\pi\varepsilon_0}\dfrac{1}{r_{surface}}\dfrac{\partial r_{surface}}{\partial z} & r_{ebeam} < r < r_{surface} \end{cases} \qquad \textbf{(59)}$$

Due to an incorrect derivation a different expression for the axial field E_z was used in the simulations. This affected the results in a way that the rectangular form of the acceptance phase-space became extra accentuated.

The ion-ion interaction is the third electrical force contribution, but this was neglected due to the intricacy to model space-charge effects caused by ions. The few injected ions and the expected low residual gas pressure could motivate the assumption, and the validity of it is discussed in sec. 3.2).

3.1.2.2 Magnetic field

SIMION has not the potentiality to handle solenoid fields directly in its potential arrays, so the field was implemented as a user defined field force. An approximation of the following form was used for the axial magnetic field [92]:

$$B_z(r,z) = \frac{B_0}{1 + exp(-A_0(z - z_0))} + \frac{B_1}{1 + exp(-A_1(z - z_1))} \qquad \textbf{(60)}$$

$$-\frac{r^2}{4}\left(\frac{B_0A_0^2\,exp(-A_0(z-z_0))\cdot(1-exp(-A_0(z-z_0)))}{(1-exp(-A_0(z-z_0)))^3} + \frac{B_1A_1^2\,exp(-A_1(z-z_1))\cdot(1-exp(-A_1(z-z_1)))}{(1-exp(-A_1(z-z_1)))^3}\right)$$

where B_0, B_1, A_0, A_1, z_0 and z_1 are magnet dependent parameters. Figure 51 shows a comparison between the OPERA 2D calculated and approximated values for B_z along the REXEBIS axis. The agreement is very good for field strengths above 10^{-3} T, but the analytic formula does not emulate the field increase at the collector iron-cylinder ending. The radial magnetic field, to the 3rd order in r, is given as:

$$B_r = -\frac{1}{2}\frac{\partial B_z}{\partial z}r + \frac{1}{16}\frac{\partial^3 B_z}{\partial z^3}r^3 \qquad \textbf{(61)}$$

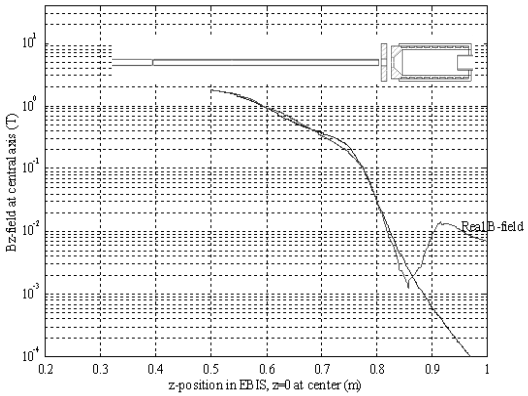

Figure 51. *A comparison between measured B_z-field along the central axis and its approximation. A drawing of collector and part of the drift tubes relates the magnetic field to the solenoid. Note the logarithmic scale.*

3.1.2.3 Ionisation process

To obtain a realistic breeding scenario the random ionisation within the trap had to be included in the model. Ions within the electron beam had at each calculation time-step a certain probability, proportional to the ionisation cross-section and electron beam current density, to be further ionised. The cross-section for ionisation was calculated with Lotz's approximate electron ionisation cross-section formula for positive ions (see sec. 2.2.1).

In a real EBIS the ions are reflected forth and back between the two longitudinal potential barriers a numerous times during trapping; the number of reflections are determined by the injection energy and confinement time. To avoid the time-consuming calculation of forth and back tracing of ions, the ionisation cross-sections were multiplied by a factor so that only one turn within the trap corresponded to a desired confinement time.

3.1.2.4 Calculation accuracy

Despite the shortened tracking length, computationally achieved by the increase of the ionisation cross-section, the ion tracking required considerable CPU-time; a normal injection/breeding/extraction run with a few hundred ions lasted several days on a 120 MHz Pentium. The tracing time-step length was 0.5 ns, and energy conservation tests were performed to examine the calculation accuracy. If mono-energetic 1^+ ions were injected and hindered from ionisation, and thereafter extracted (i.e. still as 1^+ ions), the final energy spread was $\sigma(E_{out}(1^+))$~2.3 eV. An upper estimation of the spread caused by energy non-conservation for 8^+ ions would then be $\sigma(E_{out}(8^+))<8\cdot 2.3$ eV~18 eV.

3.2 Space-charge simulations

When performing beam tracing the space-charge from the propagating beam is one of the main complications, and it is usually overcome with so called Self-Consistence Calculations (SCC). In the SIMION simulations the ion space-charge effect was omitted, and the following calculations will motivate the approximation, at least in a region without external fields. The ion-beam space-charge effect inside the trap is on the other hand laborious to estimate.

3.2.1 Model description

After extraction from the trap and collector regions the ions enter a field free region where they propagate in a bunch, all with approximately equal axial velocities, repelling each other via Coulomb interaction. The number of ions per unit length n_{ion} is dependent on the extraction time t_{ext}, the extraction voltage U_{ext} and the number of trapped ions N_{ion} (see Box 5). In the simulations a fraction of the total pulse was cut out and all ions within the test bunch were traced repeatedly until a self-consistent solution was found (approximately three iterations were required). The test bunch length ΔL must be chosen much larger than the beam radius (even after space-charge blow-up) to minimise the influence from the end boundaries (i.e. the axial ends of the test bunch where the ions only experience Coulomb forces from the bunch centre). Very long test bunch lengths ΔL were tested with consistent results.

3.2.2 Space-charge simulation results

For typical REXEBIS extraction conditions (given in Box 5), the beam radius increase is 0.01 mm over a 0.2 m drift distance, with an emittance growth of $2\cdot 10^{-3}$ π·mm·mrad. The emittance increase should be compared with the nominal value of about 10 π·mm·mrad. Thus, the radius and emittance increase due to space-charge can safely be neglected.

Inside the trap region there exists a strong electrical force from the electron beam and a magnetic field from the solenoid, so the above field-free calculations are not valid. The Debye length (the distance it takes for a plasma to shield itself from an applied continuos electric field) inside the trap equals:

$$\lambda_D = \sqrt{\frac{\varepsilon_0 k T_e}{e^2 n_e}} \qquad \textbf{(62)}$$

Due to the directed electron beam flow in an EBIS, the Debye length is different in axial and radial direction, for the REXEBIS λ_D(axial)~$9\cdot 10^{-4}$ and λ_D(radial)~$1\cdot 10^{-4}$ m.

Assuming that the trap contains 10^6 ions, each mm^3 will contain ~6000 ions, thus the Coulomb interaction between the ions can not be excluded. However, the magnitude of the beam blow-up due to the space-charge is difficult to estimate, and SIMION does not support Self Consistence Calculations and it would be fairly difficult to include.

Box 5. Space-charge influences on beam radius and emittance.

The different steps in the SCC of the beam blow-up for an ion beam propagating exclusively under space-charge influence were:

1. Distribute $n_{ion}\cdot\Delta L$ over a cylinder with radius r_0 and length ΔL.
2. Let all ions have the same initial axial velocity and no transverse velocity component, i.e. $\varepsilon_{start}=0$.
3. Trace each ion separately over the distance L, and let it Coulomb-interact with all other ions that are moving parallel to the z-axis with no transverse velocity components this first trace.
4. Record the positions for all ions during the trace.
5. Retrace each ion separately over the distance L, and let now the ions Coulomb-interact with all other ions at their positions from the last trace.
6. Repeat (4) and (5) until a convergent solution is obtained.
7. Read final beam-radius and transverse velocities and calculate the emittance increase.

Simulation conditions

Number of trapped ions $N_{ion}=1\cdot 10^7$
Initial beam radius $r_0=0.1$ mm
Extraction voltage $U_{ext}=20\,000$ eV
Ion charge $q_{ext}=8^+$
Ion mass $m_{ion}=30$ u
Test bunch length $\Delta L=1$ mm >>r

Simulation results

Radius increase after 0.2 m drift $\Delta r=0.01$ mm
Emittance increase $\Delta\varepsilon=2\cdot 10^{-3}$ mm·mrad

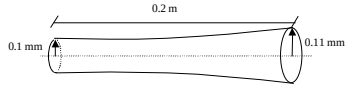

$$n_{ion} = \frac{N_{ion}}{t_{ext}\sqrt{\frac{2U_{ext}q_{ext}}{m_{ion}}}} = \frac{10^7}{100\cdot 10^{-6}\sqrt{\frac{2\cdot 20000\cdot 8e}{30u}}} \approx 100000 \qquad \textbf{(63)}$$

3.3 Acceptance and emittance

Radioactive ions are valuable and difficult to produce in large amounts, therefore the requirement on the beam transport efficiency, including the REXEBIS, is high in the REX-ISOLDE project. To guarantee the efficiency, extensive analyses of the EBIS injection and extraction have been performed, analytically as well as with simulations. To our knowledge, complete injection and extraction simulations of an EBIS have not been performed before, so therefore we have developed a model and implemented it in SIMION. Even if the simulations started off with the specific aim to determine the REXEBIS emittance, they soon became more general involving for instance investigations of the emittance dependence on ion charge and mass, as well as on magnetic field strength in the EBIS. Hence, the results of the analysis presented in this chapter are in most cases of general applicability, also on other EBISs.

In the REXEBIS we will utilise ion injection, i.e. already 1^+ ionised ions are injected in the EBIS for further breeding. This procedure is somewhat more complicated than gas injection, at which gas atoms/molecules are let into the ionisation region by diffusion, where they are ionised and trapped. The reason for the difficulty is to inject the ions in a proper way, so they are trapped within the electron beam and not bounce at the magnetic mirror when they try to enter the EBIS. If the ions enter the EBIS with too large radii or divergence, they will either oscillate too violently in radial direction due to the electrostatic force from the electron beam, or pick up a too large azimuthal momentum due to the magnetic field, and are for those reasons reflected back. In other words, an effective injection requires a small ion beam radius and little divergence. The injected ions will distribute their energy between potential energy in the electron beam well and kinetic energy (longitudinal, azimuthal and radial momentum) depending on the injection conditions.

Some of the simulations were performed with gas injection conditions since that imitates the way the residual gas is ionised. The atoms are then ionised at random radius (within the electron beam), with no initial kinetic energy (the thermal velocity is negligible compared with the electron beam potential well energy).

Due to the axis-symmetrical geometry of an EBIS, the horizontal and vertical phase space plots are in principle identical, and in this report they are often referred to as the transverse phase space.

3.3.1 Emittance definitions

Since acceptance and emittance are vital for the evaluation of beam properties, we will here shortly explain what emittance is, and define a few measures. For a more extensive treatment we refer to for instance ref. [130] or to the notes from CERN Accelerator School [143]. Neglecting mutual interaction and coupling between the three movement directions of a particle, the emittance is defined for each degree of freedom; horizontal, vertical (transverse emittances) and longitudinal.

3.3.1.1 Transverse emittance/acceptance

The transverse emittance ε, horizontal or vertical, is a measure of the parallelism of the beam and it is proportional to the area filled by the trajectories in the phase space plot. Smaller phase space area, i.e. smaller emittance, means a better quality of the beam, implying better beam focusability or parallelism. The phase space plot in turn is a plot of the x-x´ or y-y´ values for all particles in the beam at a certain longitudinal position z (the beam propagates along the z-direction), where x´=dx/dz and y´=dy/dz (Figure 52). In this context one often speaks about phase space ellipses because with linear focusing elements the trajectories follow elliptical paths in phase space, so elliptical phase space distributions remain elliptical[8]. We define the emittance as the area filled by the trajectories in a phase space plot. That means for an ellipse the emittance is the product of the two semi-axes of the ellipse multiplied by π. To easier calculate the emittance value, a phase space plot can be converted to upright position. In reality, that equals a translation in z-direction to the focal point of the beam.

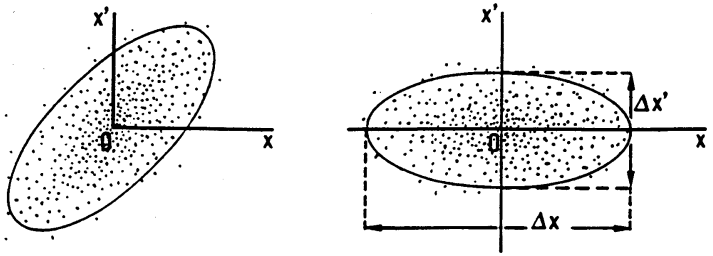

Figure 52. *A set of points representative for a beam in the (x,x´) phase space; tilted (left) and upright (right) emittance ellipses.*

According to Liouville's theorem the phase space is invariant in an ideal focusing system, that is in a system without dissipative forces, without particle loss (or gain), and where the applied forces and beam-generated forces act over large length scales in comparison with the interparticle spacing. In other words, the emittance is a conserved quantity when a beam is subject to reversible processes. Nonetheless, non-linear forces can warp the phase space of the distribution, enlarging the practical phase space volume[9]. When there is acceleration involved, the normalised emittance is conserved, defined as $\varepsilon_N = \varepsilon\beta\gamma$ where β and γ are the relativistic quantities.

Above the emittance was defined as the total phase space *area*, while others prefer to divide this value with π and designate that the emittance. The confusion is widespread! However, throughout this document the term 'geometrical emittance' refers to our "area"-definition, and the used encircling area

[8] Nevertheless, in this chapter we will encounter a rhomboidal phase space defining the acceptance of an EBIS.
[9] With practical phase space area (or volume) we mean the acceptance phase space area that exists in accelerators, for instance an ellipse.

has either been an ellipse or a rhomboid, no strange butterfly-shaped areas. In some cases this definition is not completely unambiguous since a real beam has no clear envelope in phase space. A practical definition is to define the emittance as the area of the ellipse containing 95% of all the particles in its interior.

Sometimes even such a definition is not satisfying enough, especially if the phase space has become so twisted and bent that its area is not more representative of the spread of the particles. Then a statistical definition, which not relates the emittance to any contour limiting area occupied by the points, is appropriate. Such a definition was given by Lapostolle [144]:

$$\varepsilon_{RMS} = 4\sqrt{\langle x^2\rangle\langle x'^2\rangle - \langle x\cdot x'\rangle^2} \quad mm\cdot mrad \qquad \textbf{(64)}$$

and it is called either 'effective emittance' or 'RMS emittance'. For many realistic beam distributions ε_{RMS} is the emittance that contains 85-90% of the beam. In our work we have preferred not to make comparisons between geometrical emittance values and RMS emittance values. Note that the RMS emittance is not a conserved quantity. (If a straight line in the phase space becomes curved, then the RMS emittance is no longer zero, while that it still the case for the geometrical emittance (using a non-elliptic contour).)

3.3.1.2 Longitudinal emittance

The longitudinal emittance ε_L for a pulsed beam is the area of the time-energy space, i.e. $\varepsilon_L = \Delta E\cdot\Delta t$ π·eV·s, where ΔE is the energy spread and Δt the pulse length. Also here definitions excluding the π exist. To exemplify, the REXTRAP has an estimated longitudinal emittance of ~5 π·eV·s, which means that it can deliver a short pulse with large energy spread, or vice versa.

3.3.1.3 Further explanations and comments

The classification of ions into 0%, 95% and 100% groups denotes how large fraction of the confinement time inside the EBIS (at least) the ions spent within the electron beam. That means, ions that are injected perfectly into the electron beam potential belongs to the 100% set, while the ions within a 95%-set are not fully trapped but spend at least 95% of there time within the electron beam. The shorter time inside the beam is due to worse injection conditions (i.e. a high injection energy in combination with large initial ion trajectory divergence or radius), resulting in larger trajectory radii inside the confinement region and only occasional crossing of the electron beam. Due to the different conditions inside the EBIS for 95% and 100%-ions, they make up different phase spaces and acceptance/emittance values. 0%-ions have only the requirement to enter the trap region without necessarily crossing the electron beam.

In the presented transverse phase space plots '+' denotes ions only partly trapped within the electron beam (<100%-ions) while '*' denote fully trapped ions (100%-ions). Judging from the plots one may think that the phase spaces are hollow, or worm-stung like a Swiss cheese, since there are + signs scattered inside the ellipses. This is not the case, and it is a consequence of the ions not being fully trapped within the phase space in the other transverse plane.

Another detail that may cause confusion is a varying extraction voltage. Even though the ions will be extracted from the REXEBIS at a voltage of 15-22.5 kV, we have chosen to carry out some emittance simulations with 60 kV extraction voltage; just to facilitate comparison between injection acceptances (performed at 60 kV) with extraction emittances. However, the conversion between different extraction voltages is trivial. For example, the 20 kV extraction voltage emittance is related to the 60 kV emittance as: $\varepsilon_{20\,kV} = \varepsilon_{60\,kV}\cdot\sqrt{\frac{60000}{20000}}$, and in the 20 kV phase space plot the divergence values are increased with the same factor as compared to the 60 kV plot.

One limitation in our simulations concerns the determination of the geometrical acceptance/emittance values. What we have done is to include all ions in an upright phase space plot within either an ellipse or a rhomboid and from that determined the geometrical area, i.e. the emittance. However, the inclusion of the ions was done by eye and therefore somewhat arbitrary, so where the statistics were low, the error bars became considerable.

The reader may complain about the poor statistics for the simulations presented in sec. 3.3.3 to 3.3.6, and the complaints are motivated in most cases. The reason for the lacking statistics is the long time needed to complete a run. One simulation had to be performed a number of times before we finally got all conditions correct. The excuse for the latter is a long and fairly complicated user program added to SIMION, and the literally thousands of buttons/options available in the same program.

Finally, we should clarify that the term acceptance is a measure of what emittance value a system can accept as input.

3.3.2 Analytical acceptance expression

An analytical expression for the acceptance was derived following the outline of an emittance determination for ECR sources presented in ref. [145]. The formula was adapted for an EBIS by taking into account the electron beam potential, which induces a large emittance/acceptance contribution. In an ECR, the ions move only with thermal velocities inside the plasma, while in an EBIS the kinetic energy can measure several hundred electron volts. This fact makes a large difference for the acceptance expression. The following derivation gives the geometrical acceptance, as defined above, for ions that are trapped 100% of the time inside a *non-compensated* electron beam.

The motion of a charged particle in an axially symmetric magnetic field can be described by a Hamiltonian function:

$$H = \frac{1}{2m}\left[\left(\frac{p_\theta(kinetic)}{r}\right)^2 + p_r^2 + p_z^2\right] + U(r) = \frac{1}{2m}\left[\left(\frac{p_\theta(canonical)}{r} - qA_\theta\right)^2 + p_r^2 + p_z^2\right] + U(r) \qquad \textbf{(65)}$$

where $A_\theta = \frac{1}{2}B(z)r$, q the charge, r the radial position, p_θ, p_z, p_r the momenta, and U(r) the electrical potential. The canonical momentum in the azimuthal direction p_θ(canonical) is a constant of motion, since the Hamiltonian does not depend on the azimuthal angle θ. The canonical, kinetic and magnetic momenta are related as:

$$p_\theta(canonical) = p_\theta(kinetic) + qA_\theta r \qquad \textbf{(66)}$$

In contrast to the emittance derivation for an ECR source, the kinetic momentum p_θ(kinetic) can not be assumed to be close to zero inside an EBIS due to the non-compensated electron beam potential. However, the azimuthal momentum is conserved, that means $p_{\theta out}$(canonical)=$p_{\theta in}$(canonical), and since the magnetic field outside the EBIS equals zero, eq. 66 becomes:

$$p_{\theta out}(kinetic) = p_{\theta in}(kinetic) + qA_\theta r_{in} \qquad \textbf{(67)}$$

(Subscript 'in' and 'out' denotes inside and outside the EBIS, respectively). We have assumed the magnetic field to be constant within the EBIS, and then at a certain point in the extraction zone suddenly decrease to zero. Consequently, r_{in}=r_{out} and the canonical momentum of the ion is completely transferred into kinetic energy after passing the fringe field. Nevertheless, the derivation is valid for any shape of the shaping field, as was shown in ref. [146]. We would now like to transform to Cartesian coordinates and therefore write eq. 67 as:

$$\left(p_{yout}\cos\theta - p_{xout}\sin\theta\right) = \left(p_{yin}\cos\theta - p_{xin}\sin\theta\right) + \frac{qB}{2}r_{in} \qquad \textbf{(68)}$$

using the relation $A_\theta = \frac{1}{2}B(z)r_{in}$ and leaving out the 'kinetic' notation. For projection in the x-x' phase space (equals a rotation of the coordinate system), the θ-value to be used should equal either π/2 or 3π/2 and r_{in}=|x_{in}|. However, since the maximum p_{xout} value is searched for, θ must be 3π/2. Then the above equation is reduced to:

$$p_{xout} = p_{xin} + \frac{qB}{2}\left|x_{in}\right| \qquad \textbf{(69)}$$

If the longitudinal momentum p_0 outside the EBIS is much larger than the transverse momentum, one can make the approximation $p_{xout} \approx p_0 \cdot x'_{out}$. The longitudinal injection momentum is related to the extraction

voltage U_{ext} as $p_0 \approx \sqrt{2mqU_{ext}}$ as long as the longitudinal momentum inside the EBIS is small compared with p_0. Hence, after division with p_0 on both sides, we obtain:

$$x'_{out} = \frac{p_{xin} + \frac{qB}{2}\left|x_{in}\right|}{p_0} = \frac{mv_{xin} + \frac{qB}{2}\left|x_{in}\right|}{\sqrt{2mqU_{ext}}} \qquad \textbf{(70)}$$

The maximum acceptance is obtained from the phase space ellipse as $\alpha_{max}=x_{outmax}\cdot x'_{outmax}\cdot\pi$, and since we require the ions to be within the electron beam completely, the maximum trajectory position $x_{outmax}=x_{inmax}=r_{ebeam}$. What is still missing is to maximise x'$_{out}$, and that is accomplished by setting $x_{in}=r_{ebeam}$[10] in the second term and to find the maximum kinetic momentum in x-direction inside the EBIS, that means we would like to maximise p_{xin} or v_{xin}. This is done in Box 6, and when inserting the expression for the maximum v_{xin} in eq. 70, we obtain:

$$x'_{outmax} = \frac{m\cdot\left(\frac{qBr_{ebeam}}{2m} + \sqrt{\frac{q^2B^2r_{ebeam}^2}{4m^2} + \frac{q\rho_l}{2\pi\varepsilon_0 m}}\right) + \frac{qB}{2}r_{ebeam}}{\sqrt{2mqU_{ext}}} = \frac{\left(\frac{qBr_{ebeam}}{2} + \sqrt{\frac{q^2B^2r_{ebeam}^2}{4} + \frac{q\rho_l m}{2\pi\varepsilon_0}}\right) + \frac{qBr_{ebeam}}{2}}{\sqrt{2mqU_{ext}}} \qquad \textbf{(71)}$$

Hence, the maximum geometrical acceptance α_{max} equals:

$$\alpha_{max} = x_{outmax}x'_{outmax}\pi = \pi\frac{r_{ebeam}}{\sqrt{2U_{ext}}}\cdot\left(Br_{ebeam}\sqrt{\frac{q}{m}} + \sqrt{\frac{qB^2r_{ebeam}^2}{4m} + \frac{\rho_l}{2\pi\varepsilon_0}}\right) \qquad \textbf{(72)}$$

where r_{ebeam}, U_{ext}, q, m and ρ_l represent electron beam radius (m), ion injection potential (V), ion charge (C), ion mass (kg) and electron-beam charge per meter (C/m). Thus, all ions that enter the EBIS without any interaction with other particles, and are required to be fully trapped in the electron beam, must fit in a phase space region with this area. We note that two terms originate from the magnetic field, while the second term in the squareroot is due to the space-charge from the electron beam. In the case of a dominating space-charge, the acceptance formula is reduced to:

$$\alpha_E \approx \pi\frac{r_{ebeam}}{\sqrt{2U_{ext}}}\cdot\sqrt{\frac{\rho_l}{2\pi\varepsilon_0}} \qquad \textbf{(73)}$$

that means it becomes mass and charge independent and proportional to the squareroot of the electron beam charge per meter ρ_l. Contrary, when the electron-beam space-charge is small or compensated by positive ions, the acceptance is both mass and charge dependent and proportional to the B-field:

$$\alpha_B \approx \pi\frac{r_{ebeam}}{\sqrt{2U_{ext}}}\cdot\left(Br_{ebeam}\sqrt{\frac{q}{m}} + \sqrt{\frac{qB^2r_{ebeam}^2}{4m}}\right) \qquad \textbf{(74)}$$

Let us now insert values for $^{30}Na^+$ ion injection into the REXEBIS in eq. 72. It is clear that the magnetic field influence on the acceptance is negligible (assuming a non-compensated beam). The geometrical acceptance for 20 keV injection energy equals:

$$\alpha_{max}(REXEBIS) = \frac{\pi r_{ebeam}}{\sqrt{2U_{ext}}}\cdot\left(0.9 + \sqrt{0.2 + 214}\right) \approx 11.2\,\pi\cdot mm\cdot mrad \qquad \textbf{(75)}$$

[10] This assignment is correct since maximum v_{xin} occurs for $x_{in}=r_{ebeam}$ as shown in Box 6.

Box 6. Ion kinetic energy within electron beam.

The maximum velocity for an ion that has to be confined within an electron beam is not $\sqrt{2q\Delta U/m} = \sqrt{q\rho_l/2\pi\varepsilon_0 m}$ as one may guess, if an axial magnetic field is present. Instead the highest v_x value is obtained for ions that circle at the electron beam edge r_{ebeam}. For an ion circling at a constant radius r within the electron beam applies $F_{cent}=F_B+F_E$, that means:

$$\frac{mv_\theta^2}{r} = F_{cent} = F_E + F_B = \frac{q\rho_l}{2\pi\varepsilon_0}\frac{r}{r_{ebeam}^2} + qv_\theta B \qquad (76)$$

Solving for v_θ gives:

$$v_\theta = \frac{1}{2}\frac{qB}{m}r \pm \sqrt{\left(\frac{1}{2}\frac{qB}{m}r\right)^2 + \frac{q\rho_l}{2\pi\varepsilon_0 m}\left(\frac{r}{r_{ebeam}}\right)^2} \qquad (77)$$

The maximum v_x occurs as mentioned for $r_{in}=r_{ebeam}$ and with a positive squareroot:

$$v_x = \frac{1}{2}\frac{qB}{m}r_{ebeam} + \sqrt{\left(\frac{1}{2}\frac{qB}{m}r_{ebeam}\right)^2 + \frac{q\rho_l}{2\pi\varepsilon_0 m}} = \frac{1}{2}\frac{qB}{m}r_{ebeam} + \sqrt{\left(\frac{1}{2}\frac{qB}{m}r_{ebeam}\right)^2 + \frac{2\Delta U}{m}} \qquad (78)$$

3.3.3 Simulated acceptance

To determine the acceptance phase space a set of ions were "injected" into the EBIS. The ions were initialised with uniform distributions in the x-x' and y-y' spaces at the 2nd bender focus. They were then traced into the EBIS using the model described in sec. 3.1, and those that were captured were classified as accepted. Thereafter the x-x' and y-y' initial conditions for the accepted ions were plotted in two plots, representing the horizontal and vertical acceptance phase spaces. Due to too restrictive initialisation in the divergence directions (-10 mrad<dx/dz<10 mrad and -10 mrad<dy/dz<10 mrad), most of the acceptance phase plots are cut at ±10 mrad. The initial energy spread was 59 999<Ekin<60 001 eV, which is somewhat higher than the predicted energy spread from the REXTRAP. (The REXTRAP should approximately have a longitudinal emittance of 5 eV·µs and with an extraction time of 10 µs the energy spread equals 0.5 eV.) When not specifically stated, the injected elements were $^{30}Na^+$ ions.

3.3.3.1 Acceptance phase space shape

First after some simulations, when the statistics were good enough, we realised that the upright acceptance phase space for the REXEBIS had the shape of a rhomb (see for instance Figure 53 and 54). We had different theories to what could be the cause of this rhomboidal shape: either the magnetic field in combination with the electrostatic potential from the electron beam, or solely the fringe field from the electron beam. Our tests showed that the size and shape of the rhomboid was independent of the magnetic field (which is in agreement with the analytical acceptance expression derived in sec. 3.3.2), and therefore the first solution was ruled out. Moreover, inside the drift tubes the phase space was elliptic, but outside the collector the shape was rhomboidal. These facts suggest that the odd shape originates from the collector region, and that it is created by the electrostatic fringe field that occurs in the collector region where the electron beam is absorbed. A few comments to this statement are given in Appendix 4.

3.3.3.2 Verification of analytical acceptance formula

To verify the analytically derived acceptance formula (eq. 72) the acceptance phase spaces for 100%-ions injected into the REXEBIS were simulated, and a geometrical acceptance value was determined from these plots. The ions were injected with an excess energy of ~280 eV above the axis potential in the fully compressed electron beam region. Actually, the needed excess energy to fill the acceptance phase space is ~220 eV (see Box 6).

The analytical expression predicts a geometrical acceptance of 11.2 π·mm·mrad≈35 mm·mrad, which agrees very well with the rhomboid area which measures $\sim\left(\frac{1.6\cdot 10.5}{2}\right)\cdot 4 \sim 34$ mm·mrad (see Figure 53). One should keep in mind that the theoretical estimation gives an upper limit for the acceptance, and that it is fairly difficult to decide the exact extension of the rhomboid. Nevertheless, several independent simulations support the result of the theoretical expression.

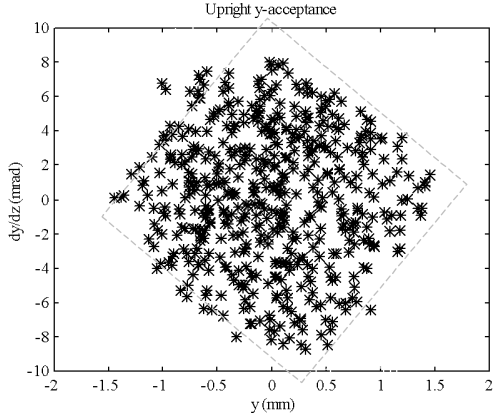

Figure 53. *Transverse acceptance phase space plot and enclosing rhomboid for 100%-ions with 60 keV injection energy. The tilt of the rhomboid is due to free beam space drift and the einzel lenses.*

As was seen in sec. 3.3.2, the term originating from the electron beam is completely dominating for the REXEBIS acceptance. That means the acceptance should be mass, charge and B-field independent. The latter independence was verified by testing different magnetic fields strengths; the acceptance phase spaces for B=2 and 5 T were found to be similar. Tests with different masses (A=30 and 100) and charges (Q=1^+ and 10^+) were also performed, however, the starting conditions were not completely unambiguous so no conclusions could be drawn about these parameter's independence, even if the acceptance phase spaces turned out to be similar.

3.3.3.3 Beam aberrations and effective EBIS acceptance

In Figure 54 an indication of a spiralling form is seen for the 0%-ions (it has been indicated with arrows). Unfortunately, the starting conditions were such that the initial divergence was cut at ±10 mrad, which means that most of the likely tails are not shown. Nevertheless, special injection simulations showed that the present REXEBIS system can not accept larger divergence values than ~12 mrad without introducing aberrations to the beam. The absolute maximum divergence is 14 mrad (then the trajectories touch the walls). The radial starting position at the 2nd bender can reach at least 5 mm without any noticeable distortion.

We have seen that the acceptance formula eq. 72 predicts the acceptance for 100%-ions quite well, however, the acceptance for 95%-ions might be of more interest from an EBIS design point of view. We will argue for that below, and illustrate the REXEBIS acceptance with a phase space plot for 95%-ions.

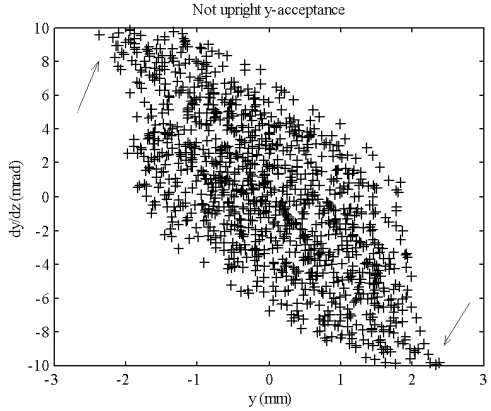

Figure 54. *Transverse acceptance phase space plot for 0%-ions. The arrows indicate beginning aberration wings. (NB! The phase space is not upright as in all other plots.)*

As already pointed out, the classification of ions into 0%, 95% and 100% groups denotes how large fraction of the confinement time inside the EBIS (at least) the ions spent within the electron beam. To have an efficient charge breeding, the ions should be

completely confined within the beam, i.e. all ions should be of the 100% sort. On the other hand, if a 5% prolongation of the breeding time is acceptable, also 95%-ions become useful. For 95%-ions, the acceptance phase space is enlarged, as can be seen if one compares the phase space plots in Figure 55 (100% and 95%-ions); the geometrical acceptance increases from 11 π·mm·mrad to $\sim\left(\frac{2\cdot 13}{2}\right)\cdot 4$ mm·mrad≈17 π·mm·mrad.

The reason for the acceptance increase is a larger mean radius inside the trap at injection for 95%-ions compared to 100%-ions. A larger mean radius at injection is obtained by higher injection energy and less restriction initial radius and divergence, i.e. a larger acceptance as is explained in Appendix 4. Nevertheless, very soon after entering the trap region, the ions traverse the electron beam, and are then immediately ionised from 1^+ to 2^+ (or higher). When that happens, the mean radius shrinks and most of the ions become trapped within the electron beam. Thus, the time fraction spent within the electron beam for these ions will be close to 100%. In fact, the acceptance can be enlarged until one runs into aberration problems caused by too narrow lenses and drift tubes (for the REXEBIS case this happens at about $\left(\frac{5\cdot 12}{2}\right)\cdot 4$ mm·mrad =38 π·mm·mrad). The conclusion is that the effective acceptance can be expanded by raising the ion injection energy a few hundred eV, to the cost of not fully trapped ions. Though, one has to keep in mind that if the time within the electron beam goes down for instance to 50%, it implies a broader charge-state distribution and fewer ions in the correct charge-state.

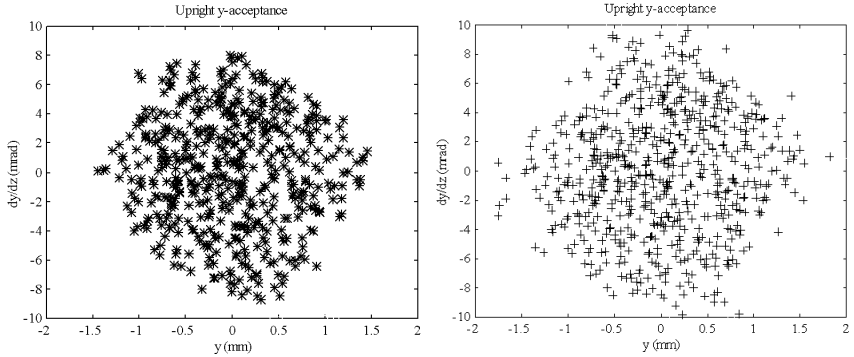

Figure 55. *Transverse acceptance phase space plot for 100% (left) and 95%-ions (right). The acceptance increases from 11 to 17 π·mm·mrad when the lower percentage value is accepted. (NB! The starting divergence values are cut at ±10 mrad.)*

3.3.4 Radial redistribution during charge multiplication

3.3.4.1 Ion trajectories within the trap region

Inside the trap region the ion is bound to the electron beam and its motion is a combination of the radial oscillation in the electrostatic field from the beam, on which is superimposed the azimuthal cyclotron motion around the magnetic field. The result is a rapid precessing transverse oscillation around the beam centre, plus a relatively independent bouncing between the end barriers. Figure 56 shows typical trajectories for ions trapped in an electron beam of uniform current density. It is important to stress that the ions are trapped to the beam even when their trajectories take them outside it.

Typical frequencies for the motions in the REXEBIS are:

- radial – $f_{radial}\approx \frac{1}{2\pi}\sqrt{\frac{q\rho_I}{2\pi\varepsilon_0 r_{ebeam} m}} \approx 40$ MHz
- azimuthal – $f_{azimuthal}$=Larmor frequency= $\frac{qB}{4\pi m}\approx 4$ MHz
- axial – $f_{axial}=\frac{v_z}{2L}\approx$10-20 kHz

Due to the high number of oscillations under a confinement, their phases are essentially random.

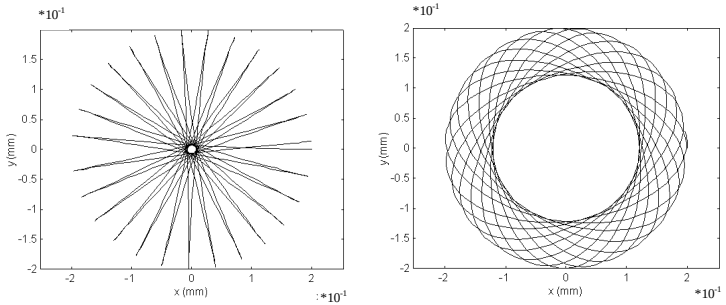

Figure 56. *Typical radial trajectories of ions trapped in an electron beam with uniform density; the left ion was started with no kinetic energy while the right had an initial azimuthal momentum. In both cases, the ion attempts to fall radially to the centre of the beam, but is reflected away from the axis by the axial magnetic field.*

3.3.4.2 Radial distribution

Inside the trap region the successive ionisation causes the radial distribution of the ions to change from a broader to a more narrow distribution closer to the beam axis. This can be intuitively understood by a simple energy argument: At the point of ionisation the momentum and kinetic energy are unchanged, but the depth of the electrostatic potential increases. Thus, the ions will on average not reach as large radii as for the lower charge-state.

In addition, the radial and azimuthal velocity distributions change as well, but that will not be treated here. It is possible to calculate the radial distribution as function of charge-state and velocity distributions, using classical Hamilton formalism, and a simplified example of that is given in ref. [51], however, the mathematics are rather tedious.

To illustrate the shift in radial distribution with increasing charge-state we have plotted the distributions in Figure 57 for an average charge-state <Q> of 1.0, 2.8 and 6.0 (the pictures are snapshots at different breeding times). The mean radius decrease with increasing <Q> is unambiguous. As will be seen in sec. 3.3.5.4, the emittance decreases too with increasing charge-state, and this phenomenon is mainly

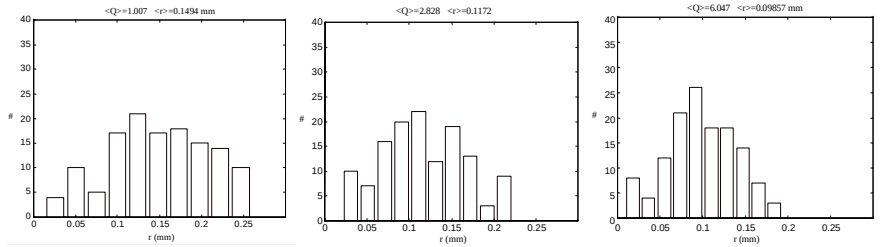

Figure 57. *Radial trajectory distribution inside the trap region for different charge-states (<Q>=1.0, 2.8 and 6.0). The mean radius decreases with increasing charge-state.*

attributed to the radius shrinkage[11]. One should point out that the amount of radius shrinkage is solely dependent on the average charge-state, and not on the ion mass (in a first approximation). This will have consequences for the REXEBIS emittance values, because all elements should be charge bred to Q/A~1/4, i.e. the heavier elements will have a higher charge and thereby a smaller average radius which results in a smaller emittance, than the lighter elements.

Figure 58 shows the radial distribution of the accepted ions at the focus outside the EBIS (the ions are initialised with a uniform distribution over –2.5<x<2.5 mm, –2.5<y<2.5 mm).

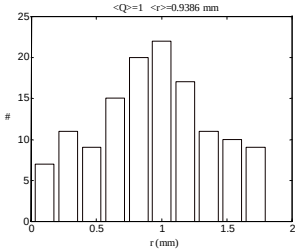

Figure 58. *Radial trajectory distribution for the accepted ions at start at the 2nd bender focus outside the EBIS.*

3.3.5 Simulated emittance

3.3.5.1 General emittance considerations

The emittance simulations that are presented here are mainly performed with an extraction voltage of 60 kV to allow for an easy comparison with the acceptance simulations that also were carried out with a 60 keV beam. One notices that the phase space is rhomboidal for lower charge-states in a similar way as for the acceptance phase space, but the feature washes out for beams with higher charge-states (see Figure 59).

The first of two emittance tests was to check the dependence on the B-field. Two complete injection-breeding-extraction cycles were performed: one with a magnetic field of 2 T, and the other with a field strength of 5 T. The average charge for the extracted ions was <Q>=6$^+$, and U_{ext}=20 kV. Though the statistics were somewhat lacking, the conclusion was that the emittance does not vary with the magnetic field (see Table 16). This result is of major importance from an EBIS design point of view, since it shows that one does not have to keep the B-field strength low to obtain a small emittance. However, one should keep in mind that this result was obtained with a non-compensated beam (i.e. the electrostatic potential contribution to the emittance outweighed the contribution from the magnetic field). For a compensated beam the emittance will increase with the B-field.

	Emittance (π·mm·mrad)	
	B=2 T	B=5 T
Geometrical	10	11
RMS	2.55	2.60

Table 16. *Transversal emittance values for B=2 T and 5 T, U_{ext}=20 kV.*

The second parameter to be varied was the ion charge, and its effect on the emittance is treated in the next section.

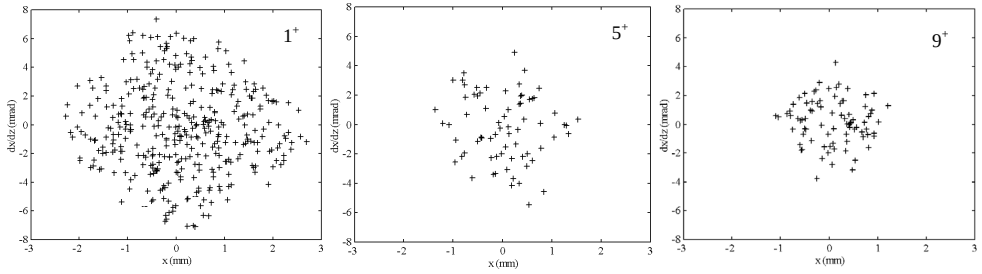

Figure 59. *Transverse emittance phase space plots for 0%-ions of charge-state 1$^+$, 5$^+$ and 9$^+$, U_{ext}=60 kV.*

[11] Transformations of the radial and azimuthal velocity distributions also affect the emittance value.

3.3.5.2 Emittance dependence of the charge-state

From eq. 72 one may conclude that the emittance should be independent of the ion charge as long as the EBIS is operated under such conditions that the electron beam term dominates over the terms originating form the magnetic field, and the ions are distributed uniformly over the beam. However, the latter premise is not fulfilled for a distribution with highly charged ions as was seen in sec. 3.3.4, since the highly charged ions are confined close to the beam axis and therefore r_{in} becomes smaller than in the case for low-charged ions.

By varying the breeding time during the simulation, different charge-states were obtained covering 1$^+$ to 11$^+$. The ions were sorted after charge, and extraction phase spaces were plotted for each charge-state. From the plots the RMS emittances were derived. One should point out that the statistics for the higher charge-states were embarrassingly poor. Figure 60 shows the emittance values as function of extracted ion charge Q (Figure 59 illustrates the same phenomenon). The RMS emittance decreases with increasing charge-state.

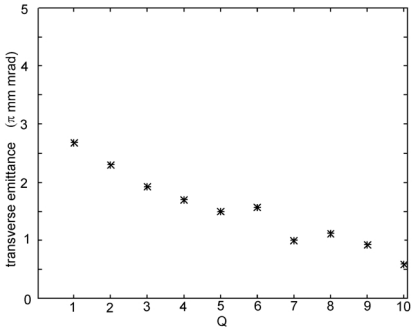

Figure 60. *RMS emittance values vs. charge-state for 100% and 0%-ions, U_{ext}=60 keV. The emittance decreases with increasing charge-state.*

One might argue that the emittance should drop with the square root of Q, which equals saying the normalised emittance is constant. This hypothesis was tested and rejected. Instead the emittance decrease is due to the radial redistribution to smaller trajectory radii inside the trap region for higher charge-states. Similar behaviour of the emittance has also been noticed in ECR ion sources [147,148].

3.3.5.3 Residual gas emittance

In the onset of our investigations we focused on the emittance from the injected ions, which is of importance for the beam transport and the injection into the RFQ. Nevertheless, the emittance of the residual gas might be of more importance since it could be the limiting factor for the resolution of the mass separator; a too large residual gas emittance, and the injected ions are not separable from the unwanted gas ions.

To simulate the residual gas emittance the atoms were ionised randomly within the electron beam with no initial kinetic energy[12]. As rest-gas ^{16}O was used. Figure 61 shows an upright phase space plot for Q=4$^+$ and 5$^+$ for 60 kV extraction voltage. The emittance ellipse had an extension of ~10 π·mm·mrad, although the main part was found within 4 π·mm·mrad. Note that this simulation is carried out with a modified beam optics system allowing for a larger divergence. This has no effect on the actual size of the emittance.

Due to the maximum emittance for low-charged ions, the worst residual-gas emittance case, with a Q/A-value close to 1/4.5, would correspond to He^{1+}. However, helium is not very abundant as a rest-gas, so O^{4+} probably generates a representative emittance.

[12] To be able to extract the ions they were given an initial axial momentum corresponding to around 5 eV, which is low and it should not affect the result.

The REX-ISOLDE mass analyser is able to separate beams with a Q/A resolution of 150 for transverse emittances smaller 40 π·mm·mrad (4σ) and energy spread <50 eV/Q. From the picture one concludes that the absolute rest-gas emittance value falls within the limit, but that the beam needs focusing.

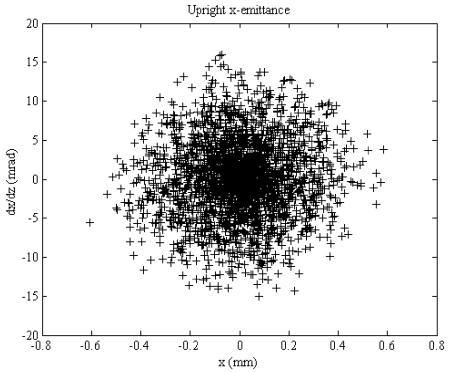

Figure 61. *Phase space plot from residual gas $^{16}O^{4+}$ and $^{16}O^{5+}$ extracted with 60 kV. The geometrical emittance is 0.6·15 π·mm·mrad. The true REXEBIS residual gas phase space would be stretched $\sqrt{3}$ in x'-direction due to the lower extraction voltage of 20 kV. This simulation has been carried out with modified beam optics, therefore the large divergence.*

3.3.5.4 Injected ion emittance

As was hinted at in the previous section, the emittances may differ between injected ions and residual gas ions. For instance, if one arranges a narrow injection of the ions into the bottom of the electron beam well, one will end up with a small emittance. On the other hand, if there is little overlap between the injected ion beam and the electron beam, the extracted beam will show a high emittance. However, the difference between residual gas and injected ion emittances should be minor as long as the ion injection conditions are energetically correct and the ions are distributed over the whole electron beam radius.

One may ask why the emittance plots in Figure 61 (residual gas) and Figure 62 (ion injection) are different? The reason for this is twofold. First of all, and most important, the final charge-state is higher in the injected ion case (i.e. the emittance is smaller). Secondly, the statistics for the ion injection was poor, and possibly not the whole acceptance phase space was filled by the injected ions.

The ions in Figure 62 were extracted with an voltage of 60 kV, so to obtain the true REXEBIS phase space the divergence values have to be multiplied by $\sqrt{60/20}$, which gives an emittance of ~9 π·mm·mrad. With the two variable einzel lenses we have the ability to reshape the phase space, and fine-tune it for different ions.

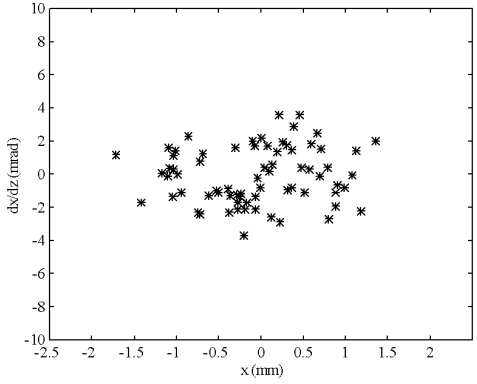

Figure 62. *Emittance phase space plot for ^{30}Na ions charge bred to 7^+ or 8^+. The ions were fully trapped, i.e. they were of 100% type. The extraction voltage was 60 kV, that means for the real REXEBIS the phase space would be stretched $\sqrt{3}$ in x'-direction due to a lower extraction voltage of 20 kV.*

So what will the largest emittance out of the REXEBIS be, and for what conditions does it occur? As will be shown in the next section the emittance decreases with increasing charge-state, that means an extracted beam of 1^+ ions will have the largest emittance. In fact, the emittance will be the same as the acceptance, multiplied by the injection/extraction voltage correction, that is $\sqrt{60/20}$ ·11 π·mm·mrad= 19 π·mm·mrad. Thereby an upper limit for the REXEBIS emittance should have been stated. Nevertheless, faulty injection conditions can make the emittance even larger. We saw in sec 3.4.3.3 that the acceptance could measure 17 π·mm·mrad for 95%-ions, which gives an emittance (for 1^+) of around 30 π·mm·mrad. Even higher values are obtained for less confined ions (i.e. lower 'percentage value ions'). Such high emittance values come close to the limit of the mass analyser (40 π·mm·mrad). One has to keep in mind that this worst case scenario assumes a poor injection condition, and no charge breeding (ions extracted as 1^+)!

To conclude, the simulations gave a REXEBIS emittance of around 10 π·mm·mrad (with 20 kV extraction voltage) for $^{30}Na^{7+}$ ions; somewhat higher for ions with lower charge-state. If the ions are injected within the specified 3 π·mm·mrad phase space, the emittance will be even lower than 10 π·mm·mrad.

3.3.6 Energy spread

The REXEBIS platform voltage is adjusted so the injected ions have an energy of ~100 eV when they propagate within the trap region, and since the electron-beam potential-depth ΔU=100 eV, the ions are energetically trapped within the electron beam. The ionisation is a random process that occurs at different radii and therefore at different beam potential. That means the ions achieve a varying energy depending on where they are ionised, which is the cause of the breeding energy spread (also called ionisation heating). The energy spread of the extracted beam is an important parameter, maybe not so much from the point of view of the RFQ, but to be able to perform an exact Q/A selection in the mass analyser, the energy may not vary too much. An upper estimation of the energy spread yields $\Delta E_{extract}=q\cdot\Delta U$ (non-compensated electron beam, which is approximately the case for the REXEBIS). This is a highly conservative estimation; thus, the energy spread for the REXEBIS was simulated to moderate the prediction.

The $^{30}Na^{1+}$ ions were injected from the 2nd bender focus with an initial uniform energy variation of 60 000±1 eV, $\sigma(E_{in})$=0.6 eV. While the ions were confined within the trap region, the trap potential was increased 300 eV, i.e. 1^+ ions should have an extraction energy of 60 300 eV. Only ions that were trapped within the electron beam at least for 95% of the time were recorded, but since the breeding time was varied, a set containing all charge-states was obtained. In this section the extraction energy per charge, i.e. $\Delta E_{ext}/Q$, at the 2nd bender focus for an extraction voltage U_{ext}=60 000 V is presented[13].

In Figure 63 the extracted beam energies per Q are plotted for Q=2,4,6,8 and 10. We can see that higher charge-states lead to lower extraction energies as expected, since the highly charged ions accumulate around the beam axis. The minimum extraction energy does not go below 60 200 eV, i.e. 60 300 eV minus 100 eV (the depth of the electron beam potential), which is correct.

It seems as if the energy spread does not vary with the charge, but the statistics are rather poor. An average energy spread per Q for all charge-states would be $\sigma(E_{out})$~15 eV.

These results are naturally valid also for U_{ext}=20 keV, and we can conclude that simulations assign an energy spread that is significantly lower than the estimation of 50 eV/Q, which has been used as input for the mass separator design. The presented results were obtained from ion injection, but since the conditions are similar for gas injection, the outcome is not expected to change drastically for residual gases.

The energy spread from an EBIS has been measured several times, for instance at CRYSIS, but then with a highly compensated trap. The obtained result was an energy spread of 57 eV/Q for a 300 mA electron beam at 17.4 keV. This value exceeds my simulation prediction by far, and can not be ascribed to electron-ion or ion-ion heating processes, nor faulty injection (gas injection was used), but is merely due to the high electron beam compensation. (The first ions in the extracted pulse leave a compensated trap and have therefore a high energy, while the last extracted have a lower energy due to a more attracting electron beam.) Remember that the REXEBIS will have a low degree of compensation.

[13] Due to minor energy conservation problems when the ions passed the collector region, the energy variation caused by the breeding was determined by recording the energy at z=410 mm when the ions entered and left the trap region.

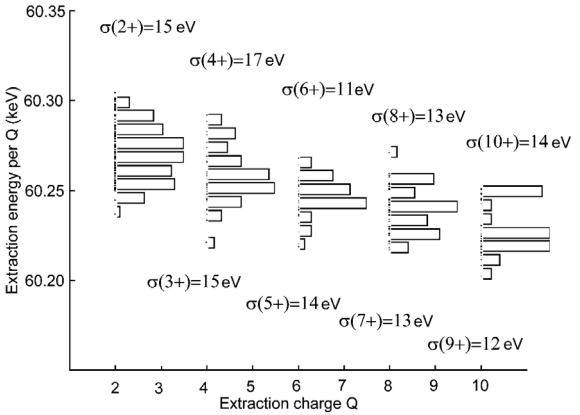

Figure 63. *Extraction energy per Q versus charge-state for ions injected into the REXEBIS. Histograms for the energy spread (even charges) are plotted vertically in connection to corresponding charge-state. (From the listed energy spread values a numerical error of σ~3.5 eV should be subtracted.)*

3.4 Phase space correlation in extracted EBIS ion beam

3.4.1 Introduction

Ions starting inside a cylindrically symmetrical magnetic field have after extraction from the field a rotational kinetic momentum corresponding to the magnetic vector potential they started in (see Figure 64). The consequence is an increase in the transverse emittance, so even if one started with zero emittance inside the EBIS, after extraction it would be non-zero. However, there exists a correlation between the transverse phase spaces [149,150], and ion optical elements, such as skew quadrupoles (a quadrupole rotated 45° to the horizontal plane), have the ability to partially decorrelate the phase spaces. The magnetic field from the lens induces a complete compensation of the azimuthal velocity in one direction, while increasing it by a factor two in the other direction as shown in Figure 65. So if one started with, an unfortunately utopian, zero emittance inside the EBIS, the skew quadrupole would arrange the ion movements so that the emittance in one transverse plane would be zero, and in the other increase by a factor two compared with the non-compensated beam emittance.

For the Mass separator following the REXEBIS in the REX-ISOLDE system, the emittance is of vital importance for the mass separation resolution. By improving the emittance in one direction (the bending

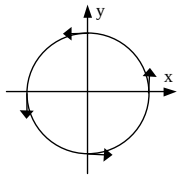

Figure 64. *Azimuthal velocity components due to the coupling between phase spaces [149].*

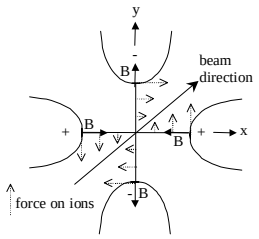

Figure 65. *The effect of a skew quadrupole counter-acting the azimuthal velocity in one plane [149].*

direction), as suggested above, the mass resolution can be improved. This opportunity raised the demands for an investigation of the beam correlation out of an EBIS, and the need for decorrelating optics. Thus, a complete injection, breeding and extraction cycle for the REXEBIS was simulated to determine degree of correlation.

3.4.2 Results

The result from the investigation is presented in Figure 66 in the form of a velocity vector plot, i.e. a plot indicating the velocity vectors for the extracted ions at the 2nd bender focus. One can see that the velocity directions are fairly randomly distributed, and no azimuthal correlation as the one in Figure 64 is observed. The way we quantified the correlation was by plotting a histogram of the azimuthal velocity component, see Figure 67, and from that compare the mean azimuthal velocity $< v_\theta >$ with the standard deviation $\sigma(v_\theta)$. The result was an insignificant correlation, $< v_\theta >$=65 m/s, compared with the standard deviation, $\sigma(v_\theta)$ =1100 m/s. The fact that the mean azimuthal velocity is so small compared with the standard deviation, is due to the large transverse energy spread inside the EBIS, causing the ions to move with high velocity in random directions, and this random movement swamps the velocity correlation induced by the extraction from the axial magnetic field.

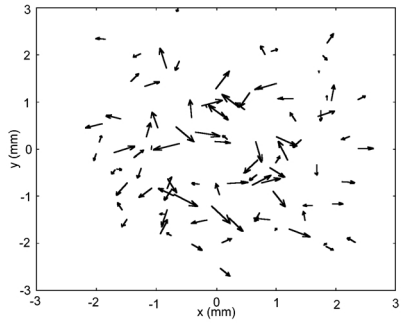

Figure 66. *Velocity vector plot for a beam extracted from REXEBIS.*

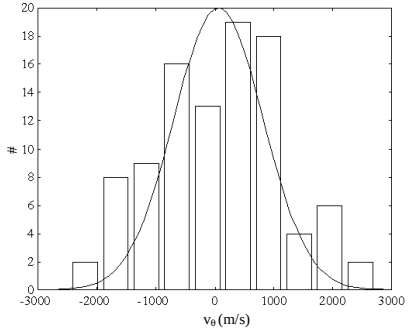

Figure 67. *v_θ histogram with $< v_\theta >$=65 m/s and $\sigma(v_\theta)$ =1100 m/s.*

3.4.3 Conclusions on phase space correlation

Introducing a skew quadrupole after the EBIS would in principle decrease the azimuthal velocity in one direction, while it is increased in the other. Though, for the REXEBIS conditions, the initial ion-energy inside the EBIS is so large, and the velocity so randomly distributed, that the azimuthal velocity coupling caused by the extraction from the axial magnetic field is drowned. Hence, adding a skew quadrupole can not compensate for the collective ion movements, and therefore not improve the emittance significantly. For an ECR the effect is more pronounced due to the smaller initial energy spread, which would also be the case for an EBIS with higher trap compensation.

3.5 CRYSIS emittance – simulation and measurements

3.5.1 Introduction

There is a large discrepancy between measured and theoretically expected emittance from CRYSIS, the EBIS for the CRYRING at the Manne Siegbahn Laboratory. A theoretical estimation (see sec. 3.3.2) gives an upper limit for the geometrical emittance of ~17 π·mm·mrad at an expulsion voltage of 3.5 kV, which should be compared with a measured emittance of 70 π·mm·mrad (2σ). It is supposed that the ion beam fills the collector exit, or the following narrow einzel-lens system, and that large aberrations are introduced in either of these regions. To verify the suspicion, and to validate the predictability of the developed EBIS model, the CRYSIS geometry was implemented in SIMION.

A sketch of the electrostatic surfaces with potentials is found in Figure 68. The CRYSIS model was similar to the REXEBIS implementation, with modified electron beam and magnetic field. In contrast to the REXEBIS simulations, all ions were extracted with one charge-state, $Q=14^+$.

3.5.2 Ion starting conditions

The extracted ions were of $^{40}X^{+14}$ type, and the position of ionisation from $Q_{ion}=13^+$ to 14^+ (no further ionisation) was assumed to occur uniformly over the electron-beam cross-section, even if the ionisation is more likely to occur at the radial turning points where the ion spends most of the time. The uniform ionisation distribution results in an underestimation of the emittance. Two different electron-beam radii were simulated: r_{ebeam}=0.15 and 0.4 mm. To include the effects from ion heating and a compensated trap, the ions were initiated with a total energy such that the ions were not necessarily energetically confined within the electron beam, i.e. the ions could temporarily leave the electron beam radially ($r_{ion}>r_{ebeam}$). The initial kinetic energy was randomly distributed between zero and the maximal electron-beam potential-energy[14] ($q_{ion}\cdot\Delta U$), and the velocity direction was chosen randomly within the whole solid angle.

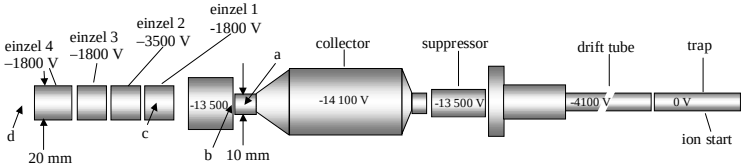

Figure 68. *CRYSIS structure with trap, collector, small einzel lens and positions for the snapshots.*

Electron-beam current I_e	0.2 A
Electron-beam radius r_{ebeam}	0.15 and 0.4 mm
Electron-beam current-density j_e	280 and 40 A/cm^2
Electron-beam energy E_e	10 keV
Electron-beam potential-depression ΔU	-30 V
Magnetic field B	2 T
Extraction voltage U_{ext}	3500 V
Extracted ion type	$^{40}X^{+14}$
Initial radius r_{start}	<0.15 and 0.4 mm
Initial energy E_{start}	<$q_{ion}\cdot\Delta U$=420 eV

Table 17. *CRYSIS and ion parameters for the two different electron beam radius cases.*

3.5.3 Beam compensation

For a non-compensated trap with no heating, the ions are all trapped within the electron beam (assuming proper ion injection or neutral gas in-flow). On the other hand, with an increasing compensation degree, the rigidity reduces, i.e. the radial oscillation frequency ω_p decreases with the growth of the ion space-charge, and the amplitude of the ion oscillation swells. Since the ions then spend more time outside the electron beam, the breeding has to be increased to retain the desired charge-state. Ion heating due to Coulomb collisions may also produce ions with enough energy to leave the electron beam temporarily. For these reasons we have allowed the ions to have a non-confining (within the electron beam) starting energy, but the magnitude was somewhat arbitrary.

3.5.4 Results

The investigation focused on the ion beam properties at the collector exit and in the first einzel lens after the collector. In Figure 69 and Figure 70 the beam profiles at the narrow collector exit (a) and at the first einzel-lens cylinder (c) are plotted ('+' denote ions only partly trapped in the electron beam; '*' denote fully trapped ions). The collector exit radius is ~5 mm, and the einzel lens radius ~10 mm. The collector

[14] The magnitude of the upper energy limit was chosen somewhat arbitrarily and is in reality dependent on ion heating and boiling-off effects, that are difficult to estimate in a compensated trap.

aperture is filled to approximately 50% and 90% for r_{ebeam}=0.15 and 0.4 mm, respectively. At the middle of the first cylinder in the einzel lens the aperture is filled to 35% and 50%.

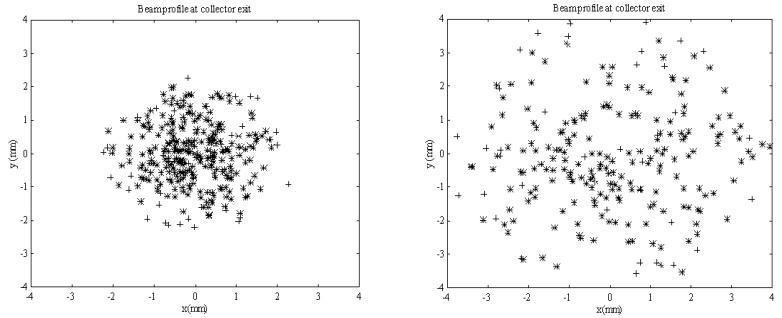

Figure 69. *Ion beam profiles at the collector exit (a) for r_{ebeam}=0.15 (left) and 0.4 mm (right). Collector radius ~5 mm.*

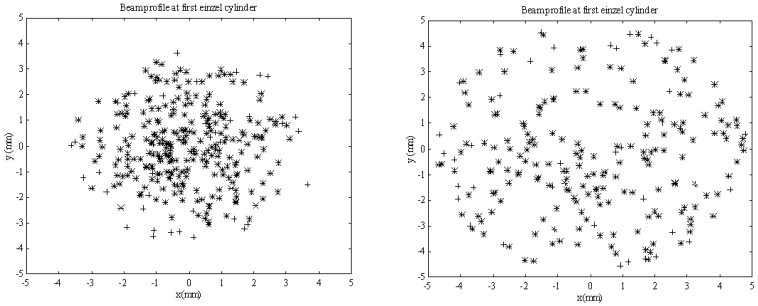

Figure 70. *Ion beam profiles at the einzel lens (c) for r_{ebeam}=0.15 mm (left) and 0.4 mm (right). Einzel lens radius ~10 mm.*

In Figure 71 the beam propagation from the end of the collector through the einzel lens are found. Note that all ions, also ions that have spent only part of their time inside the electron beam, are included.

A series of phase space snap shots were taken at the positions marked in Figure 68, and they are presented in Figure 72 (shifted to upright shape) together with the corresponding geometrical emittance in Table 17. It was notoriously difficult to estimate the geometrical emittance values (see sec. 3.3.1.1 for a definition), so the error-bars are of the order of 50%. From the two first values (a and b) it is clear that the phase space is only slightly distorted after passing through the collector exit, and the emittance values (see Table 17) agree well with the energy-adjusted theoretical value (an upper limit) obtained from eq 72[15].

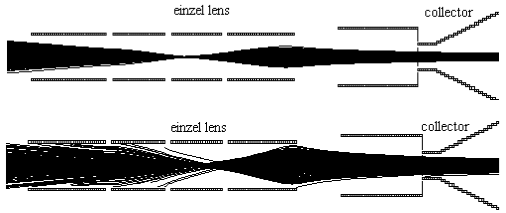

Figure 71. *Extracted beam for r_{ebeam}=0.15 (top) and 0.4 mm. Trajectories for all ions are included.*

[15] To be correct, eq 72 gives an expression for the acceptance. That means, a non-uniform distribution of ions within the electron beam, as in the case for ions that have been ionised to a high charge-state and therefore been attracted to the beam axis, will produce a lower emittance than what the expression predicts.

However, at the centre of the first einzel-lens cylinder (c), and after the last einzel-lens cylinder (d), the phase space is distorted with spiralling arms that explain why the simulated values exceed the theoretical by far.

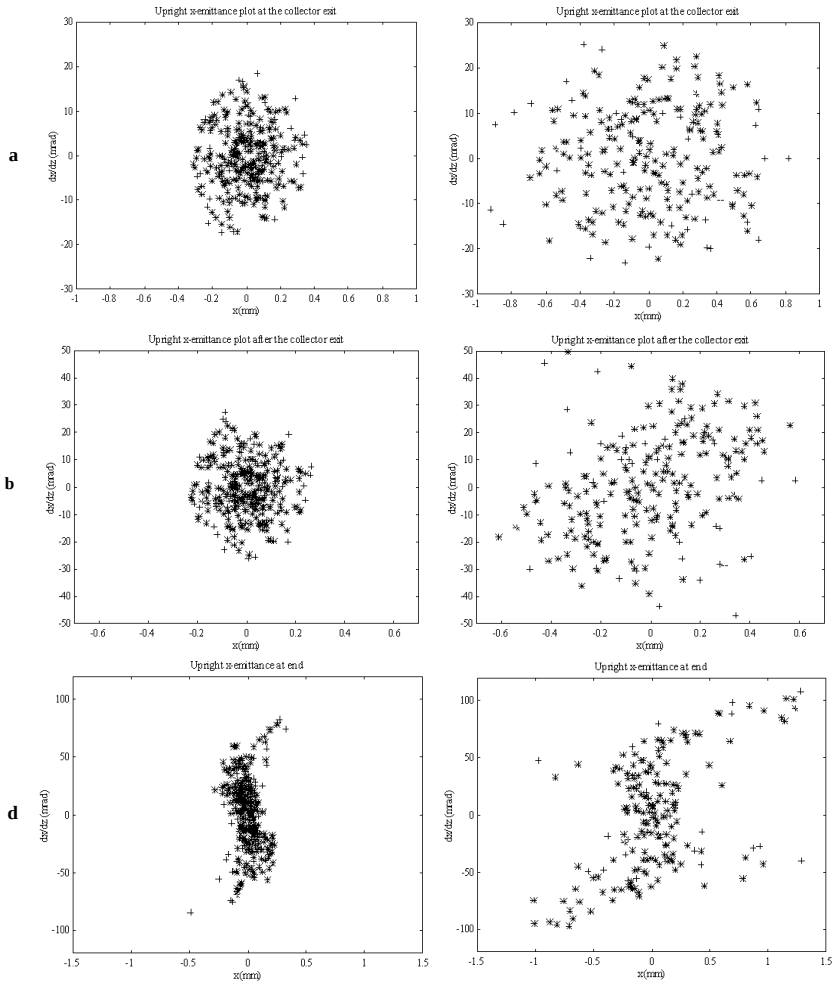

Figure 72. *Transverse phase space plots (translated to upright position) for r_{ebeam}=0.15 mm (left) and 0.4 mm (right). Recording positions: (a) at collector, (b) after collector, (d) after einzel lens.*

After leaving the drift tube region with the well-focused electron beam and the strong magnetic field, the ions start to repel each other due to the Coulomb force. The space-charge blow-up results in a larger beam diameter in the collector exit, which may lead to beam distortions. The SCC of the beam propagation from sec. 3.2 could not be used because of too high beam current. A conservative analytical estimation gave a beam radius increase at the collector of 1.2 mm. Thus, when inspecting Figure 53, we can

conclude that quite a few electrons will touch the collector exit, and this causes naturally further beam distortion and emittance increase.

		r_{ebeam}=0.15 mm		r_{ebeam}=0.4 mm	
Position	Beam voltage (V)	Theory ε_x	Simulation ε_x	Theory ε_x	Simulation ε_x
		Emittances in (π·mm·mrad)		Emittances in (π·mm·mrad)	
a	~14 000	8.5	6	28	20
b	13 600	8.5	6	28	22
c	1800	24	30	86	200
d	3500	17	21	61	120

Table 18. *Non-normalised transversal geometrical emittance values for CRYSIS at different axial positions. Note the varying beam energy.*

3.5.5 CRYSIS simulation conclusions

The results from the simulation indicate that the beam is distorted in the entrance of the first einzel lens cylinder. The final emittance value is strongly related to the electron beam radius inside the EBIS since the emittance grows linearly with r_{ebeam}, and the beam distortion adding to the inherent emittance increases also with r_{ebeam}. The measured emittance value of 70 π·mm·mrad can therefore very well be explained by an aberrated ion beam created in an electron beam with a radius r_{ebeam} of 0.2-0.3 mm. The results from this investigation also validated the implementation of the EBIS model in SIMION.

3.6 Continuous injection mode

3.6.1 Motivation

Continuous injection, also titled slow injection, is an injection mode where the 1^+ ions are continuously introduced into the EBIS during the confinement period. This method is well adapted for primary ion sources with very low intensity where the collection of ions in the EBIS can continue for the whole breeding period without running into space-charge limitations. The method is for instance regularly used at CRYSIS at the Manne Siegbahn Laboratory. It would also be suitable for radioactive ion beams produced at on-line isotope separators since the radioactive beam is essentially DC and the intensity is moderate (proposed by Haas in ref. [151]). Subsequently the Penning trap would be redundant in the accelerator chain since the need for efficient bunching disappears. Moreover, one is then no longer restricted by the space-charge limitation of the Penning trap. This, however, assumes a high trapping efficiency of the EBIS and a high-quality emittance from the on-line separator to be successful.

In this section we will briefly touch upon the method, because it might come in question for future radioactive beam post accelerators. To our knowledge no theoretical studies have been carried out on the continuous injection mode, and one has so far assumed that the trapping efficiency can be arbitrary high. We have developed a few qualitative arguments that show that the maximally obtainable efficiency for an ion beam with finite energy spread and emittance is less than 100%. These will be put forward here, as well as some comments on continuous injection tests performed on the Dioné EBIS at Saclay [152] that might explain their poor experimental results.

3.6.2 Theory

The theory for continuous injection is simple: the single-charged ions are injected over a potential barrier at the beginning of the confinement region into an electron beam of sufficient current density so that ionisation to Q>1 occurs before a round trip inside the region is finished (see Figure 73). The probability for trapping in the confinement region is large under the right injection circumstances, but not 100%, as will be shown in the next section. The trapping efficiency is dependent on the ion injection energy, the barrier potential height, the electron beam potential depth, and the barrier position. The ions that are trapped are after finished confinement extracted in the usual way, i.e. the outer barrier is lowered and the ions leave the source.

There is a difference in extracted charge distribution for ions that are pulsed or continuously injected. In the latter case the ions are continuously fed into the trap region, resulting in a broader charge distribution, and a smaller fraction within the peak charge-state than for pulsed injection. This is illustrated in two charge distribution plots in Figure 74: one for continuous injection and the other for pulsed injection. Both were simulated with the same confinement time. A broader charge-state distribution results in a smaller fraction of ions within the peak charge-state, and a lower peak charge-state means that the breeding time has to be extended, which is disadvantageous for short-lived radioactive nuclei.

At extremely low injection intensities the collection time can be of considerable length (if there are no lifetime restrictions set by the radioactive ions). Then the trapped ions must be cooled by light ions (see sec. 2.2.2), and one has to make sure that the trap does not become compensated by residual gases.

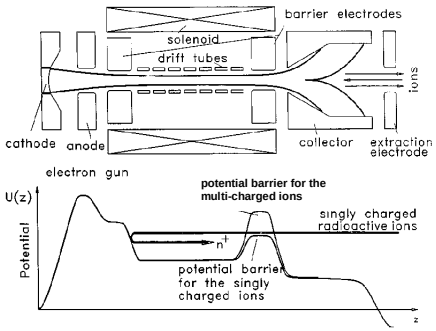

Figure 73. *Potential distribution along the axis in an EBIS using continuous injection mode [153]. The sketch is not displaying that some ions remain singly charged, and that some multi-charged ions have enough energy to leave the trap.*

Effectively, a high efficiency for an EBIS means that practically all of the injected ions also are extracted and not lost for one or another reason. There are two measures for the efficiency that will be used onwards – the total and the partial efficiency defined as:

$$\text{Total efficiency} = \frac{\text{number of extracted ions}}{\text{number of injected ions}}$$
$$\text{Partial efficiency} = \frac{\text{number of extracted ions in peak charge state}}{\text{number of injected ions}} \qquad \textbf{(79)}$$

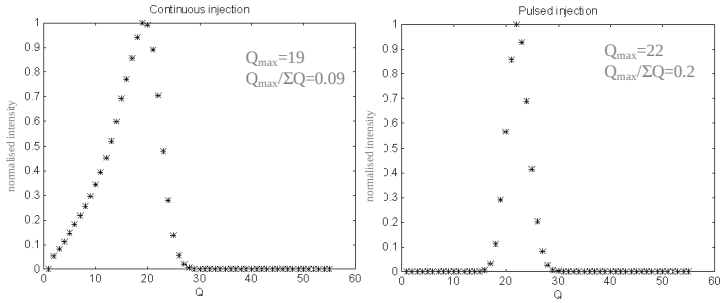

Figure 74. *Charge-state distributions for continuous (left) and pulsed (right) injection. The confinement time is in both cases 20 ms; electron beam energy 5 keV; electron current density 200 A/cm^2; ion species Xe.*

3.6.3 Potential settings and injection energy

As mentioned in the introduction we have developed a few theoretical arguments associated with the injection conditions that show that the trapping efficiency, and thereby the total and partial efficiencies, for continuous injection is bound to be less than 100%. Important parameters for these arguments are the:

- injected ion beam emittance ε
- injected ion-beam energy-spread ΔU_{in}
- injected ion beam energy U_{in}
- barrier potential $U_{barrier}$
- electron beam potential well ΔU
- beam axis potential U_{beam}

and their definitions can be found in Figure 75.

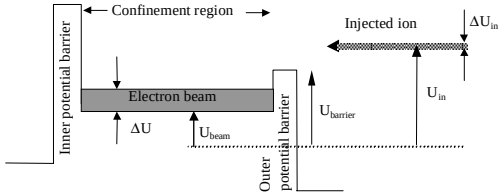

Figure 75. *Potential and energy definitions for continuous injection.*

3.6.3.1 Ion energy contra barrier potential

At injection single-charged ions have to climb the outer potential barrier, and therefore the barrier must of course be lower than the lowest injection energy U_{in}-ΔU_{in}/2 if all ions should have the possibility to enter the confinement region. However, this potential requirement is necessary but not enough since the ion beam has also a finite emittance. Ions entering the EBIS with a large trajectory radius or divergence oscillate in the electron beam (large radial momentum) and/or pick up azimuthal momentum from the solenoidal magnetic field, so they may bounce at the outer potential barrier because of a lack in axial momentum. In other words, the acceptance shrinks with decreasing U_{in}-$U_{barrier}$. From this point of view, the threshold should be as low as possible compared with the ion energy (however, there is no need to go below the bottom of the electron beam potential well).

3.6.3.2 Ion energy contra electron beam potential

Inside the confinement region the ions should have an energy less than $\Delta U+U_{beam}$. Otherwise the ions are not completely energetically trapped within the electron beam, and have therefore the possibility to elude ionisation by circling around the electron beam. Such ions can leave the trap after one bounce, and are then lost. Thus, for this reason the injection energy should be low, but not too low, since that leads to a decrease in the acceptance (see sec. 3.3.3.3), and definitively not lower than U_{beam} because then they are energetically disqualified to enter the trap. Note that the trap potential U_{beam} grows linearly while ΔU decreases linearly with increasing beam compensation. Thus, possibly the injection energy U_{in} and the outer potential barrier $U_{barrier}$ should vary with the compensation degree.

3.6.3.3 Requirements for trapping

The ions are not automatically trapped even if they are ionised inside the confinement region. The following energy/potential relation must be fulfilled for the ion to be trapped at ionisation from 1^+ to 2^+:

$$U_{in} + U_{beam} + U_{ionisation} < 2U_{barrier} \qquad \textbf{(80)}$$

where $U_{ionisation}$ is the potential within the electron beam at the position of ionisation[16]. That means that a higher potential barrier or lower injection energy give a larger trapping probability. This requirement is in contradiction with the ones specified in the two previous sections. Moreover, since U_{beam} increases with the electron beam compensation, the barrier ought to follow. What further increases the trapping probability is ionisation to higher charge-states than 2^+, and this is obtained by a higher electron beam current density.

The optimal settings for a high efficiency are dependent on the energy spread of the injected beam, the emittance of the primary ion source, the ionisation cross-section, the compensation etc, and are always a compromise between a large acceptance and a high trapping efficiency.

3.6.3.4 Pre-ionisation

During the transport from the collector to the confinement region, the ions move more or less within the electron beam and can therefore already there be ionised to higher charge-states. This is undesirable since it means that the ions will probably bounce at the outer potential barrier and not enter the confinement

[16] The ions can be trapped even if the relation is not fulfilled as long as they have a large radial oscillation or azimuthal oscillation, which disqualifies them to climb the outer potential barrier on when trying to leave the trap.

region. To avoid this, the transport time should be minimised, i.e. the velocity should be high and this is obtained by applying a potential to the drift tubes which is well below the injection energy.

3.6.4 Experimental results

At CRYSIS in Stockholm continuous injection is used regularly with an acceptable efficiency for injection of weak 1^+ ion currents from DC sources (<1 μA). No dedicated experiments to verify the optimised total efficiency has been carried out, but crude measurements of the total efficiency for Pb^{55+} and Ar^{18+} breeding give values of 0.5 and 2%, respectively. One has to keep in mind that these are non-optimised values, with possible ion heating affecting the result.

In connection with the design of REX-ISOLDE, measurements of the total efficiency for continuous injection were carried out on the Dioné EBIS at Saclay [152]. Primary 1^+ ions of nitrogen were injected continuously during the confinement period, and after 38 ms the ions very extracted with N^{5+} as the most abundant charge-state. They reported a total efficiency of very poor 0.04%. The reason for this extraordinary low efficiency was probably a fully compensated electron beam. The number of injected 1^+ ions ($8.5\cdot10^{10}$ ions ⇔ $13.6\cdot10^{-9}$ C) exceeded the electron-beam space-charge (~$3\cdot10^{-9}$ C) by a factor of 4, and after charge breeding to $<Q>=5^+$, yet another factor 5 of the number of ions ought to be lost. Thus, just by using more moderate injection conditions, a factor 20 could be gained in efficiency. Furthermore, the outer potential barrier was set as low as possible to minimise the primary ion acceleration when they entered the confinement region. This setting is not necessarily the optimal as was shown in the previous section. The author's own explanations for the poor result are the low electron current (I_e=60 mA) and the high energy with which the ions enter the trap. That could be correct since the former condition leads to a small EBIS acceptance, which the injection might not have been tuned for.

3.6.5 Conclusions on continuous injection

There are several advantages with continuous injection, but to be efficient it imposes higher requirements on the injected beam properties. We have presented some arguments showing that the total efficiency can not reach 100% due to the compromise between a large acceptance and a large accepted injected ion energy spread on one hand, and a high trapping probability on the other. In other words, the total efficiency is a combination of the acceptance and trapping probability, and both can not be optimised simultaneously. It is important to stress that the acceptance is smaller for continuous injection compared with pulsed injection, so even if a primary ion source (the source injecting ions into the EBIS) has an acceptable emittance for pulsed injection, it might produce a beam with too large emittance for continuous injection.

The optimal settings for a high efficiency are most likely an injection energy just below the upper electron beam potential, with an outer potential barrier height adjusted to strike a balance between a high acceptance and high trapping probability. Since the beam axis potential axis varies in time with the electron beam compensation, the injection energy and barrier height might have to be adjusted in accordance.

No absolute numbers for the trapping and total efficiencies have been calculated since it is a complicated and intricate business, due to the fact that there is a correlation between the position in the injection phase space and the trapping probability[17]. Even if the Dioné EBIS at Saclay showed a very poor total efficiency for continuous injection (0.04%), runs at CRYSIS indicate a much higher efficiency, and it is the belief that it can reach at least several percent, which means that it would become an attractive alternative to the Penning trap – EBIS arrangement.

[17] Depending on where the ions start in the injection phase space, they will end up at different trajectories within the electron beam, and thereby be ionised at different positions/potentials. That means thereexists a correlation between the position in the initial phase space and the trapping probability. In addition, ionisation to higher charge-states may occur that complicates the situation even more.

Part IV – Conclusions

A summary of the REXEBIS design and construction has been presented in this report. The EBIS will fulfil the requirements specified by REX-ISOLDE, that is to:

- charge breed ions with A<50 to a Q/A-value >1/4.5 within 20 ms
- accept an injected ion beam delivered by the Penning trap with a transverse emittance of 3 π·mm·mrad at 60 keV, an energy spread of 5 eV, and a pulse length of 10 μs
- deliver a beam with an geometrical emittance <40 π·mm·mrad at 20 kV extraction voltage and an energy spread <50 eV/Q
- charge breed $<10^7$ ions per pulse
- manage a repetition rate up to 100 Hz

This has been proved viable by extensive simulations and calculations. The design is based on a 0.5 A electron beam produced in a magnetic field of 0.2 T that is compressed by a 2 T solenoidal field to a current density of >200 A/cm^2. The 2 T magnetic field is provided by a warm-bore superconducting solenoid, thus giving easy accessibility to the inner structure but no cryogenic pumping. The EBIS is switched between 60 kV (ion injection) and ~20 kV (ion extraction).

The electron beam is produced by an immersed gun, which is fairly insensitive to axial displacement. The design allows a certain degree of freedom in electron beam current and current density. The inner structure with its few drift tubes is placed inside the warm bore, and most of the details are manufactured in titanium due to its possibly gettering property. The electron collector design is novel, yielding: a low fraction of electrons that re-enter the trap region; small aberrations on the ion beam; a high pumping conductance. Simulations showed that the fraction of electrons that re-entered the trap region is less than 0.25%. This value is considerably lower than the result from a simulation performed on a similar system, and it is attributed to a more realistic model, and a better designed collector.

Heating problems connected to baking of the inner structure, or heating of the collector by the electron beam, were demonstrated to be insignificant. We developed a simple method to verify the magnetic field straightness, and found the traced central field line to be within a cylinder of radius 0.1 mm concentric with the geometrical axis for the full EBIS length (-800<z<800 mm). The field mapping procedure has the advantage that it cancels possible bending of the test tube that holds the hall probe, which otherwise can affect the result more than the sag due to the tube weight.

Ion heating by the electron beam is small for the REXEBIS (less than a few eV), and will not cause ion losses from the potential well. It was proven that the drift tube alignment does not have to be better than within 1 mm, a factor 10 less accurate than previously claimed, nor does the magnetic field homogeneity need to be 0.1%, rather some percent. The electron beam scalloping is neither that hampering for the functionality of the REXEBIS since the central potential ripple is only ±5 V, which should be compared with an electron beam potential well of ~100 V. Though, a more severe problem is Penning trapping of secondary electrons at the post anode or at the inner barrier. The build-up of negative space charge may create electron beam instabilities. Spitzer heating of the secondary electron might be enough to eject them, and simulations showed that an applied asymmetric radial electric field could promote the electrons to leave the trap. Experimental tests on the EBIS are the only confident way to determine if Penning trapping is a real problem. If that should be the case, the use of the optional post anode must be excluded.

Estimations of the vacuum in the trap region showed that the residual gas pressures originating from surface out-gassing and Ar backflow from the Penning trap can be kept at an acceptable level with the help of vacuum fired material, turbo and NEG pumps, and an effective differential pumping between the REXTRAP and the REXEBIS. An Ar pressure of $1\cdot10^{-12}$ torr should be attainable, and the other rest-gas partial pressures were calculated to be: $p(H_2)=5\cdot10^{-12}$, $p(CO)=3\cdot10^{-12}$, $p(CO_2)=2\cdot10^{-12}$, $p(CH_4)=5\cdot10^{-13}$ torr. Assuming these partial pressures, the extracted ion spectrum from the EBIS can contain residual gas peaks that are two magnitudes of order larger than the injected ion peaks in some cases, which should be manageable by the mass separator. The pressure is of no worry from an electron-beam compensation point of view.

A design study of an emittance meter dedicated to record the extracted beam properties has been carried out. It is of so-called pepperpot type, consisting of a two-dimensional array with a fluorescent plate some centimetres behind, and a recording CCD camera. Tests performed on CRYSIS with a low quality CCD camera and a P47 fluorescent plate were very promising, though, one has to keep in mind that the REX-ISOLDE ion intensities are very low, and the only possibility to obtain a reasonable signal is to use a pilot beam or gas injection. The idea to use a drift tube arrangement to retard the injected 60 keV beam and to allow an extraction at around 20 kV was abandoned for practical reasons, and instead it was decided to switch the REXEBIS platform between injection and extraction. Several design proposals for the high voltage switching have been presented and investigated, however, due to the construction delicacy and the needed manpower; it was decided to buy a commercial switching power supply.

A complete EBIS was modelled in the ion-tracing program SIMION. The time-dependent model included magnetic and electrical fields as well as charge breeding, though, it did not deal with collective plasma effects. For EBIS conditions similar to those in the REXEBIS (i.e. moderate Q/A, non-compensated trap and low residual gas pressure) the single-particle model is valid, and complete injection, breeding and extraction cycles were simulated to certify the high injection and extraction efficiencies necessary for the REXEBIS. Beam optics parameters such as drift tube potentials, lens positions and voltages, accepted beam tilt and displacement tolerances at the focal points were also settled using the EBIS model. The simulations should ensure an injection and extraction efficiency close to 100%.

The rhomboidal shape of the acceptance phase space might be explained by the fact that the ions are injected into a region with non-linear field, more exactly a cubic field, in this case caused by the fringe field from the electron beam when it is absorbed at the collector. A slightly wrong implementation of the electron beam model may have accentuated this feature. An analytical acceptance expression for an EBIS was derived and verified with simulations. The formula implies that the acceptance for an EBIS with parameters similar to the REXEBIS is independent of ion mass, charge and magnetic field as long as the electron-beam potential-well is not compensated. The acceptance into the trap increases if the injection energy is increased a few hundred eV above the outer barrier potential, although the average time spent within the electron beam decreases. In principle the acceptance is limited by the beam optics elements and the drift tubes if one is not concerned about how well the ions are injected into the electron beam well.

The emittance was found to be charge-dependent. The reason for the decrease in emittance with increasing charge-state is the change in mean ion trajectory radius within the trap when the ions are successively charge bred. In other words, the radial distribution of the ions becomes more axially centred with higher charge-state. The energy spread of the extracted beam is caused by the charge breeding heating, and was estimated to be 15 eV/Q (1σ). This low value is valid for an uncompensated electron beam.

The maximal geometrical acceptance was determined to 11 π·mm·mrad for $^{30}Na^{1+}$ ions with 60 keV injection energy. The emittance was shown to be independent of the magnetic field, which is an important observation since it is often claimed that the emittance is directly proportional to the B-field. The latter statement is in principle only true for a compensated trap. The residual gas emittance, represented by $^{16}O^{4+}$ ions, had a geometrical emittance of about 20 π·mm·mrad (20 kV). If $^{30}Na^{1+}$ ions are injected correctly into the REXEBIS (within the electron beam), a geometrical emittance of about 10 π·mm·mrad (20 kV) should be obtained for $^{30}Na^{7+}$ ions; somewhat higher for ions with lower charge-state, and vice versa for higher charge bred ions. If the ions are injected within the specified 3 π·mm·mrad phase space, the emittance will be even smaller. The absolute maximum emittance occur for ions that are not fully trapped within the electron beam and not charged bred, i.e. they are extracted as 1^{+}. Then the emittance can amount 30 π·mm·mrad or even higher values.

Ion beam simulations showed that any possible correlation between the two emittance transverse phase spaces for the extracted ions is insignificant for the REXEBIS: the correlation is small with a mean azimuthal ion velocity $< v_\theta >$=65 m/s much smaller than the standard deviation $\sigma(v_\theta)$ =1100 m/s. The low degree of correlation is due to the large transverse energy spread inside the EBIS, causing the ions to move in random directions. Thus, the adding of a skew quadrupole does not affect the emittance significantly.

The simulations of the ion beam extraction from CRYSIS suggested that the large discrepancy between measured and theoretically expected emittance could be explained by aberrations in the collector exit and the succeeding narrow einzel lens. The final emittance value is strongly related to the electron beam radius inside CRYSIS since the inherent emittance grows linearly with it. Also the beam distortion adding to the inherent emittance increases with the electron beam radius. The measured emittance value of 70 π·mm·mrad (2σ) can therefore very well be explained by an aberrated ion beam created in an electron beam with a radius of 0.2-0.3 mm. An open collector design in combination with a wider einzel lens would most certainly reduce the problem and decrease the emittance.

Finally, the advantages with continuous ion injection into an EBIS called for an investigation of the hitherto obtained poor efficiency for that mode. We have presented some arguments showing that the total efficiency can not reach 100% since it is a combination of the acceptance and trapping probability, and both can not be optimised simultaneously. It is important to stress that the acceptance phase space is decreased for continuous injection as compared to pulsed injection mode, so even if the primary ion source has an acceptable emittance for pulsed injection, it is not necessarily the case that it is enough confined for continuous injection. The optimal settings for a high efficiency are most likely an injection energy just below the upper electron beam potential, with a potential barrier height adjusted to strike a balance between a high acceptance and high trapping probability. Even if the Dioné EBIS at Saclay showed a very poor total efficiency for continuous injection (0.04%), tests at CRYSIS indicate a much higher efficiency, and it is our belief that it can reach at least several percent, which means that it would become an attractive alternative to the Penning trap – EBIS arrangement.

A compilation of the most important design parameters for the REXEBIS is presented on the next page.

Acknowledgements

This experiment is funded by the Knut and Alice Wallengerg Stiftelse, Sweden.

Solenoid	
Central magnetic field	variable between 0.1and 2.0 T
Field homogeneity over ±400 mm on axis	0.25% (measured) 0.3% (specified)
Field straightness	$r_{central}$<0.1 mm over -800<z<800 mm (measured) $r_{central}$<0.5 mm over -825<z<825 mm (specified)
Relative field decay	$13 \cdot 10^{-6}$ h^{-1} (measured) $5 \cdot 10^{-6}$ h^{-1} (specified)

Inner structure	
Trap length	100, 230, 332, 464, 696 or 798 mm
Trap capacity	$6 \cdot 10^{10}$ charges
Number of drift tubes	6
Drift tube inner radius	5 mm
Electron-beam energy	5 keV
Electron-beam radius	0.25 mm
Electron-current density	>200 A/cm^2 (~250 A/cm^2)
Tube-to-beam axis voltage	-750 V
Electron beam potential depth	107 V
Beam ripple	±5 V
Drift tube material	titanium

Collector	
Collector voltage relative to cathode	2000 V
Suppressor voltage relative to cathode	1500 V
Extractor voltage relative to collector	-17 000 V
Power dissipation	1000 W
Material	OHFC
Electron load	<8 mA/cm^2
Direct reflected, back-scattered and secondary electrons	<0.1%, 0.1%, 0.05%

Electron gun	
Gun type	Semi-immersed
Cathode material	LaB_6 310-crystal orientation
Cathode temperature T_c	1750 K
Cathode life-time	1 year
Cathode current density j_c	25 A/cm^2
Cathode diameter	1.6 mm
Magnetic field at cathode B_c	0.2 T
Electron beam current I_e	0.46 A
Anode voltage U_{anode}	6500 V
Perveance P	0.87 A/V$^{3/2}$
Post anode voltage $U_{post\ anode}$	~10 000 V (optional)
Compression	from 25 to >200 A/cm^2 (~250 A/cm^2)
ω_L/ω_p in full field	5.1
Radial gun misalignment Δr_c	<1.3 mm
Gun tilt $\Delta(dr/dz)_c$	<4 mrad
Axial gun misalignment Δz_c	<±5 mm

Turbo pumps	
Two 180 *l*/s	One 260 *l*/s
Compression N_2 >$1 \cdot 10^{12}$, He $2 \cdot 10^8$, H_2 $5 \cdot 10^5$	Compression N_2 >$1 \cdot 10^9$, He $3 \cdot 10^5$, H_2 $1.3 \cdot 10^4$

NEG pumps	
H_2 pumping speed	0.5 *l*/cm^2·s
O_2, N_2 and CO_x pumping speed relative H_2	65%, 15% and 40%
Hydrocarbon sorption efficiency relative H_2	<0.1%

Ion beam properties (simulated)		
Specified geometrical acceptance	3 π·mm·mrad (60 kV)	
Maximum geometrical acceptance	11 π·mm·mrad (60 kV)	
Geometrical emittance	<19 π·mm·mrad (20 kV)	
Extracted energy spread per Q	15 eV (1 σ)	
	Injection	Extraction
Tilt	±0.3°	±1°
Transversal displacement	±5 mm	±20 mm

A compilation of the most important design parameters for the REXEBIS.

Commonly used symbols

A	mass number
α	acceptance (mm·mrad)
B	magnetic field (T)
B_z	axial magnetic field (T)
e	elementary charge ($1.6 \cdot 10^{-19}$ C)
E_e	electron beam energy (eV)
ε_0	permittivity constant ($8.854 \cdot 10^{-12}$ Fm^{-1})
ε	emittance (mm·mrad)
h	Planck constant ($6.626 \cdot 10^{-34}$ J·s)
I_e	electron beam current (A)
j_e	electron-beam current-density (A/m^2)
k	Boltzmann's constant ($1.38 \cdot 10^{-23}$ J/K)
m_e	electron mass ($9.1 \cdot 10^{-31}$ kg)
N	neutron number
ω_c	cyclotron resonance frequency (rad/s)
p	pressure (1 Pa=$1 \cdot 10^{-2}$mbar=$7.6 \cdot 10^{-3}$ torr)
q	ion charge (C) or ion charge-state depending on the context
Q	ion charge-state
q_{desp}	gas desorption rate per unit area (torr·*l*/cm^2·s)
Q_{desp}	gas desorption rate (torr·*l*/s)
r and θ	cylindrical coordinates
r_t	drift tube inner radius (m)
r_{ebeam}	electron beam envelope (m)
ρ_l	electron beam charge per unit length (C/m)
S	pumping speed (*l*/s)
$\sigma_{q \to q+1}$	ionisation cross-section from q to q+1 (m^2)
T	temperature (K)
τ	breeding time (s)
u	mass number
U_e	electron beam potential relative cathode potential (V)
U_{ext}	extraction voltage (V)
U_{dec}	deceleration voltage (V)
U_t	drift tube potential relative cathode potential (V)
ΔU	electron beam potential depth (V)
v_e	electron velocity (m/s)
v_θ	azimuthal ion velocity (m/s)
Φ	magnetic flux (T/m^2)
Z	proton number

Acronyms

CCD	Charge Coupled Device
CRYSIS	CRYogenic Stockholm Ion Source (EBIS at Manne Siegbahn Laboratory)
DSSSD	Double Sided Silicon Strip Detector
EBIS	Electron Beam Ion Source
ECR	Electron Cyclotron Resonance
IH-structure	Interdigital H-structure
ISOL	Isotope Separator On-Line
LINAC	LINear ACcelerator
MCP	Multi Channel Plate
NEG	Non-Evaporable Getter
PIG	Penning Ionisation Gauge
REX-ISOLDE	Radioactive EXperiment at ISOLDE
RFQ	Radio Frequency Quadrupole

Appendix 1. Magnet blueprints: end and side view.

(The drawings have been edited due to copyright reasons. No further copying or reprint is allowed.)

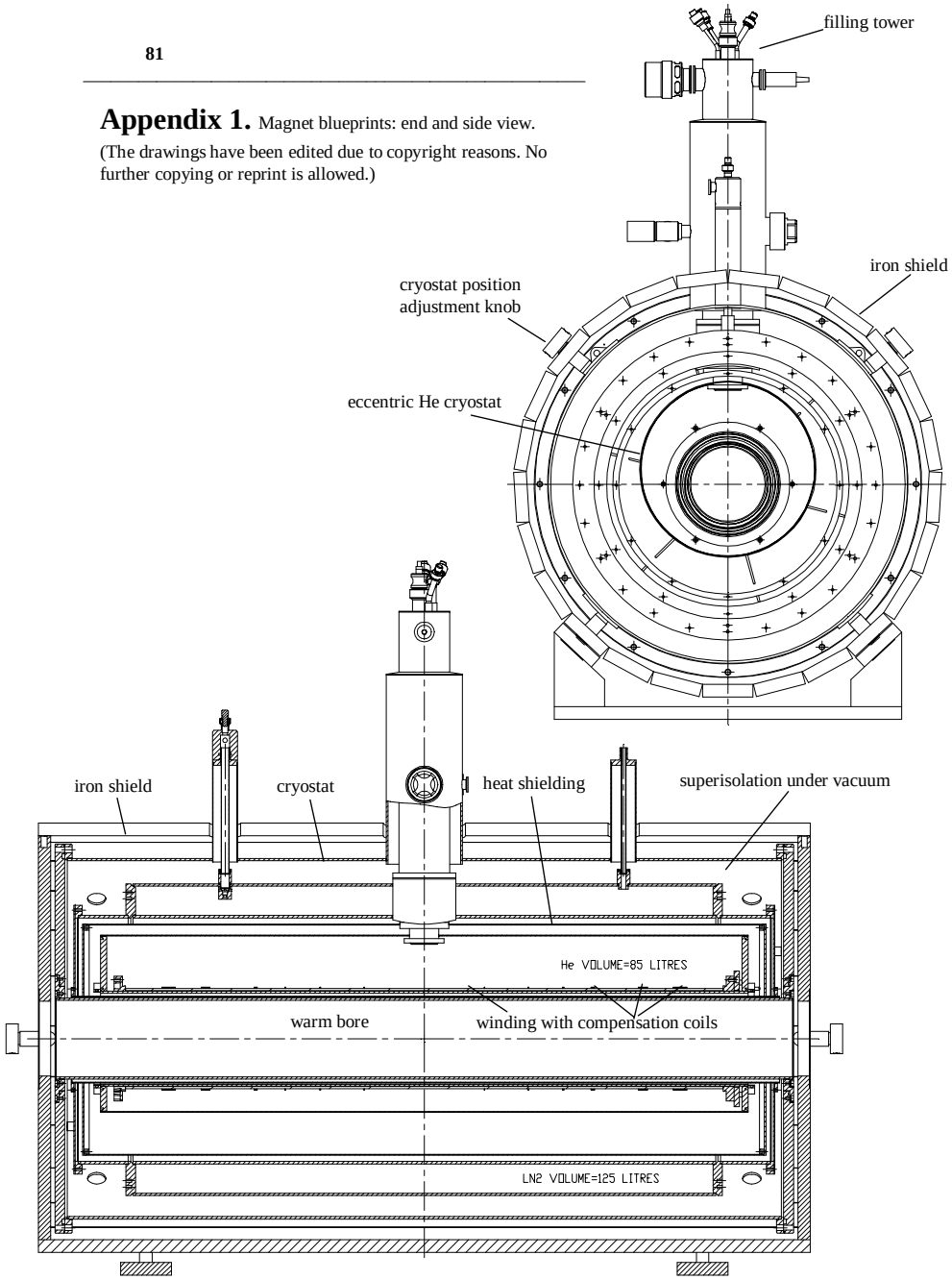

Appendix 2. Beam profiles and phase spaces at the 2nd bender at injection and extraction.

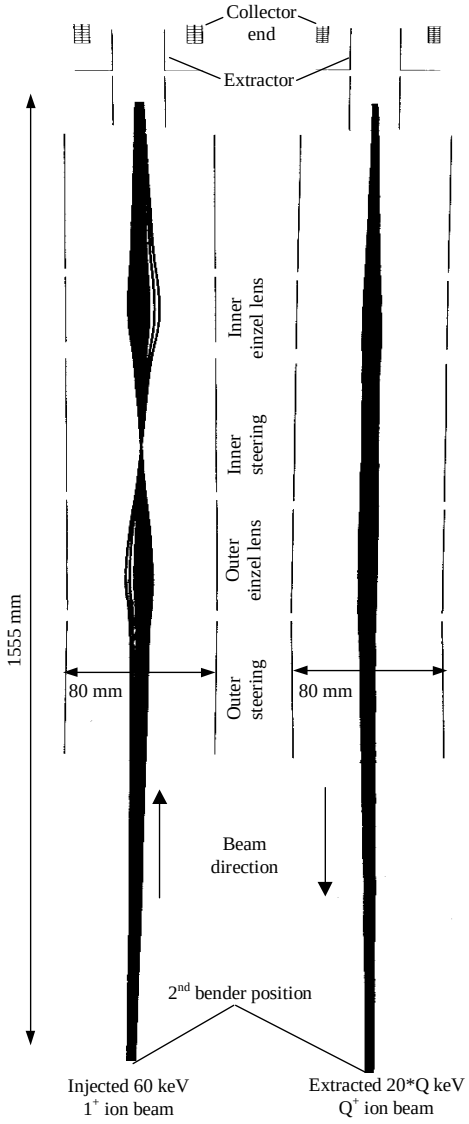

Acceptance phase space

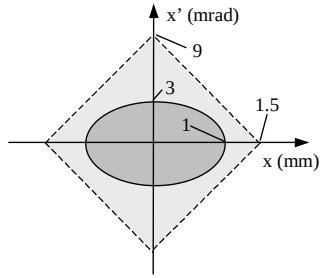

Acceptance phase space at 2nd bender focus for a 60 keV ion beam.

Ellipse: specified geometrical acceptance.
Rhomboid: simulated geometrical acceptance.

Emittance phase space

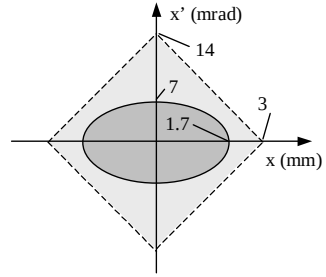

Emittance phase space at 2nd bender focus for a 20 kV extraction voltage. Note that the two lenses facilitate shaping of the phase space to a certain extent.

Ellipse: $^{30}Na^{7+}$ geometrical emittance.
Rhomboid: Geometrical emittance for poorly injected ions extracted as 1^+ (almost 'worst' case)

Appendix 3. Control system parameters

Gun platform	Cathode heater voltage	R/W	Analogue DC	Profibus
	Cathode heater current	R	-"-	-"-
	Collector voltage	R/W	-"-	-"-
	Collector current	R	-"-	-"-
	Suppressor voltage	R/W	-"-	-"-
	Suppressor current	R	-"-	-"-
REXEBIS platform	Trap 1 voltage	W	µs switching	Function generator controlled
	Trap 2 voltage	W	-"-	-"-
	Trap 3 voltage	W	-"-	-"-
	Outer barrier voltage	W	-"-	-"-
	Cathode voltage	R/W	Analogue DC	Profibus
	Cathode current	R	-"-	-"-
	Extractor voltage 1	R/W	-"-	-"-
	Extractor current 1	R	-"-	-"-
	Extractor voltage 2	R/W	-"-	(optional)
	Extractor current 2	R	-"-	-"-
	Inner einzel lens voltage	W	ms switching	Delay-gate-generator
	Outer einzel lens voltage	W	ms switching	-"-
	Gun vacuum, Pe and Pi	R	Analogue	ISOLDE controlled
	Collector vacuum, Pe	R	-"-	-"-
	OVC vacuum Full range	R	-"-	-"-
	LqHe and LqN_2 level	R	RS232	
	Magnet current	R/W	One common serial transfer	
	Field meter	R		
	2 gate valves	R/W	Digital	ISOLDE controlled
	2 turbos	R/W	-"-	-"-
Extractor platform	Extractor deflector x voltage	W	ms switching	Delay-gate-generator
	Extractor deflector y voltage	W	-"-	(optional)
Ground potential	HV platform switching	R/W	µs switching	Function generator controlled
	TOF chopper	W	TTL	Pulse synchronised with function generator
	TOF signal	R	MCA	
	Faraday cup/Channel plate	R	-"-	
	2 inner deflector x voltage	W	ms switching	Delay-gate-generator
	2 inner deflector y voltage	W	"	-"-
	2 outer deflector x voltage	W	"	-"-
	2 outer deflector y voltage	W	"	-"-
	3 cooling water flow	W	Digital	ISOLDE controlled
	Optics turbo	R/W	Digital	-"-
	Prevacuum turbo	R/W	-"-	-"-
	Gate valve	R/W	-"-	-"-
	Leak valve	R/W	-"-	-"-
	End valve	R/W	-"-	-"-
	Rough valves	R/W	-"-	-"-
	Optics vacuum, Pe and Pi	R	Analogue	-"-
	Preturbo vacuum, Full range	R	-"-	-"-

Appendix 4. Motivation for a rhomboidal acceptance phase space and its increase in size with injection energy.

Rhomboidal shape

In the simulations we noticed that the phase space outside the collector had the shape of a tilted rhomb, but inside the drift tube region, the shape was elliptic. This suggests that the odd shape is created in the collector region. Rhomboidal phase space shapes could appear non-linear field regions with cubic fields ($F_r \propto r^3$) [143], where the ellipse is distorted to a rectangular form. Since the magnetic field played an insignificant role for the size of the rhomboid, we conclude that the odd shape originates from the electrostatic fringe field that is formed when the electron beam is absorbed in the collector region.

Energy dependence

In sec. 3.3.3.3 we claimed that the size of the phase space is dependent on the ion energy, and by increasing the ion injection energy it can be enlarged. We will here in a somewhat hand-wavy style motivate that statement.

The ion injection energy is divided into several components when the ion enters the EBIS. First of all a large portion is converted into potential energy E_{pot}. It consists of the $E_{platform}$ part (the whole EBIS is on high voltage) and a radial-dependent part E(r) created by the electron beam space charge. The kinetic energy is divided into longitudinal momentum, radial oscillation and azimuthal rotation. The last motion is fairly small compared to the radial oscillation in the REXEBIS case, and therefore left out in the following argument. For an ion to be able to climb the potential hill and enter the trap region, not too much energy must be spent "unnecessarily", that means the E(r) component should be small as well as the radial oscillation inside the trap region. These two parameters are determined by the injection conditions: large initial radius and/or divergence result in large trajectory radius and oscillation inside the trap, and therefore little energy left for the longitudinal motion which is used for climbing the electrostatic potential hill. However, if the injection energy is increased, naturally the initial radius and divergence can be increased, and there will still be enough energy for the longitudinal motion.

A few 100 eV is enough to see an increase in the acceptance phase space, and if one increase the energy more, one encounters aberration problems caused by too narrow lenses and drift tubes.

References

1 Radioactive beam experiment at ISOLDE: Coulomb excitation and neutron transfer reactions of exotic nuclei, proposal to the ISOLDE committee, CERN-ISC94-25, Nov 1994

2 D. Habs, O. Kester, K. Rudolph, P. Thirolf, G. Hinderer, E. Nolte, G. Bollen, H. Raimbault-Hartmann, H. Ravn, F. Ames, L. Liljeby, K-G. Rensfelt, D. Schwalm, R. von Hahn, R. Repnow, A. Schempp, U. Ratzinger, P. van Duppen, M. Huyse, G. Walter, Nucl. Instr. Meth. B126 no.1-4 (1997) p.218-23

3 D. Habs, O. Kester, G. Bollen, L. Liljeby, K.G. Rensfelt, D. Schwalm, R. von Hahn, G. Walter and P. Van Duppen, Nucl. Phys. A616 (1997) p.29c-38c

4 The REX-ISOLDE Project, D. Habs, O. Kester, T. Sieber, A. Kolbe, J. Ott, G. Bollen, F. Ames, D. Schwalm, R. von Hahn, R. Repnow, H. Podlech, A. Schempp, U. Ratzinger, L. Liljeby, K-G. Rensfelt, F. Wenander, B. Jonson, G. Nyman, P. van Duppen, M. Hyuse, A. Richter, G. Schrieder, G. Walter, and the REX-ISOLDE collaboration, Nucl. Instr. Meth. B139 no.1-4 (1998) p.128-35

5 http://fy.chalmers.se/subatom/f2bfw/rexposter.html

6 http://www.ha.physik.uni-muenchen.de/okester/rex/rex.html

7 http://www.cern.ch/ISOLDE/

8 B. Jonson, H. L. Ravn, G. Walter, Nucl. Phys. News vol.3 no.2 (1993) p.5

9 E.D. Donets and V.I. Ilyushchenko, JINR R7-4124, 1968

10 E. Beebe, L. Liljeby, Å. Engstöm, M. Björkhage, Phy. Scr. vol.47, (1993) p.470-474

11 H. Raimbault-Hartmann, D. Beck, G.Bollen, M. König, H-J. Kluge, E-Schark, J.Stein, S. Schwarz, J. Szerypo, Nucl. Instr. Meth. B126 (1997) p.378-382

12 G. Bollen, S. Becker, H-J. Kluge, M. Konig, R.B. Moore, T. Otto, H. Raimbault-Hartmann, G. Savard, L. Schweikhard, H. Stolzenberg, Nucl. Instr. Meth. A368 (1996) p.675

13 Proc. 1st Int. Conf. on Radioactive Nuclear Beams, Berkeley (Califonia), Oct. 1989, ed. W. D. Myers, J. M. Nitschke, E. B. Norman (World Scientific, Singapore, 1990)

14 Proc. 2nd Int. Conf. on Radioactive Nuclear Beams, Lovain-la-Neuve (Belgium), Aug. 1991, ed. Th. Delbar (Adam Hilger, Bristol, 1992)

15 Proc. 3rd Int. Conf. on Radioactive Nuclear Beams, East Lansing (Michigan), May 1993, ed. D. J. Morrissey (Editions Frontieres, Gif-sur-Yvette, Cedex, France, 1993)

16 Proc. 4rd Int. Conf. on Radioactive Nuclear Beams, (Omiya), June 1996, Japan

17 European radioactive beam facilities, Statement by NuPECC (1993), ed. R.H. Siemssen

18 Report from the "NuPECC Study Group on Radioactive Beam Facilities", Nuclear Physics European Collaboration Committee Europe, 2000

19 D. Habs, D. Rudolph. O. Kester, P. Thirolf, P. Reiter, D. Schwalm, G. Walter, P. Van Duppen, J. Eberth, REX-ISOLDE Collaboration, Zeitschrift-für-Physik-A (Hadrons and Nuclei), vol.358 no.2 (1997) p.161-162

20 D. Habs, D. Rudolph, P. Thirolf, C. Fischbeck, C. Gund, D. Schwalm, J. Eberth, E. Grosse, H. Prade, H. Emling, J. Gerl, R.M. Lieder, P. Van-Duppen, C. Rossi-Alvarez, M. Pignanelli, Particle-and-Nuclear-Physics (UK) vol.38 (1997) p.111-26

21 H. Scheit et al., CERN IS379 P114

22 L. Axelsson et al., CERN-ISC 98-23 ISC-P105

23 B. Jonson et al., CERN-ISC 98-11 ISC-P100

24 A. N. Ostrowski et al., CERN-ISC 97-25 ISC-P-93

25 B. Jonson et al., CERN-ISC 97-27 ISC I27

26 M. V. Andrés et al., CERN-ISC 97-10 ISC I21

27 R. Chapman et al., CERN-ISC 93-12 ISC I6

28 M. Wiescher, CERN-ISC 94-21 ISC I11

29 L. Campajola, CERN-ISC 97-1 ISC I20

30 N. Forton, Phys. Rev. Lett. 70 (1993) p.2383

31 G. Gwinner et al., Phys. Rev. Lett. 72 (1994) p.3795

32 D. Beck CERN-ISC 99-13 ISC-P111

33 D. Forkel-Wirth et al., CERN-ISC 94-27 ISC I13

34 G. Weyer et al., CERN-ISC 94-24 ISC I12

35 H. Haas et al., CERN-ISC 94-29 ISC I15

36 J. Äystö, G. Bollen, A. C. Mueller, G. Pollarolo, A. Povès, K. Riisager, M. Schädel, A. Shotter, J. Vervier, 'EXOTIC NUCLEI AND RADIOACTIVE BEAMS: Highlights and Perspectives in Europe', (Report to the European Nuclear Physics Collaboration Committee), March 1997

37 J. Vervier, Nuclear-Physics-A, vol.A616 no.1-2 (1997) p.97-106

38 B. Laune, AIP-Conference-Proceedings (USA), no.392 pt.1 (1997) p.381-384

39 The SPIRAL Radioactive Ion Beam Facility, May 1994, Ganil R 9402

40 http://ganinfo.in2p3.fr/spiral/presentation.html

41 P. G. Bricault, R. Baartman, G. Dutto, S. Koscielniak, R. E. Laxdal, R. Poirier, L. Root, P. W. Schmor, G. Stanford, eds. C. Hill, M. Vretenar., Proceedings of 18th International LINAC Conference (LINAC 96), Geneva, Aug. 1996, vol.1 p.399-401

42 http://www.triumf.ca/isac/lothar/isac.html

43 Oak. J. B. Ball, International Symposium on Nuclear Structure Physics Today, Changli, Taiwan, May 1993, Nucl. Phys. A570 no.1-2 (1994) p.15c-22c

44 http://www.phy.ornl.gov/hribf/hribf.html

45 From the REX-ISOLDE drawing library at LMU Munich, Sektion Physik

46 H. L. Ravn, P. Bricault, G. Ciavola, P. Drumm, B. Fogelberg, E. Hagebø, M. Huyse, R. Kirchner, W. Mitig, A. Mueller, H. Nifenecker, E. Roeckl., Nucl Instr. Meth. B88 (1994) p.441-461

47 G. Bollen, Nucl. Phys. A616 no.1-2 (1997) p.457c-468c

48 Stein, diploma thesis, Mainz University, 1994

49 G. Bollen et al. J. Appl. Phys. 68 (1990) p.4355

50 G. Bollen, et al., Nucl. Instr. Meth. A368 (1996) p.675

51 R. W. Schmieder, 'Physics of highly-ionised atoms', Plenum, New York, 1989, p.321-376

52 H. Haseroth, C. E. Hill, Proc of the 6th International Conference on Ion Sources, 1995, Sept. ed. P. Schmor, Rev. Sci. Instrum. 67 (1996) no3 p.945

53 A.O. Nier, T.R. Roberts, and F.J. Franklin, Phys. Rev. 75 (1949) p.346

54 A. Schempp et al., Nucl. Inst. Meth. B10/11 (1985) p.831

55 J. Friedrich et al., IEEE-PAC91, San Francisco, (1991) p.3044

56 C.-M. Kleffner, et al., EPAC92, (1992) p.1340

57 E. Nolte, et al., Nucl. Inst. Meth. 158 (1979) p.311

58 R. von Hahn et al., Nucl. Inst. Meth. A328 (1993) p.270-274

59 R. von Hahn et al., Proc. of the EPAC92, (1992) p.1313

60 J. Eberth et al., Nucl. Instr. Meth. A369 (1996) p.135

61 P. J. Sellin, P. J. Woods, D. Branford, T. Davinson, N. J. Davis, D. G. Ireland, K. Livingston, R. D. Page, A. C. Shotter, S Hofmann, R. A. Hunt, A. N. James, M. A. C. Hotchkis, M. A. Freer, S. L. Thomas, Nucl. Instr. Meth. A311 no.1-2 (1992) p.217-23

62 P. Sortais, Nucl. Instr. Meth. B98 no.1-4 (1995) p.508-16

63 R. Geller. 'Electron cyclotron resonance ion sources and ECR plasmas', IOP Publishing Ltd, London, 1996

64 R. Keller, in 'The Physics and Technology of Ion Sources', ed. I. G. Brown, New York, Wiley-Interscience, 1989

65 H. Haseroth, C. E. Hill, Proc of the 6th International Conference on Ion Sources, 1995, Sept. ed. P. Schmor, Rev. Sci. Instrum. 67 (1996) no3 p.945

66 E.D. Donets, 'Electron Beam Ion Sources', chapter 12 in 'The physics and Technology of ion Sources', ed. I. G. Brown, New York, John Wiley & Son, 1989, p.245-279

67 R. W. Schmieder, Physics of highly-ionised atoms, New York, Plenum, 1989, p.321-376

68 R. Becker 'Characterization of ion sources', chapter 2/section 11 in 'Handbook of Ion Sources', ed. B. Wolf, CRC Press Inc. 1995

69 W Lotz, Z. Phys 206, (1967) p.205

70 W Lotz, Z. Phys 216, (1968) p.241

71 T. A. Carlsson, C. W. Nestor Jr, N. Wasserman, J. D. McDowell, ATOMIC DATA 2 (1970) p.63-69

72 V. Kalagin, V. P. Ovsyannikov, JINR preprint E9-96-I28 (1996)

73 Y. S. Kim, R. H. Pratt, Phys. Rev. A27 (1983) p.2913

74 A. Müller, E. Salzborn, Phys. Lett. A62 (1977) p.391

75 R. Becker, Proc 3rd EBIS Workshop 1985, Ithaca, eds. V. Kostroun and B.W. Schmieder, p.185

76 L. Spitzer, Physics of fully ionised gases, (Interscience, New York, 1956)

77 G. Drentje, J. Sijbring, KVI Annual Report 1983

78 M. Mack, J. Haveman, R. Hoekstra, A. G. Drentje, 7th Int. Workshop on ECR Ion Sources (Julich) 1986, ed H. Beuscher p.152

79 R. Becker, H. Klein, W. Schmidt, IEEE Trans. Nucl. Sci. NS-19 (1972) p.125

80 M. A. Levine, R. Marrs, R. W. Schmieder, Nucl. Inst. Meth. A237 (1985) p.429

81 E. Beebe, L. Liljeby, A. Pikin, E. D. Donets, D. Habs, K. Janko, O. Tengblad, P. van Duppen, the ISOLDE collaboration, Nucl. Instr. Meth. B93 (1994) p.378-381

82 Borg. S, H. Danared, L. Liljeby, Proc. 3rd international EBIS workshop, ed. V. O. Kostroun, Ithaca, New York (1985) p.47

83 L. Liljeby, Å. Engström, International symposium on electron beam ion sources and their applications, AIP Conf. Proc. no.138, Upton, New York (1988) p.27

84 E. Beebe, L. Liljeby, Å. Engström, M. Björkhage, Status report on the Stockholm electron beam ion source, The 5th International Symposium on Electron Beam Ion Sources and their Applications, Dubna: EBIS-5 Publishing group, 1992, ed. D. D. Donets, I.P. Yudin

85 K. Halbach, R. F. Holsinger, "SUPERFISH - A Computer Program for Evaluation of RF Cavities with Cylindrical Symmetry", Particle Accelerators 7 (1976) p.213-222

86 R. Rao, F. Wenander, A preliminary design of the electron beam optics of the electron beam ion source for REX-ISOLDE, Nucl. Instr. Meth. A416 (1998) p.210-220

87 K. Amboss, Proc. 2nd EBIS Workshop, Saclay-Orsay, ed. J. Arianer, (1981) p.59

88 H. Nishihara, M. Tereda, J. Appl. Phys. 39, (1968) p.4573

89 H. Nishihara, M. Tereda, J. Appl. Phys. 41, (1970) p.3322

90 M. P. Stöckli, C. L. Cocke, J. A. Good, P. Wilkins, International symposium on electron beam ion sources and their applications, ed. A. Hershcovitch, Upton New York, (1988) p.281

91 Superconducting Magnet System, Operator's Handbook, Oxford Instruments, June 1997

92 W. B. Herrmannsfeldt, SLAC-Report-331 1988

93 OPERA 2D ver. 1.5, Vector Fields Oxford, England

94 G. R. Brewer, 'Focusing of high-density electron beams', chapter 3.3 in 'Focusing of charged particles II', ed. A. Septier, Academic Press London 1967

95 G. Herrmann, J. Appl. Phys. 29 (1958) p.127

96 D. Hestenes, 'New foundations for classical mechanics', D. Reidel Publishing Company (1986)

97 F. Chen, 'Introduction to plasma physics and controlled fusion', Plenum New York, (1984) p.142

98 Technical bulletin no.3, FEI Co, USA

99 J. L. Laclare, G. Leleux, 2nd EBIS workshop, Saclay-Orsay, ed. J. Arianer, (1981) p.128-136

100 M. P. Stöckli, Rev. Sci. Instr. vol.69 no.2 (1998) p. 649-651

101 I. Tammaru, Phy. Scr. vol.T71 (1997) p.50-59

102 A. Pikin, E. N. Beebe, M. Björkhage, L. Liljeby, Å Engström, Experimental study of RF oscillations in the Stockholm cryogenic electron beam ion source, to be published

103 W. Pirkl, RF measurements on CRYSIS, MSL annual report 1997, Stockholm

104 R. Becker, Int. Rep. 9-94, Institut für Angewandte Physik der Universität Frankfurt

105 Physics Handbook, ed. C. Nordling, J. Österman, Studentlitteratur Lund Sweden, 1987

106 Plisulate, Thinsulate technical data, M. H Detrick Company Ltd, England

107 Bygg 1 Allmänna grunder, 3:e upplagan, redaktör W. Tell, AB Byggmästarens förlag, Stockholm 1961, kapitel 15

108 B. Bernstein, S. K. Trehan, Nucl. Fusion 1 (1960) p.3

109 A. I. Hershcovitch, P. A. Politzer, Phys. Rev. Lett. 36 (1976) p.1365

110 A. I. Hershcovitch, A. E. Kponou, Nucl. Instr. Meth. Phys. Res. A330 (1993) p.144-149

111 J. Dietrich, Nucl. Instr and Meth. A298 (1990) p.35

112 J. Dietrich, R. Becker. Proc. Fifth Int. EBIS symp. ed. E. D. Donets, Dubna (1992) p.147-165

113 Ch. Goldstein, M. Malard, Proc. 2nd EBIS Workshop, Saclay-Orsay, eds. J. Arianer and M. Olivier, Orsay, (1981) p.149

114 E. H. Darlington, J. Phys, D: Appl. Phys. 8 (1975) p.85

115 H. Bruining, Physica 5 (1983) p.901

116 E. H. Darlington, V. E. Cosslett, J. Phys. D: Appl. Phys. 5 (1972) p.1969

117 Jablonski, J. Gryko, J. Kraaer, S. Tougaard, Phys. Rev. B, vol.39 no.1 (1989) p.61-71

118 H. Kanter, Ann. Phyz. (Ser 6) 20 (1957) p.144

119 H. E. Bishop, Ph.D. Thesis, University of Cambridge, U.K. 1966

120 Ingenjörshandboken, I Allmän del, ed. C. A. Strömberg, Nordisk Rotorgravyr, (1947) p.286

121 The Matworks Inc. http://www.mathworks.com/

122 L. Bagge, Manne Siegbahn Laboratory, Private communication

123 F. J. Norton, J. Appl. Phys, v.28 (1957) p.34

124 Technical bulletin from SAES GETTERS S.p.A, Milano Italy

125 R. S. Vaughan-Watkins, E. M. Williams, Vacuum vol.28 no.10/11 p.459-465

126 M. Q. Ding, E. M.Williams, Vacuum vol.39 no.5 (1989) p.463-469

127 M-H. Achard, R. Calder, A. Mathewson, Vacuum vol.29 no.2 p.53-65

128 R. S. Vaughan-Watkins, E. M. Williams, 8th Int. Vac. Cong. Sept 1980 vol.II p.387-390

129 H. Danared, Manne Siegbahn Laboratory, Private communication

130 S. Humphries Jr., 'Charged particle beams', John Wiley & Sons Inc, New York, 1990

131 M. Sarstedt, R. Becker, H. Klein, A. Maaser, J. Muller, R. Thomas, M. Weber, Nucl. Instr. Meth. B99 (1995) p.721-724

132 J. Camas, G. Ferioli, R. Jung, J. Mann, IEEE Proceedings from 1993 Particle Accelerator Conference, vol.3 p.2498-2500

133 M. Domke, CHR. Dorn, P. Forck, H. Kraus, A. Peters, P. Strehl, 3rd European workshop on beam diagnostics and instrumentation for particle accelerators, Frascati (Rome) - Italy 12-14 October 1997

134 J. Collier, G. Hall, H. Haseroth, H. Kugler, A. Kuttenberger, K. Langbein, R. Scrivens, T. R. Sherwood, J. Tambini, O. B. Shamaev, B. Yu. Sharkov, A. Shumshurov, S. M. Kozochkin, K. N. Makarov, Yu. A. Satov, Rev. Sci. Instr. 67 (3) March (1996) p.1337-1339

135 Product information from Keithley Instruments Inc, http://www.keithley.com

136 A. Paal, Manne Siegbahn Laboratory, Private communication

137 Behkle Electronic GmbH, Frankfurt, Germany, 'Fast high voltage transistor switches, model series HTS'

138 Profibus information homepage, http://www.profibus.com

139 W. Heinze, R. Maccaferri, Nucl. Instr. Meth. A352 (1994) p.147-149

140 P. Schmidt, The REX-Trap – REX-EBIS Control system, Internal report ISOLDE, Feb. 1998

141 D. A. Dahl, J. E. Delmore, A. D. Appelhaus, Rev. Sci. Instr. Vol.61 (1990) p.607

142 J. Axelsson, 'Ion injection into Electron Beam Ion Source', diploma thesis, Manne Siegbahn Laboratory Stockholm, 90-13 ISSN-1100-214X

143 e.g. CERN Accelerator School Fifth advanced accelerator physics course, ed. S. Turner vol.II Geneva 1995

144 P. M. Lapostolle, IEEE Trans. Nucl. Sci. NS-18 no.3 (1971) p.1101

145 W. Krauss-Vogt, H. Beuscher, H. L Hagedoorn, J. Reich, P. Wucherer, Nucl. Instr. Meth. A268 (1988) p.5-9

146 W. Krauss-Vogt, Berichte der KFA-Jülich, Nr- 2043 (Feb. 1986)

147 P. Sortais et al. 13th International Workshop on ECR Ion Sources, College Station, TX, USA, (1997) p.83

148 J. Mandin, 'Etude experimentale et simulation des conditions d'extraction d'un faisceau d'ions multicharges d'une source a resonance cyclotronique electronique', PhD thesis GANIL T 97 01

149 J. L. Hagedoorn, J. I. M. Botman, On the motions of ions in a cylindrically symmetrical magnetic field, Internal report GSI-90-29

150 J. I. M. Botman, H. L. Hagedoorn, The beam emittance of cyclotrons with an axial injection system (source unknown)

151 H. Haas et al., Proc. 1st Int. Conf. on Radioactive Nuclear Beams, Berkeley (Califonia), Oct. 1989, ed. W. D. Myers, J. M. Nitschke, E. B. Norman (World Scientific, Singapore, 1990) p.59

152 B. Visentin, P. van Duppen, P.A. Leroy, F. Harrault, R. Gobin, the Isolde collaboration, Nucl. Instr. Meth. B101 (1995) p.275-279

153 U. Köster, O. Kester, D. Habs, Rev. Sci. Instr. Vol.69 no.3 p.1316-1321

154 E. D. Donets, Phy. Scr. T71 (1997) p.5